The Role Of NMDA Receptor Co-Agonists In Dendritic Integration

Dissertation

zur

Erlangung des Doktorgrades (Dr. rer. nat.)

der

Mathematisch-Naturwissenschaftlichen Fakultät

der

Rheinischen Friedrich-Wilhelms-Universität Bonn

vorgelegt von

Kirsten Bohmbach

aus

Stade

Bonn, Juli 2020

Angefertigt mit Genehmigung der Mathematisch-Naturwissenschaftlichen Fakultät der

Rheinischen Friedrich-Wilhelms-Universität Bonn

1. Gutachter: **Professor Dr. Christian Henneberger**

Institut für Zelluläre Neurowissenschaften

Universität Bonn

2. Gutachter: **Professor Dr. Michael Hofmann**

Institut für Zoologie

Universität Bonn

Tag der Promotion: 27. Januar 2021

Erscheinungsjahr: 2021

Sit down before fact as a little child,
be prepared to give up every conceived notion,
follow humbly wherever and to whatever abysses nature leads,
or you will learn nothing.

Thomas Huxley

ABSTRACT

The integration of synaptic inputs is the fundamental function of neurons. This integration does not only take place at the soma, but also dendrites can actively shape the input-output computations of a neuronal network. In the CA1 region of the hippocampus, dendrites of pyramidal cells integrate inputs either linear or, under specific circumstances, supralinear. For instance, synchronous, spatially clustered inputs at apical oblique dendrites have been shown to evoke dendritic spikes. Likewise, specifically timed activation of Schaffer collateral and perforant path fibers results in large dendritic plateau potentials. These two types of nonlinear integration are highly dependent on NMDA receptor recruitment. Glutamate uptake and dynamic supply of co-agonists can modulate NMDA receptor recruitment. Astrocytes take up the majority of the released glutamate. Moreover, they are one possible source of NMDA receptor co-agonists. In astrocytes, the release of gliotransmitters, such as the NMDA receptor co-agonist D-serine, is evoked by calcium transients.

With my thesis, I aim to unravel the role of astrocytes in different types of dendritic integration through modulation of glutamate uptake or NMDA receptor co-agonist supply. Furthermore, the recruitment and relevance of astrocytic, calcium-dependent, dynamic supply of D-serine under behaviorally relevant activity patterns were explored. Conclusively, the consequence of disrupting dynamic co-agonist supply on learning and memory in vivo was investigated. To this end, whole-cell patch clamp recordings in combination with microiontophoretic glutamate application, electrical stimulation and two-photon excitation fluorescence microscopy as well as behavioral experiments were used.

My data showed that glutamate uptake in the CA1 region of the hippocampus was more tightly regulated at small compared to large spines. Accordingly, the probability of evoking a dendritic spike was increased at the latter. Moreover, my results indicated that local dendritic integration can be modulated by exogenous co-agonists but also through cannabinoid-evoked astrocytic calcium transients that induce the release of endogenous NMDA receptor co-agonist. Endocannabinoids can be mobilized through neuronal depolarization. In my experiments, I therefore used axonal stimulation of CA1 pyramidal cells at different frequencies to investigate whether endogenously mobilized cannabinoids could modulate dendritic integration. Endocannabinoids evoked a similar effect on the integration as exogenous cannabinoids or direct NMDA receptor co-agonist application. I demonstrated that this modulation depends on CB1 receptors and the release of the NMDA receptor co-agonist D-serine. The data showed an unexpected dependency of the frequency of neuronal activation on the dendritic integration. Typically, the mobilization of endocannabinoids is increased with increasing depolarization and action potential number. Interestingly, the opposite was observed. While action potentials evoked at a frequency of 10 Hz increased the threshold and amplitude of dendritic spikes, axonal stimulation at 40 Hz did not. Additional experiments revealed that hyperpolarization-activated cyclic nucleotide-gated (HCN) channels, which are known for the relevance in establishing the neuronal resonance, are required for the frequency-dependent modulation of dendritic integration. Importantly, specific knock-out of CB1 receptors in astrocytes disrupted the positive feedback loop and resulted in selective impairment of spatial reversal learning in a passive place avoidance task and altered long-term object recognition and location memory. Astrocytic calcium transients are the key step in linking neuronal activity to the release of D-serine. To gain a better understanding of these astrocytic calcium transients, the relationship between the pre-event baseline and the peak or amplitude calcium concentration was investigated. Spontaneous and

evoked astrocytic calcium transients were monitored in situ and in vivo by two-photon excitation microscopy. These experiments revealed an overall positive relationship between the pre-event baseline and the peak calcium concentration. Contrastingly, the transient's amplitude and the pre-event baseline concentration correlated negatively with each other. While influx of extracellular calcium mediated the former, the latter was depending on store-dependent calcium release. This relationship poses interesting possibilities on how the intracellular calcium concentration of astrocytes could shape the release of gliotransmitters and synaptic transmission.

My thesis revealed a previously unknown, behaviorally relevant, frequency-dependent positive feedback loop that links pyramidal cell activity to their dendritic integration. Through endocannabinoid mobilization and astrocytic calcium transients, a subsequent increase in D-serine is evoked. D-serine in turn increases the recruitment of NMDA receptors and hence, promotes supralinear dendritic integration through a decreased threshold and increased amplitude of dendritic spikes. The findings not only expand our understanding of astrocytic glutamate clearance and astrocytic calcium transients but also underline the importance of astrocytes for learning and memory through gliotransmission.

TABLE OF CONTENTS

1 INTRODUCTION

Every day, we are confronted with ever changing circumstances and surroundings. In order to respond to new situations appropriately, our brains need to be able to update our assessments and adjust our behavioral responses accordingly. This requires a high degree of flexibility. Existing experiences and knowledge need to be applied to new situations. For example, when your favorite shop moves into another street in town, the existing positive memory needs to be connected with the new spatial information. In other words, prior formed memories need to be associated with new sensory cues to result in the appropriate behavioral response. The hippocampus, a highly specialized region in our brain, plays a crucial role in learning, memory and the association of features that define the context. My thesis aimed to increase our understanding of how input integrations in the hippocampus are shaped. Therefore, I investigated how astrocytes can modify certain neuronal computations and ultimately, identified the behavior that this requires.

1.1 THE HIPPOCAMPUS

1.1.1 ANATOMICAL STRUCTURE

The hippocampus is a highly conserved brain region located in the medial temporal lope. It has a dorsal (the most rostral part) and a ventral part (the most caudal part). While the dorsal part is thought to be most important for spatial navigation (Moser et al., 1993, 1995), the ventral part has been implicated in emotional learning (Henke, 1990; Kjelstrup et al., 2002). The functional system containing the hippocampus is known as the hippocampal formation (Figure 1.1). It consists of three main substructures: the dentate gyrus, the hippocampus proper and the subiculum (Amaral and Lavenex, 2007). The hippocampus proper, also called cornu ammonis (CA), can be further separated in three distinct regions: CA1, CA2 and CA3 (Lorente De Nó, 1934). The functional relevance in the formation of memory and unique structural properties of the hippocampal formation have made it one of the most well-studied systems of the brain. While the cerebral cortex has a multi-layered organization with reciprocal connection, each region of the hippocampal formation has a single principal cell layer with distinct, unidirectional-connected intrinsic networks (Amaral and Lavenex, 2007). This neuroanatomical organization allows researching the features of each network separately.

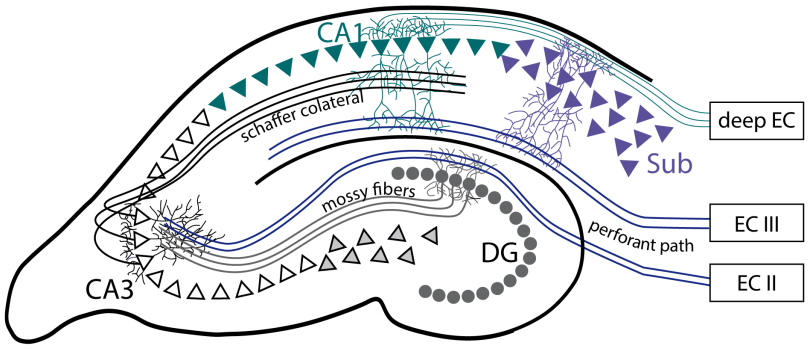

Figure 1.1. Schematic overview of the trisynaptic circuit. The dentate gyrus (DG) granule cells receive input via the perforant path from neurons of the entorhinal cortex layer two (EC II). Its axons, the mossy fibers, emanate from the DG to pyramidal cells in CA3. CA3 neurons in turn innervate CA1 pyramidal cells via the Schaffer collaterals. Additional inputs onto CA1 pyramidal cells originates from layer three neurons in the EC (EC III). The circuit ends with axons from CA1, terminating in the subiculum (Sub) or the deep layers of the EC (deep EC).

The main information path through the hippocampal formation has been described as a the trisynaptic circuit (Figure 1.1; Andersen et al., 1971). The first synaptic connection is formed between neurons of the entorhinal cortex layer 2 and the principal cell layer of the dentate gyrus granule cells along the perforant pathway. The granule cell axons travel along the mossy fiber pathway to innervate CA3 pyramidal cells, the second synaptic connection. The third connection is formed between CA3 and CA1 pyramidal cells by the Schaffer collateral fibers. The CA1 was thought to be the main output structure, with axons innervating the deep layers of the entorhinal cortex and the subiculum. While this pathway might describe the main information route through the hippocampal formation, it has been established that the circuit is far more complex (Amaral and Lavenex, 2007; Amaral and Witter, 1989). Next to the trisynaptic pathway, CA3 and CA1 receive direct inputs from the entorhinal cortex along the perforant path. While the entorhinal cortex and the subiculum are the major input and/or output structures, there are additional, mainly neuromodulatory inputs from and/or outputs to the neocortex, amygdaloid complex, basal forebrain, hypothalamus, brain stem and the thalamus. Furthermore, associational, commissural and longitudinal fibers from CA3 and CA2 innervate hippocampus proper.

1.1.2 The CA1 Microcircuit

The CA1 region of the hippocampal formation has been studied extensively because of its importance in memory encoding and the ease of obtaining intra- and extracellular recordings from this network. Therefore, a tremendous amount of knowledge on synaptic transmission, integration and plasticity derives from the CA1 microcircuit. Like the other CA regions, CA1 is structured into several morphological distinct strata (Amaral and Lavenex, 2007). The pyramidal cell nuclei are densely packed in the stratum pyramidale (SP) from where they send their basal dendrites to the stratum oriens (SO) and one to two apical trunk dendrites to the stratum radiatum (SR) (Figure 1.2). The apical trunk dendrite gives rise to two sets of small dendrites: oblique branches in the stratum radiatum (proximal apical) and tuft branches in the stratum lacunosum moleculare (SLM, distal apical). Each stratum receives inputs from different structures. While the tuft dendrites in the stratum lacunosum moleculare are mainly innervated by entorhinal cortex layer 3 neurons (Andersen et al., 1966; Steward, 1976) and thalamic projections (Dolleman-van Der Weel and Witter, 1996), oblique branches in the stratum radiatum and basal dendrites in the stratum oriens receive their major input from the Schaffer collateral fibers. CA1 pyramidal cells (PC) have a single axon that emerges from the soma or a basal dendrite (Thome et al., 2014). It then passes through the stratum oriens to the alveus, from where it continues to its various target regions.

CA1 PCs receive their excitatory inputs onto small protrusions on their dendrites, so-called spines. The shape of these spines can vary (Harris et al., 1992). For example, thin spines are elongated protrusions with only small heads. Mushroom spines, on the other hand, have a large head and a narrow neck. In total, a CA1 PC has several ten thousand spines (Megías et al., 2001), which are not evenly distributed along the strata. The overall density of spines is the highest in the stratum oriens and stratum radiatum, and the lowest in the stratum pyramidale. Since the total dendritic length in the stratum radiatum is longer than in the stratum oriens, more than half of all spines are located in the stratum radiatum.

Approximately 10 % of the cells found in CA1 are GABAergic interneurons (Aika et al., 1994; Woodson et al., 1989). Inhibitory synapses are usually formed symmetrically, targeting the dendrite, soma or axon directly. Albeit the low number, a large variety of GABAergic neurons can

be found within the CA1 microcircuit (for review see Klausberger and Somogyi, 2008; Somogyi and Klausberger, 2005). Interneurons are classified based on their target region and expression of certain marker proteins, resulting in at least 21 different types (Klausberger and Somogyi, 2008). Inhibition is distributed differently along the dendritic tree of pyramidal cells than excitation. While the soma and axon receive no excitatory innervation, they are targeted by basket and axo-axonic cells, respectively. Distinct subtypes of dendritic-targeting interneurons modulate the inputs into the microcircuit differentially. Inhibition of Schaffer collateral inputs in the stratum oriens and radiatum is performed by bistratified or ivy cells. However, some basket cells target proximal dendrites, too. Oriens-lacunosum moleculare (OLM) cells modulate perforant path inputs but are themselves inhibited by interneuron-specific interneurons (Chamberland et al., 2010; Tyan et al., 2014). Moreover, a variety of long-range inhibition from other brain regions are present in the CA1 microcircuit (Klausberger and Somogyi, 2008; Melzer et al., 2012).

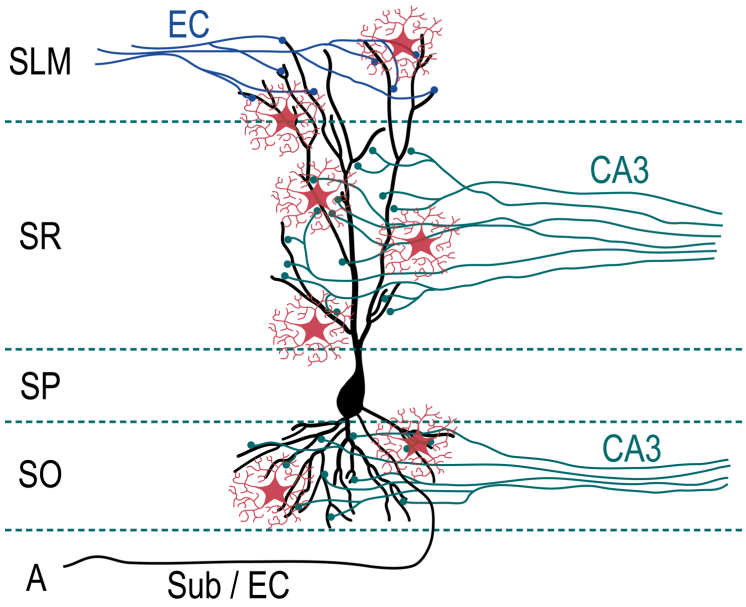

Figure 1.2. Schematic of the CA1 microcircuit. The nucleus of CA1 pyramidal cells is located in the stratum pyramidale (SP). One or two apical trunk dendrites are sent to the stratum radiatum (SR) and further ramify into the apical oblique dendrites, innervated by CA3 neurons (turquoise fibers), and the apical tuft dendrites in the stratum lacunosum moleculare (SLM), innervated by the entorhinal cortex (EC, blue fibers). Basal dendrites in the stratum oriens are innervated by fibers from CA3. The axons of CA1 pyramidal cells are located basally and travel through the alveus (A) to the subiculum (Sub) or EC. Astrocytes can be found throughout all strata (red).

In addition to the neurons, glial cells are present in the CA1 microcircuit. Glial cells in the central nervous system can be subdivided into different types with distinct functions. In the brain, the three major classes of glial cells are oligodendrocytes, microglia and astrocytes. Oligodendrocytes are mainly found in the white matter, where they create myelin sheaths to insulate axons. Microglia are the immune cells of the brain. Astrocytes are the most abundant type of glial cells in the hippocampus. Across strata, their number slightly differs (Ogata and Kosaka, 2002). They are densely packed in the stratum lacunosum moleculare and sparser in the stratum pyramidale. In the stratum radiatum of CA1 they are evenly distributed and each of them occupies its own territory (Bushong et al., 2002). With their fine processes they are in close proximity to neuronal

synapses (Gavrilov et al., 2018; Ventura and Harris, 1999; Wolff, 1968). Owing to their electrically-passive nature, it was long thought that astrocytes are mainly supporting neurons by clearance of neurotransmitters, ion homeostasis and metabolic support (Kuffler, 1967). However, more recent findings show that astrocytes play a more active role and can modulate neuronal transmission (for a detailed description of astrocytes see section 1.3).

1.1.3 Memory and Plasticity

The hippocampus, and with it the CA1 microcircuit, exerts a central role in the encoding and storage of new memories. However, memory processed by the hippocampus is not omnifarious. In general, three types of memory are distinguished: sensory, short-term and long-term memory. Sensory memory is a very short-lasting memory of sensory input, e.g., visual, auditory or tactile. It allows to transfer and integrate relevant sensory information to short-term memory even if the relevance is realized shortly after the input. Accordingly, we are able to recall a row of four letters even though we have only seen them for a fraction of a second (Sperling, 1960). Short-term memory is often called working memory since it describes the temporal storage of information required to fulfill complex tasks (Baddeley, 1992). Long-term memory, as the name describes, refers to long-term storage of information ranging from hours to a lifetime. Two main types, declarative and non-declarative memory, can be distinguished and are stored differentially in the brain (Brem et al., 2013). Implicit, non-declarative memory refers to unconscious memory and is further divided into several subtypes. Procedural memory is one subtype. It stores, for instance, the motor sequence required for playing a certain piano piece. Another subtype is associative memory, which links one stimulus to a related one, as studied in classical Pavlovian conditioning. Habituation, sensitization and priming are further subtypes of unconscious memory. Depending on the subtype, implicit memory is stored in the cerebellum, striatum, neocortex or the limbic system. Declarative, explicit memory refers to memories that are formed about the environment. Facts and meanings without further context are termed semantic memory, while experiences and contextual memory are termed episodic memory. Observations made on patients with brain damage have established a major role of the hippocampus in declarative memory (Scoville and Milner, 1957). The most famous patient is “H.M”. As a treatment of his severe epilepsy, he received a temporal lobectomy, meaning a complete removal of the hippocampus and surrounding cortical areas. After the surgery, he had no more seizures. Thereafter, however, he suffered from an inability to form new memories. The removal of the hippocampus is thought to be the cause of this defect.

Encoding of Memory Through Plasticity

How are memories encoded? The output pattern of a network is based on specific input patterns. Hence, encoding of memories could be represented by alteration of the input-output transformation of network connection. This will lead to altered output of the network that are thought to enable appropriate behavior. This basic principle underlying plasticity, known as the Hebbian theory, has been postulated seventy years ago:

> *“When an axon of cell A is near enough to excite a cell B and repeatedly or persistently takes part in firing it, some growth process or metabolic change takes place in one or both cells such that A's efficiency, as one of the cells firing B, is increased.”*
>
> (Hebb, 1949)

Several studies have recapitulated the effect of hippocampectomization in rodents, making them the appropriate model for experimental investigations of the cellular mechanisms of memory. However, owing to the lack of suitable experimental setups, it was only in the late 60s and early 70s that Bliss and Lomo (1973) observed the first long-term changes in synaptic transmission. High frequency stimulation of perforant path axons led to hours-long changes in the dentate gyrus of anaesthetized rabbits. Specifically, they observed an increase in the population excitatory postsynaptic potentials (EPSPs) and the population spike. This means not only potentiation of the synaptic input but also an enhanced somatic excitability of the dentate gyrus granule cells is induced. This phenomenon has been termed long-term potentiation (LTP) and has been used to investigate the effects of thousands of compounds and conditions on memory formation at a cellular level ever since. LTP is not a phenomenon that is restricted to the hippocampus. It is rather a term describing a variety of processes in different brain regions that result in long-term alterations of synaptic transmission (for review Malenka and Bear, 2004). Thus, LTP has been described to underlie simple associative learning, a form of intrinsic memory formation (Maren, 2005; McKernan and Shinnick-Gallagher, 1997; Rogan et al., 1997).

LTP in the CA1 region of the hippocampus was first described in acute guinea pig brain slices in 1975 (Schwartzkroin and Wester, 1975). This approach was then used to study the underlying mechanism in detail and thereby, unraveling the key features already postulated by Hebb: input specificity, associativity, cooperativity and persistence. At a cellular level this means postsynaptic depolarization and presynaptic glutamate need to coincide to activate NMDA receptor-dependent calcium influx (Ascher and Nowak, 1988; Collingridge et al., 1983; Gustafsson et al., 1987; Kelso et al., 1986; Lynch et al., 1983; MacDermott et al., 1986; Malinow and Miller, 1986; Mayer et al., 1984; Morris et al., 1986; Nowak et al., 1984). Intracellularly, the influx of calcium activates signaling cascades that result in altered AMPA receptor expression and changes in spine morphology. Using single spine two-photon uncaging, it was discovered that repetitive activation of a single spine results in morphological changes (Matsuzaki et al., 2004). While the stimulated spine is turned into a large mushroom spine, the morphology of neighboring spines was unaltered. This suggests that spine morphology indicates a physical trace of memory. The morphological adaptations are accompanied by an increase in AMPA receptor-mediated current, indicating an increase in number and/or posttranslational modification of the receptor (Boehm et al., 2006; Kopec et al., 2006; Lee et al., 2000, 2003; Matsuzaki et al., 2004; Okamoto et al., 2004; Patterson et al., 2010). Calcium/calmodulin-dependent protein kinase II (CaMKII) and calmodulin have been shown to be key regulatory proteins in this process by linking the calcium influx to structural adaptations (Barria et al., 1997; Faas et al., 2011; Hayashi et al., 2000; Kristensen et al., 2011; Lee et al., 2009; Lu et al., 2010; Opazo et al., 2010; Otmakhov et al., 2004; Tomita et al., 2005). During the late phase of LTP (several hours after induction) adaptation of the local protein synthesis can be observed (Fonseca et al., 2006; Frey et al., 1993; Govindarajan et al., 2011; Stanton and Sarvey, 1984).

Opposed to LTP, long-term depression (LTD) describes the long-lasting decrease in synaptic strength. Several types of LTD, among the major forms mediated by either NMDA receptor or metabotropic glutamate receptors (mGluRs), have been described. Depending on the receptor's location, different downstream effectors are suggested. Postsynaptic LTD relies, as LTP, on calcium dependent signaling through CaMKII and calmodulin (Barria et al., 1997; Coultrap et al., 2014; Lee et al., 1998, 2000; Okamoto et al., 2004; Snyder et al., 2001; Tomita et al., 2005; Xiao et al., 2001). In contrast to LTP, however, the result is a decrease of AMPA receptor conductance

through a decrease in receptor density and altered kinetics by posttranslational modifications. Presynaptic LTD is the result of a long-term suppression of glutamate release (Enoki et al., 2009; Faas et al., 2002; Fitzjohn et al., 2001; Watabe et al., 2002). Heterosynaptic LTD is a subtype of presynaptic LTD, in which presynaptic release is inhibited through retrograde endocannabinoid signaling (details in section 1.1.5; Yasuda et al., 2008). Investigating protocols inducing long-term alterations in synaptic efficacy reveled a striking dependence of the spike timing and order in determining potentiation or depression. While presynaptic input preceding or timed together with postsynaptic depolarization induced LTP, reversing the input sequence lead to LTD. Furthermore, a precise time-interval between pre- and postsynaptic activation is required, leading to the name: spike-timing-dependent plasticity (STDP; Song et al., 2000).

1.1.4 The Role of NMDA Receptors in Plasticity

NMDA receptor recruitment is a crucial step in many types of synaptic plasticity. The NMDA receptor (Figure 1.3) is a heteromeric complex formed out of different subunits, e.g., two GluN1 and two GluN2 subunits (Salussolia et al., 2011). Binding of its ligands, glutamate and additionally one of the co-agonists D-serine or glycine, results in opening of the channel pore (Johnson and Ascher, 1987; Kleckner and Dingledine, 1988; Kolhekar et al., 1994; Matsui et al., 1995; Mothet et al., 2000; Paoletti and Neyton, 2007; Vyklický et al., 1990). However, for current flow through the channel pore, depolarization is necessary to relieve the otherwise present magnesium block (Ascher and Nowak, 1988; Mayer et al., 1984; Nowak et al., 1984). Only when ligand binding coincides with depolarization, sodium and calcium influx as well as potassium efflux can take place. Therefore, the magnesium block meets a requirement of Hebbian plasticity as it makes coincidence detection of presynaptic and postsynaptic activity possible. But other biophysical characteristics are important for the role of NMDA receptors in learning and memory, too. Compared to AMPA receptors, NMDA receptors display rather slow kinetics owing to the slow glutamate unbinding (Forsythe and Westbrook, 1988). Therefore, AMPA receptors provide rapid depolarization while NMDA receptors mediate its duration. Accordingly, NMDA receptors set the interval that allows summation of synaptic input. Another distinct property of NMDA receptors is its permeability for calcium (MacDermott et al., 1986). This calcium influx allows the interaction with calcium-dependent enzymes that are required for the induction of LTP or LTD.

But how can the same receptor regulate two opposing mechanisms? Their subcellular location has been suggested as one important factor. NMDA receptors can be found within the synapse, but also at extrasynaptic sites. The latter means on dendrites, the spine neck, or at perisynaptic sites, e.g., within 100 nm of the release site (Harris and Pettit, 2007; Petralia et al., 2010). Typically, synaptic receptors are activated during low frequency presynaptic activity (Harris and Pettit, 2007) while extrasynaptic NMDA receptors are activated by elevated levels of ambient glutamate (Fleming et al., 2011; Meur et al., 2007; Moldavski et al., 2020), glutamate released by astrocytes (Fellin et al., 2004) or glutamate spill-out from the synapse (Kullmann et al., 1999; Rusakov and Kullmann, 1998). Moreover, different downstream effector pathways have been described for the different locations. While synaptic receptors are thought to promote survival through activation of calcium/CREB signaling and suppression of apoptosis, extrasynaptic ones suppress the former and activate the latter (Hardingham et al., 2002). Furthermore, plasticity is proposed to be steered by the activation of distinct receptor pools. In the cortex, increasing glutamate spill-out out of the synapse and hence, increasing the activation of extrasynaptic NMDA receptors, resulted in the induction of LTD (Massey et al., 2004). However, another study has

suggested that in the hippocampus LTP can be induced through extrasynaptic NMDA receptors (Yang et al., 2017).

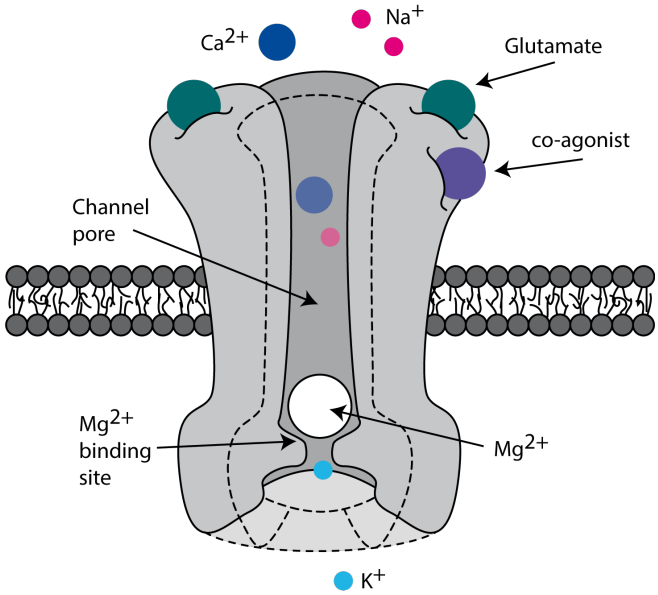

Figure 1.3. Schematic of the NMDA receptor. The NMDA receptor requires several criteria to be met for pore opening: (1) Glutamate binding; (2) Co-agonist binding of D-serine or glycine; (3) Relief of the magnesium block through depolarization. Only if all three requirements are fulfilled at the same time (coincidence detection) influx of sodium and calcium as well as efflux of potassium ions occures.

In addition, the subunit composition of NMDA receptors influences its channel properties and has been proposed to influence plasticity differentially. Neurons in the hippocampus predominantly express di- and tri-heteromeric receptors containing the GluN1, GluN2A and/or GluN2B subunit (Ascher and Nowak, 2009; Paoletti and Neyton, 2007). Especially the GluN2 subunit is crucial in determining many biophysical properties and channel kinetics of the NMDA receptor. Receptors containing the GluN2B subunit display a higher affinity for and slower unbinding of glutamate (Paoletti, 2011). The magnesium unblock is slower, as well (Clarke and Johnson, 2006). Accordingly, di-heteromeric GluN2A-GluN1-containing receptors display faster kinetics than GluN2B-GluN1 containing ones (Rauner and Köhr, 2011). Tri-heteromeric receptors show intermediate kinetics. In addition, a differential affinity for the co-agonist glycine and D-serine has been suggested (Matsui et al., 1995; Papouin et al., 2012), but the physiological relevance is undetermined. Importantly, the interaction with downstream proteins differs between the GluN2 subunits. For example, the GluN2B subunit interacts more with CaMKII than the GluN2A one (Barria and Malinow, 2005; Bayer et al., 2001). Owing to the distinct signaling of CaMKII during LTP and LTD (Coultrap et al., 2014), a differential contribution of GluN2 subunits to plasticity has been postulated. Some studies have suggested a selective involvement of the GluN2A subunit in LTP and of the GluN2B subunit in LTD (Brigman et al., 2010; Liu et al., 2004; Massey et al., 2004; Papouin et al., 2012; Sakimura et al., 1995). However, a substantial amount of evidence contradicts a strict subunit-dependent separation (Berberich et al., 2005; Clayton et al., 2002; von Engelhardt et al., 2008; Miwa et al., 2008; Morishita et al., 2007; Tang et al., 1999; Wang et al., 2009; Weitlauf et al., 2005). In line with the distinct interaction of the GluN2B subunit with CaMKII, it was shown, that indeed the distinct C-terminus of the GluN2 subunits is responsible for the differential induction of plasticity (Foster et al., 2010). Accordingly, Foster et al. showed

the importance of GluN2B for LTP. Interestingly, modelling of the charge transfer has predicted the opposite (Erreger et al., 2005). The slow kinetics of the GluN2B subunit have resulted a larger contribution of this subunit during LTD induction. Vice versa, the GluN2A-dependent, faster charge transfer has been enhanced during LTP induction. Furthermore, a distinct subcellular distribution was suggested for the different NMDA receptor subunits (Stocca and Vicini, 1998). However, others have failed to show this (Harris and Pettit, 2007). The contradicting results concerning the association of a distinct receptor pools with distinct forms of plasticity suggest rather complex interaction. Likely, the balance in recruitment of NMDA receptors at different locations and/or the ratio of different subunits have been suggested to control induction of LTP and LTD (Iacobucci and Popescu, 2017; Paoletti et al., 2013).

1.1.5 The Role of Endocannabinoids in Plasticity

Next to NMDA receptor-dependent LTP and LTD, endocannabinoids have been shown to evoke long-term plastic changes in the hippocampus. Moreover, endocannabinoids also shape the basal synaptic transmission in the CA1 microcircuit. Accordingly, their role of them in learning and memory has been studied.

The knowledge of the psychoactive and medical properties of cannabis dates back several thousand years (Touw, 1981). In Europe, the therapeutic potential of the plant was researched already at the beginning of the 19th century (O'Shaughnessy, 1843). Nevertheless, it took until the end of the 20th century to identify the first endogenous cannabinoid (Devane et al., 1992). Nowadays, we distinguish between several endocannabinoids, although most research focuses on two: anandamide (AEA) and 2-arachidonoylglycerol (2-AG). Each endocannabinoid has a specific biosynthesis that is mediated by a cascade of several enzymes located at the postsynapse (for review see Di Marzo, 2011). Common steps are the requirement of membrane depolarization, elevation of the intracellular calcium concentration and/or activation of metabotropic receptors (Kim et al., 2002; Neu et al., 2007; Ohno-Shosaku et al., 2001; Varma et al., 2001). Degradation of AEA and 2-AG is performed by fatty acid amide hydrolase (FAAH) or monoacylglycerol lipase (MAGL) at the post- or presynapse, respectively (Gulyas et al., 2004; Straiker et al., 2009). More recently, it is has been shown that also astrocytes mobilize and degrade endocannabinoids (Smith et al., 2020; Viader et al., 2015).

Notably, endocannabinoids are produced on demand and are not stored in vesicles (Hashimotodani et al., 2013). Nevertheless, the time course from stimulation to receptor activation is considerably fast at physiological temperatures, namely 20-50 ms (Heinbockel et al., 2005). Because of their lipophilicity it is presumed that endocannabinoids are mobilized by diffusion through the membrane and can exert their action only locally on neighboring neurons or astrocytes (Di Marzo et al., 1998; Piomelli et al., 2000), with an action range of approximately 10 µm (Chevaleyre and Castillo, 2003).

Once mobilized, endocannabinoids in the brain mainly bind to two G-protein coupled receptors, the CB1 and CB2 receptor. Whereas the CB2 receptor shows weak expression in the brain (Galiègue et al., 1995; Schatz et al., 1997) that is confined to microglia (Carlisle et al., 2002; Klegeris et al., 2003; Walter et al., 2003), CB1 receptors are expressed throughout the brain (Herkenham et al., 1990), with a particularly high expression in the hippocampal CA1 microcircuit (Liu et al., 2003). Here, the most prominent CB1 receptor expression can be found in the presynaptic terminals of cholecystokinin (CCK)-positive GABAergic interneurons (Marsicano and Lutz, 1999). CCK-positive cells show different morphologies and functional connections to

CA1 pyramidal cells (Bezaire and Soltesz, 2013; Freund and Buzsáki, 1996). While CCK-positive basket cells contact the soma and proximal dendrites of CA1 pyramidal cells with their axon, other subtypes inhibit dendrites in the stratum radiatum or lacunosum moleculare. However, independent of their morphology, CB1 receptors have been described in most subclasses of CCK-positive interneurons (Ali, 2007; Ali and Todorova, 2010; Klausberger et al., 2005; Neu et al., 2007; Pawelzik et al., 2002; Wilson et al., 2001). Expression of CB1 receptors has also been described in excitatory boutons (Kawamura et al., 2006) and astrocytes (Bonilla-Del Río et al., 2019; Gutiérrez-Rodríguez et al., 2018; Han et al., 2012; Navarrete and Araque, 2008), albeit to a lesser extent.

SHORT-TERM PLASTICITY

The most-well described mechanisms by which endocannabinoids influence neuronal transmission in the CA1 microcircuit is depolarization-induced suppression of inhibition (DSI, Alger et al., 1996; Pitler and Alger, 1992, 1994) and, to a lesser extent, depolarization-induced suppression of excitation (DSE, Ohno-Shosaku et al., 2002). Notably, both forms of short-term plasticity require retrograde signaling from the postsynapse to the presynapse. A depolarization of the postsynaptic neuron results in an increase of the calcium concentration (Lenz and Alger, 1999; Lenz et al., 1998; Pitler and Alger, 1992; Wang and Zucker, 2001), which will stimulate the production and mobilization of endocannabinoids (Ohno-Shosaku et al., 2002a; Wilson and Nicoll, 2001; Wilson et al., 2001). In addition, activation of mGluRs or M1/M3 metabotropic acetylcholine receptors (AChRs) can facilitate the mobilization of endocannabinoids (Edwards, 2005; Kim et al., 2002; Martin and Alger, 1999; Ohno-Shosaku et al., 2002b, 2003; Varma et al., 2001). At the presynapse, the $G_{\beta\gamma}$-subunit of the CB1 receptor inhibit voltage gated calcium channels (VGCC) (Brown et al., 2003; Hoffman and Lupica, 2000; Sullivan, 1999; Twitchell et al., 1997; Wilson et al., 2001). Thereby, the presynaptic increase in calcium is reduced and the release of neurotransmitters inhibited (Szabó et al., 2014). Notably, DSI is mainly observed for somatic inhibition (Lee et al., 2010; Younts et al., 2013). Many experiments have tried to unravel the endocannabinoid identity responsible for DSI and DSE. However, a large variety of pharmacological and genetic approaches have resulted in contradicting results (Beltramo et al., 1997; Chevaleyre and Castillo, 2003; Di Marzo, 2011; Edwards, 2005; Gao et al., 2010; Makara et al., 2005; Min et al., 2010; Pan et al., 2009; Szabo et al., 2006). Nevertheless, direct measurements of the 2-AG concentration in response to stimulation have strongly supported its role in DSI (Tanimura et al., 2010). Moreover, the existence of a preproduced pool of 2-AG has been proposed (Edwards, 2005; for review and discussion see Alger and Kim, 2011).

While the underlying mechanisms of DSI and DSE are well-characterized in vitro and in situ, evidence for their recruitment in vivo has been mostly correlative. The use of CB1 receptor knock-out animals does not permit the segregation of short and long-term plastic effects of endocannabinoids. However, the stimulation patterns that evoke DSI could serve as an indication. In hippocampal slices, the impact of DSI scales with number and frequency of postsynaptic APs (Fortin et al., 2004). Hence, DSI could be evoked by short bursts that mimicking firing pattern of CA1 pyramidal cells that are observed during behavioral experiments (Dubruc et al., 2013). The resulting DSI has been postulated to shape spike-time precision during place cell formation. While these findings strongly support a role of DSI in vivo, to my knowledge there is no evidence that documents the occurrence of DSE under physiological conditions.

Long-term Plasticity

Endocannabinoids have been shown to mediate long-term plasticity in various brain regions and by various mechanisms (for review see: Lutz and Marsicano, 2009; Xu and Chen, 2015). This section will focus on three mechanisms observed in the hippocampus. Repetitive stimulation of excitatory inputs has been shown to evoke heterosynaptic, presynaptic-form of LTD of inhibitory inputs (iLTD) that depends on endocannabinoid signaling (Chevaleyre and Castillo, 2003; Edwards et al., 2008; Kang-Park et al., 2007; Lafourcade and Alger, 2008; Zhu and Lovinger, 2007). Notably, endocannabinoid-evoked LTD of excitatory inputs is only observed during development (Yasuda et al., 2008). Through the repetitive activation of postsynaptic mGluRs, endocannabinoids are mobilized and through CB1 receptors trigger iLTD (Chevaleyre and Castillo, 2003). In contrast to DSI, an increase in postsynaptic calcium is not necessary. Accordingly, iLTD cannot be evoked for perisomatic inputs, likely caused by the lack of mGluRs. Thus, iLTD is recruited solely in interneurons targeting dendrites in the stratum radiatum. Interestingly, iLTD changes the input-output coupling in CA1 pyramidal cells and therefore, can participate in the induction of heterosynaptic LTP in a frequency-dependent manner (Chevaleyre and Castillo, 2003, 2004). Strikingly, the induction of iLTD is spatially restricted. Only with 10 µm of the stimulated spine, iLTD was observed. Likely, iLTD is, as DSI, mediated by the mobilization of 2-AG (Xu et al., 2014). Another interesting heterosynaptic plasticity mediated by endocannabinoids required dual pathway activation of CA1. Low frequency activation of entorhinal inputs to the stratum lacunosum moleculare results in mobilization of endocannabinoids and depotentiation of Schaffer collateral inputs in the stratum radiatum that previously have experienced LTP (Izumi and Zorumski, 2016, 2019). Next to endocannabinoids, also signaling by dopamine, GABA and adenosine is required. This so termed LTP-D is thought to provide a mechanism of synaptic resetting, since it does not influence basal transmission. Precise pairing of Schaffer collateral with perforant path inputs could also result in plastic changes selectively at the former. This heterosynaptic plasticity is termed input-timing-dependent plasticity (ITDP) and depends on the delay between inputs to both pathways (Dudman et al., 2007). Interestingly, the induction of ITDP requires iLTD of CCK-positive, Schaffer collateral-associated interneurons mediated by endocannabinoids (Basu et al., 2013). In accordance with a role of endocannabinoids in plasticity, substantial evidence of altered learning and memory has been found (for review see Marsicano and Lafenêtre, 2009). However, the diverse release mechanisms, locations and signaling mechanisms of endocannabinoids do not allow distinction of the underlying mechanism involved. One interesting recent finding, in contrast to many studies in situ, describes the role of AEA in long-term potentiation in adult animals without involvement of iLTD (Zimmermann et al., 2019). Through overexpression of the degrading enzyme fatty acid amide hydrolase (FAAH), the concentration of AEA was decreased selectively in the hippocampus. Interestingly, this has resulted in an increased magnitude of LTP without influencing iLTD, excitatory LTD, DSI or DSE in slices. Furthermore, these mice displayed impairment of spatial and aversive memory.

1.1.6 Spatial Learning and Memory

Many experiments state the existence of LTP and LTD in vivo (Barrionuevo et al., 1980; Heynen et al., 1996; Levy and Steward, 1979; Staubli and Lynch, 1990; Thiels et al., 1994, 1996). Nevertheless, evidence that relates these plastic changes to behavioral output is mainly correlative. Using the Morris water maze (MWM), a link between NMDA receptors, LTP and spatial memory has been demonstrated. In this task, rodents need to escape a pool filled with

opaque water by finding a hidden platform. While in the beginning the platform is discovered through random navigation, repetition evokes learning of the platform's location based on spatial clues outside the maze (Morris, 1981; Morris et al., 1982, 1986). Spatial learning deficits can be evoked through pharmacological blockade of NMDA receptors or intrahippocampal lesions (Davis et al., 1992; Morris, 1989; Morris et al., 1982, 1986). The first regional specific results were obtained using a genetically modified mouse, lacking the GluN1 subunit specifically in CA1 PCs. These mice did not only exhibit learning deficits in the MWM (Tsien et al., 1996), but also showed impaired place fields in CA1 (McHugh et al., 1996). In general, these results show the importance of NMDA receptors in the hippocampus for spatial learning.

Place fields are another important advancement in understanding the underlying mechanism of hippocampal learning and memory. By recording single cell responses in the freely moving rats, O'Keefe identified different types of cells in the CA1 region based on distinct firing patterns (O'Keefe, 1976; O'Keefe and Dostrovsky, 1971). Place cells fire action potentials (APs) only when the animal is in a certain location in space independent of the exploratory behavior. The second type of cells discovered, the displace cells, show firing patterns independent of the location of the animal but rather seem to correlate with its motor behavior and rhythmic activity in the theta range (O'Keefe, 1976). O'Keefe postulated that these cells encode some distance-related parameter like acceleration or velocity. Based on these and other observations made, O'Keefe and Nadel have proposed that the hippocampus functions as a cognitive map (O'Keefe and Nadel, 1978), an idea first introduced by Tolman (1948). However, this map is not limited to spatial information, as a more recent study has shown that a map of social space is stored within the hippocampus, too (Tavares et al., 2015). Therefore, the cognitive map represented in the hippocampus is rather a topological than a geometrical map, based on its connectivity and not on distances and angels (Dabaghian et al., 2014). Wilson and McNaughton (1993) have shown that during exploration of a novel environment inhibition is suppressed. Moreover, they suggested that the new spatial information creates a condition in which synaptic modifications are favored. A decreased inhibition will also increase the signaling that has been suggested to underlie place cell induction: behavioral timescale synaptic plasticity (Bittner et al., 2015; Grienberger et al., 2017). Inputs from the entorhinal cortex can initiate dendritic plateau potentials (for detail see section 1.2.4), resulting in an long-lasting depolarization spreading through the neuron (Grienberger et al., 2014). Hence, excitatory inputs arriving simultaneously throughout the dendritic arbor are potentiated (Bittner et al., 2015, 2017). A revisit to the same location/situation is thought to recruit these inputs. However, these now potentiated input will result in a larger, ramp-like depolarization and eventually recruit AP firing within the place field of the cell (Bittner et al., 2015; Diamantaki et al., 2018; Epsztein et al., 2011; Harvey et al., 2009). While this form of plasticity does not meet the requirements postulated by Hebb, it allows rapid, one trial learning as required for survival-related behavioral output.

Investigating the spatial learning abilities of rodents in the MWM or other tasks (for review see Sharma et al., 2010) and recording place cell activity has led to a more detailed understanding of the hippocampus in learning and memory, but also to contradicting results. Several studies have suggested that hippocampal NMDA receptors are not universally required for spatial learning (Bannerman et al., 1995, 2003a, 2008, 2012; Cain et al., 1996; Jeffery and Morris, 1993; Korol et al., 1993; Saucier and Cain, 1995; Sutherland et al., 1993). It is important to distinguish between allocentric and egocentric spatial learning. While self-centered spatial learning does not require

the hippocampus, spatial learning based on environmental cues does. Learning of the MWM task can be achieved by both learning strategies, which can explain the contradicting results observed.

Changes in the environment cause rearrangement of place cells and fields in CA1 (Deshmukh and Knierim, 2013; Lenck-Santini et al., 2005; Lever et al., 2010; Manns and Eichenbaum, 2009). In these situations, the microcircuit seems to be in enhanced state, thus, allowing plastic changes in synaptic transmission during novelty exploration (Larkin et al., 2014). In line with these observations, it is suggested that the CA1 microcircuit of the hippocampus plays an important role in integrating the current situation into already experienced ones (Brun et al., 2002; Lee et al., 2004; Vago and Kesner, 2008). While CA3 sends on "known" information, i.e., memory retrieval (Brun et al., 2002; Larkin et al., 2014; Lee et al., 2004), the perforant path connections are required for spatial novelty detection (Brun et al., 2002; Vago and Kesner, 2008). Accordingly, dopamine, an important modulator of novelty detection, specifically has modifies inputs from the latter (Vago and Kesner, 2008). Interestingly, a different contribution of LTP and LTD during the exploration is also proposed. While a facilitation of LTP has been observed in simple but novel environments, exploration of a novel, complex environment has enhanced LTD (Dong et al., 2012; Goh and Manahan-Vaughan, 2013; Goh and Manahan-Vaughan, 2013; Kemp and Manahan-Vaughan, 2004; Li et al., 2003). Accordingly, a relevance of the hippocampus in behavioral flexibility is suggested (Mahut, 1971). This requires the adaptation of an existing memory to incorporate new information. Interestingly, LTD has been implicated to play a prominent role in behavior flexibility (Kim et al., 2011; Morice et al., 2007; Nicholls et al., 2008).

1.1.7 Rhythmic Activity and Oscillations

The anterograde amnesia of the patient H.M after the removal of the temporal lobe suggests an encoding of new declarative memories in the hippocampus (Scoville and Milner, 1957). However, his previous memories were not affected. This suggests that long-term memory is stored elsewhere in the brain. Therefore, coordinated activity along different brain regions will be necessary to transfer the information. Synchronized neuronal activities, so-called oscillations, are suggested to dynamically coordinate many cognitive functions and brain states (Buzsáki and Draguhn, 2004; Engel et al., 2001; Klimesch, 1999). There are several oscillations, which can be observed in the hippocampus. These oscillation have distinct frequency bands and differ with respect to their behavioral relevance.

Delta Oscillations

Delta oscillation (< 4 Hz) are mainly observed during non-REM sleep (McCormick and Bal, 1997). While these oscillations are most prominent in the neocortex and thalamus (Neske, 2016), also in the hippocampus delta oscillations are observed (Wolansky et al., 2006; Zhang et al., 2012). These are usually associated with a state of deactivation as present during sleep or anesthesia (Wolansky et al., 2006). Interestingly, hippocampal delta oscillations during slow wave sleep (SWS) have been shown to enhance memory performance (Marshall et al., 2006). Furthermore, EEG recordings have shown an increase in delta power activity following a hippocampal-dependent memory task (Binder et al., 2012). Moreover, the replay of previously experienced behavior, e.g., place cell patterns, occurs mostly during SWS (Ji and Wilson, 2007). Accordingly, SWS has been proposed to support the consolidation of hippocampal memories (Marshall and Born, 2007).

THETA OSCILLATIONS

Theta rhythm (4-10 Hz) is a highly regular activity that can be observed not only in the hippocampus but throughout most of the brain (Canolty et al., 2006; Leung and Borst, 1987; Mitchell and Ranck, 1980; Paré and Collins, 2000; Vertes et al., 2001). However, it is strongest in the hippocampal fissure between dentate gyrus and CA1 (Winson, 1974). Two different types defined by their sensitivity to atropine are distinguished (Kramis et al., 1975). Atropine-sensitive type 2 theta has a low frequency and is not dependent on movement. It is often observed during anesthesia or phases of immobility, e.g., decision points or predator-dependent freezing (Sainsbury et al., 1987). Interestingly, type 2 theta can be induced by stimulation of OLM interneurons in the ventral hippocampus. Varying the activity of OLM cells and, hence, type 2 theta power influenced risk-taking behavior and innate anxiety of mice (Mikulovic et al., 2018). Type 1 theta is atropine-resistant. Its frequency is higher and correlates with the animal's speed of movement (Kramis et al., 1975; Vanderwolf, 1969). It is thought to put the hippocampus in an active state necessary for memory functions (Buzsáki, 2002; Tanaka et al., 2018). The mechanism is unclear. However, involvement of cholinergic activity via the medial septum/diagonal band of Broca and excitation via entorhinal cortex are postulated to be necessary (Buzsáki, 2002; Mysin et al., 2019). In the dorsal hippocampus especially cholinergic inputs to CA1 PCs and not inhibitory neurons, as well as NMDAR activation in the entorhinal cortex have been essential in setting the theta power during an open-field task and the performance in the Y-maze (Gu et al., 2017).

Interestingly, neurons are more likely to respond to inputs at a distinct frequency, termed resonance frequency (Hutcheon and Yarom, 2000). In CA1 PCs, the resonance frequency lies in the theta band (Hu et al., 2002; Nolan et al., 2004). This frequency is determined by two distinct mechanisms. On the one hand, the membrane time constant (τ_m) defines the low pass filtering properties as it determines how fast the membrane potential can respond to these changes in current. On the other hand, hyperpolarization-activated cyclic nucleotide-gated (HCN) and their resulting h-current (I_h) form a high pass filter (Buzsáki and Draguhn, 2004; Hutcheon et al., 1996). Owing to their slow activation and deactivation kinetics, HCN channels are not able to respond in a timely manner to high frequency activations. However, low frequency inputs allow HCN channels to open and counteract the depolarization. Accordingly, inputs at intermediate frequencies have a high impedance (Z_D) that results in the resonance peak.

BETA OSCILLATIONS

Beta-range activity (10-30 Hz) in the hippocampus has been be observed specifically during the exploration of a novel environment (Berke et al., 2008). Interestingly, the power in beta activity has been low during the first lap and increases strongly during the second. The more place cells have become spatially selective, the more the power of beta oscillations has decreased. Hence, the amount of beta-rage activity has dropped after only a couple of minutes. On a cellular level, it has been suggested that hippocampal basket cells modulate beta oscillations (Bibbig et al., 2007; Gurevicius et al., 2007). Also, the occurrence of beta activity and synchronization between different brain regions could be revealed in different studies. It has been shown that reward related memory paradigms enhance beta activity (Lansink et al., 2016; Mas-Herrero et al., 2015). In the hippocampus, this increase in beta band has been observed in a district subset of CA1 PCs (Lansink et al., 2016). In line with a relevance of beta oscillations in the hippocampus during these specific memory tasks, the neuronal activity in the ventral striatum has been specifically phase-

locked to it. Furthermore, processing of odor information is commonly associated with beta oscillations in CA1 (Allen et al., 2016; Igarashi et al., 2014; Martin et al., 2007). Recently, it has been shown that this activity not only occurs simultaneously with beta oscillations in the olfactory bulb but is driven by it, suggesting a beta-rage activity-dependent communication between the two brain areas (Lockmann et al., 2018).

GAMMA OSCILLATIONS

Gamma-range activity occurs more in burst-like pattern during certain theta phases (Canolty et al., 2006; Colgin et al., 2009; Lisman and Idiart, 1995; Soltesz and Deschênes, 1993; Stumpf, 1965). Not the whole population of CA1 PCs fires at gamma frequency, rather small subsets of neurons participate in these burst-like patterns (Jensen and Colgin, 2007; Lisman and Idiart, 1995; Senior et al., 2008). It is thought that gamma oscillations are coordinating unconscious neuronal activity, like integrating information learned or determining aspects to be remembered (Colgin and Moser, 2010). This is in line with findings from Lundqvist et al. (2016) that have shown a correlation between encoding or decoding neuronal activity and changes in the gamma burst rate in the prefrontal cortex. They have postulated that gamma oscillations modulate, which sensory information is incorporated into working memory. In the CA1 region of the hippocampus two separate forms of gamma oscillations are observed, each of them occurring during a different phase of theta (Bragin et al., 1995; Colgin et al., 2009). Slow gamma (< 80 Hz) oscillations are coherent between CA1 and CA3 (Colgin et al., 2009; Combe et al., 2018). Furthermore, CA1 PCs respond to activation of Schaffer collaterals preferably with AP firing in the slow gamma range. These oscillations can be observed when the animal tries to retrieve information, e.g., when the animal pauses at a cross point trying to remember where it already was and which way to go next (Johnson and Redish, 2007; Lopes-Dos-Santos et al., 2018). In line with this, slow gamma oscillations correlate well with spatial associative memory formation, like it is required for the object location task (Trimper et al., 2017). Fast gamma (> 80 Hz) oscillations in CA1 are phase-locked to the medial entorhinal cortex and hence, are coupled to inputs in stratum lacunosum moleculare (Bragin et al., 1995; Colgin et al., 2009). These inputs are thought to integrate location information into ongoing encoding (Brun et al., 2002, 2008; Colgin et al., 2009; Fyhn et al., 2004; Hafting et al., 2005; Lopes-Dos-Santos et al., 2018). For example, humans performing a virtual MWM task showed that increased high gamma activities has correlated with better performance in the task and, therefore, faster memory formation (Pu et al., 2018). In line with this, also in rats, high gamma power has been selectively and significantly increased during exploration of a novel object in a novel location compared to the familiar one (Zheng et al., 2016).

PHASE PRECESSION

Phase precession describes the action potential firing of an individual neuron relative to the oscillatory activity of the surrounding cells. Since theta activity is synchronized throughout the brain, it is assumed that the occurrence of neuronal activity relative to the theta phase strongly influences its effect on the entire network and the resulting behavior. The phase precession of place cells is probably the most well-known examples of this relationship (O'Keefe and Recce, 1993). O'Keefe and Reece showed that CA1 PCs typically fire at the peak of each theta cycle, called in phase. However, place field related firing is found to be out of phase. The maximum firing rate at the center of the place field is precisely anti-phase to the local theta oscillations, meaning at its trough. This phase precession is considered important for the encoding of spatial information. Thus, the degree of novelty correlates with the theta phase shift and corresponding place cell

remapping (Lever et al., 2010). But also the likelihood of inducing LTP or LTD is dependent on the theta phase (Huerta and Lisman, 1995, 1996; Hyman et al., 2003). Interestingly, low and fast gamma oscillations are likewise phased-locked to the theta cycle (Colgin et al., 2009). This is thought to represent the place and movement path of an animal and to set a behavioral state of the animal that is relevant for decisions (Amemiya and Redish, 2018; Senior et al., 2008). Additionally, the coherence of theta between the hippocampus und the prefrontal cortex can be directly correlated with the behavior outcome. The more strongly both brain regions were synchronized, the better the performance was in behavioral tasks (Benchenane et al., 2010; Gruber et al., 2018).

1.1.8 Differences Along the Longitudinal Axis of the Hippocampus

While the gross organization within the hippocampal formation is remarkably similar, functional differences are found along the longitudinal axis. For example, the frequency of theta oscillations is comparable between the dorsal and ventral hippocampus, however, a phase shift of 180° is observed (Patel et al., 2012). Furthermore, the ventral hippocampus has a reduced number of place cells with wider place fields compared to the dorsal hippocampus (Jung et al., 1994; Kjelstrup et al., 2008; Maurer et al., 2005; Royer et al., 2010). The differential spatial precision correlates with the distinct function and connectivity of the two parts. The dorsal hippocampus is strongly connected to cortical networks while subcortical networks, e.g., amygdala and hypothalamus, are connected to the ventral hippocampus (Groen and Wyss, 1990; Kishi et al., 2006; Moser and Moser, 1998; Siegel and Tassoni, 1971). Accordingly, spatial learning relies heavily on the dorsal hippocampus, while the ventral part is relevant in emotional processing (Bannerman et al., 1999, 2002, 2003b; Hock and Bunsey, 1998; Moser et al., 1993, 1995; Pothuizen et al., 2004). However, this distinction is ambiguous. Rather fine and particular variations in behavioral tasks can cause changes in the relevance of a distinct part of the hippocampus for the task performance. For example, Komorowski et al. (2013) suggested, that the dorsal CA3 allows rapid association within a context while the ventral CA3 mediates more general information across different contexts. As a result, an increased relevance of ventral CA3-CA1 connection during spatial reversal learning has been proposed. During the early training sessions mice often use egocentric learning strategies while spatial reversal learning requires spatial strategies (Shah et al., 2019). In line with these findings, Kleinknecht et al. (2012) found that lesions to the ventral hippocampus selectively disrupt spatial learning strategies, while the dorsal part is involved in general spatial exploratory behavior. The connection between subcortical systems and the hippocampus is thought to regulate the integration of emotional and motivational values to declarative memory. Accordingly, damages to the ventral hippocampus cause a decrease in innate anxiety (Bannerman et al., 2002; Kjelstrup et al., 2002; McHugh et al., 2004; Pentkowski et al., 2006). However, Hunsaker and Kesner (2008) have found an involvement of the dorsal hippocampus in fear-related memory encoding and retrieval. While the ventral CA1 has been involved in the retrieval of contextual fear, the dorsal one has been involved in encoding and retrieval. While further experiments are required to understand the fine, functional distinctions along the longitudinal axis of the hippocampus, the differences are ubiquitous. Accordingly, it is important to take these differences into account when designing and interpreting behavioral tests.

1.2 Dendritic Computations in CA1 Pyramidal Cells

CA1 PCs receive ten thousand of inputs onto their spines throughout their dendritic tree. These inputs arrive via two major input pathways, the Schaffer collaterals and the perforant path. CA1 PCs integrates information from these two distinct inputs and generate output in form of APs. To evoke an AP, the EPSPs need to propagate several hundred micrometers along the dendrites to the soma. Here, the potentials are summed up. If the depolarization is sufficient an AP will be generated at the axon initial segment located at the beginning of the axon close to the soma. However, dendrites do not only create the necessary surface for synaptic input and form the connection to the soma, but their morphology, cable properties and distribution of ion channels can actively shape synaptic integration and thereby influence the output of the CA1 microcircuit.

1.2.1 Dendrites – From Cable to Active Integrator

Wilfried Rall compared dendrites to electrical cables to understand their role in propagation and summation of synaptic input (Rall, 1962). As specified in his model, a neuron can be illustrated by several compartments that are electrically connected through an axial resistance (R_a). Synaptic input can be regarded as a local depolarization caused by the influx and efflux of certain ions. The local difference between the membrane potential (V_m) and the reversal potential (E_{rev}) determines the driving force for each ion to pass the membrane through the opened channels and pores. Together with the synaptic conductance (G_{syn}), the individual driving forces shape the amplitude of the EPSP. The membrane capacitance (C_m) and membrane resistance (R_m) determine how fast the membrane potential can respond to these changes in current, i.e., membrane time constant (τ_m). Owing to the dendritic R_a, EPSPs are attenuated and slowed down during the propagation from the synapse to the soma. This dendritic filtering of input inevitably reduces the influence distal synaptic inputs have on somatic depolarization (Magee and Cook, 2000; Rinzel and Rall, 1974; Spruston, 2008). A reduction dendritic diameter with increasing distance from the soma counteracts the distance-dependent dendritic filtering. Therefore, the impedance (Z_D) increases and causes lager local EPSPs for synaptic input of the same G_{syn} (Jaffe and Carnevale, 1999; Nevian et al., 2007). Taken dendritic branching is taken into account, shunting of the current can be caused by the decrease in R_m. An important parameter that Rall provided is the space constant (λ, Rall, 1964). It describes the length of a dendrite that reduces a potential to 63% of its maximum. The space constant can further be used to describe the stretch of dendrite in which synapses are more likely to interact. Activation of several synapses with in λ results in a strong depolarization, reducing the driving force and, hence, resulting in sublinear summation of input. Dendritic branch points decrease Z_D locally and, therefore, cause a linear integration measured at the soma (Abrahamsson et al., 2012).

However, the contribution of voltage-dependent conductances were not taken into account by Wilfried Rall's model. Large, local depolarization can result in the activation of voltage-gated ion channels and receptors and thereby in- or decrease the local depolarization in amplitude and duration (Cash and Yuste, 1999; Migliore and Shepherd, 2002; Williams and Stuart, 2000). A detailed description of active conductances and how they influence dendritic integration would be beyond the scope of my thesis and can be found elsewhere (for review see Magee, 2016). Briefly, their distribution along the dendritic tree can directly influence and shape the propagation of the depolarization towards or from the soma.

1.2.2 Action Potential Backpropagation

If the depolarization arriving at the soma is sufficient, APs are initiated at the axon initial segment. From there these all-or-nothing events propagate along the axon to innervate other cells. However, APs in CA1 PCs can also propagate back into the dendritic tree. These back propagating APs (bAPs) do not only travel into the apical trunk, but also into basal and apical oblique dendrites and, to a certain extent, even propagate into the apical tuft dendrites (Antic, 2003; Inoue et al., 2001; Spruston et al., 1995; Williams and Stuart, 2000). Locally at the dendrites, the depolarization evoked through bAPs can relieve the magnesium block of NMDA receptors and thus, make the induction of LTP or LTD possible (Song et al., 2000; Stuart et al., 1997). The morphology of the dendritic tree, especially the number of dendritic branch points is a key factor in regulating the spatial spread of bAPs (Larkum et al., 2001; Rall, 1964; Schaefer et al., 2003). Additional, the density of voltage-gated channels and distribution of inhibition plays a role (Hoffman et al., 1997; Lorincz and Nusser, 2010; Magee and Johnston, 1995; Tsubokawa and Ross, 1996). The inactivation of sodium channels in dendrites has been shown to be longer than observed at the soma (Colbert et al., 1997; Jung et al., 1997; Mickus et al., 1999). This increases the failure of dendritic propagation during repetitive stimulation as observed experimentally (Spruston et al., 1995). Accordingly, a firing rate in the beta frequency will result in a persistent decrease of the AP amplitude with increasing spike number (Jung et al., 1997). Counterintuitively, repetitive firing also can enhance back propagation (Short et al., 2017; Williams and Stuart, 2000). This is the result of temporal summation of APs during short, physiological-like bursts at a frequency of 80-300 Hz. In line with the efficiency of propagation, attenuation and/or summation local calcium influxes have been observed (Inoue et al., 2001; Short et al., 2017; Spruston et al., 1995; Williams and Stuart, 2000). Back propagation of APs into a specific dendrite can additionally be enhanced by local synaptic input, increasing the probability of LTP induction and dendritic spike or plateau initiation (Hoffman et al., 1997; Larkum et al., 1999, 2001; Sjöström and Häusser, 2006; Stuart and Häusser, 2001; Takahashi and Magee, 2009; Watabe et al., 2002).

1.2.3 Linear and Supralinear Dendritic Integration in Apical Oblique Dendrites

For the generation of APs, EPSPs and IPSPs are summed temporally and spatially. However, passive propagation to the soma causes a loss of the temporal information by lengthening the response. This is counteracted by conductances that shorten EPSPs. On the other hand, currents that increase the length of EPSPs likewise increase the time interval for summation. In CA1 pyramidal cell basal and apical oblique dendrites synchronous but spatially distributed or smaller subthreshold inputs are typically summed linearly (Figure 1.4 A; Cash and Yuste, 1999). However, under certain circumstances so called dendritic spikes can be evoked (Figure 1.4 B; Gasparini et al., 2004; Losonczy and Magee, 2006; Losonczy et al., 2008; Müller et al., 2012; Remy et al., 2009). These regenerative, all-or-nothing events require synchronous activation of spine clusters on a single dendritic subcompartment. Dendritic spikes have a characteristic time course that is most visible in the first derivative. After a slow initial start of the EPSP, a short-lasting but fast, component is activated. This is followed by another slow component. This time course is directly related to the local conductance. Initially, synaptic conductance through the activation of AMPA receptors and, to a lesser extent, through NMDA receptors and VGCC is taking place. This local depolarization leads to the activation of voltage-gated sodium channels (VGSC), resulting in an all-or-nothing regenerative response that is comparable to an AP. This local depolarization efficiently repels the magnesium ions blocking the channel pore of NMDA receptors. Owing to the slow unbinding of glutamate, influx of sodium and calcium through the receptor can take place. This precisely timed, local recruitment of conductances causes a supralinear summation of the

EPSPs. The increased depolarization leads to the recruitment of additional VGCC. While this increases the local influx of calcium, VGCCs appear not to affect the depolarization at the soma (Losonczy and Magee, 2006). Notably, the same conductances, albeit to a lesser extent, also modulate the subthreshold linear summation of EPSPs. Cash and Yuste (1999) showed that blockade of VGSC, VGCC and NMDA receptors results in sublinear summation of EPSPs. For the occurrence of supralinear integration several requirements need to be fulfilled. Experimentally it was determined that spines need to be activated with an interstimulus interval of less than one millisecond and should not be distributed more than 20 µm from each other (Gasparini et al., 2004; Losonczy and Magee, 2006). These circumstances allow the most efficient recruitment of VGSC and NMDA receptors. Furthermore, proximal dendrites are more likely to display dendritic spikes than distal once. Dendritic spikes are observed at two different strengths, defined by the steep slope of the sodium conductance (Losonczy et al., 2008; Remy et al., 2009). While weak dendritic spikes, which are characterized by a small maximum slope of the sodium channel component, are strongly attenuated in their propagation towards the soma, strong spikes, with a larger maximum slope, are not. Repetitive activation of dendritic spikes increases this attenuation. Interestingly, Losonczy et al. (2008) observed the majority of strong dendritic spikes in the proximal primary dendritic branches. This so-called dendritic branch strength is modulated by Kv4.2 in an acetylcholine-dependent manner. Induction of branch strength plasticity does not only increase the passive propagation but also directly changes the local inhibition, making strong spikes inhibition-resistant (Müller et al., 2012). Accordingly, AP output from weak spikes is evoked by the slow NMDA receptor-dependent peak, leading to imprecisely timed APs (Losonczy et al., 2008). Contrarily, strong dendritic spikes require less synaptic input to evoke an AP and will result in precisely-timed output through the peak of the fast sodium channel component.

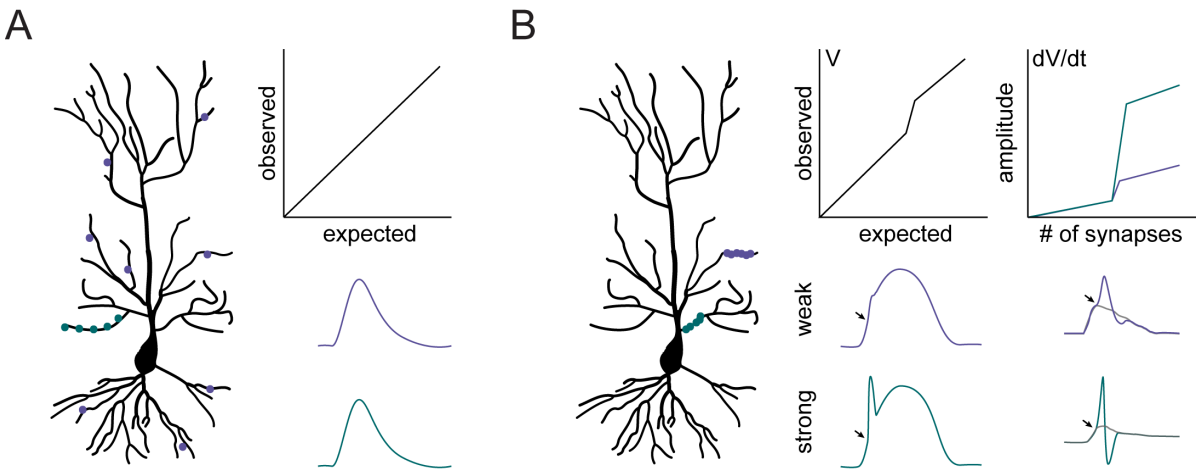

Figure 1.4. Dendrites integrate inputs differentially depending on the spatial and temporal pattern of inputs. (A) Activating synapses spatially distributed over the dendritic tree (purple) or a single dendrite (turquoise) results in a linear summation. Accordingly, the observed depolarization at the soma scales with the expected depolarization from the arithmetic sum of single spine potentials. **(B)** Supralinear integration can be induced when spatially clustered inputs are activated synchronously. Here, a sudden increase in the somatic depolarization (V) in relation to the expected one is observed. The nonlinearity is caused by dendritic spikes. Distal dendrites are more likely to evoke weak dendritic spikes (purple), while strong dendritic spikes are elected predominantly at proximal dendrites (turquoise). The differences in dendritic spike strength is visible in the amplitude of the first derivative of the somatic depolarization (dV/dt). Dendritic spikes cause a steep increase in the amplitude owing to the evoked sodium conductance (start marked by arrow).

1.2.4 Dendritic Plateau Potentials in Apical Tuft Dendrites

Apical tuft dendrites of CA1 PCs can perform nonlinear input integrations as well. Precisely-timed input to both major input pathways, i.e., Schaffer collateral and perforant path, evokes dendrites plateau potentials in the stratum lacunosum moleculare (Figure 1.5; Takahashi and Magee, 2009). Similar plateaus have been observed in pyramidal cells throughout the brain (Pérez-Garci et al., 2006; Schiller et al., 1997). Their activation requires the recruitment of AMPA and NMDA receptors as well as VGCCs (Schiller et al., 1997; Takahashi and Magee, 2009). Their propagation to the soma is usually inhibited by HCN channels (Tsay et al., 2007) and long-lasting inhibition through $GABA_B$ receptors (Pérez-Garci et al., 2006). However, in combination with a depolarization, evoked through AP firing or input through Schaffer collaterals, the propagation probability of plateau potentials to the soma can be increased (Larkum et al., 1999; Takahashi and Magee, 2009). At the soma, these dendritic plateau potentials present a long-lasting after depolarization and are hence, able to cause burst firing of CA1PCs (Magee and Carruth, 1999; Takahashi and Magee, 2009).

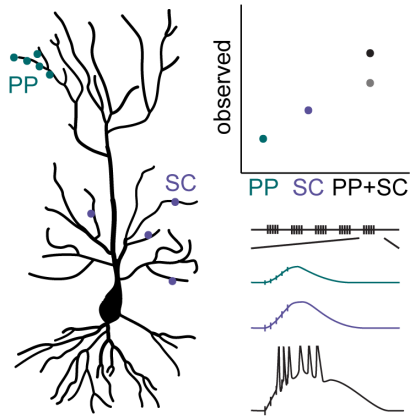

Figure 1.5. Precisely-timed input evokes dendritic plateau potential in apical tuft dendrites. Theta burst pattered, simultaneous activation of perforant path input (PP, turquoise) and Schaffer collateral fibers (SC, purple) evokes dendritic plateau potentials (black) that are characterized by a long-lasting after depolarization and consequently burst firing of action potentials at the soma. The somatic depolarization is larger than expected from summing up the potentials for each pathway (grey).

1.2.5 Dendritic Integration Shapes Learning and Memory

For the occurrence of dendritic spikes and plateaus in vivo, physiological input needs to arrive in a clustered and/or well-timed manner. Several studies have shown, that synapses in vivo are indeed activated and change their strength in small dendritic clustered (Bollmann and Engert, 2009; Fu et al., 2012; Kleindienst et al., 2011; Roth et al., 2020; Takahashi et al., 2012). Likewise, the relative timing of Schaffer collateral and perforant path inputs to each other favors the occurrence of dendritic plateau potentials (Bittner et al., 2015). Accordingly, the presence of regenerative dendritic events in response to physiological stimuli has been demonstrated in different brain regions in vivo (Bittner et al., 2015; Chen et al., 2013b; Cichon and Gan, 2015; Grienberger et al., 2014; Larkum and Zhu, 2002; Lavzin et al., 2012; Palmer et al., 2014; Sheffield and Dombeck, 2015; Sheffield et al., 2017; Waters et al., 2003; Xu et al., 2012). Owing to their large local calcium influxes and the strength in generating AP output, supralinear dendritic integration, like dendritic spikes and plateaus, can influence the neuronal network on different levels. As a result enhanced AP output is observed (Grienberger et al., 2014; Lavzin et al., 2012; Palmer et al.,

2014; Smith et al., 2013). Furthermore, a relevance of nonlinear dendritic integration for visual (Sivyer and Williams, 2013; Smith et al., 2013) and sensory perception (Lavzin et al., 2012; Palmer et al., 2014; Xu et al., 2012) or spatial navigation has been shown (Bittner et al., 2015; Grienberger et al., 2014; Sheffield and Dombeck, 2015; Sheffield et al., 2017). In addition, an increase in strong dendritic spike probability was observed after exposure to an enriched environment (Makara et al., 2009). Overall, these results suggest that dendritic integration of inputs describes a physiologically relevant mechanism in regulating neuronal computation and behavioral output. NMDA receptor activation is crucial for dendritic integration. However, recruitment of these receptors requires the presence of a co-agonist. Thus, supply of D-serine or glycine could influence dendritic integration. Astrocytes are a possible source of the co-agonist D-serine. Accordingly, astrocytes could shape dendritic integration, neuronal output computations and the corresponding behavioral output through dynamic supply of the NMDA receptor co-agonist D-serine. My thesis aims to investigate this hypothesis.

1.3 ASTROCYTES

For a long time neuroglia, or simply glia, were considered as a form of connective tissue keeping the neurons in place (Virchow, 1859). They were therefore named glia after the Greek term for glue and this perception persisted for many years. The diversity of glial cells was discovered using cellular histology, leading to the differentiation between astrocytes, oligodendrocytes and microglia (Kettenmann and Verkhratsky, 2008). Astrocytes received their name because of the star-like morphology (Lenhossék, 1895). Further characterization has led to the differentiation between fibrous, white matter and protoplasmic, gray matter astrocytes (Andriezen, 1893). This section will focus on the characteristics of protoplasmic astrocytes found in the gray matter. Protoplasmic astrocytes are able to release gliotransmitters that have been shown to influence synaptic transmission, neuronal computations and behavior. Hence, astrocytes fulfill an important role in regulating learning and memory.

1.3.1 ASTROCYTE MORPHOLOGY

Astrocytes in the gray matter have a complex morphology (Figure 1.6 A). From their rather small soma several major branches emanate that further arborize into fine and fussy processes resulting in a sponge-like morphology (Bushong et al., 2002; Livet et al., 2007; Ogata and Kosaka, 2002). Each astrocyte occupies its own territory of approximately 66,000 μm^3. Overlap is only found at the boarder of the territory (Figure 1.6 A&B). Interestingly, nearly all astrocytes also contact blood vessels through distinct processes, called endfeet. Furthermore, astrocytes form a large functional syncytium through extensive gap junction coupling (Anders et al., 2014; Giaume et al., 2010; Gutnick et al., 1981; Kuffler, 1967). Nevertheless, astrocytes are not a homogenous group of cells (for review see Khakh and Deneen, 2019; Khakh and Sofroniew, 2015). For instance, the presence of the glial fibrillary acidic protein (GFAP) has long been considered a robust molecular marker for astrocytes. However, some astrocytes do not express GFAP in sufficient amounts to be detectable by immunohistochemistry (Walz and Lang, 1998). Moreover, GFAP levels can vary substantially between brain regions (Batiuk et al., 2020; Chai et al., 2017; Emsley and Macklis, 2006). Accordingly, further molecular differences between regions have been identified (Batiuk et al., 2020; Boisvert et al., 2018; Chai et al., 2017; Degen et al., 2012; Duran et al., 2019; Gokce et al., 2016; Lin et al., 2017; Morel et al., 2017, 2019; Zeisel et al., 2015). More than that astrocytes are a morphologically and functionally diverse group. In the CA1 stratum radiatum, astrocytes have an elongated shape orientated perpendicular to the pyramidal cell layer (Anders et al., 2014; Bushong et al., 2002; Nixdorf-Bergweiler et al., 1994; Wallraff et al., 2006). Astrocytic gap junction coupling is found to be organized anisotropic, too (Anders et al., 2014). Astrocytes in the CA1 stratum lacunosum moleculare are more densely-packed and round in shape (Nixdorf-Bergweiler et al., 1994; Ogata and Kosaka, 2002; Shimada et al., 1992; Wallraff et al., 2006). Accordingly, their territories tend to be smaller, than in the other layers of the CA1 (Ogata and Kosaka, 2002). Similarly, micro vessels are more dense in the stratum lacunosum moleculare, suggesting a correlation between astrocyte and micro vessels number (Shimada et al., 1992). Recently, molecular differences between stratum radiatum and lacunosum moleculare astrocytes have been identified (Batiuk et al., 2020).

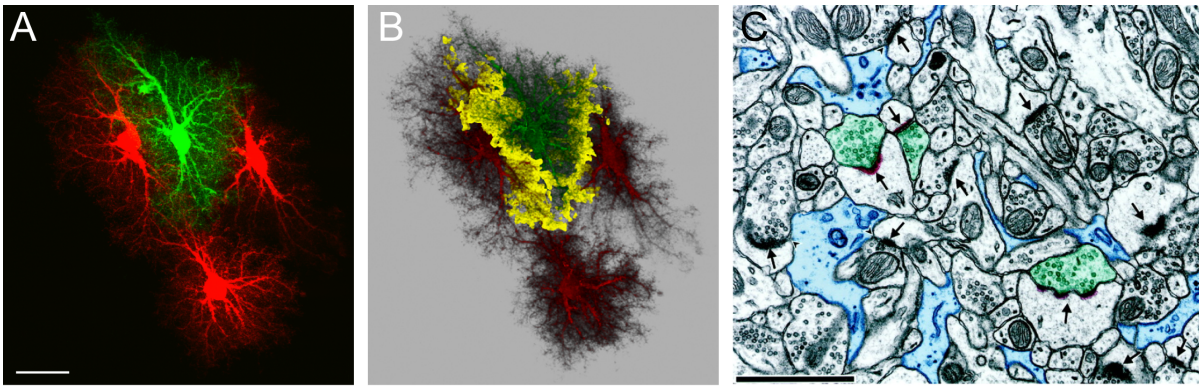

Figure 1.6. Astrocyte morphology. (A) The image shows four astrocytes in the CA1 stratum radiatum filled with fluorescent dyes illustrating their nonoverlapping territory (scale bar: 20 µm). **(B)** 3D reconstruction of a Z-stack of the same astrocytes as in (A). The yellow area marks the overlap between the green and red dye: ~5 % of the territory. **(C)** Electron microscopy image of the stratum radiatum. Arrows mark the postsynaptic density (dense black area) and the green coloring the presynapse containing small microvesicles. Astrocytes (blue) are in close contact with spines (scale bar: 1 µm). *Images in A&B are from Cell Image Library (CIL) Dataset CCDB:28 (Bushong et al., 1999). Image in C is from Ventura and Harris, (1999) – copyright 1999 Society for Neuroscience.*

1.3.2 Astrocytic Functions in a Neuronal Network

Because of their electrically-passive nature, it was long thought that astrocytes were mainly fulfilling supportive roles for neurons (Kuffler, 1967). They have been shown to be an important regulator of ion homeostasis, pH and osmolarity (Kettenmann and Ransom, 2013). For example, the extracellular concentration of potassium is regulated through clearing and buffering by astrocytes (Figure 1.7). Another important task of astrocytes is the metabolic support for neurons and the regulation of blood flow. Through their end feet located on small capillary vessels they participate in the blood brain barrier, take up glucose and can influence the local blood flow. Glucose is then transferred with aid of the lactate shuttle to neurons. However, more and more studies have demonstrated also an active participation in synaptic transmission. Since their fine processes are in close proximity to neuronal synapses (Gavrilov et al., 2018; Ventura and Harris, 1999; Wolff, 1968), they can locally influence synaptic transmission. There, astrocytes clear the released glutamate from the synaptic cleft (Figure 1.7; Danbolt, 2001). By determining the spatial and temporal extent synaptic transmission and plasticity is shaped. Furthermore, fine astrocytic processes show fluctuations in the intracellular calcium concentration (Agarwal et al., 2017; Asada et al., 2015; Di Castro et al., 2011; Kanemaru et al., 2014; Shigetomi et al., 2010, 2013a). These calcium transient can occur spontaneously (Gee et al., 2014; Nett et al., 2002), as response to neuronal activity (Porter and McCarthy, 1996; Wang et al., 2006) or as calcium waves spreading through the astrocytic territory (Cornell-Bell et al., 1990; Dani et al., 1992; Hirase et al., 2004; Newman and Zahs, 1997; Nimmerjahn et al., 2004). Neurons in turn respond with changes in activity to changes in astrocytic calcium (Nedergaard, 1994; Parpura et al., 1994). This effect is likely caused by the release of gliotransmitters (Figure 1.7). Although astrocytes are not electrically excitable, changes in their intracellular calcium concentration and the subsequent release of gliotransmitter suggests that there are excitable in a different manner. Accordingly, reciprocal signaling between neurons and astrocytes can be an important regulator of synaptic transmission and plasticity. Hence, astrocytes are nowadays considered as an active partner in the tripartite synapse (Araque et al., 1999; Perea et al., 2009). This section will focus on the astrocytic regulation of synaptic transmission through glutamate clearance and calcium-dependent release of gliotransmitters.

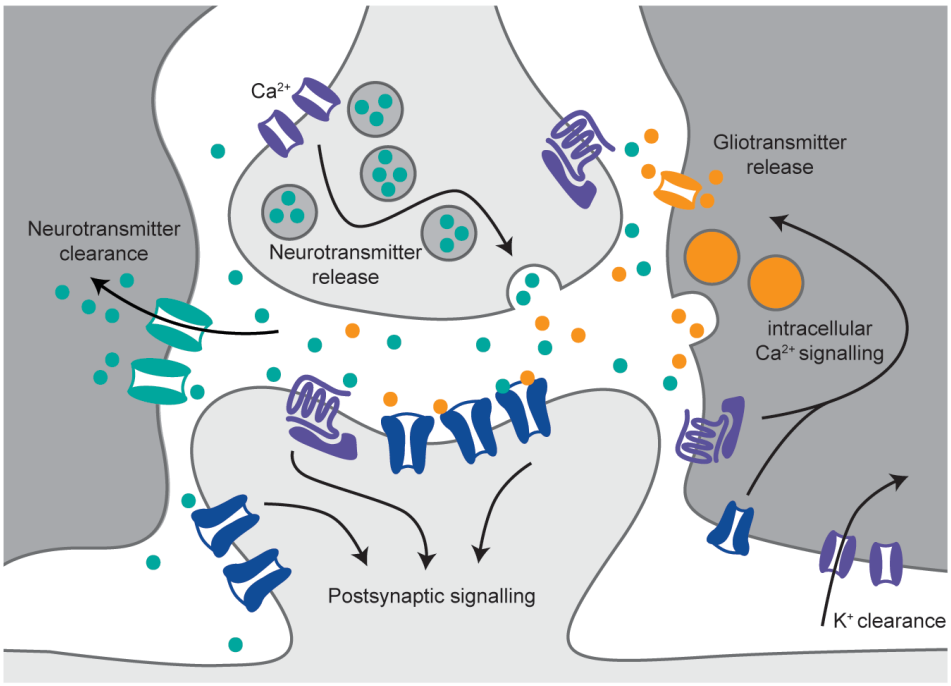

Figure 1.7. Illustration of astrocyte functions at the synapse. Astrocytes fulfill several functions in supporting and mediating neuronal signal transduction. Neurotransmitters (turquoise) released by the presynaptic terminal (upper light gray part) propagate to the postsynapse (lower light gray part) evoking a change in potential. Astrocytes (dark gray) control the magnitude of this signaling by neurotransmitter clearance. Additional, neurotransmitters can activate astrocytic ionotropic or metabotropic receptors causing an increase in the intracellular calcium concentration. This in turn evokes the release of gliotransmitters (orange). Following release, the gliotransmitters can activate pre- or postsynaptically located receptors and modulate neuronal signaling. Moreover, neuronal activation increases extracellular potassium. Astrocytes regulate neuronal excitation by clearance of it.

1.3.3 The Role of Astrocytes in Glutamate Clearance

While neurons express a small number of glutamate transporters (Holmseth et al., 2012), the majority of glutamate clearance is performed by astrocytes (Danbolt, 2001). Through expression of the glutamate transporter type 1 (GLT1 or EAAT2) and the glutamate aspartate transporter (GLAST or EAAT 1) astrocytes take up approximately 90 % of the total glutamate (Bergles and Jahr, 1997; Danbolt, 2001; Danbolt et al., 1992, 2016; Holmseth et al., 2012; Kiryk et al., 2008; Lehre et al., 1995; Matsugami et al., 2006). Glutamate uptake requires the co-transport of sodium (Danbolt, 2001). Hence, the sodium gradient established by Na^+/K^+-ATPases regulates the efficiency of glutamate clearance from the synapse (Rose et al., 2009). Different cortical regions display distinct glutamate uptake properties (Romanos et al., 2019). The functional impact of these is more pronounced during an increased glutamate load, evoked through high frequency stimulation. Likely this differential uptake ability is modulated by Na^+/K^+-ATPases. This suggests that glutamate uptake regulates the susceptibility to pathologies. Accordingly, a decreased expression of Na^+/K^+-ATPases has been shown to facilitates the initiation of cortical spreading depression (Capuani et al., 2016) and promotes the recruitment of NMDA receptors (Romanos et al., 2020). Excessive extracellular glutamate is observed in many pathologies, e.g., epilepsy (Albrecht and Zielińska, 2017; Findley et al., 2019). Impairing glutamate uptake increased the extracellular glutamate and induced excitotoxicity (Rothstein et al., 1996). The activation of extrasynaptic NMDA receptors is directly regulated by glutamate clearance (Asztely et al., 1997; Diamond, 2001; Moldavski et al., 2020; Mulholland et al., 2008) and an increased tonic activation of these receptors causes cell death (Hardingham et al., 2002).

However, glutamate clearance has been shown to regulate not only cell survival but also synaptic transmission. Ambient glutamate levels in the hippocampus are usually low, leading only to small tonic NMDA receptor currents (Angulo et al., 2004; Cavelier and Attwell, 2005; Meur et al., 2007; Sah et al., 1989). Blocking the glutamate transporters, however, considerably increases these tonic currents. It is postulated that these tonic currents modulate neuronal input/output functions (Sah et al., 1989). One possible mechanism of this effect is through an increased recruitment of perisynaptically-located mGluRs in interneurons (Huang et al., 2004). As a consequence, an increase in interneuron excitability and inhibition of CA1 PCs is evoked.

Impaired glutamate uptake has been shown to change NMDA receptor recruitment and consequently an enhance short- and impair long-term potentiation (Barnes et al., 2020; Katagiri et al., 2001). In addition, glutamate clearance also regulates the activation of neighboring synapses and spines (Arnth-Jensen et al., 2002; Barbour and Häusser, 1997; Scimemi et al., 2004). Specifically extrasynaptic NMDA receptor recruitment is increased by an enhanced concentration of ambient glutamate (Fleming et al., 2011; Meur et al., 2007; Moldavski et al., 2020) or glutamate spillover from neighboring synapses (Kullmann et al., 1999; Rusakov and Kullmann, 1998). In turn increased recruitment of extrasynaptic receptors has been implicated in enhancing LTP (Yang et al., 2017), LTD (Massey et al., 2004; Yang et al., 2005) and the occurrence of dendritic NMDA receptor spikes (Chalifoux and Carter, 2011). However, synaptic transmission does not only depend on glutamate clearance but can also shape it. Increased diffusion of GLT1 is observed as response to neuronal activity (Al Awabdh et al., 2016; Murphy-Royal et al., 2015). Impairing this diffusion leads to prolonged dwell time of synaptic glutamate and subsequent decreased kinetics of EPSPs. Slowing of glutamate uptake is observed in response to increased frequencies of neuronal activity (Armbruster et al., 2016). Interestingly, the late-phase of LTP results in an increase of glutamate uptake evoked through protein synthesis and expression of GLT1 in astrocytes (Pita-Almenar et al., 2006, 2012).

Especially the fine astrocytic perisynaptic processes (PAPs) are particularly enriched in glutamate transporters (Sakers et al., 2017). Hence, proximity of astrocyte processes has been shown to be an important regulator of glutamate clearance in other brain regions by regulating the activation of presynaptic glutamate receptors (Oliet et al., 2001). Furthermore, induction of neuronal plasticity induces changes in the PAPs in the somatosensory cortex (Perez-Alvarez et al., 2014). In the hippocampus, a retraction of astrocytic processes from the synapse facilitates glutamate spillover and NMDA receptor recruitment during burst stimulation (Tanaka et al., 2013). This decreased glutamate clearance also results in an impaired spatial reference memory and contextual fear memory. Also hippocampal LTP is accompanied by structural changes in the synapse and adjacent glial cells (Bernardinelli et al., 2014; Lushnikova et al., 2009). Inducing structural remodeling at the neuropil, by activation of PAR1 on astrocytes, leads to changes in glutamate clearance as well as short- and long-term plasticity (Sweeney et al., 2017). Similarly, connexin 30 has been identified to regulate the morphology of PAPs and accordingly is found to affect hippocampal long-term plasticity and learning (Pannasch et al., 2014). In line with a plasticity-dependent regulation of astrocyte spine coverage is that thin spines in the dentate gyrus are preferentially in contact with astrocytes (Medvedev et al., 2014). Interestingly, in the CA1 region only half of the glutamatergic spines have been identified to have an astrocytic process in close proximity (Ventura and Harris, 1999). Whether this is caused by spine size-dependent regulation of astrocyte coverage is so far unknown. However, it suggests the intriguing possibility of differential synaptic transmission depending on the spine size by the strength of local,

astrocytic glutamate uptake. Accordingly, glutamate spillover and recruitment of synaptic, extrasynaptic or presynaptic NMDA receptors or mGluRs might be regulated in a spine size dependent manner. This could result in a differential probably of these spines to undergo certain short and long-term plastic changes or regulate the probability of evoking dendritic spikes. This thesis explores the hypothesis of spine-size-dependent glutamate clearance and spine-size-dependent dendritic integration in the CA1 microcircuit.

1.3.4 Astrocytic Calcium Transients

Astrocytic calcium changes are observed as a response to various neurotransmitters and modulator, e.g. acetylcholine, ATP, endocannabinoids, GABA or glutamate (for review see Guerra-Gomes et al., 2018; Perea et al., 2009). Increases in intracellular calcium concentration can be observed in small microdomains throughout the astrocyte territory (Agarwal et al., 2017; Asada et al., 2015; Di Castro et al., 2011; Kanemaru et al., 2014; Shigetomi et al., 2010, 2013a), with the most occurring in the small processes (Asada et al., 2015; Shigetomi et al., 2013a). Using 3D super-resolution microscopy, a recent study has suggested that single spines are targeted by small, node-like astrocytic structures that exhibit calcium transients (Arizono et al., 2020). Notably, calcium transients in these nodes appear to be synapse-specific and the majority of them does not propagate to neighboring spines. Since membrane permeable calcium indicators, e.g. Fluo-4-AM, were and are frequently used to study astrocytic calcium transients, their frequency is often underestimated. Bulk-loading targets only 10% of the astrocytic territory (Reeves et al., 2011), and hence, selectively underestimates transients occurring in the periphery (Shigetomi et al., 2013a). Using genetically encoded calcium indicators, a frequency of up to two calcium events per minute is suggested (Gee et al., 2014; Shigetomi et al., 2013a). Although the source of these intrinsic fluctuations are still under debate, the basic properties of the possibly underlying mechanisms are understood (for review see Bazargani and Attwell, 2016; Berridge et al., 2003). An important role in mediating astrocytic calcium is been suggested for the endoplasmatic reticulum. Calcium entry from the extracellular space leads to activation of inositol triphosphate (IP3) receptors and, possibly, ryanodine receptors and sequentially the release of more calcium. Accordingly, pharmacological inhibition of store-operated calcium release reduces the amplitude and/or frequency of calcium transients in astrocytes (Araque et al., 1998a; Arizono et al., 2020; Henneberger et al., 2010; Jennings et al., 2017; Jourdain et al., 2007; Kang et al., 1998; Okubo et al., 2020; Vaarmann et al., 2010). Mice with a selective knock-out of the IP3 receptor in astrocytes are shown to have a strong reduction in frequency and/or amplitude of calcium transients (Agarwal et al., 2017; Fiacco et al., 2007; Kanemaru et al., 2014; Li, 2005; Petravicz et al., 2008; Sherwood et al., 2017; Srinivasan et al., 2015). However, some have failed to show a change of the frequency and/or amplitude, specifically in the fine astrocytic processes (Rungta et al., 2016; Srinivasan et al., 2015). Recently, also mitochondria have been suggested to play a role in the regulation of calcium transients in astrocytic microdomains (Agarwal et al., 2017).

Increases in the intracellular calcium concentration of astrocytes can be evoked through numerous mechanisms that cause the influx of extracellular calcium and/or from intracellular stores (Verkhratsky et al., 2012). The extracellular calcium concentration correlates proportionally with the frequency of spontaneous astrocytic calcium transients (Shigetomi et al., 2012; Wu et al., 2019). On the other hand, increasing the extracellular calcium concentration could increase their frequency (Parri and Crunelli, 2003). Interestingly, increasing the intracellular calcium buffering capacity results in a similar result. Modelling suggests that these effects are modulated by the formation of IP3 (Lavrentovich and Hemkin, 2008). However, IP3

receptor activation does not only depend on IP3, but is modulated by the cytosolic calcium concentration (Foskett et al., 2007; Hituri and Linne, 2013). IP3 receptors show a bell-shaped dependency on the calcium concentration inside the cell. While low intracellular calcium concentrations increase their open probability, high concentrations inhibit the receptor. Astrocytes have been shown to have varying resting calcium concentrations, resulting in two distinct groups (Zheng et al., 2015). This suggests that the probability of IP3 receptor opening and thus the frequency of spontaneous calcium transients between these cells vary. TRPA1 is implicated in the regulation of the resting calcium concentration in astrocytes (Shigetomi et al., 2012, 2013b). Next to a 40 % decrease of the basal calcium concentration, application of a TRPA1 channel blocker results in a nearly complete block of spontaneous calcium transients. Furthermore, it is found that the reduction in calcium transients resulted in a reduced extracellular D-serine concentration (Shigetomi et al., 2013b). This suggests an interesting relationship between the astrocytic resting calcium concentration and the release of gliotransmitters. In addition, modelling the characteristics of astrocytic calcium transients in dependency of the intracellular calcium concentration suggests a regulation of the peak calcium concentration by the former (Lavrentovich and Hemkin, 2008). To my knowledge, this relationship has not yet been confirmed experimentally. In general, the parameters that are shaping astrocytic calcium transients are poorly understood. Nevertheless, their role in mediating the release of gliotransmitters and the subsequent modulation of synaptic transmission underlines their importance. Knowing the parameters that control astrocytic calcium transients might advance our understanding of their role in gliotransmitter release and synaptic transmission. An exciting question, which is addressed by my thesis, is the involvement of the resting calcium concentration in shaping astrocytic calcium transients.

1.3.5 Gliotransmitter Release

Many studies have shown that calcium transients evoke the release of gliotransmitters, e.g., glutamate, ATP/adenosine and D-serine. Albeit some studies have failed to show this dependency (for review and discussion on the controversy see: Bazargani and Attwell, 2016; Rusakov et al., 2014), the release of gliotransmitters by astrocytes is generally accepted. It is postulated that gliotransmitters are released through small vesicles, similar to those observed in neurons. But other pathways, as reversed transport have been suggested as well. The investigation and presence of the underlying release mechanisms has been a topic of numerous studies that are summarized and discussed elsewhere (Bohmbach et al., 2018; Petrelli and Bezzi, 2016; Verkhratsky et al., 2016). In the following sections I laid the focus on two gliotransmitters, glutamate and D-serine, which are known regulators of NMDA receptors. Accordingly, astrocytic release of these compounds can modulate dendritic integration.

Glutamate

One of the earliest described and best studied gliotransmitters is glutamate (Bezzi et al., 2004; Hua et al., 2004; Innocenti et al., 2000; Jeremic et al., 2001; Montana et al., 2004; Parpura et al., 1994; Pasti et al., 2001). Parpura and Haydon (2000) investigated the calcium concentration required for the release of astrocytic glutamate in cultured astrocytes. They showed that even small increases of 55 nM in the intracellular calcium concentration are sufficient to cause gliotransmission. Similar to neurons, a cooperative binding of calcium ions to evoke release has been shown in astrocytes (Kreft et al., 2004; Parpura and Haydon, 2000). Araque et al. (1998) observed in co-cultures that astrocytic glutamate evokes NMDA receptor-dependent slow

depolarizing inward currents (SICs) in neighboring neurons. It should be noted that cultured astrocytes show an altered morphology and expression of proteins and receptors. Conclusions should therefore be drawn carefully from these studies. Importantly, glutamate release from astrocytes and SICs are also observed in situ (Angulo et al., 2004; Fellin et al., 2004; Kang et al., 2005; Mariotti et al., 2016; Navarrete and Araque, 2008; Parri et al., 2001; Perea and Araque, 2005). Furthermore, it has been shown that SICs are evoked by extrasynaptic GluN2B-containing NMDA receptors (D'Ascenzo et al., 2007; Fellin et al., 2004; Shigetomi et al., 2008) through store-dependent increase of astrocytic calcium and SNARE-dependent vesicular release of glutamate (Kang et al., 2005; Mariotti et al., 2016). Notably, these studies were mostly conducted in slice preparations from juvenile rodents or in different brain regions. The observation of SICs in the hippocampus of adult mice requires specific pharmacological interventions like blocking potassium conductance, decreasing synaptic transmission or increasing NMDA receptor recruitment (Angulo et al., 2004; Gómez-Gonzalo et al., 2017; Perea and Araque, 2005). While SICs are mediated by postsynaptic receptors, also the activation of presynaptic mGluRs and NMDA receptors has been reported (Min and Nevian, 2012; Navarrete and Araque, 2010; Navarrete et al., 2012; Perea and Araque, 2007). Similar to SICs, glutamate is thought to be released through calcium-dependent vesicular fusion. Targeting presynaptic receptors, glutamate mediates the presynaptic release probability and induction of LTP. Notably, other studies have failed to evoke SICs or changes in synaptic transmission after inducing astrocytic calcium transients through various methods (Agulhon et al., 2010; Fiacco et al., 2007). Both studies used expression of exogenous receptors or uncaging of exogenous compounds to evoke astrocytic calcium transients. Therefore, it is possible that these are not coupled to the same release machinery as endogenously evoked transients. Accordingly, using the same technique a recent study showed that designer drug activated receptors do not effect plasticity induction in wild type mice but selectively in a genetically modified mouse model with impaired astrocyte calcium signaling (Huang et al., 2020). Furthermore, astrocytic glutamate release has been proposed to be mediated by BEST1 and TREK 1 channels (Oh et al., 2012; Park et al., 2013; Woo et al., 2012, 2018). Nevertheless, a functional relevance of astrocytic, calcium-dependent glutamate release in vivo is described (Navarrete et al., 2012; Poskanzer and Yuste, 2016). Jourdain et al. (2007) showed that in the molecular layer of the dentate gyrus astrocyte processes contain small microvesicles, located close to extrasynaptic GluN2B-containing NMDA receptors. Accordingly, activity-dependent activation of P2Y1 receptors causes the release of glutamate from astrocytes and results in an increase in synaptic strength. The structural and functional evidence suggests that astrocytic glutamate release is occurring under physiological conditions in the dentate gyrus. Whether SICs are recruited under physiological or pathophysiological conditions needs to be determined. Since an increased occurrence is observed in an Alzheimer's mouse model (Gómez-Gonzalo et al., 2017), the latter is suggested.

D-SERINE

Another interesting gliotransmitter is D-serine. Because NMDA receptor activation requires the presence of a co-agonist, astrocytes can regulate NMDA receptor recruitment, and thus LTP and LTD, through the release of the co-agonist D-serine. The first evidence for astrocytic D-serine release has been found through staining and using astrocyte cultures (Schell et al., 1995, 1997). Moreover, serine racemase, the enzyme catalyzing the transformation of L-serine to D-serine, has been found primarily in astrocytes (Wolosker et al., 1999). Mothet et al. (2005) showed that astrocytic D-serine release is depending on intracellular, store-dependent calcium increases.

Using electron microscopy, D-serine has been shown to be located in small microvesicles together with elements of the release machinery in culture (Martineau et al., 2013) and in adult astrocytes in the hippocampus (Bergersen et al., 2012). Functional evidence on a potential role of astrocytic D-serine release derives from mixed cultures (Yang et al., 2003). While LTP could not be induced in pure neuronal cultures, it has been possible in mixed ones. The authors identified that D-serine release is responsible for the observed effect. D-serine is also able to modulate plasticity in acute brain slice. In situ experiments by Henneberger et al. (2010) showed that the induction of LTP in the CA1 of the hippocampus depends on D-serine. By interfering with astrocytic calcium increases, astrocytic D-serine production or the vesicular release machinery the induction of LTP has been impaired, providing strong evidence for astrocytic, calcium-dependent, vesicular release of D-serine. A more recent study showed the involvement of IP3 receptors in the release of D-serine in the hippocampus (Sherwood et al., 2017). Likewise, LTP induction in vivo is depending on astrocytic D-serine release (Robin et al., 2018). Recently it was even suggested that the astrocytic release of D-serine alone, without neuronal depolarization or high frequency stimulation, is sufficient to induce LTP (Adamsky et al., 2018). The importance of astrocytic calcium and D-serine for LTP is further supported by the fact that a decrease in the resting calcium concentration also impairs LTP induction (Shigetomi et al., 2013b). Recently, a dependence of the intrahippocampal D-serine concentration in situ and in vivo and wakefulness has been discovered (Papouin et al., 2017). Increased general activity results in a higher extracellular D-serine concentration, a process depending on acetylcholine-mediated astrocytic calcium increase and subsequent release of the co-agonist. Consequently, LTP induction is favored during the dark, active phase. Moreover, vesicular D-serine release from astrocytes is described in other brain regions. In the dentate gyrus, vesicular release of D-serine by astrocytes is regulating the dendritic maturation of adult born neurons (Sultan et al., 2015). In the supraoptic nucleus of the hypothalamus astrocytic coverage and hence, co-agonist availability, determines the NMDA receptor recruitment and consequently, LTP induction (Panatier et al., 2006). Through regulation of the synaptic D-serine concentration, astrocytes modulate the activity threshold for LTP induction between virgin and lactating rats. Albeit the large amount of functional and morphological evidence suggesting astrocytic release of D-serine, the Wolosker laboratory proposed that neuronal release through Asc-1 could be the major source of D-serine (Kartvelishvily et al., 2006; Rosenberg et al., 2010, 2013; see for review Wolosker et al., 2016).

1.3.6 Behavioral Relevance of Gliotransmission

Similar to the evidence in vitro and in situ, contradicting results concerning the behaviors modulated by reciprocal signaling between neurons and astrocytes have been found (for review see Oliveira et al., 2015). Especially in the context of hippocampus-dependent spatial memory, various effects of selective interruption or activation of astrocyte signal transmission have been observed.

One way to disrupt gliotransmission in astrocytes is through the expression of a dominant negative (dn)SNARE protein. While this has not impacted the performance of undisturbed animals in a novel object and an object location memory tasks, it has been sufficient to prohibit the effects of sleep deprivation on the memory performance (Halassa et al., 2009). However, another study showed that impairment of the same pathway through expression of the tetanus toxin has resulted in an impaired performance (Lee et al., 2014). Similar results have been obtained in mice lacking the cannabinoid 1 (CB1) receptor specifically in astrocytes (Robin et al., 2018). Furthermore, astrocytic CB1 receptors have been shown to disinhibit exogenously-evoked

impairment of spatial working memory in the MWM (Han et al., 2012). Overexpression of serine racemase and consequently an increase in D-serine, however, has not impaired long-term spatial memory examined with the same task (Otte et al., 2013). Similarly, a lack of the IP3 receptor 2 has neither impaired long-term memory nor reversal learning examined with the MWM (Petravicz et al., 2014). However, using an IP3 'sponge' to disrupt astrocyte calcium signaling has resulted in impaired MWM long-term memory (Tanaka et al., 2013). Interestingly, activating or deactivating G_s-coupled activation of astrocytes has evoked a reduction or enhancement, respectively (Orr et al., 2015). Also concerning contextual fear conditioning varying results have been obtained. While expression of a dominant negative SNARE protein has not affected the memory performance (Halassa et al., 2009), Papouin et al. (2017) showed that daily fluctuations of vesicular-released D-serine from astrocytes can. Similarly, artificial activation of astrocytic Gq-dependent signaling during learning has increased contextual fear memory (Adamsky et al., 2018). While overall these results demonstrate that astrocytic gliotransmission potently modulates hippocampal memory performance, the discrepancy between studies highlights the complexity of the underlying mechanism and the need for careful examination. It is important to ensure that, for example, genetic alterations are inducible to avoid developmental adaptations. Furthermore, subtitle differences in the behavioral design are known to influence the required brain regions (for example the dorsal or ventral hippocampus, see 1.1.8) and different astrocytic signaling can underlie the observed effect. Furthermore, daily fluctuations in the extracellular D-serine concentration can influence learning and memory as well. Accordingly, behavioral experiments with a careful design and/or a location specific astrocytic alteration will make conclusions more specific. In addition, any genetic or pharmacological intervention should be examined for effects on exploratory or anxiety-related behavior as these are common confounders for behavioral testing.

1.3.7 Astrocytic Endocannabinoid Receptors

While most research focused on unraveling the function of the endocannabinoid system with a neuron-centric view, recent investigations have shown that also astrocytes express CB1 receptors (Bonilla-Del Río et al., 2019; Gutiérrez-Rodríguez et al., 2018; Han et al., 2012; Navarrete and Araque, 2008). Electron microscopy has revealed that between 35-55 % of CA1 stratum radiatum astrocytes show CB1 receptor staining, with nearly all receptors being located within 400-1200 nm of a synapse (Bonilla-Del Río et al., 2019; Gutiérrez-Rodríguez et al., 2018; Han et al., 2012). Similar to neuronal CB1 receptors, astrocytic ones have been described to be activated in response to high-frequency stimulation of Schaffer collaterals or depolarization of CA1 pyramidal cells in rodents, in situ and in vivo, and in human tissue (Andrade-Talavera et al., 2016; Navarrete and Araque, 2008, 2010; Navarrete et al., 2013; Robin et al., 2018), whereas the mobilization is positively regulated by the length of the depolarization or the number of APs (Navarrete and Araque, 2008, 2010). Moreover, the activation of astrocytic CB1 receptors has led to an increase in the overall intracellular calcium and/or an increase of the calcium transient frequency in astrocytes (Gómez-Gonzalo et al., 2015; Navarrete and Araque, 2008, 2010; Navarrete et al., 2013; Robin et al., 2018). The efflux of calcium from intracellular stores has been required for this effect. While these recordings were performed with cell membrane permeable dyes, Eva M. Schönhense has confirmed the effect in whole-cell patch clamp recordings from astrocytes filled with the fluorescent indicators Fluo-4 and Alexa Fluor 594 in our laboratory (Figure 1.8). Application of the CB1 receptor co-agonist WIN55,212-2 has evoked a significant increase in the ratio of both fluorescent indicators. In the presence of the inverse agonist AM251, no change has been observed. This shows that indeed CB1 receptors are responsible for the

increase in intracellular calcium. Furthermore, the number of astrocytes that have shown an increase in the fluorescent ratio have been quantified. Under control conditions approximately 80 % of the astrocytes have responded to bath application of the CB1 receptor agonist. These have been significantly more, than observed in AM251. Importantly, the number of (non)responding astrocytes observed in our laboratory is in line with the findings of others (Navarrete and Araque, 2008).

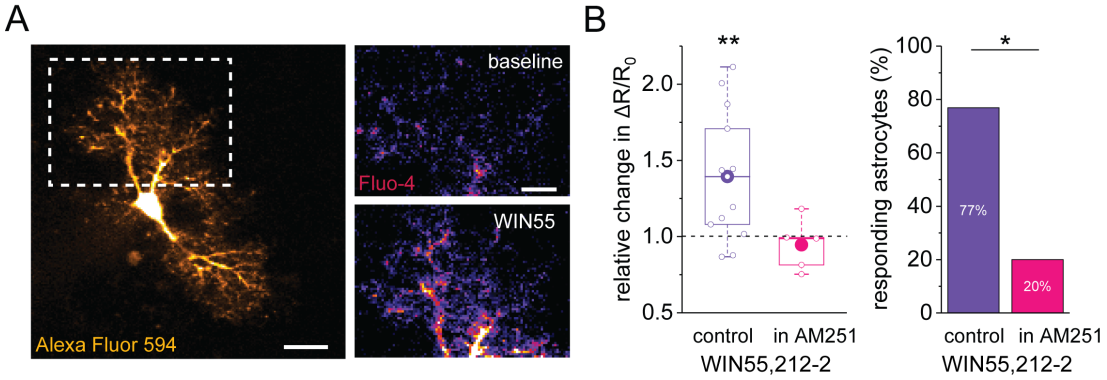

Figure 1.8. Activation of CB1 receptors increases astrocytic Ca^{2+}. (A) Left: Example of an astrocyte filled with Alexa Fluor 594 (40 µM) and Fluo-4 (200-400 µM) via the whole-cell patch-clamp pipette (scale bar: 10 µm). Right: Sum of Fluo-4 fluorescence intensity over 10 frames (scale bar: 5µm) during baseline and after application of the CB1 receptor agonist WIN55,212-2 (10 µM) for the marked area marked on the left. **(B)** Changes in astrocytic calcium concentration were monitored through the fluorescence ratio of Alexa Fluor 594 and Fluo-4 (background-subtracted). Left: WIN55,212-2 significantly increased the fluorescence ratio (1.39 ± 0.12, n = 13, p = 0.005, one-population Student's t-test). In the presence of the inverse CB1 receptor agonist AM251 (5 µM), the effect was absent (0.95 ± 0.08, n = 5, one-population Student's t-test). Right: A significantly smaller number of astrocytes responded (increase > 5%) to application of WIN55,212-2 in the presence of AM251 than without (p = 0.047, Fisher's exact test). *Figure adapted from the Master thesis of E.M. Schönhense (2015) with permission.*

Since CB1 receptors are coupled to $G_{i/o}$ in neurons, the increase in astrocytic calcium is a surprising result. Usually $G_{i/o}$-coupled GPCRs do not increase calcium. However, it has been suggested that the downstream effectors of the CB1 receptor are cell-type specific (reviewed by Stella, 2010). Support for a G_q-dependent mechanisms has been found in cultured hippocampal neurons and HEK cells, where the agonist WIN55,212-2 has been shown to enable $G_{q/11}$-dependent calcium release from internal calcium stores (Lauckner et al., 2005). Furthermore, Navarrete and Araque (2010) showed that astrocytic calcium increase through CB1 receptors is pertussis toxin resistant. Activation of store-dependent calcium release in astrocytes has likewise been described for other compounds signaling through $G_{i/o}$-coupled receptors, however, those have been modulated by the $G_{\beta\gamma}$-subunit of the receptor (Durkee et al., 2019). Regardless of the intracellular mechanism, an increase of the cytosolic calcium concentration in astrocytes evokes the release of gliotransmitters. Astrocytic CB1 receptor activation in the hippocampus is proposed to result in the release of glutamate (Gómez-Gonzalo et al., 2015; Han et al., 2012; Navarrete and Araque, 2008, 2010; Navarrete et al., 2013) or D-serine (Andrade-Talavera et al., 2016; Robin et al., 2018). Accordingly, astrocytic CB1 receptors are implicated in short- and also in long-term plasticity of synaptic transmission. Navarrete and Araque (2010) observed that a depolarization of five seconds or a train of somatic-evoked APs in a CA1 pyramidal cell in situ results in a transient increase or decrease of the synaptic release probability in a subset of recordings, respectively. Interestingly, both forms are mediated by CB1 receptors, however only the potentiation requires an increase in astrocytic calcium. Subsequent release of glutamate is

shown to activate presynaptic mGluRs and thereby, transiently modulating the presynaptic release probability. The same signaling cascade has been demonstrated to modulate long-term plasticity as well. Gómez-Gonzalo et al. (2015) depolarized one neuron to -30 mV for three minutes and another to 0 mV for five seconds to evoke plasticity. This pairing protocol has evoked endocannabinoid-dependent LTP at more distant synapses through astrocytic glutamate release. In contrast, iLTD is usually observed only within a few micrometers (Chevaleyre and Castillo, 2004). In juvenile mice, astrocytic CB1 receptors have also been shown to mediate LTD. Using a post-before-presynaptic activation pairing protocol, Andrade-Talavera et al. (2016) induced a form of LTD that required endocannabinoid mobilization, astrocytic calcium signaling and subsequent release of D-serine. Through activation of presynaptic NMDA receptors, the presynaptic release probability has been altered resulting in a long-term depression of synaptic transmission. Notably, all these experiments were conducted in situ. Owing to the specific induction paradigms that often required a prolonged artificial depolarization of neurons, the relevance in vivo needs to be determined. However, the general role of astrocytic CB1 receptors has been investigated in vivo. Han et al. (2012) showed that endocannabinoid-mediated iLTD is preserved in glutamatergic or GABAergic CB1 receptor knock-out mice in vivo, but impaired in astrocyte-specific knock-out mice. Furthermore, they showed that the exogenous cannabinoid THC increases the magnitude of long-term depression in slices and results in an impaired spatial memory in mice. Importantly, the behavioral impairment is specifically mediated by astrocytic CB1 receptors. Hence, Han et al. has suggested that astrocytes are a key regulator in the endocannabinoid mediated long-term plasticity and spatial memory. The results of Robin et al. (2018) support these hypotheses by showing that astrocyte-specific CB1 receptor knock-out mice exhibit impaired LTP in vivo that can be restored by the application of exogenous D-serine.

Overall, these data support the theory that astrocytic CB1 receptors are a powerful mediator of synaptic transmission in the hippocampus. By increasing the frequency of astrocytic calcium transients, the release of gliotransmitters is evoked. This in turn modulate the recruitment of NMDA receptor, which changes synaptic transmission on a short- and long-term time scale. However, alterations of memory performance have only been described after application of an exogenous cannabinoid. In addition, strong induction protocols were used to induce the mobilization of endocannabinoids from neurons. These protocols question the relevance of the described mechanisms under physiological conditions. To address the physiological relevance of astrocytic CB1 receptor activation, my thesis investigated neuronal activity patterns, which mimic behavioral relevant oscillations, in their potency to modulate NMDA receptor recruitment. Specifically, I determined the influence of CB1 receptor-dependent astrocytic D-serine release on supralinear dendritic integration as well as spatial learning and memory.

1.4 AIMS AND OBJECTIVES

The main function of neuronal networks is to integrate inputs in order to generate meaningful output. Dendrites, as the main input receiving structure, participate in this function. They act as a coincidence detector for local activation, a process that is believed to play an important role in spatial navigation (Bittner et al., 2015; Sheffield and Dombeck, 2015; Sheffield et al., 2017). NMDA receptor activation is shown to be crucial for dendritic integration (Cash and Yuste, 1999; Losonczy and Magee, 2006). Notably, the NMDA receptor is a coincidence detector itself: It requires the presynaptic release of glutamate, postsynaptic depolarization and the binding of a co-agonist, glycine or D-serine (Ascher and Nowak, 1988; Johnson and Ascher, 1987). The main goal of this thesis is to understand if and how NMDA receptor recruitment during dendritic integration is shaped by astrocytes and its behavioral relevance. To address this, the following aims and objective were formulated:

1) To understand how dendritic integration can be shaped by astrocytes.

In order to investigate dendritic integration, a suitable technique to activate small clusters of spines is required. To this end, I first established the use of microiontophoretic stimulation with glutamate in acute hippocampal slices. Then, different forms of dendritic integration were investigated by using a combination of whole-cell patch clamp recordings, microiontophoretic stimulation, electrical stimulation, two-photon excitation microscopy and pharmacological interventions in the CA1 microcircuit of the hippocampus to test the following hypotheses:

a. Astrocytic glutamate uptake is differentially regulated at spines of different size and thereby modulates dendritic integration.

   In order to study the functional impact of differential glutamate uptake, I measured the effect of pharmacological blockade of the uptake on the NMDA receptor-mediated calcium responses of single spines. Relative changes in dependence of the spine size addressed this hypothesis. Furthermore, it is known that spine enlargement caused by long-term potentiation occurs in clusters (Kleindienst et al., 2011; Takahashi et al., 2012). Therefore, I determined whether the size of spines influenced the way inputs were integrated in the respective dendrite.

b. D-serine release through activation of astrocytic CB1 receptors and the subsequent increase in astrocytic calcium modulates dendritic integration.

   NMDA receptor recruitment is essential for the different types of dendritic integration and hence, a possible modulation by its co-agonist D-serine is suggested. I used pharmacological blockade of NMDA receptors and the saturation of their co-agonist site to determine the range of a possible dynamic modification of linear and supralinear dendritic integration of apical oblique dendrites as well as dendritic plateau potentials in apical tuft dendrites. Since the pharmacological activation of astrocytic CB1 receptors evokes astrocytic calcium transients (Navarrete and Araque, 2008; Schönhense, 2015), and possibly, the release of D-serine (Robin et al., 2018), I determined whether pharmacological activation of these receptors can influence dendritic integration through the NMDA receptor co-agonist binding site.

c. Endocannabinoids-dependent activation of astrocytic CB1 receptors takes place during behaviorally relevant network activities.

   Endocannabinoids are released in dependence of neuronal depolarization and/or increases in calcium (Di Marzo, 2011). I investigated the extent of neuronal activity required to recruit astrocytic CB1 receptor-dependent signaling. Therefore, the effect the depolarization of a single neuron and the recruitment of several neurons has on dendritic integration was determined. For the latter, I retrogradely stimulated CA1 pyramidal cells at patterns that resemble delta, theta, beta and gamma oscillations. Combining these recordings with pharmacological interventions permitted me to draw conclusions about the involvement of CB1 receptors and the identity of the released co-agonist. Finally, a mouse line with an inducible, astrocyte-specific knock-out of the receptor was used to establish that astrocytic CB1 receptors mediated the observed effects

2) To understand during which behavior signaling through astrocytic CB1 receptors is recruited, and thus, modulation of dendritic integration can take place.

Mice with an inducible, astrocyte-specific knock-out of CB1 receptors were subjected to several behavioral tests to explore their role in spatial learning and memory. Specifically, the role of astrocytic CB1 receptors in general exploratory and anxiety-related behavior, spatial working memory as well as long-term object identity and location memory was examined. In addition, a passive place avoidance task was used to test the role of astrocytic CB1 receptors in fear-related spatial memory and its flexibility during changes in the environment.

3) To investigate the role of the intracellular resting calcium concentration in shaping astrocytic calcium transients

Astrocytic calcium transients are the key step in regulating neuronal transmission through, for example, endocannabinoids. However, parameters that shape astrocytic calcium transients are unknown. The resting calcium concentration is an interesting candidate for this, as it could shape the influx of calcium (Foskett et al., 2007; Lavrentovich and Hemkin, 2008). The expression of a calcium-sensitive fluorescent protein in astrocytes was used to record spontaneous astrocytic calcium transients in situ and in vivo. The relationship between the pre-event baseline and the peak or the amplitude calcium concentration of each transient was analyzed. To unravel the underlying mechanisms, the role extracellular and intracellular, store-dependent calcium influx play in shaping astrocytic calcium transients was determined.

2 MATERIAL AND METHODS

2.1 ANIMALS

All animals were housed under twelve-hour light/dark conditions and were allowed ad libitum access to food and water. For the experiments, either three to five weeks old male Wistar rats (Charles River Laboratories) or six to ten weeks old male wild type (Charles River Laboratories) and/or transgenic (own breeding) C57BL/6N mice from both genders were used. All experiments were conducted in full compliance with national and institutional guidelines.

2.1.1 TRANSGENIC ANIMALS

To induce a cell-type specific knock-out or knock-in of a gene, the cre-lox recombination system was used. In this model, the target gene (or a part of it) is flanked by two loxP sequences ("floxed"). Only when the cre-recombinase is present within the nucleus, it recognizes the two LoxP sequences and removes the sequence in between. Therefore, in the $CB1^{f/f}$ line (Table 1), the cannabinoid 1 (CB1) receptor gene is removed upon cre presence in the nucleus and a cell type specific knock-out can be generated. In the mouse lines Ai14 (Table 1) and PC-G5-tdT (Table 1) a stop codon in front of tdTomato or GCaMP5g-IRES-tdTomato, respectively, is floxed. Therefore, the indicators are expressed selectively. Cell-type specific promoters are used to express cre. This can be either done ubiquitously or, to avoid developmental influences, upon injection of tamoxifen. The GLAST-cre ER and creERT2 mouse (Table 1) expresses a modified estrogen receptor (ER or ERT2, higher affinity for tamoxifen than estrogen) dependent on the Slc1a3 (GLAST, EAAT1) promoter, a protein selectively expressed by astrocytes. By using different combinations of these transgenic mouse lines or stereotactic injections with recombinant adeno-associated viruses (rAAV), the generation of astrocyte or neuron-specific knock-in or knock-out is possible.

Table 1. Transgenic mice strains, their background and reference.

Short name	Long name	Background	Reference
GLAST-creERT2	$Slc1a3^{tm1(cre/ERT2)Mgoe}$	C57BL/6N	(Mori et al., 2006)
GLAST-creER	Tg(Slc1a3-cre/ERT)1Nat	C57BL/6J	(Wang et al., 2012b) JAX Mice 012586
Ai14	$Gt(ROSA)26Sor^{tm14(CAG-tdTomato)Hze}$	C57BL/6J	(Madisen et al., 2010) JAX Mice 007908
PC-G5-tdT	$Polr2a^{Tn(pb-CAG-GCaMP5g,-tdTomato)Tvrd}$	C57BL/6N	(Gee et al., 2014) JAX Mice 024477
$CB1^{f/f}$		C57BL/6N	(Marsicano et al., 2003)

2.1.2 TAMOXIFEN TREATMENT

To induce the expression of cre in GLAST-cre ER(T2) mice, the administration of tamoxifen is required. For this purpose, 20 mg tamoxifen (Sigma) were dissolved in 1 ml sunflower oil (Sigma) containing 10 % ethanol (AppliChem) by sonication for at least 15 minutes. To activate cre activity, the mice were injected with 1.5 mg of tamoxifen once daily for five consecutive days by intraperitoneal (i.p.) injections. After at least two weeks of recovery, the animals were used for experiments.

2.1.3 STEREOTACTIC INJECTIONS OF RAAVS

A rAAV containing cre under a Ca^{2+}/calmodulin-dependent protein kinase II promotor fragment of 0.4 kb (CaMKII0.4; AAV1.CaMKII0.4Cre.SV40, V4567MI-R, PennCore) was injected bilaterally into the ventral hippocampus of PC-G5-tdT mice to selectively express the calcium indicator GCaMP5g in CA1 pyramidal cells (PCs).

First, the animals were deeply anesthetized (Fentanyl, Rotexmedica, 0.05 mg/kg bodyweight; Midazolam, Rotexmedica, 5.0 mg/kg bodyweight; Medetomidin, Cepitor from CPPharma, 0.5 mg/kg bodyweight; i.p. injection volume 0.1 ml/10 g bodyweight). The eyes were then covered with a cream (Bepanthen® eye and nose crème) and the head fur was shaved off. After ensuring that the animal was asleep by checking the toe reflexes, the head was fixed in a stereotactic frame (Model 901, David Kopf Instruments). Before making a small incision, the skin was locally anaesthetized with lidocain (1 x 10 mg puff, Xylocain, Astra Zeneca). As landmark for the injection, the intersections of the skull sutures bregma and lamda were used. Those areas are particularly visible when the skull is cleared from remaining periosteum and dried. By comparing the height of bregma and lamda it can be ensured that the skull was fixed levelled (<0.2 mm difference in height). Next, the coordinates for the ventral hippocampus were determined relative to bregma (anterior -3.5 mm, lateral -/+3 mm, ventral -2.5 mm). After marking the point of injection with a surgical marker, a small hole was drilled with a dental drill and the beveled needle nanosyringe (nanofil 34G BVLD, WPI) was slowly inserted into the brain. Then, 0.5 µl of viral particles (2.94×10^{13} VP/ml) dissolved in PBS were injected slowly under the control of a microinjection pump (100 nl/min, WPI). After a recovery period of at least five minutes, the needle was retracted slowly, and the procedure repeated for the other hemisphere. At the end of the surgery, the incision was sutured using antibacterial absorbable thread (Ethicon) and treated with an antibiotic cream (Refobacin 1 mg/g, Gentamicin). Then, the anesthesia was stopped by i.p. injection of the corresponding antagonists (Naloxon, Puren, 1.2 mg/kg bodyweight; Flumazenil, Anexate from Hikma, 0.5 mg/kg bodyweight, Atipamezol, Antisedan from Ventoquinol, 2.5 mg/kg bodyweight; injection volume 0.1 ml/10 g bodyweight). To ensure that the animal had no pain, analgesia was injected i.p. 30 minutes before ending the narcosis as well as 8, 16 and 24 hours afterwards (Buprenorphin, Buprenovet from Bayer, 0.05 mg/kg bodyweight; injection volume 0.1 ml/20g bodyweight). Experiments with these animals were conducted three to five weeks after surgery.

2.2 Acute Hippocampal Slice Preparation

For the preparation of acute brain slices the animal were deeply anesthetized with isoflurane (Consense), decapitated and their brain was quickly removed and placed into ice-cold $aCSF_{sucrose}$ (artificial cerebrospinal fluid, containing in mM: sucrose 105, NaCl 60, KCl 2.5, $MgCl_2$ 7, NaH_2PO_4 1.25, ascorbic acid 1.3, sodium pyruvate 3, $NaHCO_3$ 26, $CaCl_2$ 0.5 and glucose 10; osmolarity 300-310 mOsm). Next, forebrain and cerebellum were removed, hemispheres separated and the dorsal part trimmed before gluing it onto the slicing block. With a vibratome (7000SMZ-2, Campden Instruments) 300 µm thick horizontal slices were cut and left for recovery in 34°C warm $aCSF_{sucrose}$ for 15 minutes before transferring them to normal aCSF (containing in mM: NaCl 131, KCl 2.5, $MgSO_4$ 1.3, NaH_2PO_4 1.25, $NaHCO_3$ 21, $CaCl_2$ 2 and glucose 10; pH 7.35-7.45; osmolarity 297-303 mOsm) at room temperature. There the slices were allowed to recover for at least one hour before starting the experiments. All chemicals, unless stated otherwise, were obtained from AppliChem.

2.3 Electrophysiological Measurements in Combination with Two-Photon Excitation Fluorescence Imaging

2.3.1 Whole-Cell Patch Clamp Recordings

For recordings, the slices were transferred into a submersion-type recording chamber mounted on a Scientifica two-photon excitation fluorescence microscope with a 40x/0.8 NA objective or 60x/1 NA objective (Olympus), placed onto a self-built grid and superfused with 34° C warm aCSF. A single CA1 PC was whole-cell patched using a Multiclamp 700B amplifier (Molecular Devices) with a borosilicated glass pipette (3-5 MΩ resistance, GB150F-10, Science Products) containing an intracellular solution (containing in mM: KCH_3O_3S 135, HEPES 10, di-Tris-Phosphocreatine 10, $MgCl_2$ 4, Na_2-ATP 4, Na-GTP 0.4, Alexa Fluor 594 hydrazide 0.04 (Thermo Fisher Scientific), Fluo-4 pentapotassium salt 0.2-0.4 (Thermo Fisher Scientific), pH adjusted to 7.2 using KOH, osmolarity 290-295 mOsm). Cells were kept in the current clamp mode, unless stated otherwise. Data acquisition was performed using Clampex (Axon Software). Data were filtered with a humbug (filtering of electrical interference, Quest Scientific, Canada), low-pass Bessel filter and digitized at 40 kHz. Using a femtosecond Ti:sapphire pulse laser Vision S (Coherent, US) with the laser power adjusted to a fluorescent intensity comparable to the one obtained with a power of 2-3 mW at the slice surface, both fluorescent dyes were excited at λ = 800 nm. The emitted photons were collected and recorded using photon multiplier tubes (Scientifica) depending on the filters at either λ_{green} = 500-550 nm or λ_{red} = 590-650 nm. The light-microscopic morphology was visualized with Dodt optics. Acquisition of the images was performed using ScanImage Software (Pologruto et al., 2003) using MATLAB (MathWorks).

Electrophysiological recordings were analyzed using Clampfit (Axon Software). The analysis of imaged was performed with Fiji/Image J (NIH) and Matlab. Numerical data were analyzed with Excel (Microsoft), OriginPro (Origin Lab Corporation) and Matlab.

2.3.2 Synaptic and Local Dendritic Potentials

CA1 PCs were distinguished from other cells in the stratum pyramidale mainly by their morphology (apical trunk dendrite and spines) and their membrane potential (app. -70 mV). Only cells with an access resistance (R_a) of less than 20 MΩ and with less than 20 % change during the time course of the recording were included in the analysis.

To evoke local dendritic potentials a microiontophoretic system (MVCS-C-01C-150, NPI) was used. A borosilicated glass pipette (60-90 MΩ resistance, GB150F-10, Science Products), filled with 150 mM glutamic acid (pH adjusted to 7.0 with NaOH) and 50 µM Alexa Fluor 594 hydrazide (Thermo Fisher Scientific), was placed in close proximity (< 1 µm) to a spine on an apical oblique dendrite under the control of two-photon excitation fluorescent microscopy. Leakage of glutamic acid from the microiontophoresis evokes either weak somatic depolarization, noise-like variations in the membrane potential or a local increase in the Fluo-4 intensity. To prevent such leakage a small, positive retain current (< 8 nA) was constantly applied. The iontophoretic stimulation duration was adjusted (< 0.8 ms) to induce reliable somatic excitatory postsynaptic potentials (EPSPs), dendritic spikes and action potentials (APs) with increasing stimulation intensity (25 to 50 pA steps until the occurrence of an AP, 3 s interstimulus interval). All experiments were conducted in the presence of 50 µM picrotoxin (abcam Biochemicals), to block $GABA_A$ receptors, therefore, the CA3 and CA1 region were separated before starting the experiment. After recording the dendritic integration at baseline with increasing iontophoretic stimulation intensities, a drug was bath-applied for three to five minutes and the integration recorded again. In a subset of experiments, baseline recordings were performed in the presence of a drug as indicated. In case of experiments with DAAO (D-amino acid oxidase, Sigma), the slices were incubated for at least 50 minutes in the enzyme before the start of the recording. The following drugs at the respective concentrations were used: 5 µM AM251 (abcam), 0.17 U/ml DAAO (Sigma), 50 µM D-APV (abcam), 10 µM D-serine (Sigma), 10 µM NBQX (abcam), 0.5 µM Ro 25-6981 (abcam), 1 µM WIN55,212-2 mesylate (Sigma), 10 µM ZD7288 (Tocris).

For the analysis of the somatic membrane potentials several parameters were compared between the baseline recording and the one after drug application to determine the respective influence of drug:

- The first somatic potential with clear kinetic of an EPSP was considered as a purely AMPA receptor mediated response (Figure 2.1 A, black). This response will be called initial EPSP (iEPSP) from here on forth. iEPSPs are considered comparable to single spine EPSPs recorded with other techniques. The amplitude of iEPSPs were compared.
- The last three EPSPs prior to the induction of AP firing (linear integration) or the last EPSP prior to a dendritic spike (supralinear integration; Figure 2.1 A, purple) are called subthreshold EPSPs from here forth. Subthreshold EPSP are large amplitude EPSP evoked by stimulating multiple spines. Hence, NMDA receptors and voltage-gated channels will contribute to their potential. The amplitude of subthreshold EPSPs were compared.
- In dendrites that integrate their inputs supralinear dendritic spikes were evoked (Figure 2.1 A, turquoise trace). To determine the effect of the applied drug on dendritic spikes, three distinct parameters were used. The first one is the microiontophoretic stimulation intensity necessary to evoke a dendritic spike, henceforth called threshold stimulus. The microiontophoretic current corresponds to the amount of glutamate ejected from the microiontophoresis and, therefore, illustrates the synaptic activation required to evoke a

dendritic spike. The second parameter indicates the recruitment of voltage-gated sodium channels during the spikelet of the dendritic spike (Figure 2.1 B, turquoise). To calculate this, the first derivative of the last EPSP prior to the first dendritic spike was subtracted from the latter. The peak amplitude of this trace (Figure 2.1 C) make measuring the maximum slope of the sodium spikelet without influence by the underlying EPSP possible. The third analyzed parameter corresponds to the recruitment of NMDA receptors during dendritic spikes. For this the amplitude of the slow component of the dendritic spikes was used (Figure 2.1 B, purple), henceforth called NMDA receptor component amplitude.

All comparisons were made by averaging two recordings. Notably, the amplitudes of somatic potentials were always compared between responses that were evoked with the same microiontophoretic stimulation intensity. This means that similar amounts of glutamate were ejected to stimulate the dendrite.

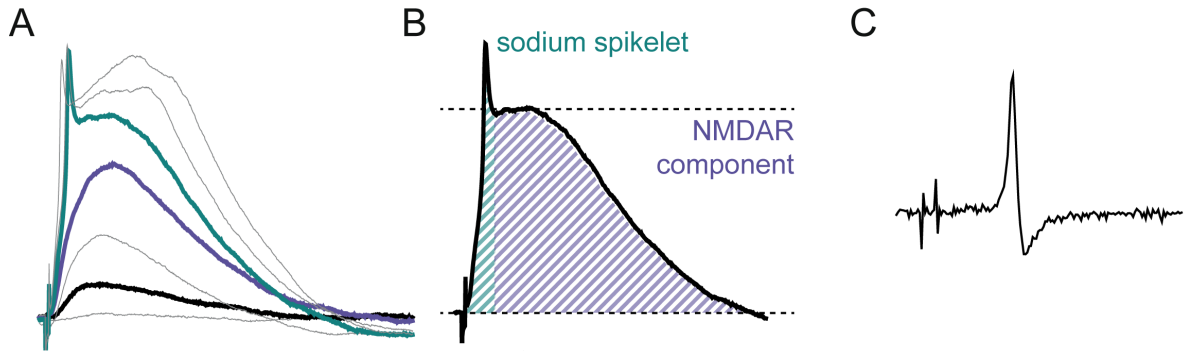

Figure 2.1. Illustration of dendritic integration analysis. (A) Iontophoretic stimulation with increasing stimulation intensities evokes iEPSP (black), subthreshold EPSP (purple) and dendritic spikes (turquoise). **(B)** Dendritic spikes have two main components: a fast sodium spikelet (turquoise) and slow component mediated, among others, by NMDA receptors (purple). The amplitude of the NMDA receptor component is illustrated by dashed lines. **(C)** First derivative of a dendritic spike subtracted by the first derivative of the subthreshold EPSP. The peak amplitude is the maximum slope of the sodium spikelet.

During whole-cell patch clamp recordings the neurons were filled with Alexa Fluor 594 (40 µM). After the electrophysiological recording a stack of the dye fluorescence of the dendritic segment with the iontophoresis (512 x 512 pixel, 15-33 µm^2, z distance 0.5-1 µm) and the cell itself (512 x 512 pixel, 150-330 µm^2, z distance 1-2 µm) was taken. The former images were used to determine the relative spine size. With Fiji/Image J, regions of interest (ROIs) were then placed around the spines with a size of 0.65 x 0.65 µm. For each ROI the intensity was plotted along the z-axis, the background was subtracted and the intensity was normalized to the baseline. This curve was then fitted with a Gaussian using OriginPro and the integral was taken as the spine size. To calculate the relative size of the stimulated spine, the median of 5 to 15 spine sizes was calculated and then compared to the initial spine. Spines with a size above one were considered big and spines with a size below one were considered small.

2.3.3 NMDA Receptor-Mediated Responses

NMDA receptor responses were recorded using either Scientifica two-photon excitation fluorescence microscope with a 40x/0.8 NA objective or 60x/1 NA objective or Olympus FV10MP microscope with a 25x/1.05NA objective (Olympus). A CA1 PC was whole-cell patched and filled with the calcium-insensitive indicator Alexa Fluor 594 (40 µM) and the calcium-sensitive indicator Fluo-4 (200 µM) as described (see section 2.3.1). The microiontophoretic system was used for local stimulation. Therefore, the iontophoresis pipette filled with glutamic acid (150 mM, pH adjusted to 7.0 with NaOH) and Alexa Fluor 594 (50 µM) or 633 (50 µM) was placed in proximity to an apical oblique dendrite (~4 µm) to stimulate several spines at the same time. For the isolation of NMDA receptor responses the membrane potential of the CA1 PC was clamped to -20 mV and the aCSF contained 1 µM Tetrodotoxin (TTX, Na^+ channel blocker, Tocris), 20 µM nifedipin (L-type calcium channel blocker, Sigma), 20 µM LY341495 (group II metabotropic glutamate receptor antagonist, Tocris), 10 µM MPEP hydrochloride ($mGluR_5$ antagonist, abcam) and 10 µM NBQX (AMPA receptor antagonist, abcam). Glutamate uptake was blocked through bath-application of 200 nM TFB-TBOA (EAAT1 and EAAT2 blocker, Tocris) for at least eight minutes. Line scanning through up to six spines (~ 400 Hz) was performed in quadruplets with an inter-event interval of 30 ms during baseline and after application of aCSF (control), TFB-TBOA or APV (50 µM). Using a femtosecond Ti:sapphire pulse laser Vision S (Coherent, US) with the laser power adjusted as described, both fluorescent dyes were excited at λ = 800 nm. The emitted photons were collected and recorded using photon multiplier tubes depending on the setup and filters at either λ_{green} = 500-550 nm or 515-560 nm and λ_{red} = 590-650 nm or 575-630 nm. Acquisition of the images was performed using ScanImage Software using MATLAB or Olympus Fluoview 4.2. Analysis was performed using Fiji/Image J and Excel. The intensity profiles over time for each indicator were averaged for every spine and corrected for the corresponding background intensity. Then, the ratio of the Fluo-4 and Alexa Fluor 594 fluorescence was calculated. The pre-event baseline (R_0), the peak (R_{max}), the baseline normalized amplitude $\Delta R/R_0$ and the decay time constant were analyzed. For the analysis of the decay constant, the ratio was fitted with a mono exponential decay using OriginPro. Spine sizes were calculated as described in section 2.3.2.

2.3.4 Alveus Stimulation

Antidromic activation of CA1 PCs can be achieved through stimulation of their axons in the alveus. To ensure selective axonal stimulation, an incision was made between CA1 and the subiculum that spares the alveus. A clustered bipolar stimulation electrode (CE2F75, FHC) was placed on the subiculum site of the incision while a field-recording pipette (borosilicated glass, 2-4 MΩ resistance, GB150F-10, Science Products) filled with aCSF was positioned in app. 500 µm distance at the boarder of stratum oriens and stratum pyramidale of CA1. For the analysis of the population spike, recorded in the stratum pyramidale, the amplitude ($A_{popspike}$) is a good measure for the recruitment of PCs. It is calculated by using the EPSP (A_1), population spike (A_2) and hyperpolarization amplitude (A_3, Figure 2.2).

The stimulation intensity was adjusted to 80 % of maximum amplitude of the population spike, with a minimum amplitude of 0.8 mV. The experiments were conducted in the presence of 50 µM picrotoxin.

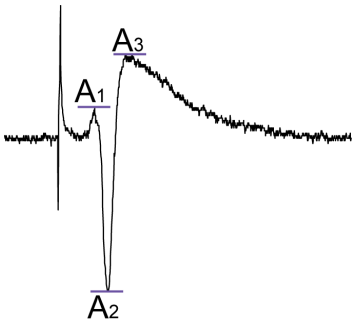

Figure 2.2. Illustration of a population spike. The amplitude of the excitatory post-synaptic potential (A1), population spike (A2) and hyperpolarization (A3) are illustrated.

If alveus stimulation was combined with recordings of dendritic integration, the field-recording pipette was removed and a CA1 PC was whole-cell patched in the same area (±70 µm) and dendritic potentials were evoked using the microiontophoretic system, as described before. Instead of drug application, the alveus was stimulated at different frequencies (4, 10, 20 or 40 Hz) for one second, five seconds before the iontophoretic stimulation with an interstimulus interval of ten seconds. Analysis was performed as described in section 2.3.2.

2.3.5 Neuronal Recruitment during Alveus Stimulation

To determine the amount of responding CA1 PCs, mice expressing the calcium indicator GCaMP5g together with tdTomato under control of the CaMKII promoter were generated by injecting PC-G5-tdT mice with a CaMKII-cre rAAV (see section 2.1.3). Slices were prepared and mounted on an Olympus FV10MP microscope with a 25x/1.05NA objective. The electrodes for alveus stimulation were placed (see section 2.3.4). Using a femtosecond Ti:sapphire pulse laser Vision S (Coherent, US) with the laser power adjusted as described, the fluorescent proteins were excited at 910 nm. The light-microscopic morphology was visualized with differential interfering contrast (DIC) optics (Olympus). To record the response of several PCs to 20 Hz alveus stimulation for one second, emitted photons were collected using photon multiplier tubes during line scannning through two to six somas at either λ_{green} = 515-560 nm or λ_{red} = 575-630 nm, depending on the filters. Acquisition of the images was performed using Olympus Fluoview 4.2. Recordings were performed in quadruplets and averaged for analysis (~2 ms per line, 1500 lines). Per slice at least 16 cells were recorded to estimate the overall percentage of responding cells. For analysis of the intensity profile over time for both indicators was corrected for background and the fluorescence ratio was calculated. The signal was then normalized to the baseline and reported as $\Delta R/R_0$. Neurons were classified as responder and nonresponders to alveus stimulation by an arbitrary threshold (>25 % increase in amplitude).

2.3.6 Extracellular Single Unit Recording

Extracellular single unit recordings allowed me monitoring of single CA1 PC firing. To investigate this during alveus stimulation, the stimulation electrode was placed in the alveus and the stimulation intensity determined, as described. Next, a borosilicate glass pipette (5-7 MΩ resistance, GB150F-10, Science Products) was placed into the PC layer during 10 Hz alveus stimulation to blindly identify single unit responses. These responses are characterized by a sharp upward reflection followed by a smaller downward reflection. The amplitude should exceed 2 mV and should not differ between several trials. Within a burst, however, the amplitude

might decrease. Recordings at 4, 10 and 40 Hz alveus stimulation were done in quadruplets. A maximum of three single unit recordings per slice were performed. For the analysis, the single unit response relative to the number of stimuli was determined and averaged over the recording trials.

2.3.7 Astrocytic Calcium Imaging using Genetically-Encoded Indicators in situ

PC-G5-tdT mice were crossbred with GLAST-creERT2 mice and injected with tamoxifen as described (see section 2.1). Acute hippocampal slices were prepared and mounted on the Scientifica two-photon excitation fluorescence microscope with a 40x/0.8 NA objective or 60x/1 NA objective (Olympus) or Olympus FV10MP microscope with a 25x/1.05NA objective. Using a femtosecond Ti:sapphire pulse laser Vision S (Coherent, US) with the laser power adjusted as described, both fluorescent proteins were excited at λ = 910 nm. The emitted photons were collected and recorded using photon multiplier tubes depending on the setup and filters at either λ_{green} = 500-550 nm or 515-560 nm and λ_{red} = 590-650 nm or 575-630 nm. Acquisition of the images was performed using ScanImage Software using MATLAB or Olympus Fluoview 4.2. Astrocytes in the CA1 stratum radiatum in 40-90 µm depth with a good distinguishable territory were identified using their tdTomato fluorescence. Only cells with a low somatic GCaMP5g intensity were used since this should correspond to low intracellular calcium and hence, to healthy cells. The astrocyte was then recorded using time-lapse frame scanning (128 x 128 pixel, 80 x 80 µm, 2.96 Hz). Spontaneous calcium transients were recorded in collaboration with Daniel Minge for ten to twenty minutes in normal aCSF, in aCSF with the IP3 receptor inhibitor 2-Aminoethoxydiphenyl borate (2-APB, 100 µM, abcam) and ryanodine (10 µM, abcam) or in aCSF without calcium (zero calcium). For the stimulation of the alveus, I positioned the electrodes as described in section 2.3.4. Changes in astrocytic calcium were recorded by imaging astrocytes during baseline and 10 Hz or 40 Hz alveus stimulation (18x for 1 s, 10 s inter-stimulus interval) for three minutes each.

The analysis of all astrocytic recordings was performed by me. Before starting the analysis, the frames were z-aligned using a custom-written Matlab script (Christian Henneberger). Then, calcium responses were visually identified using Fiji/Image J and a ROI of ~ 3 x 3 µm was placed around them. The fluorescence ratio of both indicators, GCaMP5g and tdTomato, background-subtracted; was calculated per frame. For all responses of one cell or field of view the pre-event baseline (R_0), peak (R_{max}) and amplitude (R_{max}-R_0) were determined by averaging three frames. When a cell displayed at least eight calcium responses the relationship between baseline and peak or amplitude was determined using a nonparametric, unbiased approach by calculating the x-y dependency with Spearman's rank correlation coefficient (R). Owing to the nonlinear correlation between the calcium concentration and the fluorescence intensity of GCaMP5g the correlation coefficients obtained for baseline and amplitude needed to be corrected by subtracting 0.38 (for detailed explanation, see section 3.1 and King*, Bohmbach* et al., 2020).

Additionally, the frequency of calcium transients per cell was determined. Astrocytic calcium events are not very frequent (1-2 per minute, Gee et al., 2014) and therefore their frequency can vary a lot between cells. For the frequency analysis only cells with at least one transient in each condition were used. In some cases, the astrocytes were sorted into responders and nonresponders. A cell that showed an increase in the amount of calcium transients relative to its baseline was considered a responder. If the number of events remained unchanged or decreased, it was classified as a nonresponder. To analyze the global astrocytic calcium concentration, a

single ROI around the astrocytic territory excluding the soma and major branches was drawn using Fiji/Image J. The integral of the ratio of the fluorescent intensity of GCaMP5g and tdTomato (background-subtracted) was calculated for at least 250 frames during baseline and treatment, nominally 0mM calcium or stimulation of the alveus, to calculate in relative change. To ensure viability of the astrocyte throughout the experiment, only cells that displayed at least one transient during the total recording were used. Cells that showed a change (increase or decrease depending on the experiment) of more than 5 % were considered responders.

2.3.8 Dendritic Plateau Potentials

Dendritic plateau potentials were evoked by a dual stimulation paradigm comparable to the one used by Takahashi and Magee (2009). A CA1 PC was whole-cell patched and kept in current clamp as described (section 2.3.1) in the presence of blockers for $GABA_A$ (50 µM picrotoxin) and $GABA_B$ receptors (5 nM CGP 55845 hydrochloride, Tocris). Schaffer collaterals were stimulated using a concentric bipolar stimulation electrode (FHC, CBARC75) placed at the boarder of CA3 and CA1 stratum radiatum. The perforant path was stimulated using a monopolar glass pipette stimulation electrode, placed in closed proximity to an apical tuft dendrite of the whole-cell patched CA1 PC. The stimulation intensity was set in such way, that a somatic EPSP of approximately 9-10 mV for Schaffer collateral and 1 mV for perforant path stimulation was evoked. After sufficient diffusion of the dye throughout the dendritic arbor (> 60 minutes), line scanning through an apical tuft dendrite (~2 ms per line, 2048 lines) was performed to monitor rapid changes in the fluorescence of the dyes. Dendritic plateau potentials were evoked by stimulating both pathways five times every 200 ms for five stimuli at 100 Hz. This was repeated four times with an interstimulus interval of 60 s for each condition. Paired recordings for baseline, in saturated D-serine (10 µM) and APV (50 µM) were performed.

The probability of dendritic plateaus was estimated for each cell by counting their occurrence for each burst during the four repetitions. Dendritic plateaus were identified based on their typical shape: a prolonged after-depolarization potential and the induction of AP bursts (Takahashi and Magee, 2009). Since the fifth burst showed the highest probability of dendritic plateaus (see section 3.4.3 and Takahashi and Magee, 2009), it was used for detailed analysis. APs were removed by calculating the first and second derivative and removal of extreme values: somatic potentials < 30 mV; first derivative < 5 mV/ms or > -5 mV/ms; second derivative < 30 mV*ms/ms or > -20 mV*ms/ms. The resulting traces were smoothed by a 50^{th} percentile filter over 50 points and the area, i.e., integral, and after-depolarization, i.e., full width at half maximum amplitude (FWHM), extracted using the peak analysis tool of OriginPro.

For analysis the signal of the recorded quadruplets was averaged. Next, the intensity profile over time for both indicators were corrected for their background intensity and the fluorescence ratio was calculated. The signal was then normalized to the baseline and reported as $\Delta R/R_0$. The overall integral, as well as the integral, peak and FWHM of the 5^{th} burst were analyzed. For the latter analysis, $\Delta R/R_0$ trace was smoothed with a 10-points adjacent averaging method and the parameters were automatically extracted using the peak analyzer tool of OriginPro.

2.4 Astrocytic Calcium Imaging in Vivo

In vivo recordings of astrocytic calcium responses in anesthetized and awake mice were performed by Andrea Delekate, Cordula Rakers from the laboratory of Gabor C. Petzold, I analyzed the recorded data. The expression of the genetically-encoded calcium indicator GCaMP5g was driven through GLASTcreER in PC-G5-tdT mice after tamoxifen injection as described in section 2.1.2.

Acute cranial windows for recordings in anesthetized mice were prepared as previously described (Delekate et al., 2014). Briefly, the mice were anesthetized with isoflurane (induction: 3 % v/v; maintenance: 1-1.5 % v/v), kept on a heating plate (37° C) and fixed in a stereotactic frame. After removal of the scalp, a 3 mm cranial window above the primary somatosensory cortex was created using a dental drill. The window was closed with agarose (1.5 %) and a cover glass. Recordings and analysis of cortical astrocytes were performed as described in section 2.3.7.

For recordings of awake mice chronic cranial windows were prepared. As for acute cranial windows, mice were anesthetized with isoflurane, kept on a heating plate and fixed in a stereotactic frame. After removal of the scalp, the skull was pre-treated with light-curable dental cement. Next, a 4 mm window above the primary somatosensory cortex was drilled, pre-sealed with super glue and a cover glass, and fixated using light-curable dental cement. Then, an aluminum holder was attached on the contralateral side of the skull using dental cement, allowing head fixation and awake imaging. Analgesia was applied 30 minutes before and for three consecutive days after surgery. Habituation to the head fixation and the treadmill (Luigs & Neumann, Germany) was started one week after surgery. On the first day, the mice were hold by their tail while running on the belt for approximately 30 minutes. On the following day, the mice were head-fixed and allowed to run freely. This was repeated until the animals were running calmly on the belt. Finally, the treadmill was positioned under the 16x objective (Nikon) of a two-photon microscope (Trim ScopeII, LaVision Bio Tec). The first imaging session took place two weeks after surgery and the mice were allowed to run on the treadmill for a maximum of 60 minutes a day. Time-lapse frame scanning of two to three astrocytes (384 x 384 pixel, 192 x 192 µm, 3.13 Hz) in 130-195 µm depth was performed for 10 minutes each. The recordings corrected for movement artifacts by alignment with a custom-written Matlab script (Petzold group). Locomotion was recorded at 20 Hz by a digital position readout device (Luigs & Neumann, Germany). For quantification and correlation, the movement was binned in three second time windows. Only transients whose peak occurred within ±6 s of a movement with a velocity of at least 1 cm/s were considered locomotion-associated. Analysis of these calcium responses was performed as described in 2.3.7.

2.5 IMMUNOSTAINING AND CONFOCAL MICROSCOPY

To determine the specificity and efficiency of the knock-out or knock-in in the transgenic animals, some mice were transcardially perfused with 4 % paraformaldehyde (PFA, Sigma) in phosphate buffered saline (PBS, containing in mM: NaCl 137, KCl 2.7, Na_2HPO_4 10, KH_2PO_4 1.8, pH 7.4; osmolarity 290). The mice were anesthetized using an overdose of ketamine and xylazin (ketamine (betapharm) 80 mg/kg bodyweight, Xylazin (Rompun, Bayer) 1.2 mg/kg bodyweight, i.p. injection volume 0.1 ml/20 g bodyweight). After ensuring that the animal was under deep anesthesia by checking the toe reflexes, the abdomen was opened along the ribcage. Next, the diaphragm was carefully removed and the ribcage cut to gain access to the chest cavity. To allow rapid perfusion of the animal, the right atrium was opened through a short cut before at least 20 ml ice-cold 4 % PFA in PBS were injected into the left ventricle. Finally, the brain was removed from the skull and placed in 4 % PFA in PBS overnight for postfixation.

The next day, after washing the brain with PBS, the forebrain and cerebellum were trimmed. The brain was then glued onto a mounting disk, placed in the cutting chamber with ice-cold PBS and cut into 50 µm thick horizontal slices with a vibratome (Leica). The slices were transferred into wells and washed three times for ten minutes with PBS. Afterwards, a blocking solution containing 10 % normal goat serum (NGS, Merck Millipore) and 0.5 % Triton (AppliChem) in PBS was applied for 2 h at room temperature to reduce nonspecific binding of the antibodies. Next, the primary antibody was applied in PBS with 5 % NGS and 0.1 % Triton overnight at 4°C. The following day, the slices were washed again three times with PBS for ten minutes before applying the secondary antibody in PBS with 2 % NGS and 0.1 % Triton for one to one and a half hours at room temperature. This step was repeated for the conjugated-streptavidin. For nuclear staining the slices were washed three times after the last antibody treatment and placed in water with 0.5 % Hoechst (33342, ThermoFisher Scientific) for ten minutes at room temperature. Last, the slices were washed and then mounted onto frosted glass microscope slides (Thermo Scientifica) with a ProLong Gold antifade mountant (Invitrogen) and left overnight for fixation at 4 °C.

The following primary antibodies were used:

- GFAP, polyclonal rabbit anti-cow GFAP 1:500 (Z0334, Dako);
- NeuN, monoclonal mouse anti NeuN 1:200 (MAB377, Chemicon).

The following secondary antibodies and compounds were used:

- anti-rabbit, polyclonal goat anti-rabbit IgG (H+L)-Alexa Fluor 488 1:500 (A11034, Invitrogen);
- anti-mouse, polyclonal goat anti-mouse IgG (H+L)-biotin 1:500 (115-065-003, Dianoca);
- anti-biotin, Alexa Fluor 647 streptavidin conjugate 1:600 (S32357, Thermo Fisher Scientific).

After at least 24 hours of post-fixation, the sections were imaged using a laser scanning confocal microscope (TCS SP8, Leica). The efficacy of the cre activation in the astrocyte specific CB1 receptor knock-out mice (aCB1KO, GLAST-CreERT2 x Ai14 x $CB1^{f/f}$) was determined by taking stacks of the hippocampal CA1 area (512 x 512 µm, 450 x 450 pixel, pixel size 1.14 µm, 2 µm z-steps) with a laser scanning confocal microscope (TCS SP8, Leica). Using Fiji/Image J, the NeuN-positive neurons and GFAP-positive astrocytes were counted based on their nuclei signal by Hoechst staining of the DNA and checked for co-localization with tdTomato in each stack. Three sections of 20 µm depth each were averaged per animal for analysis.

2.6 Behavioral Experiments

To examine the relevance of CB1 receptors in astrocytes in vivo, behavioral experiments with the astrocytic knock-out animals were performed in collaboration with the laboratory of Heinz Beck. The design of these experiments was developed by me with the expertise of Thoralf Opitz (senior postdoctoral fellow, laboratory of Heinz Beck). The required animals for the experiments were bred, tamoxifen injected and verified by me. I monitored the experiments and analyzed the obtained data. The performance of the behavioral experiments and the corresponding handling of these animals was the responsibility of Rebekka Zölzer (technical assistance, laboratory of Heinz Beck).

Male and female GLAST-cre ERT2$^{tg/wt}$ x CB1R$^{f/f}$ x Ai14$^{fl/fl}$ were injected with tamoxifen or sham between postnatal day 21 and 28 as described. After one to two weeks of recovery, the animals were handled on five consecutive days twice for five minutes each before participating in the tests described. All animals used were housed under reversed light/dark conditions and were allowed ad libitum access to food and water. All experiments were conducted in full compliance with national and institutional guidelines. Behavioral testing was performed in a separate, quite area during the beginning of the dark phase. The room was lid with dimmed red light and spatial cures were present around the arena. All test and training sessions were recorded using a Basler acA1300-200um camera system mounted above the arena (1280 x 1024 pixels). Between animals the arena was cleaned using 70 % ethanol. Handling, training, testing and analysis were conducted blind for the treatment the mice received.

For the analysis of the behavior experiments EthoVision XT14 (Noldus) was used. The mice locomotion was traced automatically by three points (nose, center, tail), unless stated otherwise. The tracing was then checked and, if necessary, manually corrected. For each of the tests, specific areas of interest were drawn in the software to access the relevant behavior. As a measure of locomotion, the total distance traveled and velocity were used.

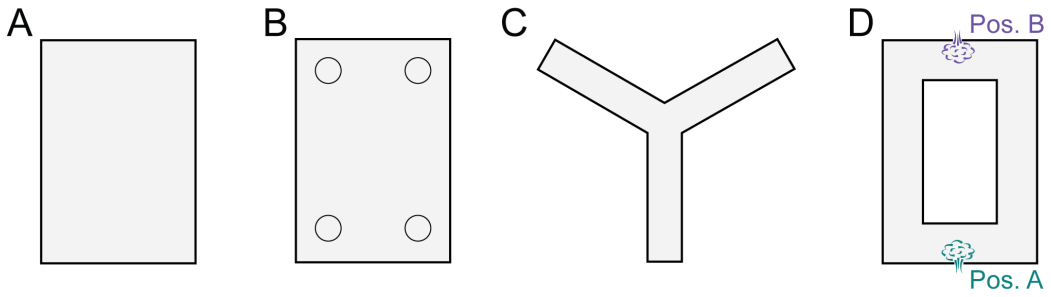

Figure 2.3 Illustrations of the mazes used for behavioral experiments. (A) open-field arena. **(B)** open-filed arena with possible positions for objects illustrated by circles. **(C)** Y-maze. **(D)** O-maze with two possible air puff positions.

2.6.1 Open-Field Test and Habituation

The open-field arena (40 x 60 cm) was constructed of dark gray PVC with 23 cm wall height and light-gray flooring (Figure 2.3 A). Mice were placed in the middle of the arena and were allowed to explore it freely. This was repeated for five consecutive days, each day for ten minutes. The open field test was conducted on the data recorded on the first day in the arena. The open-field test can be used to gain some inside on the animal's anxiety. Therefore, an outer zone in the arena was defined as an 8 cm gallery on the border of the arena, resulting in an inner zone of 24 cm x

44 cm. The two groups were compared by analyzing the cumulative duration each animal spent in the inner and outer zone. Additionally, the fecal boli deposits of the animals were counted manually.

2.6.2 Object Location and Novel Object Recognition Test

Long-term memory was investigated using the novel object recognition task (NORT) and the object location task (OLT). Both tasks were performed in the open-field arena. Objects of similar size were used (3-4 cm in diameter) and placed randomly in the corners of the arena with a distance of 9 cm from the walls (Figure 2.3 B). To allow familiarization and acquisition of the memory regarding the objects and their locations, the mice were allowed ten minutes exploration on the first day of the task. Retention of the memory was tested after a 24-hour delay by either changing one object (different in shape, texture and color) or one's location in the arena. During this test the animal's exploration of the area and objects was monitored for five to ten minutes. The positions of the objects in the arena was randomized between animals. To examine whether the animals remember the familiar object or its location, the time exploring the novel and familiar object was determined. Object exploration was defined as the nose-point being within 2 cm of the object, with body orientation towards the object. For both, the NORT and OLT, the two treatments are compared by their total exploration time (T_{total}) and the discrimination index (DI). Animals that showed excessive climbing or little exploration (T_{total} < 5 s in 10 min; $T_{novel} \vee T_{familiar}$ < 1 s in 10 min; T_{total} < 2 s in 5 min; total distance < 1 m in 5 min) as well as outliers for the analyzed parameters (mean ± 2SD) were excluded (NORT = 7; OLT = 5).

$$T_{total} = T_{novel} + T_{familiar}$$

$$DI = \frac{(T_{novel} + T_{familiar})}{(T_{novel} - T_{familiar})}$$

2.6.3 Spontaneous Alternation Test (Y-maze)

Spatial working memory was investigated using a Y-maze with three identical arms, each 40 cm long and 8 cm wide, interconnected at 120° angle (Figure 2.3 C). Each arm had a different spatial cue at the end. The mice were placed in the middle of the arena and were allowed to explore it freely for ten minutes. For the spontaneous alternation test the center point of the animal was automatically traced, checked and if necessary corrected. Owing to the inherent interest in novelty, mice have a tendency to visit the arms in alternating order. Entrance into the second half of each arm was defined as an arm visit. Zone visits, alternations and maximum possible alternations were analyzed automatically and used to calculate the alternation index (AI) and relative visits per arm for each mouse. Animals with an arm preference or aversion (relative arm visits >23 % or <8 %, respectively) were excluded (n = 3).

$$AI = \frac{alternations}{max.possible\ alternations} \times 100\%$$

2.6.4 PASSIVE PLACE AVOIDANCE TEST

The passive place avoidance test was performed in a modified open-field arena resulting in a 10 cm wide gallery, called O-maze (Figure 2.3 D). Light-sensors on each side of the gallery (position A and B) were used to activate a one-bar air puff (nitrogen gas) when the animal was disrupting the light bridge. The animal was placed in the long arm of the arena in equal distance to the possible air puff locations. The test consists of five consecutive days with specific air puff positions to test different aspect of aversive memory. Each day a single trial of ten minutes free exploration was performed. On the first day, the animals are habituated to the maze. On the second and third day, the air puff was at position A. On the fourth day the air puff was removed. Lastly, the air puff is moved to the opposite side (position B) on the fifth day. The main parameter for the analysis was the number of light bridge disruptions, and hence, air puff activations, defined as nose-point within the light bridge. Since the light bridge was present when the air puff was not, it can be used as parameter on day four and five. Additionally, latencies to the first and or last activation and interval between both were analyzed and compared between groups.

2.7 STATISTICS

Statistical analysis was performed with OriginPro. To compare categorical data the Fisher's exact test was used. For continuous data differential statistical analysis were performed depending on the distribution, number of experimental groups, dependency of the variables and the variances between the groups. All data was tested for normal distribution with the Shapiro Wilk test. Normally distributed data were reported as mean ± s.e.m. Statistical testing of one experimental group were done with a one-population Student's t-test. Results from experiments with two groups were tested if paired with the paired t-test or if independent with the Student's t-test with or without Welsh correction, depending on the equality of the variance. In case the experiment had more than two experimental groups or parameters a one-way or two-way ANOVA was used followed by post-hoc Fisher's LSD or Tukey test, as indicated. Paired data were analyzed with the appropriate repeated measures ANOVA. Nonparametric data were reported as median ± interquartile range (IQR, 25-75 %). Statistical testing of one experimental group was done with a one-population Wilcoxon signed-rank test. Two experimental parameters were tested in case of paired recordings with the Wilcoxon signed-rank test or if the data were independent with the Mann-Whitney test. For multiple parameters of paired recorded data, a Friedman ANOVA with post-hoc Wilcoxon signed-rank test was used, independent samples were analyzed with a Kruskal-Wallis ANOVA with post-hoc Mann-Whitney test. Some datasets are illustrated as box and whisker plots. The box indicates the 25th and 75th, the whiskers the 5th and 95th percentiles, the horizontal line in the box the median and the mean is represented by a filled circle. To investigate whether two groups are related, the Spearman's rank correlation coefficient was used. In graphs, statistical significance is indicated by asterisk. * for $p < 0.05$, ** for $p < 0.01$ and *** for $p < 0.001$.

3 RESULTS

3.1 THE RESTING CALCIUM CONCENTRATION SHAPES CALCIUM TRANSIENTS IN ASTROCYTES

Astrocytes can control synaptic transmission as well as learning and memory through the release of gliotransmitter (Guerra-Gomes et al., 2018). This release is mediated by astrocytic calcium transients, which occur mostly in small subcellular compartments, the so-called microdomains (Di Castro et al., 2011; Kanemaru et al., 2014). Here the influx of extracellular calcium and/or the activation of G-protein-coupled receptors can evoke a further increase in the intracellular calcium concentration by the activation of store-dependent release through IP3 and ryanodine receptors (Bazargani and Attwell, 2016). This results in an increased frequency of the transients and gliotransmitter release. The physiological principle regulating the waveform of these transients is unknown. An interesting candidate for this is the local resting concentration of calcium. It has been shown that the open probability of IP3 receptors has a bell-shaped dependency on intracellular calcium concentration (Foskett et al., 2007; Hituri and Linne, 2013). This means that small changes in the local resting calcium concentration could increase the open probability of these receptors and thus cause a larger increase in cytosolic calcium, whereas very high concentrations reduce the opening of IP3 receptors. Furthermore, higher calcium concentrations could lead to partial saturation of the cytosolic calcium buffers. Accordingly, modelling suggests that a higher resting calcium concentration results in a larger calcium transient amplitude (Klingauf and Neher, 1997). Accordingly, the local pre-event calcium concentration could shape the peak and/or amplitude of astrocytic calcium transients.

To investigate the relationship between the pre-event calcium concentration (baseline) and the events maximal calcium concentration (peak) and its change from baseline to peak (amplitude), tamoxifen-injected PC-GT-tdT x GLAST-creER/ERT2 mice expressing the genetically-encoded calcium indicator GCaMP5g and the fluorescent protein tdTomato selectively in astrocytes were used (Figure 3.2 A, left panel). This technique has the advantage that it allows the monitoring of astrocytic calcium without perturbing astrocytes through whole-cell patch clamp recordings. The intensity of the GCaMP5g can be used to examine the calcium concentration before and during calcium transients. Nevertheless, its cytosolic concentration differs per voxel owing to differences in the astrocytic volume fraction. Since the intensity of GCaMP5g depends on its cytosolic concentration and the calcium concentration, values throughout the astrocytic territory will not be comparable. To normalize for differences in the cytosolic concentration, the ratio of the GCaMP5g fluorescence and the fluorescence of the calcium insensitive protein tdTomato (background-subtracted) was calculated. It is important to note that changes in the calcium concentrations do not cause linear changes in the fluorescence intensity of GCaMP5g (Akerboom et al., 2012). Since this can influence the relationship of the baseline with the peak and/or the amplitude of calcium transients, the effect this nonlinearity has on the Spearman's rank correlation coefficients was tested (Figure 3.1 and King*, Bohmbach* et al., 2020). Using the calcium concentrations obtained through recordings with the calibrated calcium-sensitive indicator Oregon Green 488 BAPTA (OGB)-1, the corresponding calcium-bound fraction of GCaMP5g can be calculated for baseline, peak and amplitude. Both, the Spearman's rank correlation coefficient based on the estimated fluorescence and the measured calcium concentration for baseline-peak and baseline-amplitude correlations showed a linear relationship. This means a similar increase in the coefficient in both conditions. However, for the

latter the y-intercept differed with 0.38 significantly from zero. Therefore, the Spearman's rank correlation coefficients calculated for baseline/amplitude correlations hereafter were corrected to allow interpretation about the intracellular calcium concentration.

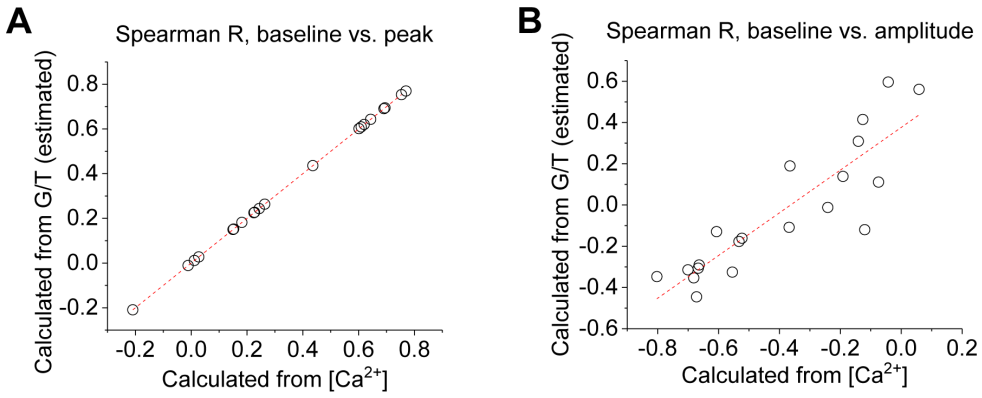

Figure 3.1. Correction of Spearman's rank correlation coefficient R for correlations obtained with the fluorescent proteins GCaMP5g and tdTomato. Estimating the corresponding GCaMP5g and tdTomato ratio (G/T) for baseline, peak and amplitude from calcium concentrations measured with a calibrated calcium-sensitive indicator demonstrated the relationship between correlations coefficients calculated using either method. **(A)** Spearman Rs for baseline-peak dependency obtained with either method overlap (n = 20, R^2 = 1, slope = 1, y-intercept = 0). **(B)** Spearman Rs for the relationship between baseline and amplitude showed a linear relationship (n = 20, R2 = 0.78). The y-intercept differed significantly from zero (y-intercept = 0.38 ± 0.062, p = 0.00001). *Note: Figure adapted from C. Henneberger, published in King*, Bohmbach* et al. (2020).*

Time-lapse frame scanning of spontaneously occurring calcium elevations was performed in acute hippocampal slices in collaboration with Daniel Minge. Transients of stratum radiatum astrocytes were visually identified, the ratio of the GCaMP5g and tdTomato fluorescence intensity (background-subtracted) was calculated and their baseline, peak and amplitude determined (Figure 3.2 A, right panel). My analysis of the relationship between the local resting and the peak calcium concentration revealed a significant overall positive correlation (Figure 3.2 B&C, gray). This means that a higher baseline calcium levels results in higher peak calcium concentration. In contrast, the amplitude of the calcium transients showed an overall negative correlation with the baseline (Figure 3.2 B&C, turquoise). My analysis revealed a similar result for spontaneous calcium transients in cortical astrocytes in vivo recorded in anesthetized mice by Andrea Delekate and Cordula Rakers from the laboratory of Gabor C. Petzold (Figure 3.2 D).

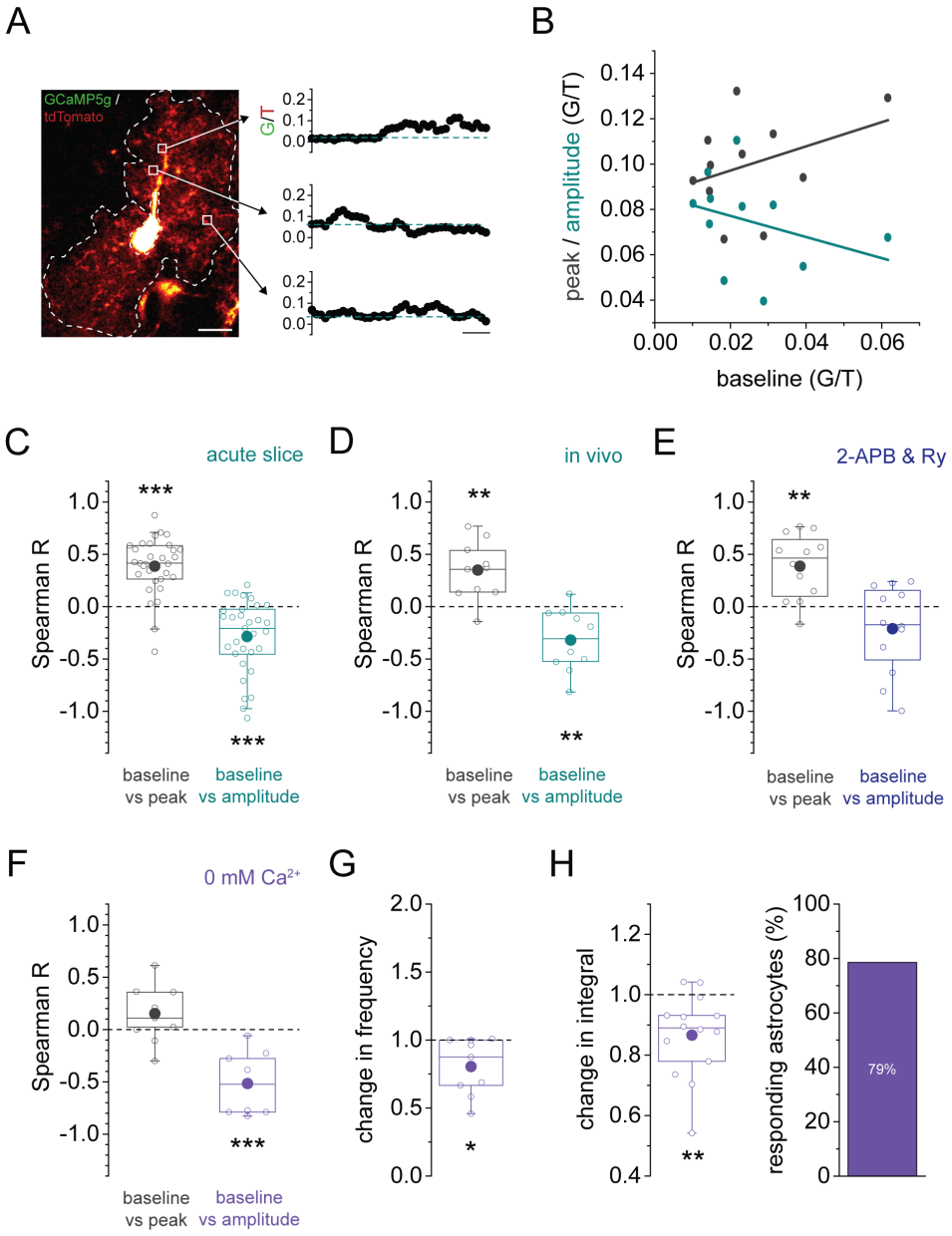

Figure 3.2. The local resting calcium concentration determines the peak and amplitude of astrocytic calcium transients. (A) Representative astrocyte expressing the calcium indicator GCaMP5g and the fluorescent protein tdTomato (scale bar: 10 µm). The fluorescence ratio of both fluorescent proteins (G/T, background-subtracted) was used to analyze the relationship between baseline, peak and amplitude of spontaneously occurring calcium transients. Representative traces did not occur simultaneously and were aligned for illustration (scale bar: 2 s). **(B)** Scatter plot illustrating the relationship between the local resting calcium concentration (baseline) and peak (gray) or amplitude (turquoise) of the G/T ratio. **(C-F)** Spearman's rank correlation coefficient R was calculated for individual cells between baseline and peak (gray) or baseline and amplitude (color, corrected values). **(C)** In acute hippocampal slices baseline and peak calcium overall correlated positively (R = +0.39 ± 0.05, n = 31, p < 0.0001, one-population Student's t-test) while baseline and amplitude correlated negatively (R = -0.29 ± 0.06, n = 31, p < 0.0001, one-population Student's t-test). **(D)** Spontaneous calcium transients of cortical astrocytes recorded in vivo in anesthetized mice showed overall a positive correlation between pre-event calcium baseline and peak (R = +0.34 ± 0.09, n = 10, p = 0.004, one-population Student's t-test) and a negative correlation with the amplitude (R = -0.32 ± 0.09, n = 10, p = 0.009, one-population Student's t-test). **(E)** In presence of 2-APB (100 µM) and ryanodine (Ry, 10 µM) the positive correlation between peak and baseline remained (R = +0.39 ± 0.09, n = 12, p = 0.001), while baseline vs. amplitude did not differ from 0 (R = -0.21 ± 0.12, n = 12, p = 0.11). **(F)** When spontaneous calcium transients were recorded in nominally 0 mM calcium, R was significantly reduced for peak, but not for amplitude. As a result, the correlation of the peak did not reach significance anymore (R = +0.153 ± 0.0908, n = 9, p = 0.13), amplitude did (R = -0.52 ± 0.10, n = 9, p = 0.0007). **(G)** Reducing extracellular calcium causes a decrease in the frequency of spontaneous calcium transients (0.80 ± 0.07, n = 9, p = 0.023, one-population Student's t-test). **(H)** The integral of the G/T ratio over time showed a significant decrease after application of aCSF with nominally 0 mM calcium (0.87 ± 0.04, n = 14, p = 0.003, one-population Student's t-test). 78.6 % of astrocytes showed a reduction of more than 5% in the integral. *Note: A subset of the displayed results are published in King*, Bohmbach* et al., 2020.*

To unravel the underlying molecular mechanism, recorded spontaneous astrocytic calcium transients in the presence of blockers for store-dependent calcium entry through inositol trisphosphate (IP)3 receptors (2-APB) and ryanodine receptors (ryanodine) were recorded by Daniel Minge in acute hippocampal slices. I analyzed how these blockers influences the described relationships (Figure 3.2 E). While the positive correlation between resting and peak calcium remained overall significant, the correlation coefficients for baseline and amplitude did not. To investigate the relevance of calcium entry from the extracellular space, spontaneous calcium transients in artificial cerebrospinal fluid (aCSF) with nominally 0 mM calcium were recorded. In this case, the opposite effect was observed (Figure 3.2 F). The correlation coefficient of baseline and peak calcium concentration was overall significantly decreased (0.31 ± 0.06 vs. 0.15 ± 0.09, n = 9, p = 0.043, paired t-test, data not shown), not reaching significance anymore. The relationship between baseline and amplitude, however, was unchanged (-0.45 ± 0.09 vs. -0.52 ± 0.10, n = 9, p = 0.34, paired t-test, not shown) and showed an overall negative correlation. Mechanistically, these results indicate, that the decrease in the amplitude of calcium transients with increasing resting calcium concentrations is regulated through store-depend release. On the other hand, the increase in the peak concentration with increasing resting calcium concentration appears to be coupled to the influx of calcium from the extracellular space.

The spontaneous calcium transients recorded in acute slices showed a mean frequency of 1.33 ± 0.20 (n = 25) events per minute with a coefficient of variation of 0.74. Inhibiting calcium entry from the extracellular space resulted in a significant decrease of the calcium event frequency (Figure 3.2 G). The total frequency of calcium transients in astrocytes is low and therefore large variations can occur. Moreover, the analysis needs to be often performed manual. To have a more unbiased parameter to detect also small differences in astrocytic calcium, the integral of the fluorescence ratio throughout the astrocyte territory was determined. A decrease of the transient frequency should lead to an overall decrease in the fluorescence ratio. Indeed, a significant reduction in the integral of the fluorescence ratio over time was found after the application of aCSF with nominally 0 mM calcium (Figure 3.2 H). In nearly 80 % of the astrocytes a decrease of more than 5 % in the integral was observed after application. Next, it was tested whether the reduction in frequency and the reduction in integral were related using the Spearman's rank correlation. Both showed a significant correlation to each other (R = +0.80, n = 9, p = 0.0099, Spearman's rank correlation), i.e., greater changes in the integral correspond to a stronger reduction in frequency. This suggests that the integral of the fluorescence ratio can serve as a crude estimate of changes in the astrocyte calcium transient frequency.

Next, we investigated whether the same relationship between baseline, peak and amplitude of the calcium concentration found for spontaneous calcium transients in anesthetized mice, could be uncovered for transients evoked by behavior in vivo. It is well known, that locomotion causes calcium increases in cortical astrocytes (Dombeck et al., 2007). Therefore, Andrea Delekate from the laboratory of Gabor C. Petzold recorded and I analyzed whether locomotion-associated calcium transients in awake, head-fixed mice running on a treadmill showed the same relationship of baseline and peak or amplitude (Figure 3.3 A). During the ten minutes of recording time, the mice travelled between 115 and 2044 cm with an average speed of 65.4 ± 18.3 cm/min. Approximately 90 % of all transients occurred within six seconds of a movement with a velocity of at least 1 cm/s and hence, were considered locomotion-associated (Figure 3.3 B). These transients showed heterogeneity within and between locomotion bursts, between the astrocytes in the field of view and within a single astrocyte (Figure 3.3 C&D).

Overall, the relationship between the parameters was comparable to the earlier experiments. The pre-event baseline and the peak showed a persistent significant positive correlation (Figure 3.3 E&F, gray), while the amplitude negatively correlated with the baseline (Figure 3.3 E&F, turquoise). These results show that in astrocytes the peak of a calcium response scales positively with the local resting concentration. This is mediated by the influx of calcium from the extracellular space. In contrast, the calcium concentration of the amplitude scales negatively with the pre-event baseline. Store-dependent calcium release underlies this relationship.

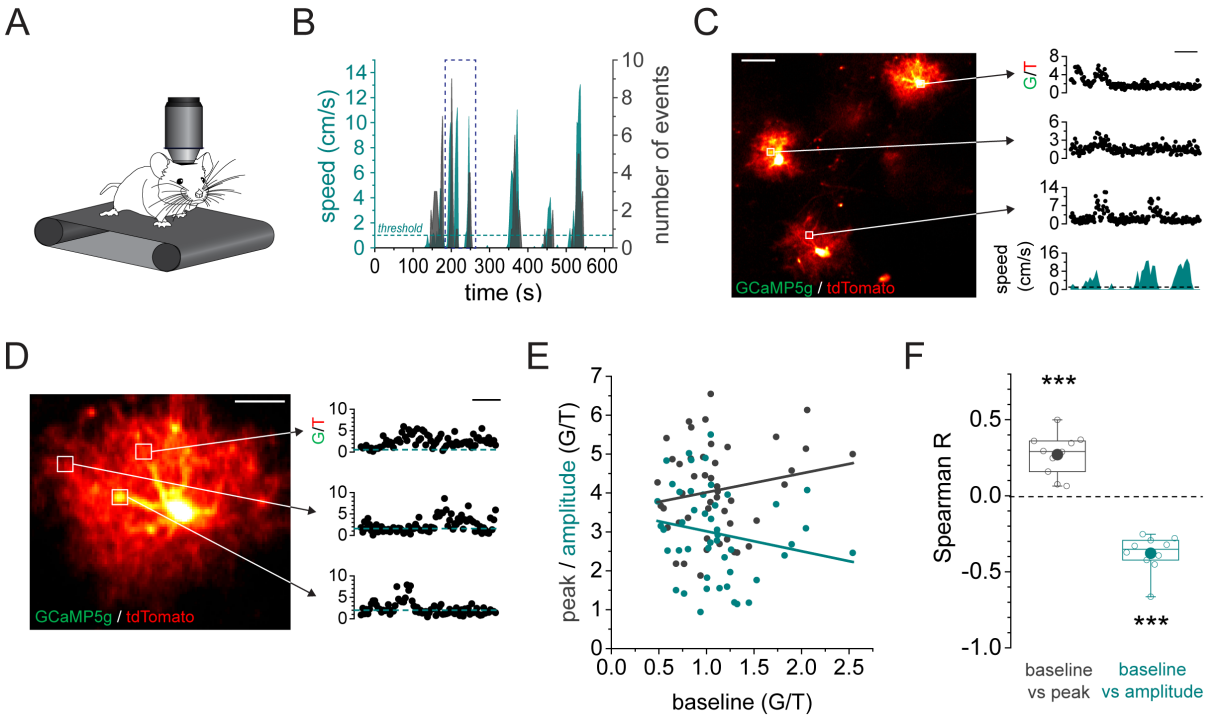

Figure 3.3. Locomotion-associated calcium transients in awake mice. (A) Schematic of the experimental setup. **(B)** Example of the number of calcium events (gray) and movement speed (turquoise; threshold 1 cm/s, dashed line) of a single mouse (time bins of 3 s), illustrating the correlation between both. **(C)** Field of view (scale bar: 50 µm) and example traces (GCaMP5g and tdTomato ratio, background-subtracted) recorded during the time window indicated by the blue dashed box in B (scale bar: 10 s). For approximately 90 % of the transients, the peak occurred 6 s before or after locomotion. **(D)** Zoom-in of a single astrocyte (upper right cell in C, scale bar: 10 µm) and representative transients (not simultaneously occurring, aligned for illustration, scale bar: 5 s). **(E)** Scatter plot illustrating the relationship between the local resting calcium concentration (baseline) and peak (gray) or amplitude (turquoise) of the G/T ratio. **(F)** The local resting concentration of locomotion-associated calcium transients in vivo correlated overall positively with the peak (R = +0.27 ± 0.04, n = 10, p = 0.0002, one-population Student's t-test) and negatively with the amplitude (R = -0.38 ± 0.04 (corrected), n = 10, p < 0.0001, one-population Student's t-test). *Note: The displayed results are published in King*, Bohmbach* et al., 2020.*

Since it has been shown, that the resting calcium concentration varies between single astrocytes (Zheng et al., 2015), the response of astrocytes to activation of, for example, endocannabinoids might vary from cell to cell. Furthermore, this would mean that the same stimulus might result in the release of gliotransmitters in one cell, but this might not happen in the neighboring cell. Since data from our laboratory suggests also large heterogeneity of the resting calcium concentrations within a single astrocytes (King*, Bohmbach* et al., 2020), the regulation of synaptic transmission might be organized in even smaller functional units. Additionally, the results showed that a decrease of the extracellular calcium leads to a decrease in spontaneous calcium transient frequency. This decrease scaled with a decrease in the integral of the fluorescence ratio within the astrocyte's territory. Accordingly, the relative change in integral might be used as an alternative indicator of changes in astrocyte calcium frequency.

3.2 Microiontophoretic Stimulation to Study Dendritic Integration

Astrocytic calcium transients can evoke the release of gliotransmitter and regulate synaptic transmission (Guerra-Gomes et al., 2018). One of the aims of my thesis is to investigate whether astrocytes are able to modulate neuronal input computations through, for example by releasing D-serine. CA1 pyramidal cells integrate synaptic input not only at the soma but also locally in dendrites summation and integration of synaptic conductance takes place. This process is called dendritic integration (Losonczy and Magee, 2006). Through distinct input computations different patterns of activation are detected. Interestingly, the activation of spatially clustered synapses in a temporally synchronous manner results in supralinear integration and hence, increased neuronal output (Losonczy and Magee, 2006). NMDA receptors have a central role in this. NMDA receptor opening requires the presence of glutamate and a co-agonist (Johnson and Ascher, 1987). Hence, I hypothesized that astrocytes can modulate dendritic integration through the supply of NMDA receptor co-agonist or local clearance of glutamate. To test this hypothesis I will use, among others, pharmacological interventions to determine their effect on the local input integration. Therefore, a technique that permits repetitive, local stimulation of a dendrite is required. A widely-used technique to investigate dendritic integration is two-photon uncaging of glutamate. This technique allows the stimulation of several individual spines through laser-activated release of glutamate from its cage. However, repetitive laser stimulation of a single spine to uncage glutamate can cause phototoxicity (Ellis-Davies, 2019). This will limit the number of repetitions that can be performed to study the integration of an individual dendrite. An alternative approach is the microiontophoretic stimulation with glutamate, which is ejected out of the pipette by an electrical current. Photo damage can be mostly excluded with this method since two-photon laser excitation is only required for positioning the pipette. However, this technique uses a point source to stimulate the dendrite with glutamate. This will result in a diffusion gradient of glutamate with increasing distance to the microiontophoresis pipette. Spines at distinct distances from the microiontophoretic pipette will be stimulated with varying amounts of glutamate. Therefore, it is important to determine the spatial extent of the ejected glutamate in the tissue to have an indication of the number of spines that are recruited. However, the spatial extent of this diffusion cannot be easily visualized.

To investigate the spatial extent and, hence, whether this method allows spatially defined activation of spines, whole-cell patch clamp recordings of CA1 PCs were performed. The neuron was filled via the patch pipette with Alexa Fluor 594 to visualize the dendritic tree. Next, the microiontophoresis pipette, filled with glutamic acid and Alexa Fluor 594, was placed in close proximity to a spine under guidance of two-photon excitation fluorescent microscopy (Figure 3.4 A). By retracting the iontophoretic pipette in 1 µm steps the spatial extent of the stimulation was estimated by the reduction in the amplitude of the evoked excitatory postsynaptic potential (EPSP) recorded at the soma (Figure 3.4 B&C). With an average stimulation intensity of 0.35 ± 0.03 µA and a duration of 0.57 ± 0.05 ms an initial EPSP of 5.57 ± 0.86 mV was evoked (n = 6, not shown). Fitting the reduction in amplitude with a mono-exponentially decaying function resulted in a length constant τ of 2.69 µm (R^2 = 0.99). The spatial extent of the released glutamate was estimated to have a radius of 16 ± 1.15 µm (n = 6). This means that spines within a radius of 16 µm will be stimulated by decreasing concentration of glutamate. Müller et al. (2012) found a radius of 12 µm using the same technique. As this is considerably smaller than estimated from my results, it should be noted that the spatial extent depends on the stimulation intensity and duration used. The stimulation intensity used here initially evoked an EPSP of more than 5 mV. In a subset of other experiments, this intensity was sufficient to evoke a dendritic spike (for example see Figure 3.5 B2). Expectedly, a rather large dendritic segment is activated. A dendritic segment of 32 µm contains on average 60 spines, however, the number can range from 30 to 120 ones (Harris and Stevens, 1989). Owing to the concentration gradient, some of these spines will be stimulated only by minor amounts of glutamate. Also two-photon uncaging requires the recruitment of more than 20 synapses within a dendritic segment of less than 20 µm for spike initiation (Losonczy and Magee, 2006). Taking the inhomogeneous glutamate concentration into account, glutamate microiontophoresis should be sufficiently spatially defined to examine local dendritic integration.

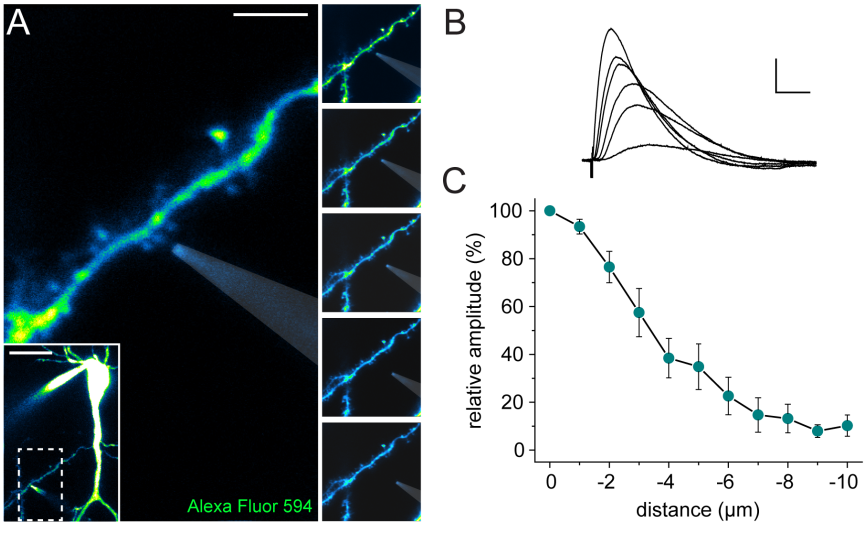

Figure 3.4. Spatial extent of microiontophoretic stimulation. (A) Sample image of an apical oblique dendrite of a CA1 pyramidal cell that was filled with Alexa Fluor 594 (40 µM) via the whole-cell patch clamp pipette to visualize the dendritic tree. A microiontophoresis pipette containing glutamic acid (150 mM) and Alexa Fluor 594 (50 µM, for visualization) was placed in close proximity (< 1 µm) to a spine (scale bar: 5 µm, inset 20 µm). To quantify the spatial extent, the distance of the iontophoretic pipette to the spine was stepwise increased while keeping the stimulation intensity and duration constant. The small insets show the retraction of the pipette in 2 µm steps from the initial position. **(B)** Corresponding traces of excitatory postsynaptic potentials (EPSPs) recorded at the soma of the whole-cell patch clamped CA1 pyramidal cell with increased iontophoretic displacement (scale bar: 2 mV, 2 ms). **(C)** Summary plot of the relative EPSP amplitude with increasing distance to the initial position (n = 6).

Next, I investigated if microiontophoresis stimulation with glutamate is indeed able to evoke different forms of dendritic integration. This requires the EPSPs to sum differentially between dendrites resulting in either no dendritic spike and linear summation or initiation of dendritic spikes and supralinear summation of synaptic inputs. Therefore, acute horizontal hippocampal slices from young adult rats were used. To increase the probability of EPSPs and dendritic spikes propagating to the soma, inhibition was blocked by the $GABA_A$ receptors antagonist picrotoxin. Since application of this antagonist can result in spontaneous, epileptiform activity from recurrent connections in CA3, a cut was made at the border of the CA3 region. Then, whole-cell patch clamp of a CA1 PC was performed and the microiontophoresis pipette was placed, as described. Using the microiontophoresis, local synaptic activation by the release of glutamate was mimicked by ejecting glutamate from the small opening of the micropipette in close proximity (< 1 µm) to a spine of a whole-cell patched CA1 PC (Figure 3.5 A1-C1). The dendrite was stimulated every three seconds with increasing amounts of glutamate while recording the resulting EPSP at the soma. The input-output computation of a dendrite was examined by plotting the stimulation intensity against the corresponding amplitude of the EPSP (Figure 3.5 A2-C2) or its maximum slope (Figure 3.5 A3-C3). These plots illustrate the distinct features of linear and supralinear integration. Stimulation of linear integrating dendrites (Figure 3.5 A2) showed the characteristic linear increase in the amplitude of the somatic potential until the occurrence of a somatic action potential (AP). Moreover, the maximum slope showed a linear increase, too (Figure 3.5 A3). In contrast, in dendrites with supralinear integration a step-wise increase in the maximum slope was detected (Figure 3.5 B3&C3). Accordingly, a deviation from linearity was also observed for the amplitude (Figure 3.5 B2&C2).

Another important feature of supralinear dendritic integration is the difference in the strength of dendritic spikes. Losonczy et al. (2008) showed that the maximum slopes of dendritic spikes are not resulting in a single population, but rather show two distinct populations. To distinguish whether microiontophoretic stimulation permits the induction of dendritic spikes with different strength, a histogram of the maximum slope of all dendritic spikes recorded was plotted. In accordance with the previously published data, also the maximum slopes evoked by microiontophoretic glutamate stimulation showed two distinct populations of dendritic spikes. Weak spikes had a small maximum slope (1st peak: 1.62 ± 0.04 mV/ms, example in Figure 3.4 B) and strong ones a larger one (2nd peak: 4.66 ± 0.14 mV/ms, example in Figure 3.4 C). These peaks are comparable to the distribution found by others with averages ranging from 0.37 mV/s to 4 mV/ms for weak dendritic spikes and 3.49 mV/ms to 8 mV/ms for strong ones in apical oblique and basal dendrites of CA1 PCs (Losonczy et al., 2008; Müller et al., 2012; Remy et al., 2009).

Overall, these results show that microiontophoretic stimulation of dendrites is a suitable technique to investigate the local dendritic integration. Although a point source is used, ejected glutamate permits a sufficient spatially-defined stimulation. Moreover, microiontophoretic stimulation can be used to distinguish distinct integration modes and dendritic spike strength present in individual dendrites. Therefore, this is a suitable technique to study the role of astrocytes in different forms of local dendritic integration.

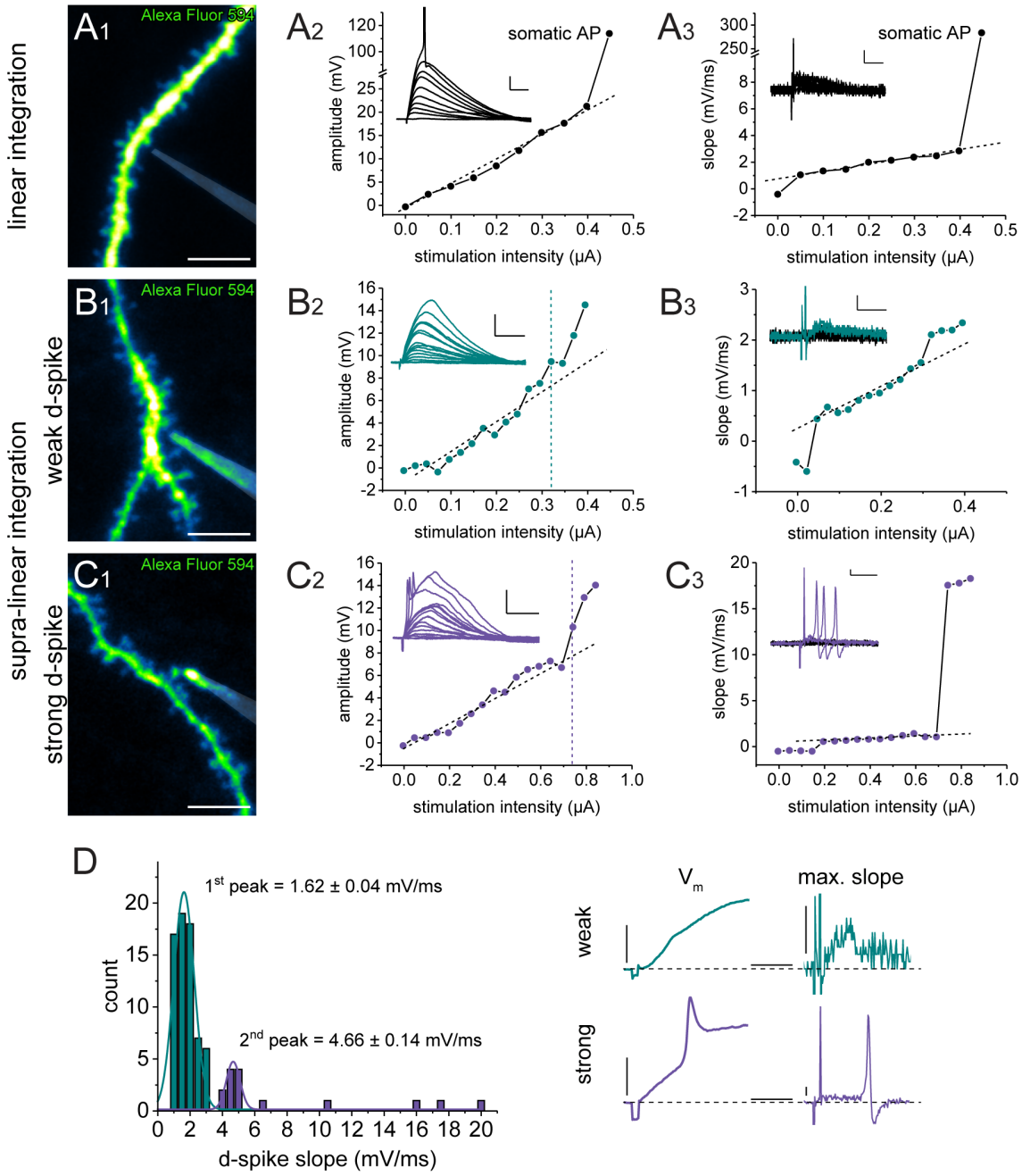

Figure 3.5. Dendrites of CA1 pyramidal cells have different modes of integrating input. While some dendrites showed a linear integration of the received input **(A)**, others displayed supralinear integration **(B&C)**. The two types of supralinear integration could be distinguished. Dendrites either exhibited weak **(B)** or strong dendritic spikes **(C)**. **(A1-C1)** For each type of integration a representative maximum intensity projection of a stimulated dendritic segment, filled with Alexa Fluor 594 (40 µM) via whole-cell patch clamp of a CA1 pyramidal cell, and the placed microiontophoresis pipette, filled with 150 mM glutamic acid and 50 µM Alexa Fluor 594 is shown (scale bar: 5 µm). **(A-C2)** The relationship between the microiontophoretic stimulation intensity (amount of ejected glutamate) and the somatic amplitude allowed the identification of the mode of integration performed by the stimulated dendritic segment. Subthreshold EPSPs followed a linear integration (dashed black line). The first dendritic spike is highlighted by a vertical dashed line and marks the point of deviation from linearity. The small insets display the corresponding voltage traces recorded at the soma (scale bar: 5 mV, 20 ms). **(A3-C3)** The nonlinearity of the dendritic integration became more obvious when the maximum amplitude of the first derivative of the somatic potential (the maximum slope) was plotted against the stimulation intensity. The small insets display the corresponding traces (scale bar: 5 mV, 20 ms or 2 mV/ms, 5 ms, respectively). **(D)** Left, frequency plot of the maximum slopes of 82 nonlinear integrating dendrites from CA1 pyramidal cells allowed the identification of the two types of supralinear integration (fitted by two Gaussian curves). The 1st peak at 1.62 ± 0.04 mV/ms corresponded to weak dendritic spikes, the 2nd peak at 4.66 ± 0.14 mV/ms to strong dendritic spikes (R2 = 0.96, n = 82). Right, dendritic spike somatic trace and its first derivative (first spike in (B) and (C)) are enlarged to illustrate the two populations observed (scale bar: 5 mV, 5 ms, 2 mV/ms, respectively). AP, action potential; d-spike, dendritic spike.

However, does microiontophoretic stimulation also permit repetitive, stable stimulation of the same dendrite? Since one of the aims of my thesis is to unravel the role of NMDA receptor co-agonists in dendritic integration, pharmacological interventions will be used. Drugs are usually applied via the bathing solution. Therefore, the position of the microiontophoresis pipette needs to be stable throughout the time course of the experiments. A comparison between different cells is not suitable for these experiments. Owing to the different distances of the dendritic segment to the soma, the potential will be differentially affected by dendritic filtering. Thus, amplitude recorded at the some will show large variations between cells. Losonczy and Magee (2006) found that the amplitude at the dendritic spike threshold was almost half when comparing proximal and distal stimulation of a single dendritic branch. This highlights the importance of performing paired measurements when investigating the effects of pharmacological interventions on, for example, the amplitude of the slow, NMDA receptor-mediated component of dendritic spikes.

To investigate the stability of the microiontophoretic stimulation, a CA1 PC was whole-cell patched, filled with Alexa Fluor 594 and the microiontophoresis pipetted positioned as before (Figure 3.6 A&B). Then, the integration of a dendrite was recorded (Figure 3.6 C). After five minutes the measurements were repeated. For the analyze several parameters were used. The amplitudes of the initial iontophoretic EPSPs (iEPSPs) should be highly sensitive to movement of the micropipette as suggested by the spatial extent of the stimulation (Figure 3.4). Notably, a much smaller stimulation intensity is required for iEPSPs. Thus, minor movements of the pipette will likely cause EPSP failure. However, the recordings did not show a difference in the iEPSP amplitude (1.21 ± 0.07 mV vs. 1.06 ± 0.12 mV, n = 5, p = 0.19, paired t-test, not shown). Next, the stimulation intensity, which corresponds to the amount of glutamate ejected, required to evoke the first dendritic spike (threshold stimulus, Figure 3.6 D) was examined. This did not differ between the two conditions. The stability of larger EPSPs was determined through the amplitude of the last EPSPs before a dendritic spike was evoked in either condition. Importantly, also these subthreshold EPSP did not change over time (Figure 3.6 E, left panel). As a measure for the contribution of NMDA receptors to dendritic spikes, the amplitude of the slow component was evaluated at a stimulation intensity, at which a dendritic spike was present in both conditions (Figure 3.6 E right panel, sample trace in A, dashed box). Lastly, the stability of sodium channel recruitment during the fast phase of the dendritic spike was estimated by the maximum slope of the first dendritic spike in each condition (Figure 3.6 F). None of these parameters changed significantly over time. These data prove the stability of the performed microiontophoretic stimulation.

In summary, microiontophoretic stimulation with glutamate is suitable to activate a defined ensemble of spines on a single dendrite. Sequentially increasing the microiontophoresis stimulation intensity, and hence, increasing the ejected amount of glutamate, the dendritic integration of postsynaptic signals can be investigated in CA1 PCs. Importantly, with this technique reliable, repetitive stimulation of the same spines on a dendrite is possible. Therefore, the effect of pharmacological interventions can be determined from one dendrite. Microiontophoretic stimulation is a suitable technique to investigate the role of astrocytes in modulating dendritic integration and spine size-dependent glutamate uptake.

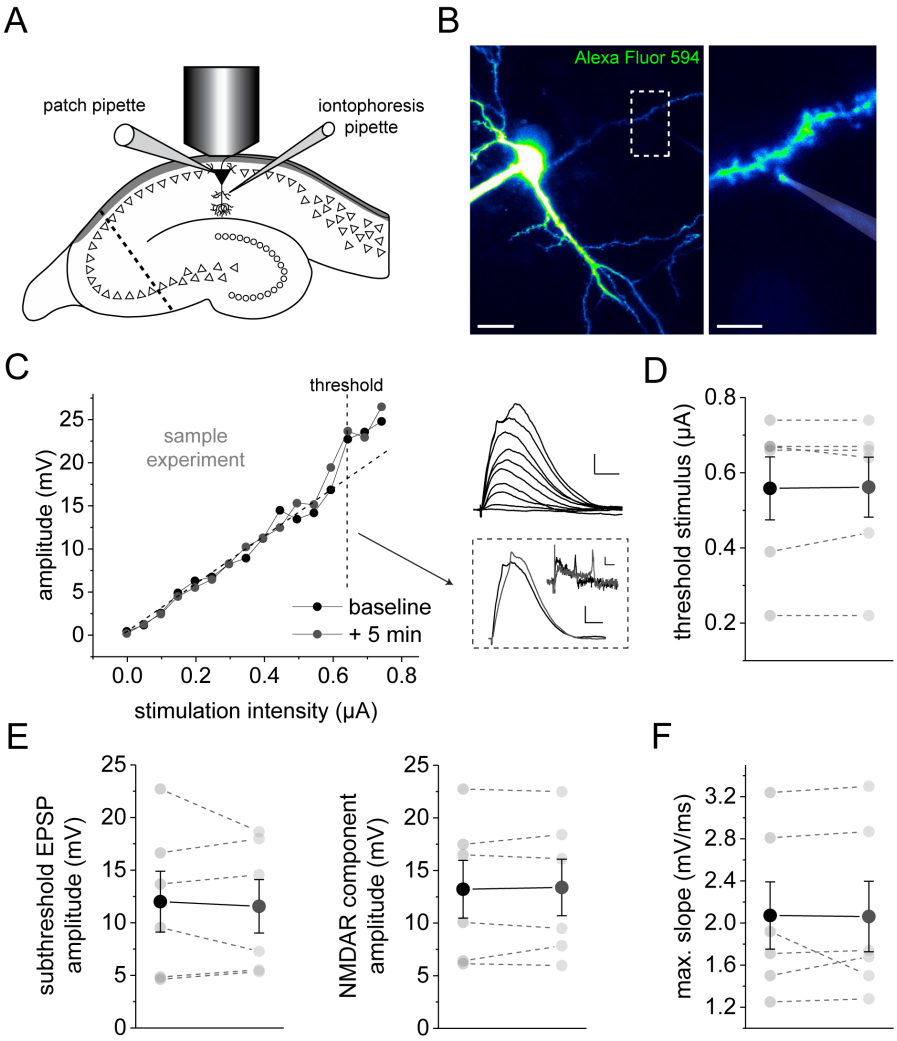

Figure 3.6. Stable evocation of dendritic spikes by microiontophoresis stimulation. (A) Schematic of the recording configuration. In the horizontal hippocampal slices, the CA3 region was separated and a CA1 pyramidal cell was whole-cell patch clamped and filled with Alexa Fluor 594 (40 µM) for visualization. The microiontophoresis pipette filled with glutamic acid (150 mM) and Alexa Fluor 594 (50 µM) was placed close to a spine on an apical oblique dendrite in the stratum radiatum. **(B)** Maximum intensity plot of a whole-cell patch clamped CA1 pyramidal cell (scale bar: 20 µm) and enlargement of the dendritic segment with the microiontophoresis pipette (scale bar: 5 µm). **(C)** Representative experiment showing the amplitude of EPSPs on a nonlinear integrating dendrite with increasing iontophoretic stimulation intensity before (black) and after a delay of five minutes (black). Right, upper inset shows the corresponding somatic voltage traces under baseline condition (scale bar: 5mV, 20ms). The first dendritic spike (threshold) is marked by the dashed line. The corresponding EPSPs for both conditions (scale bar: 5 mV, 20 ms) and their first derivative (scale bar: 1 mV/ms, 5 ms) are shown in the lower, right inset. **(D)** The stimulation intensity at the threshold of the dendritic spike (0.56 ± 0.08 µA vs. 0.56 ± 0.08 µA, n = 6, p = 0.76, paired t-test), **(E)** amplitude of large subthreshold EPSP (12.01 ± 2.89 mV vs. 11.56 ± 2.54 mV, n = 6, p = 0.64, paired t-test) and the NMDA receptor component of dendritic spikes (13.22 ± 2.74 mV vs. 13.39 ± 2.69 mV, n = 6, p = 0.63, paired t-test) as well as **(F)** the maximum slope of the first dendritic spike (2.07 ± 0.32 mV/ms vs. 2.06 ± 0.33 mV/ms, n = 6, p = 0.12, paired t-test) did not change significantly after the delay.

3.3 Glutamate Uptake and Dendritic Integration Depend on Spine Size

After establishing that microiontophoretic stimulation is a suitable technique for repeated local recruitment of locally, it was used to investigate the hypothesis of differential glutamate clearance by astrocytes depending on spine size. The majority of glutamate is taken up by astrocytes (Danbolt, 2001). Changes in the glutamate clearance in the CA1 microcircuit have been associated with, for example, differential recruitment of NMDA receptors (Katagiri et al., 2001). Since astrocytic glutamate transporters are enriched in fine perisynaptic astrocytic processes (PAPs; Sakers et al., 2017), the proximity of these to the spine have been suggested to determine the efficacy of glutamate uptake. Moreover, it has been shown that changes in plasticity are accompanied by changes in the astrocyte morphology (Bernardinelli et al., 2014; Lushnikova et al., 2009). However, it is unknown whether these changes also affect the local uptake of glutamate. Since it is assumed that plasticity also changes the size of spines, a difference in glutamate uptake between small and big spines has been suggested (Rose et al., 2018). Experiments by Michel K. Herde in our laboratory suggest that indeed the local perisynaptic glutamate concentration differs between spines of different size (Herde et al., unpublished). Whether this also results in functional different synaptic transmission is unknown.

NMDA receptor recruitment is crucial for the induction of dendritic spikes (Losonczy and Magee, 2006). NMDA receptors in CA1 pyramidal cells are not only found within the synapse but also peri- and extrasynaptic (Harris and Pettit, 2007; Petralia et al., 2010). The concentration of perisynaptic glutamate is tightly regulated by astrocytic glutamate uptake (Asztely et al., 1997). The observed increase in the perisynaptic glutamate concentration selectively at larger spines could result in an increased recruitment of extrasynaptic NMDA receptors and an increase in synaptic cross talk at selectively these spines. Accordingly, both of these effects could result in an increased probability of dendritic spike induction. To test this hypothesis, I investigated the mode of integration in relation to the size of the initially microiontophoretically stimulated spine. As described before, a CA1 PC was whole-cell patched, filled with Alexa Fluor 594 and the microiontophoresis pipetted positioned. The size of the stimulated spine could not be measured directly. The diffraction limits the z-resolution of two-photon excitation fluorescent microscopy. Therefore, an indirect, relative measurement was used to estimate the spine size. The Alexa Flour 594 intensity of the stimulated dendrite was imaged along the z-axis (Figure 3.7 A). The integral of the Gaussian curve-fitted intensity profile of several spines on a single dendrite was used to determine the relative spine size (Figure 3.7 B). The size of the stimulated spine was measured in relation to the median spine size along the dendrite. Overall, dendrites that showed a dendritic spike and supralinear integration had a significantly larger initially stimulated spine than linear integrating dendrites without dendritic spikes (Figure 3.7 C). In line with this, a significantly larger amount of the small spine (> 80 %) showed a linear integration ($p = 0.0031$, Fisher's exact test). Noteworthy, no difference in the duration of the microiontophoretic stimulation was found between both groups (0.50 ± 0.05 ms vs. 0.52 ± 0.03 ms, $n = 11/34$, $p = 0.75$, Student's t-test, data not shown) that could have confounded the observed result. These results suggest indeed, that the difference in perisynaptic glutamate concentration observed by Michel K. Herde results in an increased probability of dendritic spike induction. Furthermore, it raises the possibility that the induction of dendritic spikes is favored after LTP. However, these data do not allow conclusions to be drawn whether a differential glutamate uptake is responsible for the observed effect.

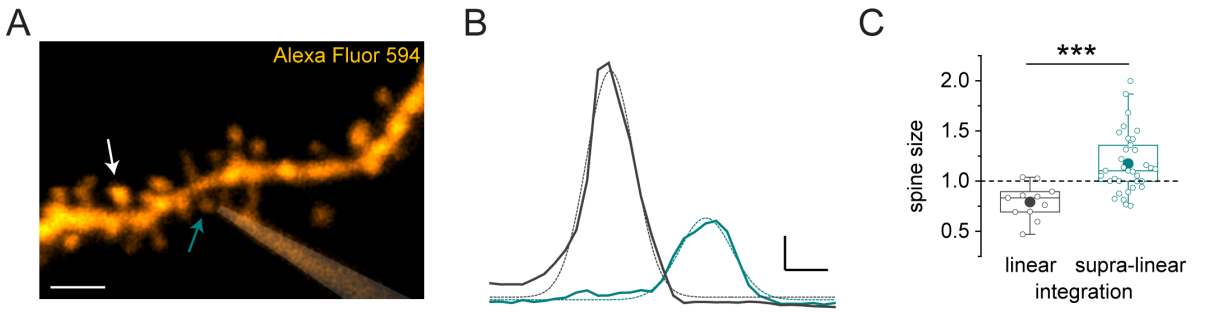

Figure 3.7. Spine size predicts of the mode of integration. (A) Maximum intensity plot of a dendrite filled with Alexa Fluor 594 (40 µM) through a whole-cell patch clamp pipette, and microiontophoresis pipette, filled with glutamic acid (150 mM) and Alexa Fluor 594 (50 µM), illustrating the different sizes of spines (white arrow – big spine, turquoise arrow – small spine, scale bar: 2µm). **(B)** Spine-size was examined through the z-axis profile of the Alexa Fluor 594 intensity (big spine – gray; small spine – turquoise). This was fitted with a Gaussian curve (dashed lines, scale bar: 1 au x 2 µm) and the integral was determined. The median integral of 5 to 15 other spines on the same dendritic segment was used to determine the relative size of the stimulated spine. **(C)** The relative size of the initially iontophoretically stimulated spine showed a significant larger relative spine size (≥ 1 big spine, < 1 small spine) in dendrites with supralinear integration compared to linear integrating dendrites without dendritic spikes (0.83 IQR 0.69-0.90 vs. 1.10 IQR 0.98-1.37, n= 11/34, $p < 0.0001$, Mann Whitney test).

To study more directly how glutamate clearance differentially modulates the activation of small and big spines, I combined whole-cell patch clamp recordings of CA1 PCs with two-photon excitation microscopy and microiontophoretic glutamate application (Figure 3.8 A). A cell was filled with Alexa Fluor 594 and the calcium indicator Fluo-4 via the patch pipette to visualize cellular morphology and monitor intracellular calcium, respectively. The microiontophoresis pipette filled with glutamate was placed in proximity of an apical oblique dendrite for stimulation of several spines at the same time (Figure 3.8 B, upper panel). The relative size of each stimulated spine was determined as described before. As a readout for the local synaptic recruitment, NMDA receptor-mediated responses were used. NMDA receptors have a high glutamate affinity and it is possibe to visualize their opening through changes in the intensity of the calcium indicator Fluo-4. Therefore, line scanning through individual spines can be used to determine their individual responses. To isolate NMDA receptor-mediated responses, the membrane potential of the whole-cell patched neuron was voltage clamped to -20 mV and voltage-gated sodium channels (VGSCs), L-type voltage-gated calcium channels (VGCCs), AMPA receptors and metabotropic glutamate receptors (mGluRs) were blocked pharmacological. The local calcium responses recorded under these conditions were mainly mediated by NMDA receptors, since blockade with the selective antagonist APV significantly reduced the calcium transient amplitude (Figure 3.8 C).

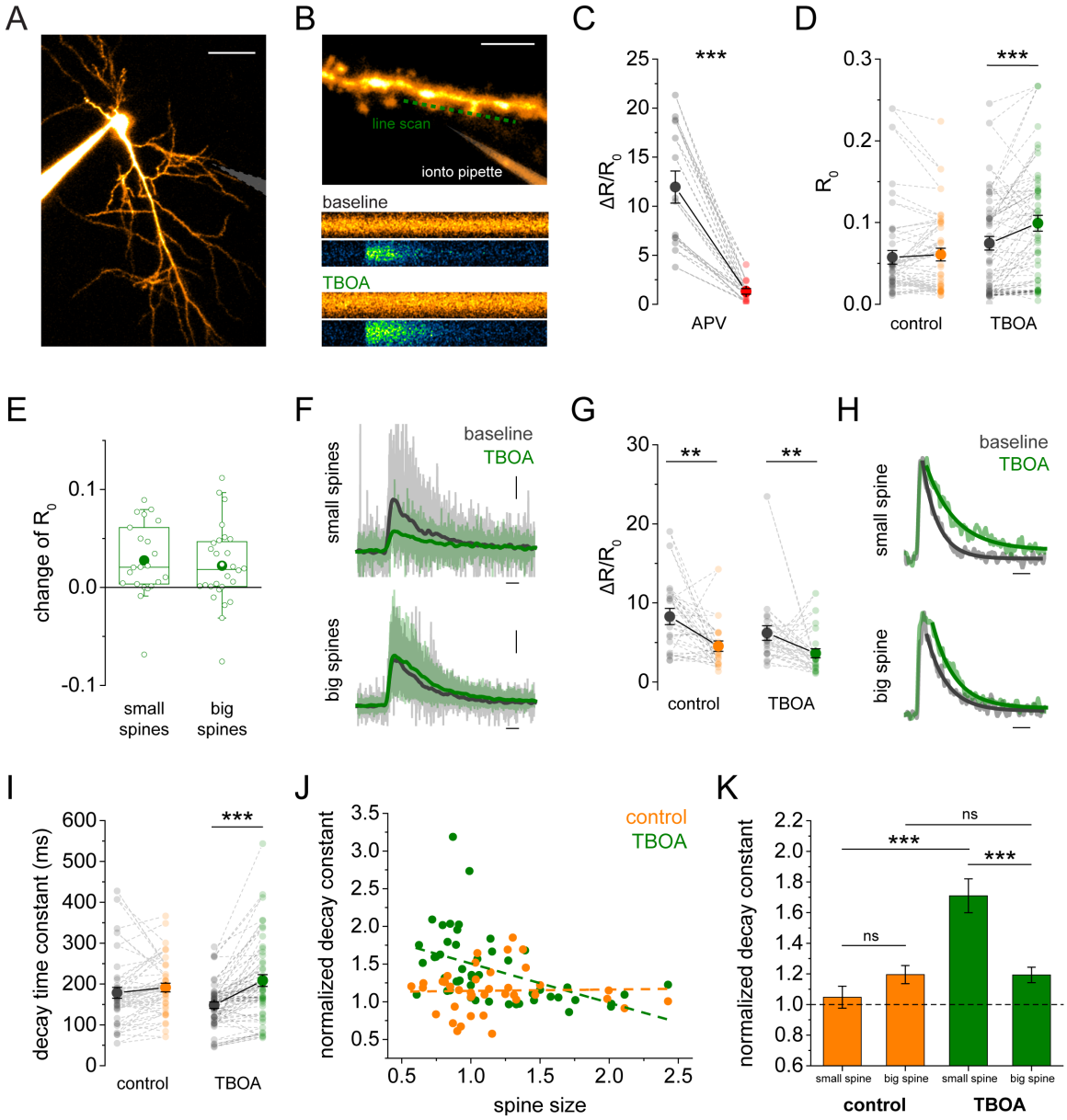

Figure 3.8. Small spines of CA1 pyramidal cells are more affected by blockade of glutamate clearance. (A) Average intensity plot of whole-cell patch clamped CA1 pyramidal cell (scale bar: 20 µm) filled with Alexa Fluor 594 (40 µM) and Fluo-4 (200 µM). **(B)** Enlargement of the dendritic segment with the microiontophoresis and line scan location (scale bar: 3 µm). Example of an intensity profile over time at baseline and after bath application of TBOA (200 nM) for Alexa Fluor 594 (orange) and Fluo-4 (green). **(C)** NMDA receptor-mediated responses were isolated by depolarizing the cell to -20 mV and the presence of blocker for mGluRs, AMPA receptors, VGSCs and L-type VGCCs. Bath application of APV significantly reduced the amplitude ΔR/R0 (11.95 ± 1.64 vs. 1.31 ± 0.28, n = 14, p < 0.0001, paired t-test). **(D)** Resting fluorescence ratio (R0) showed no difference under control conditions (0.057 ± 0.008 vs. 0.061 ± 0.008, n = 39, p = 0.40, paired t-test), but increased significantly after application of TBOA (0.075 ± 0.008 vs. 0.099 ± 0.010, n = 49, p < 0.0001, paired t-test). **(E)** No difference between the change of R0 of small and big spines was observed (0.028 ± 0.008 vs. 0.022 ± 0.008, n = 22/28, p = 0.63, Student's t-test). **(F&G)** Some traces reached saturation after application of TBOA, therefore ΔR/R0 was examined only in nonsaturated responses. **(F)** Average ΔR/R0 traces for baseline (grey) and TBOA application (green) with standard deviation for small and big spines, respectively (scale bar: 2 ΔR/R0 x 100 ms). **(G)** ΔR/R0 decreased significantly in control measurements (8.28 ± 1.02 vs. 4.53 ± 0.65, n = 20, p = 0.004, paired t-test) and after the application of TBOA (6.20 ± 0.92 vs. 3.63 ± 0.57, n = 22, p = 0.006, Wilcoxon signed rank test). **(H)** Scaled example of the response of a small and big spine with fit for the τ of the decay for baseline and after TBOA application (scale bar: 300 ms). **(I)** The decay time constant of the fluorescence ratio was unchanged in control conditions (178.50 ± 13.22 ms vs. 191.34 ± 10.63 ms, n = 39, p = 0.18, paired t-test) but significantly increased after application of TBOA (148.1 ± 7.93 ms vs. 208.5 ± 14.3 ms, n = 49, p < 0.0001, paired t-test). **(J)** The normalized decay constant showed no correlation with the spine size under control conditions (R = 0.01, p = 0.95, Spearman's rank correlation). After application of TBOA the spine size negatively correlated with the normalized decay constant (R = -0.59, p < 0.0001, Spearman's rank correlation).

(Figure legend continued on next page)

(K) Sorting spines in small and big revealed significant differences between treatment and spine size (control small 1.05 ± 0.07, n = 13; control big: 1.20 ± 0.06, n = 26; TBOA small: 1.71 ± 0.11, n = 22; TBOA big: 1.19 ± 0.05, n = 27, treatment: $p < 0.0001$, spine size: $p = 0.026$, interaction: $p < 0.0001$, two-way ANOVA). Specifically, small spines had a greater change in the decay constant compared to control experiments ($p < 0.0001$, post-hoc Tuckey test) and big spines with TBOA application ($p < 0.0001$, post-hoc Tuckey test). No difference was detected between spine size under control conditions ($p = 0.61$, post-hoc Tuckey test) and big spines between treatments ($p = 1$, post-hoc Tuckey test). *Note: The displayed results are part of the manuscript Herde et al., unpublished.*

To evaluate the role of glutamate clearance, the glutamate transporters EAAT1 and 2 were acutely blocked by bath application of TFB-TBOA and the calcium responses to iontophoretic stimulation were monitored in single spines by line scanning through them (Figure 3.8 B, lower panel). The effect of glutamate uptake blockade was examined by comparing the relative change in the local calcium response after TFB-TBOA application to that of a control recording where no drug was applied. A significant increase in the local resting calcium concentration (R0) was observed selectively after bath application of TFB-TBOA (Figure 3.8 D). However, no spine size-dependent difference was found (Figure 3.8 E). Most likely, this increase is caused by an increased recruitment of tonic NMDA receptor currents by an increase in the ambient glutamate concentration (Meur et al., 2007). The amplitude of the calcium transients showed large variations between spines (Figure 3.8 F), and an unspecific rundown in both conditions (Figure 3.8 G). Probably this effect is caused by the strong calcium influx after repetitive holding potential increases and glutamate applications at relatively distal dendrites (Rosenmund and Westbrook, 1993). The decay time constant of NMDA receptor-mediated responses has previously been used to be sensitive to changes in glutamate uptake (Armbruster et al., 2016; Romanos et al., 2019). Also in my recordings, the decay constant showed a significant increase after application of TFB-TBOA, while it remained stable under control conditions (Figure 3.8 H&I). Importantly, I observed a strong negative correlation between the normalized decay constant and the relative size of the corresponding spine only after TFB-TBOA application (Figure 3.8 J). Sorting spines according to their relative size revealed that specifically small spines were affected by the blockade of glutamate clearance.

These results suggest that iontophoretically applied glutamate has a longer dwell-time at larger spines compared to smaller ones. Furthermore, the induction of dendritic spikes is favored when relatively big spines are stimulated with the microiontophoresis. Together with the obtained data from Michel K. Herde, these observations support the hypothesis that glutamate uptake efficiency is higher at small spines than at big ones. Moreover, it suggests that astrocytes can modulate dendritic integration through the efficiency of glutamate uptake.

3.4 The Role of NMDA Receptors in Dendritic Integration

But can astrocytes also modulate dendritic integration by supplying NMDA receptor co-agonist? To address this question, I first explored the general role of NMDA receptors and the possible modulation of their recruitment during the different forms of dendritic integration. The biophysical characteristics are fundamental for the recruitment of NMDA receptors. Opening of the channel pore requires aside from glutamate also depolarization and the presence of a co-agonist (Johnson and Ascher, 1987; Matsui et al., 1995). It has been shown that both D-serine and glycine act as co-agonists of NMDA receptors. Thus, NMDA receptors are co-incidence detectors for pre- and postsynaptic activation whose recruitment can be dynamically regulated by the local co-agonist concentration. However, this required that the co-agonist binding site of NMDA receptors is not saturated. Only if an exogenously-applied co-agonist is able to modulate NMDA receptor recruitment, dynamic modulation by astrocytes is possible. The following experiments will explore this possibility for different input integrations in CA1 pyramidal cells.

3.4.1 Linear Integration in Apical Oblique Dendrites

First, the role of NMDA receptors in linear integrating dendrites was studied. In these dendrites APs were evoked before the occurrence of dendritic spikes. By gradually increasing the ejected glutamate, EPSPs of increasing size were evoked (Figure 3.9 A). Eventually the whole-cell patched neurons fired a somatic action potential (AP). This was repeated for the same dendrite after bath application of APV, a selective antagonist of NMDA receptors. To analyze the effect of the NMDA receptor blockade, the amplitude of iEPSP (small, unitary-like EPSPs) and the average amplitude of the last four EPSPs before evoking a somatic AP (subthreshold EPSPs) were used. As expected, iEPSPs showed no significant NMDA receptor-component (0.72 ± 0.13 mV vs. 0.68 ± 0.15 mV, n = 5, p = 0.62, paired t-test, not shown). However, the amplitude of subthreshold EPSPs decreased significantly after APV application (Figure 3.9 B). Having established and quantified the role of NMDA receptor recruitment in dendrites with a linear input integration, the possible modulation by NMDA receptor co-agonist supply was investigated next. Experiments were also performed under baseline condition, followed by a wash-in of saturating concentrations of D-serine (Figure 3.9 C). Accordingly, this should maximize the recruitment of NMDA receptors, if the co-agonist binding site is not already saturated under baseline condition. Expectedly, AMPA receptor-mediated iEPSPs remained unchanged by this treatment (0.98 ± 0.18 mV vs. 0.98 ± 0.13 mV, n = 5, p = 0.97, paired t-test, not shown). In contrast to blocking NMDA receptors, saturating the co-agonist site did not significantly change the subthreshold EPSP amplitude (Figure 3.9 D).

These results suggest that while NMDA receptors are efficiently recruited during synaptic activation of spines in linear integration dendrites, a modulation by additional release of NMDA receptor co-agonists, like D-serine or glycine, is not possible. Accordingly, astrocytes will not be able to dynamically modulate linear integration through the calcium-dependent release of D-serine.

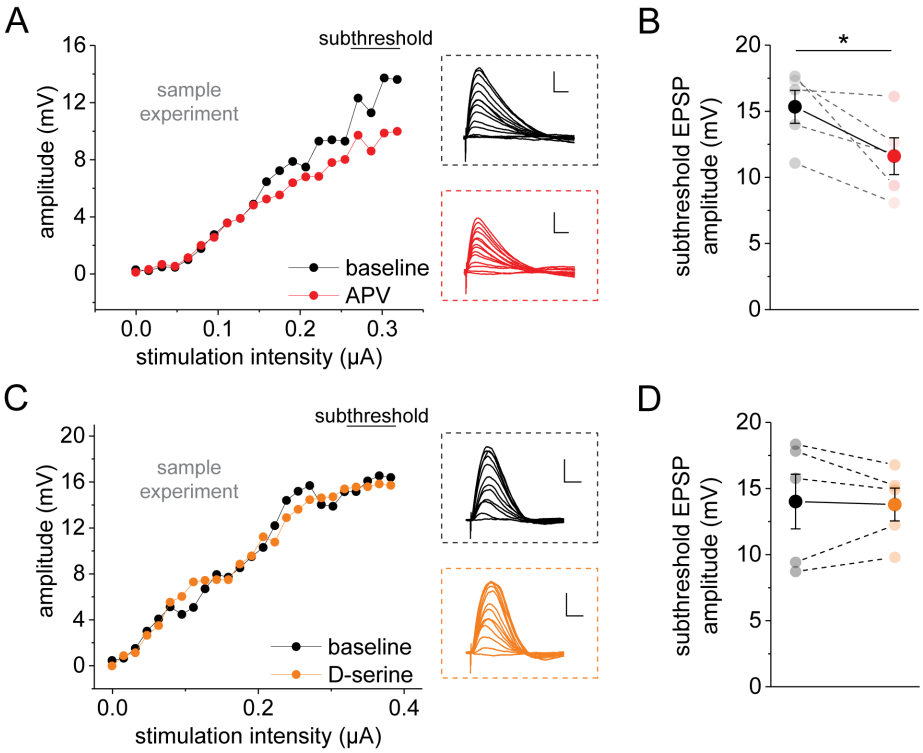

Figure 3.9. The role of NMDA receptors in linear dendritic integration. (A) Sample experiment showing the relationship between somatic amplitude and iontophoretic stimulation intensity of a linear integrating dendrite before (black) and after wash-in of the NMDA receptor antagonist APV (50 µM, red). The insets show the corresponding somatic traces (scale bar: 5 mV, 20 ms). **(B)** Large EPSPs (average of last four EPSPs before occurrence of an action potential, subthreshold EPSPs) had an APV-sensitive component (15.33 ± 1.24 mV vs. 11.60 ± 1.40 mV, n = 5, p = 0.047, paired t-test). **(C)** Amplitude of the somatically recorded voltage in dependency of the iontophoretic stimulation intensity in a sample experiment of a linear integrating dendrite before (black) and after wash-in of saturating concentrations of the NMDA receptor co-agonist D-serine (10 µM, orange). The insets show the recorded somatic potentials for both conditions (scale bar: 5 mV, 20 ms). **(D)** The amplitude of subthreshold EPSPs (14.02 ± 2.07 mV vs. 13.79 ± 1.24 mV, n = 5, p = 0.82, paired t-test) did not change significantly after the application of D-serine.

3.4.2 Supralinear Integration in Apical Oblique Dendrites

Next, the role of NMDA receptors and their co-agonists in supralinear integrating dendrites was determined. As parameters the stimulation intensity for the first dendritic spike (threshold stimulus), the amplitude of iEPSPs, subthreshold EPSPs (without dendritic spike) and the NMDA receptor component of the dendritic spike, as well as the maximum slope of the first dendritic spike were used. After recording the initial integration of a dendrite, NMDA receptors were blocked by bath application of APV (Figure 3.10 A). This resulted in a significantly higher stimulation intensity, and hence, a larger amount of glutamate, needed to evoke the first dendritic spike (Figure 3.10 B). While the amplitude of iEPSPs remained stable (1.08 ± 0.12 mV vs. 0.96 ± 0.11 mV, n = 16, p = 0.32, paired t-test, not shown), the amplitude of subthreshold EPSPs (Figure 3.10 C, left panel) and of the dendritic spike's NMDA receptor component were significantly reduced (Figure 3.10 C, right panel). Surprisingly, the maximum slope of the dendritic spike was also reduced by NMDA receptor blockade (Figure 3.10 D), although this parameter is thought to depend on the recruitment of voltage-gated sodium channels. Overall, these results highlight the importance of NMDA receptor recruitment for supralinear dendritic integration and the initiation of dendritic spikes.

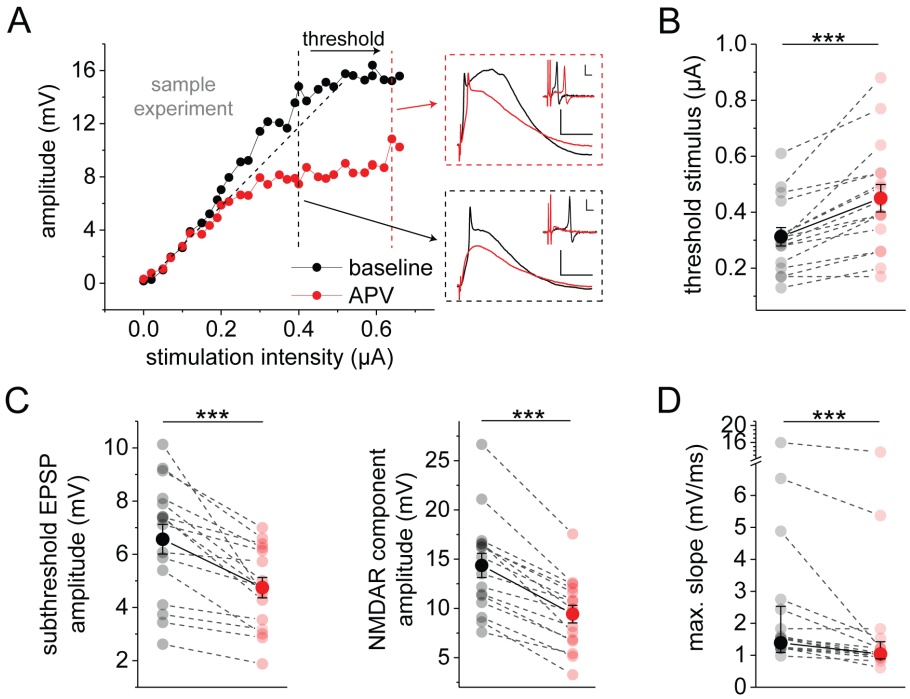

Figure 3.10. NMDA receptors play a key role in nonlinear dendritic integration. (A) Representative example of the relationship between iontophoretic stimulation intensity and somatic EPSP amplitude for a nonlinear integrating dendrite before (black) and after application of the NMDA receptor antagonist APV (50 µM, red). The first dendritic spike in each condition is marked by a color-coded dashed line, corresponding somatic traces for both conditions (scale bar: 5 mV, 20 ms) and their first derivative (scale bar: 5 mV/ms, 2 ms) are displayed. **(B)** The stimulation intensity at the threshold was significantly increased after blockade of NMDA receptors by APV (0.31 ± 0.03 µA vs. 0.45 ± 0.05 µA, n = 16, p < 0.0001, paired t-test). **(C)** The amplitude of subthreshold EPSP (6.56 ± 0.56 mV vs. 4.75 ± 0.38 mV, n = 16, p = 0.0001, paired t-test) and of the NMDA receptor component of dendritic spikes (14.36 ± 1.23 mV vs. 9.42 ± 0.90 mV, n = 16, p < 0.0001, paired t-test) showed a significant decrease. **(D)** The maximum slope was significantly reduced by APV application (1.39 IQR 1.09-2.53 mV/ms vs. 1.04 IQR 0. 89-1.42 mV/ms, n = 16, p < 0.0001, Wilcoxon signed-rank test).

It is known that NMDA receptors are formed by different subunits (Ascher and Nowak, 2009; Paoletti and Neyton, 2007) whereby the subunit composition can influence several biophysical characteristics of the receptor. Furthermore, a distinct relevance of GluN2B subunit in modulating synaptic plasticity has been suggest (Foster et al., 2010). To investigate the role of the GluN2B subunit of NMDA receptors in dendritic integration, a selective blocker, Ro 25-6981, was bath applied (Figure 3.11 A). Small iEPSPs did not change their amplitude in the presence of the GluN2B antagonist (1.04 ± 0.11 mV vs. 0.95 ± 0.09 mV, n = 15, p = 0.33, paired t-test, not shown). Similar to the results obtained with APV, Ro 25-6981 caused a significant increase in the threshold stimulus of dendritic spikes (Figure 3.11 B). In line with this, the amplitude of subthreshold EPSPs (Figure 3.11 C, left panel) and of the NMDA receptor component of dendritic spikes decreased significantly (Figure 3.11 C, right panel). In contrast to the general blockade of NMDA receptors, the maximum slope of the first dendritic spike was not influenced by selective impairment of GluN2B-containing NMDA receptors (Figure 3.11 D). This suggests that receptors containing the GluN2A-subunit in particular could modulate the recruitment of VGSCs.

Some studies have indicated an enrichment of GluN2B receptors at the peri- and extrasynaptic sites (Stocca and Vicini, 1998). This would imply that the discovered differential glutamate uptake and the proposed increase in recruitment of extrasynaptic NMDA receptors could also specifically modulate the recruitment of GluN2B-containing NMDA receptors during supralinear dendritic integration specifically. To investigate this hypothesis, the relationship between the size

of the stimulated spine and the effect of Ro 25-6981 on the threshold stimulus was investigated. However, no correlation was found (R = -0.03, n = 13, p = 0.90, Spearman's rank correlation). Accordingly, GluN2B-containing NMDA receptors are not recruited differentially in small and big spines for the initiation of dendritic spikes.

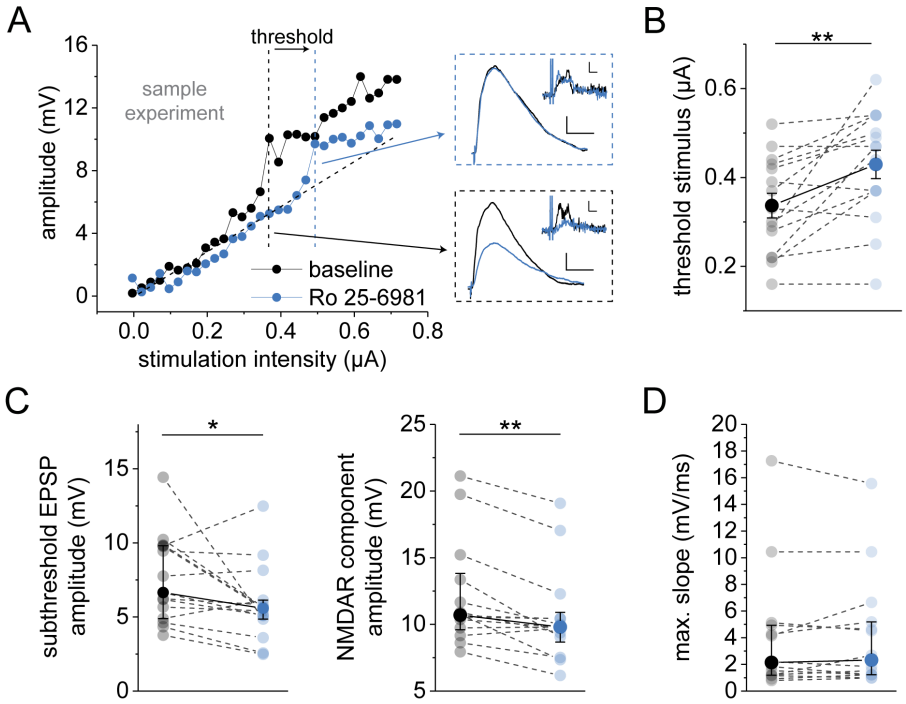

Figure 3.11. The GluN2B subunit is important for nonlinear dendritic integration. (A) Representative example of the relationship between iontophoretic stimulation intensity and somatic EPSP amplitude for a nonlinear integrating dendrite before (black) and after wash-in of the selective GluN2B-containing NMDA receptor antagonist Ro 25-6981 (0.5 µM, blue). The first dendritic spike is marked color-coded by a dashed line, corresponding somatic traces (scale bar: 2 mV, 20 ms) and their first derivative (scale bar: 1 mV/ms, 2 ms) are displayed. **(B)** The stimulation intensity at the threshold was significantly increased after blockade of NMDA receptors containing the GluN2B subunit (0.34 ± 0.03 µA vs. 0.43 ± 0.03 µA, n = 15, p = 0.0035, paired t-test). **(C)** The amplitude of subthreshold EPSP (6.65 IQR 4.89-9.81 mV vs. 5.58 IQR 4.86-6.14 mV, n = 15, p = 0.0256, Wilcoxon signed-rank test) and of the NMDA receptor component of dendritic spikes (10.7 IQR 9.60-13.83 mV vs. 9.8 IQR 8.675-10.90 mV, n = 15, p = 0.0012, Wilcoxon signed-rank test) showed a significant decrease. **(D)** The maximum slope of the first dendritic spike was not influenced by Ro 25-6981 application (2.14 IQR 1.19-4.94 mV/ms vs. 2.32 IQR 1.22-5.19 mV/ms, n = 15, p = 1, Wilcoxon signed-rank test).

My results showed the importance of NMDA receptors in supralinear dendritic integration and dendritic spikes. Therefore, a potential dynamic modification for example by astrocytic release of the NMDA receptor co-agonists D-serine, was next investigated. This means that the binding site should not be saturated under baseline conditions and a higher concentration of NMDA receptor co-agonists will further increase the recruitment of NMDA receptors. Using saturating concentrations of the co-agonist D-serine the maximum possible NMDA receptor recruitment was studied (Figure 3.12 A). Under these conditions, evoking a dendritic spike required significantly less glutamate compared to the integration in physiological D-serine concentrations (Figure 3.12 B). As expected by the results from blocking NMDA receptors, the amplitude of iEPSP remained unaffected (1.11 ± 0.13 mV vs. 0.93 ± 0.10 mV, n = 15, p = 0.11, paired t-test, not shown). Notably, the amplitude of both, subthreshold EPSP (Figure 3.12 C, left panel) and of the dendritic spike NMDA receptor component increased significantly (Figure 3.12 C, right panel). Furthermore, the maximum slope of the dendritic spike was significantly increased (Figure 3.12 D). These results

confirm the hypothesis that the binding site of NMDA receptor co-agonists at supralinear integrating dendrites is normally not saturated. Accordingly, calcium-dependent release of D-serine by astrocytes could potentially modulate dendritic integration.

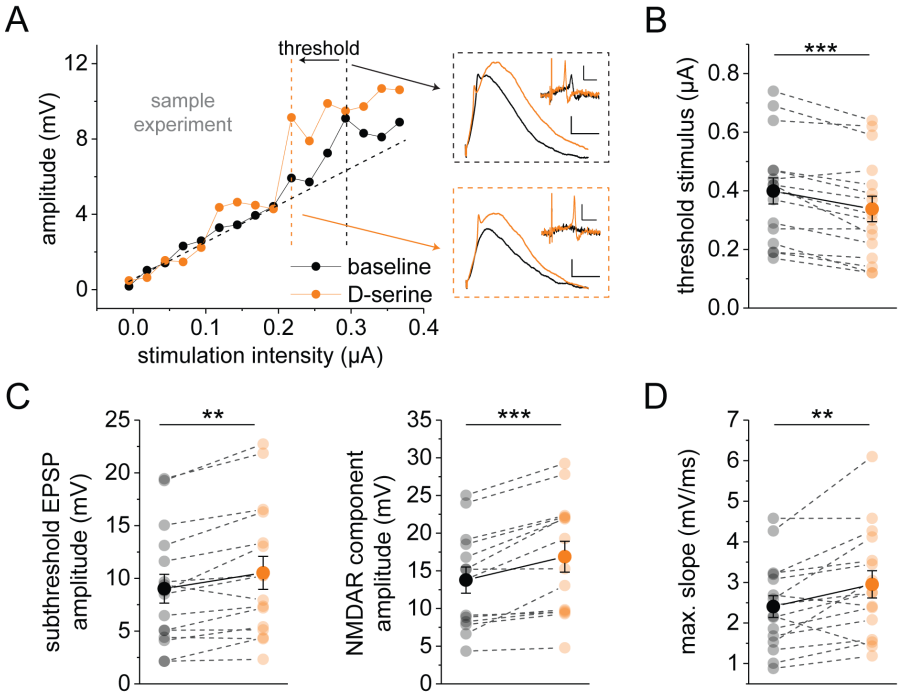

Figure 3.12. The NMDA receptor co-agonist D-serine promotes supralinear dendritic integration. (A) Representative example of the relationship between iontophoretic stimulation intensity and somatic EPSP amplitude for a nonlinear integrating dendrite before (black) and after wash-in of saturating concentrations of the NMDA receptor co-agonist D-serine (10 µM, orange). The first dendritic spike is marked by a color-coded dashed line and the corresponding somatic traces (scale bar: 2 mV, 20 ms) and their first derivative (scale bar: 2 mV/ms, 5 ms) are displayed. **(B)** The stimulation intensity at threshold was significantly decreased after D-serine application (0.40 ± 0.04 µA vs. 0.34 ± 0.04 µA, n = 15, p = 0.0001, paired t-test). **(C)** The amplitude of subthreshold EPSP (9.02 ± 1.37 mV vs. 10.52 ± 1.57 mV, n = 15, p = 0.0010, paired t-test) and of the NMDAR component of dendritic spikes (13.77 ± 1.73 mV vs. 16.87 ± 2.05 mV, n = 15, p = 0.0002, paired t-test) showed a significantly increased. **(D)** The maximum slope of the first dendritic spike was increased by D-serine (2.42 ± 0.27 mV/ms vs. 2.95 ± 0.34 mV/ms, n = 15, p = 0.0063, paired t-test).

In summary, these results show that NMDA receptors recruitment is essential for both linear and supralinear dendritic integration. In supralinear integrating dendrites the GluN2B-containing NMDA receptors contributed to most of the parameters studied. However, the maximum slope of the fast, sodium-mediated component of the dendritic spikes was uninfluenced. This suggests that specifically GluN2A-containing receptors modulate the recruitment of sodium influx. Notably, NMDA receptor co-agonists could modulate only supralinear integration with dendritic spike. Particularly surprising was that subthreshold EPSPs of supralinear integrating dendrites were also increased in their amplitude, while subthreshold EPSPs in linear integrating ones were not. This suggests that the co-agonist concentration at dendrites with and without dendritic spikes is differentially regulated. Only the former was not saturated during the initial recording. Accordingly, only supralinear dendritic integration can be controlled by the occupancy of the NMDA receptor co-agonist binding site. This suggests that astrocytes could specifically modulate this form of dendritic integration.

3.4.3 TUFT PLATEAUS – SUPRALINEAR INTEGRATION IN APICAL TUFT DENDRITES

Not only apical oblique dendrites but also apical tuft dendrites integrate inputs in a supralinear fashion. Dual stimulation of the Schaffer collaterals and the perforant path has been shown to evoke calcium plateau potentials in the tuft dendrites (Takahashi and Magee, 2009). NMDA receptors are essential of the induction of dendritic plateau potentials. Therefore, it was investigated whether apical tuft plateau potentials can be dynamically modified by supply of NMDA receptor co-agonists. CA1 PCs were whole-cell patched and filled with Alexa Fluor 594 and Fluo-4 (Figure 3.13 A&B). A bipolar stimulation electrode was placed in the stratum radiatum and a monopolar stimulation electrode in the stratum lacunosum moleculare. The Schaffer collateral and perforant path fibers were stimulated with five trains of five 100 Hz stimuli with a 200 ms interval between trains (Figure 3.13 C). During this stimulation paradigm, line scanning of the calcium-sensitive dye Fluo-4 and the calcium-insensitive dye Alexa Fluor 594 in a tuft dendrite was performed (Figure 3.13 D). This was repeated in the presence of saturating concentrations of D-serine and after application of the NMDA receptor blocker APV. The integral of the fluorescent intensity ratio (Fluo-4/Alexa Fluor 594, background-subtracted) showed a significant increase when the NMDA receptor co-agonist binding site was saturated with D-serine (Figure 3.13 E). Expectedly, blockade of the NMDA receptor resulted in a significant decrease. The probability of evoking a dendritic plateau was significantly increased by saturating concentrations of D-serine (0.45 ± 0.06 vs. 0.68 ± 0.04, n = 7, p = 0.005, paired t-test, not shown). The highest probability of plateau initiation under control conditions was during the fifth train (0.79 ± 0.08, n = 7). The effect of the D-serine application on the shape of dendritic plateau potentials was investigated in detail (Figure 3.13 F). All parameters, the area, peak amplitude and full-width at half maximum amplitude (FWHM), showed a significant increase after bath application of saturating concentrations of D-serine. Likewise, the somatically recorded potential showed a significant increase in the area and FWHM after D-serine application (Figure 3.13 G). In turn, NMDA blockade resulted in a significant decrease. These experiments indicate that dendritic plateau potentials in the tuft dendrites can be dynamically regulated in their occurrence and shape by NMDA receptor co-agonist supply.

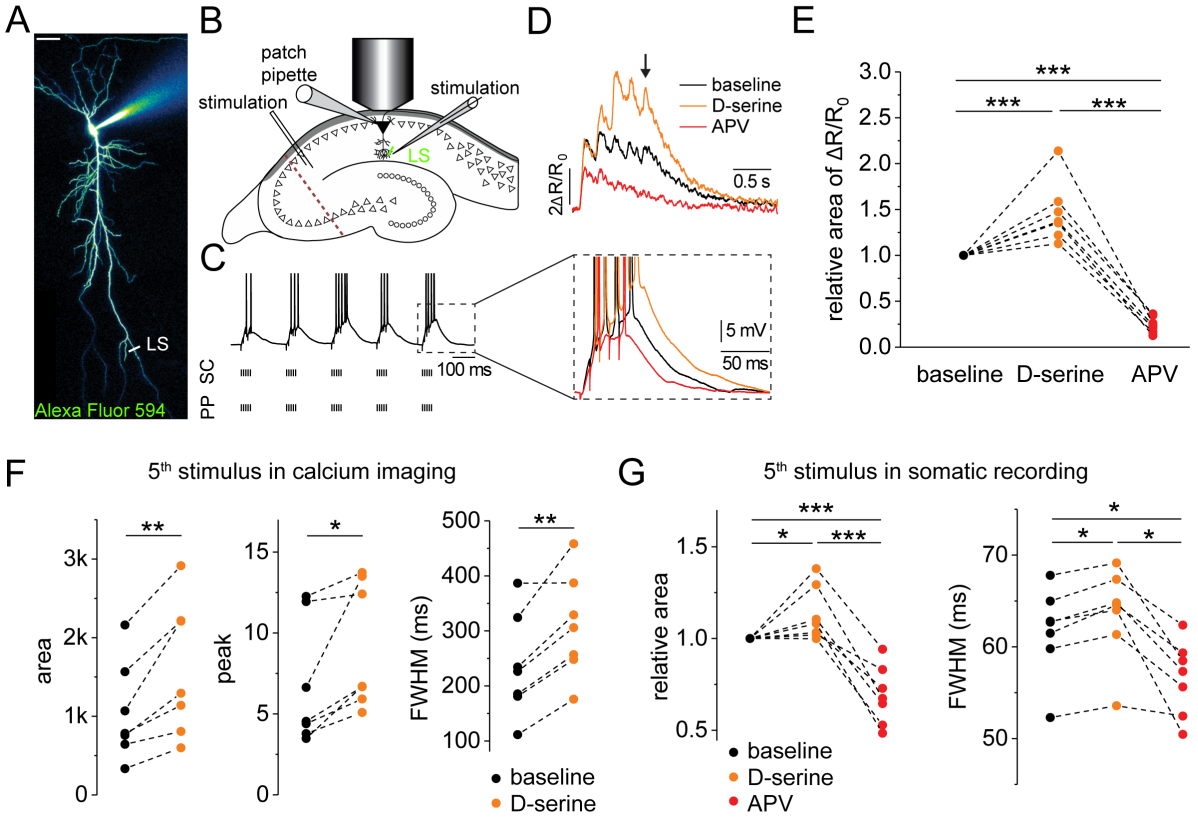

Figure 3.13. Calcium plateaus in the apical tuft dendrites can be modulated by co-agonist supply. (A) Representative CA1 pyramidal cell filled with Alexa Flour 594 (80 µM) and Fluo-4 (400 µM) via the whole-cell patch clamp pipette (scale bar: 50 µm). **(B)** Schematic of the recording configuration. A CA1 pyramidal cell was whole-cell patched, filled and stimulated with a bipolar stimulation electrode via the Schaffer collaterals (SC) and with a monopolar stimulation electrode via the perforant path (PP). During the stimulation, line scans of the fluorescence intensities in an apical tuft dendrite were performed. **(C)** Representative trace of somatic voltage during the dual pathway stimulation with five trains of five stimuli at 100Hz with a 200ms inter-train interval. The 5th burst is enlarged and shown for the three different conditions examined: baseline, bath application of saturated D-serine (10µM) and NMDA receptor blockade by APV (50 µM). **(D)** Representative trace of the fluorescence intensity ratio (Fluo-4/Alexa Flour 594, background-subtracted) during the line scan recording. The arrow illustrates the 5th train of stimulation. **(E)** The total area of the intensity ratio was normalized to the baseline condition and compared between treatments (n = 7, p = 0.00006, one-way repeated measure ANOVA with Greenhouse-Geisser correction). After saturating the NMDA receptor co-agonist binding site, the area of the intensity ratio increased significantly (1.47 ± 0.13, n = 7, p = 0.0006, post-hoc Fisher's LSD). The blockade of NMDA receptors resulted in a significant reduction in the area compared to both conditions (0.24 ± 0.03, n = 7, p < 0.001, post-hoc Fisher's LSD). **(F)** If only the 5th stimulation train was examined, the intensity ratio showed a significant increase in area (1045 ± 236 vs. 1597 ± 324, n = 7, p = 0.0048, paired t-test), peak (6.72 ± 1.44 vs. 9.15 ± 6.71, n = 7, p = 0.024, paired t-test) and full-width at half maximum (FWHM, 235.7 ± 35.06 ms vs. 308.70 ± 35.50 ms, n = 7, p = 0.0029, paired t-test). **(G)** Likewise, the change in somatically-recorded membrane potential during the 5th stimulation train resulted in significant differences in the relative area (n = 7, p = 0.00002, one-way repeated measurement ANOVA) and FWHM (n = 7, p = 0.002, Friedman ANOVA) between the treatments. In saturated D-serine, both parameters showed a significant increase (n = 7, area: p = 0.044, post-hoc Fisher's LSD; FWHM: p = 0.016, post-hoc Wilcoxon signed-rank test) and with NMDA receptor blockade a significant decrease (n = 7, area: p < 0.001, post-hoc Fisher's LSD; FWHM: p = 0.031/0.016, Wilcoxon signed-rank test).

3.5 Cannabinoid-Signaling Promotes Supralinear Integration

The results so far showed that exogenously applied, saturating concentrations of the NMDA receptor co-agonist D-serine can positively modulate dendritic integration in apical oblique and tuft dendrites. Although these results proof that the NMDA receptor co-agonist binding site is normally not saturated, no conclusion can be drawn as to whether this modulation can be recruited by astrocytes. Therefore, I investigated next, if endogenously, astrocytic-released NMDA receptor co-agonists can influence the dendritic integration in apical oblique dendrites of CA1 pyramidal cells. Calcium transients are required for the release of gliotransmitters by astrocytes (Guerra-Gomes et al., 2018). Data from our lab and others have shown that the activation of astrocytic cannabinoid 1 (CB1) receptor results in an increase of the intracellular calcium concentration (Figure 1.8; Navarrete and Araque, 2008; Robin et al., 2018; Schönhense, 2015). Increases in astrocytic calcium concentration are known to be essential for the release of the NMDA receptor co-agonist D-serine (Henneberger et al., 2010). Additionally, some studies have also suggested the release of D-serine by astrocytes through the activation of CB1 receptors (Andrade-Talavera et al., 2016; Robin et al., 2018). Therefore, the activation of CB1 receptors was used to investigate, if also endogenously released NMDA receptor co-agonists are also able to control dendritic integration.

The effect of the CB1 receptor agonist WIN 55,212-2 on supralinear dendritic integration was investigated as described before (Figure 3.14 A). Application of WIN 55,212-2 decreased the threshold stimulus for dendritic spikes significantly (Figure 3.14 B). The amplitude of iEPSPs (0.88 ± 0.08 mV vs. 0.83 ± 0.09 mV, n = 0.9, p = 0.54, paired t-test, not shown) was unchanged but significantly increased for subthreshold EPSP (Figure 3.14 C, left panel) and the NMDA receptor component of dendritic spikes (Figure 3.14 C, right panel). The maximum slope was significantly enhanced by the treatment as well (Figure 3.14 D).

While these results suggest a modulation of the dendritic integration by the release of NMDA receptor co-agonists, the possibility of CB1 receptors dependent release of glutamate should be considered (Gómez-Gonzalo et al., 2015; Han et al., 2012; Navarrete and Araque, 2008, 2010). An increase in the local glutamate concentration would likely also result in an increased recruitment of NMDA receptors and could cause a similar result. To exclude that the observed effect is caused by the release of other compounds, the experiment was repeated in the presence of saturating concentrations of D-serine. Prior saturation of the NMDA receptor co-agonist binding site should occlude all effects previously caused by NMDA receptor co-agonist release. However, if, for example, glutamate is released by astrocytes, the positive modulation caused by the activation of CB1 receptors should still be observed. WIN55,212-2 had no longer an effect on the integration when applied in saturating concentrations of D-serine (Figure 3.14 B-D). Accordingly, the observed effect on the dendritic integration is not caused by the release of other gliotransmitter.

Overall, these experiments strongly support my hypothesis that astrocytes can modulate supralinear dendritic integration. Through the activation of CB1 receptors, calcium transients are evoked that result in the release of NMDA receptor co-agonists. These NMDA receptors co-agonists cause an increased recruitment of NMDA receptors during the simultaneous activation of a cluster of spines. Hence, a positive modulation of supralinear dendritic integration is observed. This means that dendritic spikes can be evoked with less glutamate (lower threshold stimulus). Furthermore, the amplitude of the slow, NMDA receptor-mediated component of the dendritic spike is increased. Since dendritic spikes have been shown to increase the AP firing in

vivo (Palmer et al., 2014; Smith et al., 2013), it is likely that astrocytic modulation of supralinear dendritic integration will change the AP output of the CA1 microcircuit when recruited. This immediately raises the question under which behavioral conditions astrocytic CB1 receptors are activated and supralinear dendritic integration modulated.

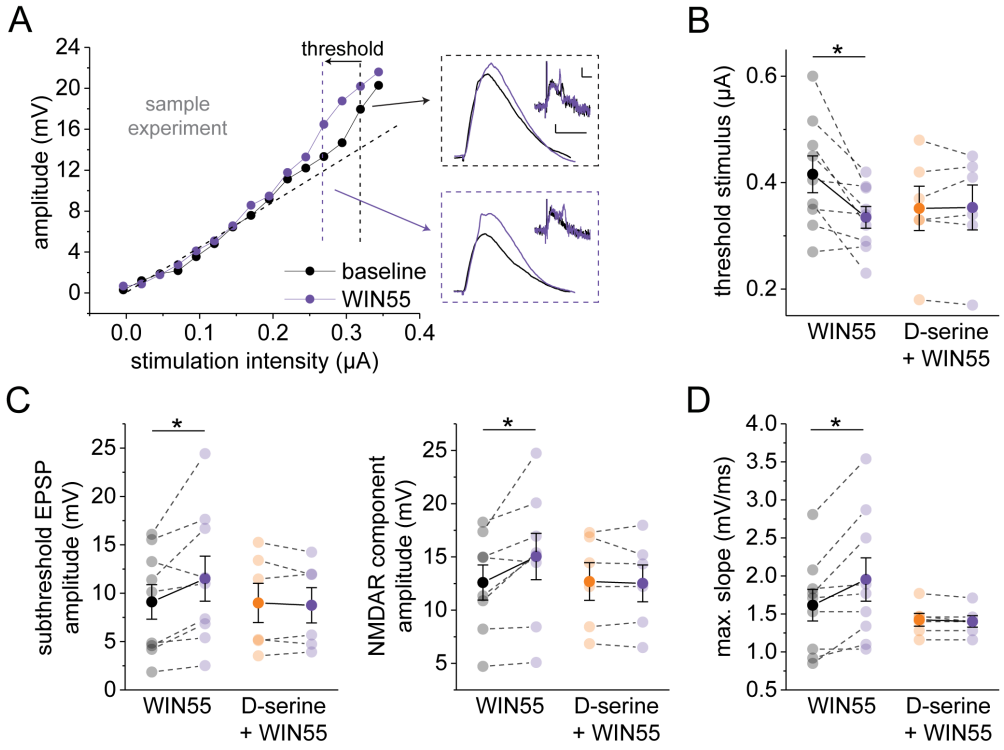

Figure 3.14. Activation of CB1 receptors promotes dendritic integration via NMDA receptor co-agonist. (A) Representative example of the relationship between iontophoretic stimulation intensity and somatic EPSP amplitude for a nonlinear integrating dendrite before (black) and after wash-in of the CB1 receptor agonist WIN 55,212-2 (1 µM, purple). The first dendritic spike is marked by a color-coded dashed line and the corresponding somatic traces (scale bar: 2 mV, 20 ms) and their first derivative (scale bar: 1 mV/ms, 5 ms) are displayed. **(B)** The stimulation intensity at threshold was significantly decreased after application of the CB1 receptor agonist (0.42 ± 0.03 µA vs. 0.33 ± 0.06 µA, n = 9, p = 0.012, paired t-test). If the CB1 receptor agonist WIN 55,212-2 was applied in presence of saturating concentrations of D-serine (10 µM) this effect was occluded (orange: 0.35 ± 0.04 µA vs. purple: 0.35 ± 0.04 µA, n = 6, p = 0.87, paired t-test). **(C)** The amplitude of subthreshold EPSP showed a significantly increase with application of the CB1 receptor agonist but not when the NMDA receptor co-agonist site was saturated (control: 9.10 ± 1.78 mV vs. 11.50 ± 2.32 mV, n = 9, p = 0.040, paired t-test; D-serine: 9.00 ± 2.03 mV vs. 8.75 ± 1.82 mV, n = 6, p = 0.52, paired t-test). The same effect was observed for the NMDA receptor component of dendritic spikes (control: 12.59 ± 1.65 mV vs. 15.04 ± 2.18 mV, n = 9, p = 0.034, paired t-test; D-serine: 12.69 ± 1.77 mV vs. 12.52 ± 1.73 mV, n = 6, p = 0.64, paired t-test). **(D)** The maximum slope of the first dendritic spike was increased by WIN 55,212-1 application under control condition (1.61 ± 0.21 mV/ms vs. 1.95 ± 0.28 mV/ms, n = 9, p = 0.018, paired t-test) but unchanged in D-serine (1.42 ± 0.08 mV/ms vs. 1.40 ± 0.08 mV/ms, n = 6, p = 0.18, paired t-test).

3.6 CA1 Network Activity Modulates Dendritic Integration

To unravel the behavior that results in the mobilization of endocannabinoids, recruits astrocytic calcium transients and subsequently modulates dendritic integration, I first explored behavioral relevant stimuli in situ. Endogenous cannabinoids are typically produced and mobilized during depolarization and/or AP firing of neurons (Ohno-Shosaku et al., 2001). Since their lipophilic structure limits their action range to only a few micrometers (Chevaleyre and Castillo, 2003), mobilization of endocannabinoids needs to occur within the astrocytic territory. Accordingly, depolarization would be required not only at the soma but also in the dendrites located in the stratum radiatum. Therefore, several stimulation paradigms were investigated for their potential role in modulating dendritic integration.

3.6.1 Depolarization of a Single Neuron Does not Regulate Dendritic Integration

Astrocytic and neuronal CB1 receptors have been shown to be recruited during the depolarization of a single neuron (Lenz and Alger, 1999; Navarrete and Araque, 2008; Ohno-Shosaku et al., 2001). However, is this sufficient to recruit NMDA receptor co-agonist release from astrocytes in the stratum radiatum and to subsequently affect dendritic integration? To address this question, subthreshold EPSPs and dendritic spikes were evoked iontophoretically before and after a whole-cell patched CA1 PC was depolarized by a current injection to fire APs (Figure 3.15 A). The amplitude of subthreshold EPSP (Figure 3.15 B, left panel) and the maximum slope of the dendritic spikes (Figure 3.15 C) remained uninfluenced by the neuronal depolarization. Surprisingly, the amplitude of the dendritic spike's NMDA receptor component showed a significant decrease (Figure 3.15 B, right panel). One possible explanation for this effect is that the prolonged depolarization and bAPs could have caused the recruitment of small conductance calcium-activated potassium channels (SK channels; Jones and Stuart, 2013). Owing to their functional coupling to NMDA receptors, the activation of these channels is known to reduce the NMDA receptor-mediated current (Ngo-Anh et al., 2005). Nonetheless, it can be concluded that the depolarization of a single neuron is not capable to enhance its supralinear dendritic integration.

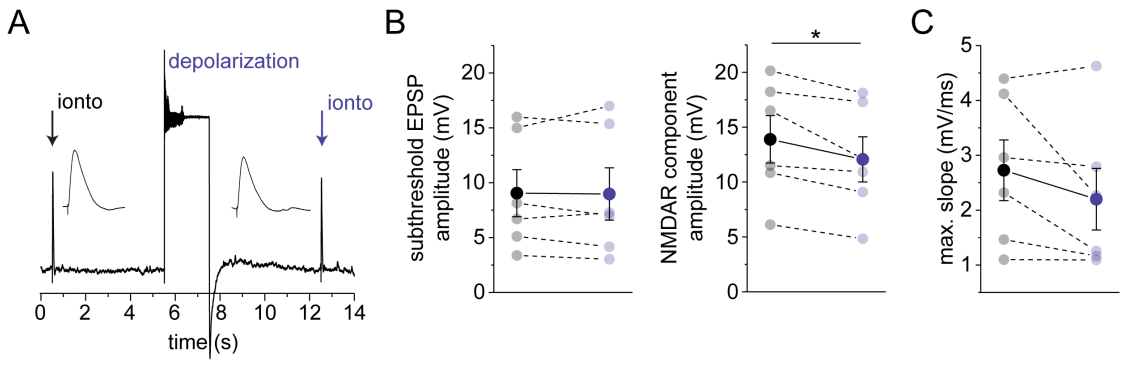

Figure 3.15. Depolarization of a single cell is insufficient to strengthen dendritic integration. (A) The influence of depolarizing a single neuron on dendritic integration was investigated by iontophoretic application of glutamate before (black) and after the whole-cell patched neuron was depolarized for two seconds with a somatic current injection to evoke action potential firing (purple). **(B)** While the amplitude of subthreshold EPSPs remained uninfluenced by the depolarization (9.05 ± 2.14 mV vs 8.97 ± 2.38 mV, n = 6, p = 0.87, paired t-test), the NMDA receptor component of the dendritic spike was significantly decreased after depolarization (13.89 ± 2.16 mV vs. 12.06 ± 2.05 mV, n = 6, p = 0.022, paired t-test). **(C)** The maximum slope of the dendritic spike showed no significant difference (2.73 ± 0.55 mV/ms vs. 2.20 ± 0.56 mV/ms, n = 6, p = 0.16, paired t-test). Ionto, iontophoretic application of glutamate.

3.6.2 Retrograde Activation of Pyramidal Cells to Mobilize Endocannabinoids

Since the depolarization of a single neuron was not able to modulate supralinear dendritic integration, the potential impact of AP firing of an ensemble of CA1 PCs was investigated. It is known that the mobilization of endocannabinoids is depending on the number and frequency of APs (Dubruc et al., 2013; Fortin et al., 2004). To test the role of different behavioral relevant neuronal activity, I wanted to activate CA1 PCs at frequencies commonly observed in regular firing patterns. During distinct tasks and behaviors, oscillations in the delta, beta, theta and low-gamma frequency band can be observed in the hippocampus (Berke et al., 2008; Senior et al., 2008; Winson, 1974; Wolansky et al., 2006). By stimulating CA1 PCs for one second with these frequencies, the potency of different AP number and frequency in modulating supralinear dendritic integration was studied.

Recruitment of neuronal ensembles can be achieved through either through orthodromic or antidromic stimulation. To avoid confounding effects caused by synaptic recruitment, antidromic stimulation of the CA1 PC axons was used. The axons of CA1 PCs are bundled in the alveus. To activate a population of CA1 PCs a bipolar stimulation electrode was placed in the alveus at the border of CA1 and the subiculum (Figure 3.16 A&B). At this border, a small incision in the stratum oriens was made to avoid unintended recruitment of other fibers that could result in synaptic activation of CA1 PCs. To analyze the recruitment, a field electrode was placed at the boarder of stratum pyramidale and oriens of CA1 to monitor the evoked population spikes. The shape of the population spike alone already suggested an axonal origin since it lacked the typical EPSP-mediated early rise (Figure 3.16 C). Quantitative analysis was performed by recording the amplitude of the population spikes under baseline conditions and after bath application of the AMPA receptor blocker NBQX (Figure 3.16 D). Comparing the amplitudes did not show any difference (Figure 3.16 E). Since the blockade of synaptic transmission by NBQX did not influence the amplitude and shape of the population spike, it was concluded that the stimulation paradigm resulted in antidromic recruitment of CA1 PC firing.

To be able to estimate the size of the CA1 PC ensemble that was recruited with antidromic stimulation, the number of recruited CA1 PCs was determined experimentally. Therefore, mice that express the calcium-sensitive protein GCaMP5g and the calcium-insensitive protein tdTomato selectively in CA1 PCs were used (Figure 3.16 F). The expression was achieved through stereotactic-injecting of transgenic PC-G5-tdT mice with a recombinant adeno-associated CaMKII-cre virus. To estimate the number of recruited neurons during antidromic stimulation, two-photon excitation microscopy of the soma of at least 16 PCs per slice was performed in the line scanning mode (Figure 3.16 G). The amplitude of the baseline-normalized intensity ratio (GCaMP5g/tdTomato, background-subtracted) was used to categorize the cells into responding and nonresponding cells. Therefore, an arbitrary threshold was defined well above the noise level. Consequently, cells with an increase in the intensity ratio during the stimulation of more than 25 % were considered to be responding cells. The result showed that on average almost half of the CA1 PCs in a slice were recruited by alveus stimulation (Figure 3.16 H).

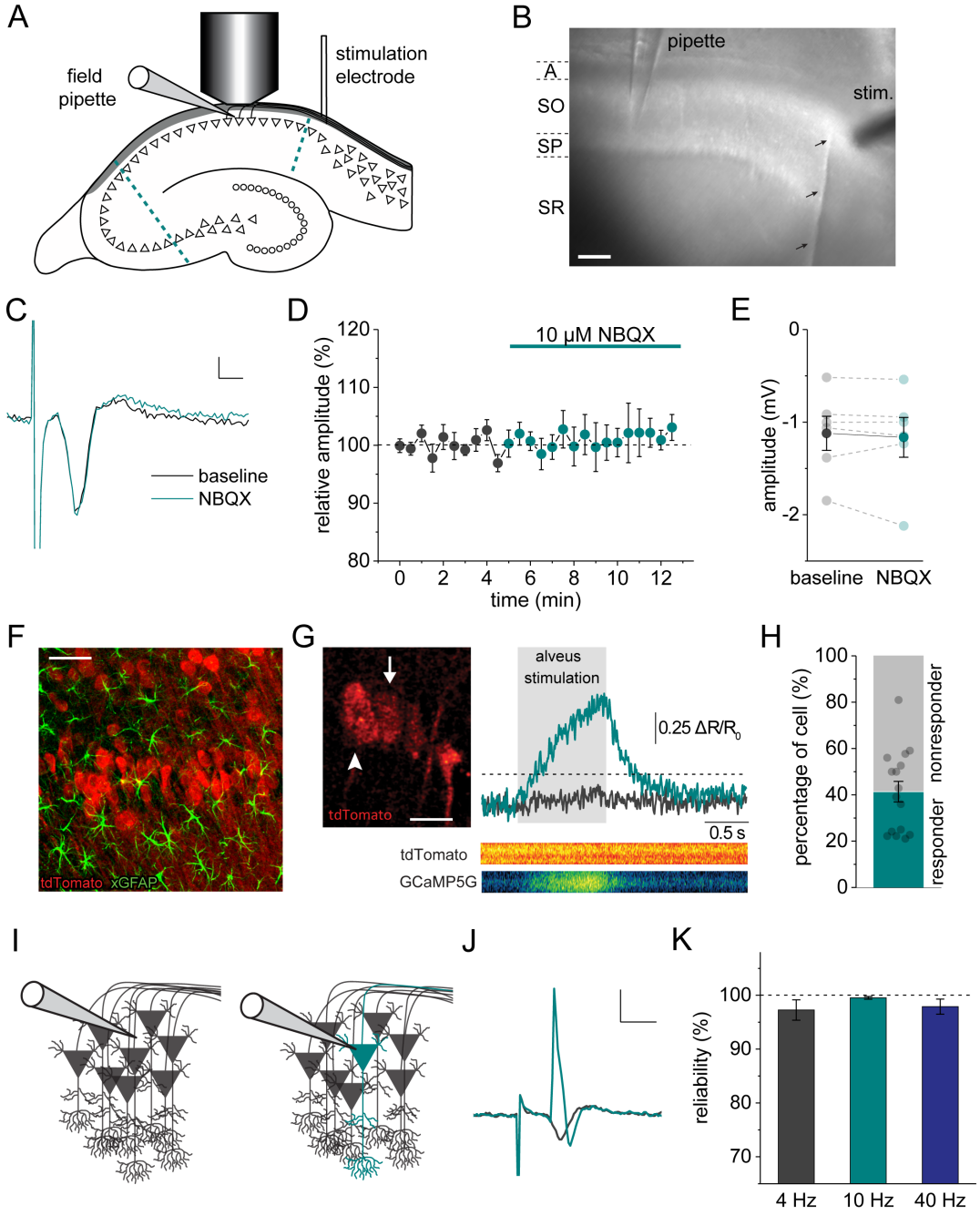

Figure 3.16. Alveus stimulation recruits a subset of CA1 pyramidal cells axonally. (A) Schematic of the recording configuration. To recruit CA1 pyramidal cell firing antidromically, a bipolar stimulation electrode was placed in the alveus above the subiculum. Retrograde recruitment of Schaffer collateral fibers in stratum oriens was prevented by an incision at the boarder of CA1 and the subiculum sparing the fibers in the alveus. The field potential was recorded with a pipette at the boarder of stratum oriens and stratum pyramidale. **(B)** Image of the electrode position and incision (arrows) in an acute hippocampal slice (scale bar: 100 µm). **(C)** Example trace of the population spike at baseline (dark gray) and after NBQX wash-in (10 µM, turquois, scale bar: 0.1 mV x 1 ms). **(D)** Time course of the relative population spike amplitude during baseline and NBQX bath application. **(E)** Comparing the population spike amplitude during baseline with the last five minutes of NBQX application did not show a significant difference (-1.12 ± 0.18 mV vs. -1.16 ± 0.21 mV, n = 6, p = 0.48, paired t-test). **(F)** Maximum projection of a confocal image stack, illustrating the expression profile of tdTomato (red) in the CA1 stratum pyramidale of PC-G5-tdT mouse after injection of a CaMKII-cre adeno-associated virus. Astrocytes were labeled through antibody staining of GFAP (green, scale bar: 50 µm). **(G)** Two-photon excitation image showing CA1 pyramidal cells expressing tdTomato (scale bar: 20 µm). Line scans through several somata were performed during stimulation of the alveus. Representative filtered traces of the ratio of GCaMP5g/tdTomato (background-subtracted, normalized to baseline) are illustrated for a nonresponding (arrowhead, gray trace) and a responding neuron (arrow, turquois trace). Cells were considered responders if the ratio increased more than 25 % over baseline (dashed line). **(H)** On average 41.36 ± 4.44 % of the cells in an acute brain slice (n = 16) responded to the alveus stimulation.

(Figure legend continued on next page)

(I, J) Schematic of the recording configuration and sample traces: First panel shows the configuration during field recording of the population spike (gray trace). The second panel shows an extracellular single unit recording, where the glass pipette is in close proximity to a pyramidal cell, allowing the detection of single unit spiking (turquoise, scale bar: 2 ms x 2 mV). **(K)** Cells that were able to follow a one second long 10 Hz stimulation reliably, were likewise able to follow stimulation at 4 or 40 Hz (n = 16, p = 0.23, One-Way Repeated-Measures ANOVA). A, alveus; SO, stratum oriens; SP, stratum pyramidale; SR, stratum radiatum; stim., stimulation electrode.

Next, the ability of CA1 PC axons to follow antidromic stimulation at different frequencies was tested. Extracellular single unit recordings allowed me to monitor single cell spiking, without the need to perform whole-cell patch clamp recordings. During field recordings of population spikes, the recording pipette was placed in the stratum pyramidale. The recorded population spikes represent the synchronized firing activity of the population (Figure 3.16 I, left panel & J, gray trace). For the measurement of extracellular single units, the recording pipette was placed in close proximity to a single CA1 PC (Figure 3.16 I, right panel). In this case, the recorded signal showed the response of the single neuron on top of the population spike (Figure 3.16 J, turquoise trace). The reliability of a neuron to follow stimulation at 4, 10 and 40 Hz was estimated. The results showed that in CA1 PCs, in which AP firing was reliably evoked with a 10 Hz stimulus, stimulation with 4 and 40 Hz also elicited consistent APs (Figure 3.16 K).

These experiments showed that the stimulation of the alveus with distinct frequencies consistently recruits approximately half of the CA1 PCs antidromically. Importantly, experiments performed and analyzed by Eva M. Schönhense in our lab showed that stimulation of the alveus is able to recruit calcium transients in astrocytes. For these experiments, time-lapse frame scanning of whole-cell patch clamped stratum radiatum astrocytes filled with the calcium-sensitive indicator Fluo-4 and the calcium-insensitive indicator Alexa Fluor 594 was performed (Figure 3.17 A). The relative change in the fluorescence ratio (Fluo-4/Alexa Fluor 594, background corrected) in response to antidromic stimulation of CA1 PCs was calculated for several subdomains of the astrocyte. Nearly 70 % of the astrocytes recorded responded with an increase in the fluorescence ratio during alveus stimulation (Figure 3.17 B, left panel). This effect was mediated by CB1 receptors, since the relative change in the fluorescence ratio was significantly decreased by the CB1 receptor inverse agonist AM251 (Figure 3.17 B, right panel).

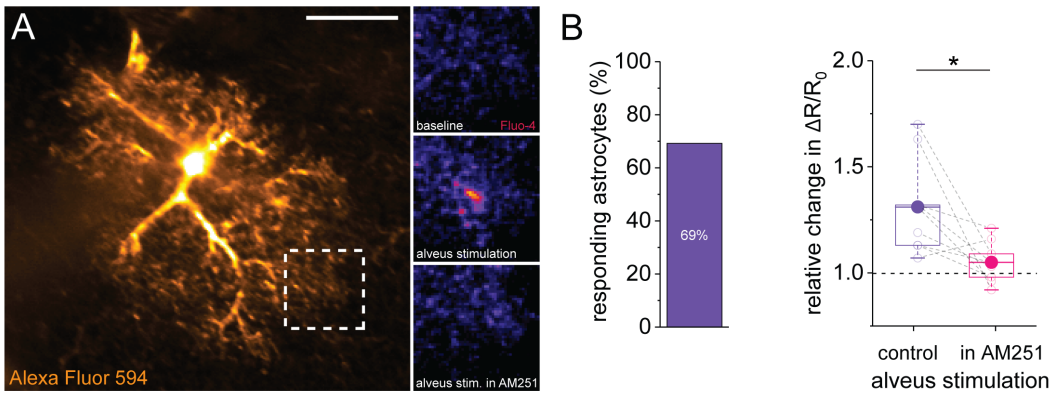

Figure 3.17. Alveus stimulation promotes astrocytic Ca^{2+} transients via CB1 receptors. (A) Example of an astrocyte filled with Alexa Fluor 594 (40 µM) and Fluo-4 (400 µM) through a whole-cell patch pipette (scale bar: 20 µm). The Fluo-4 intensity of the highlighted area (left) is displayed as an average over 20 frames during baseline, alveus stimulation and alveus stimulation in presence of the inverse CB1 receptor agonist AM251 (5 µM, right). **(B)** During alveus stimulation, 69% of the astrocytes showed an increase of at least 5% in the area of the fluorescence ratio relative to baseline. Comparing the change in fluorescence ratio of those astrocytes during alveus stimulation and alveus stimulation in AM251 revealed a significant difference (1.31 ± 0.07 vs 1.05 ± 0.03, n = 9, p = 0.016, paired t-test). *Figure adapted from the Master Thesis of E.M. Schönhense (2015) with permission.*

3.6.3 Frequency-Dependent Modulation of Supralinear Dendritic Integration By Pyramidal Cell Activity

Overall, these results show that the stimulation of the alveus stimulation consistently recruits AP firing of CA1 pyramidal cells and, more importantly, causes the mobilization of endocannabinoids. These endocannabinoids in turn promote calcium transients in astrocytes. Activation of CB1 receptors by agonist application can positively modulate dendritic integration. Thus, antidromic stimulation of CA1 PCs should modulate dendritic integration. This hypothesis was investigated next (Figure 3.18 A-C). A bipolar stimulation electrode was placed in the alveus, as previously described. Then a CA1 PC was whole-cell patch clamped, filled with Alexa Fluor 594 and the microiontophoresis pipette placed to stimulate an apical oblique dendrite. After recording the supralinear dendritic integration, CA1 PC firing was recruited by electrical stimulation of the alveus for one second, before stimulating the dendrite again iontophoretically. This was repeated for various increasing iontophoretic stimulation intensities (Figure 3.18 A, bottom panel & D). To mimic behavioral relevant activity patterns, alveus stimulation was performed at frequencies corresponding to delta (4 Hz), theta (10 Hz), beta (20 Hz) and low-gamma (40 Hz) oscillations. Strikingly, the threshold stimulus was only influenced by antidromic stimulation at 10 and 20 Hz but not at 4 and 40 Hz (Figure 3.18 E). In line with this, the amplitude of the subthreshold EPSP (Figure 3.18 F) and the dendritic spike NMDA receptor component showed a selective increase only for 10 and 20 Hz (Figure 3.18 G). Furthermore, the slope of the sodium channel component responded in the same pattern (Figure 3.18 H). The amplification of supralinear dendritic integration was most prominent for activity in the theta frequency range, since only the stimulation with a frequency of 10 Hz resulted in a significant difference compared to the other frequencies (Figure 3.18 E&G, right panel). Additionally, the duration of the potentiation of the dendritic integration was investigated. Alveus stimulation only transiently influences dendritic integration, since five minutes after the last retrograde activation of CA1 PCs, all parameters were comparable to the initial values (Table 2 A).

To determine if this modulation requires endocannabinoid signaling, the retrograde activation of CA1 PCs was repeated in the presence of the inverse CB1 receptor agonist AM251. When the endocannabinoids mobilized with alveus stimulation are unable to activate CB1 receptors, the threshold stimulus, the subthreshold EPSP's as well as dendritic spike NMDA receptor component amplitude and maximum slope of the dendritic spike were unchanged (Table 2 B). Likewise, it was investigated whether NMDA receptor co-agonists modulate the observed effects. Therefore, the experiment was performed in saturating concentrations of the NMDA receptor co-agonist D-serine. This maximizes the recruitment of NMDA receptors in such, that the release of additional NMDA receptor co-agonists is unable to influence the dendritic integration. Under these conditions all earlier observed effects were occluded (Table 2 C). While this result excludes a role of astrocytic-released glutamate, the question about the co-agonist identity remains unanswered. Both, glycine and D-serine, can regulate NMDA receptor recruitment via the same co-agonist binding site and are endogenously present in the brain. To determine the identity of the released NMDA receptor co-agonist, hippocampal brain slices were pretreated with and kept in the presence of the D-serine degrading enzyme D-amino acid oxidase (DAAO). This should cause a reduction in extracellular D-serine and a rapid degradation of newly released D-serine. When examining the effect of alveus stimulation on the dendritic integration under these conditions, no significant difference could be observed (Table 2D).

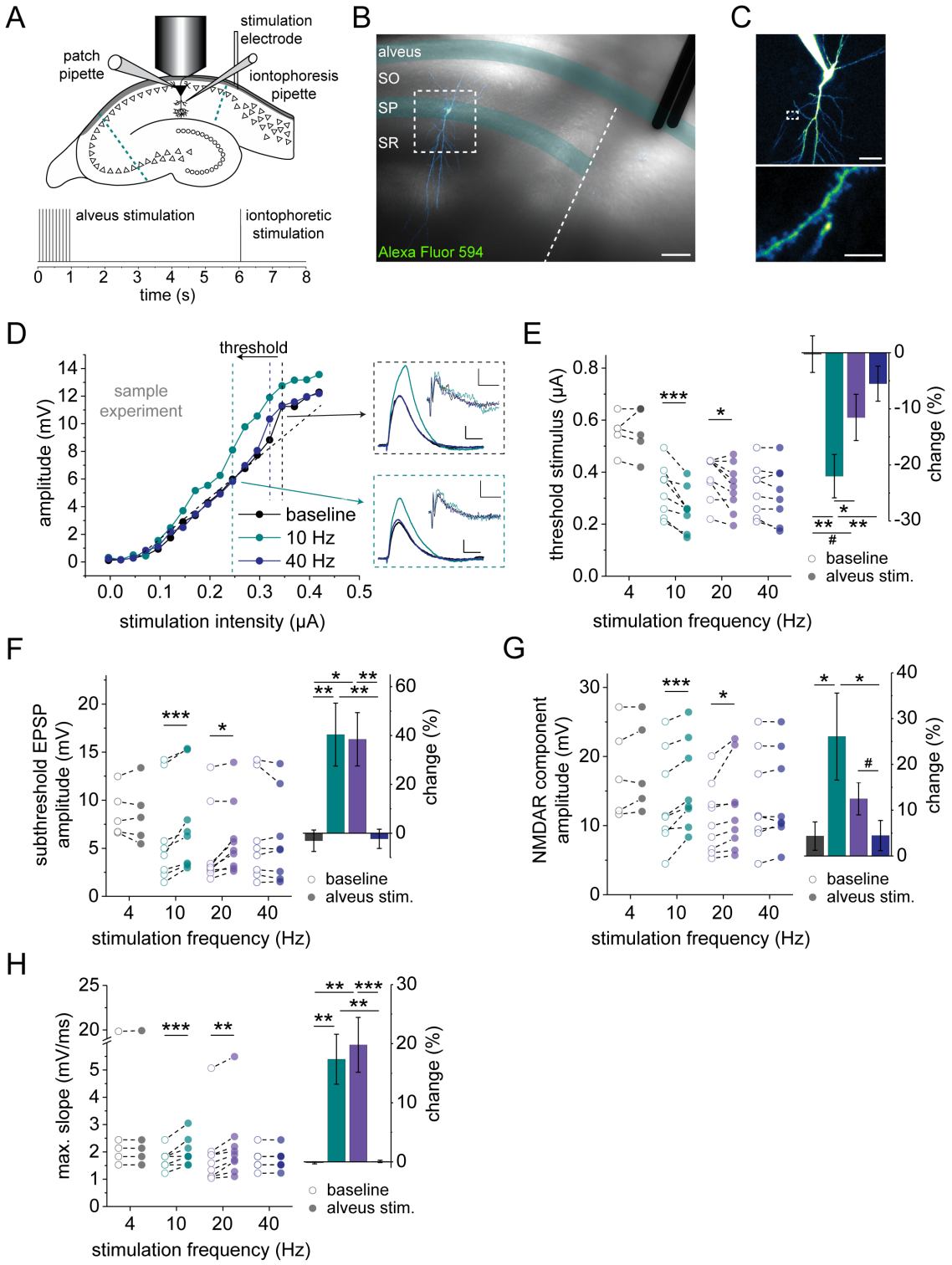

Figure 3.18. Pyramidal cell activity promotes supralinear dendritic integration in a frequency-dependent manner. (A) Schematic of the recording configuration and protocol. Incisions were made to separate CA3 recurred fibers and Schaeffer collateral fibers at the boarder of CA1 and the subiculum. A bipolar stimulation electrode is placed in the alveus above the subiculum. A CA1 pyramidal cell was filled with Alexa Fluor 594 (40 µM) via the whole-cell patch pipette and the microiontophoresis pipette filled with glutamic acid (150 mM) and Alexa Fluor 594 (50 µM) placed near a spine on an apical oblique dendrite. The lower inset depicts the protocol. Stimulation of the alveus for one second at 4, 10, 20 or 40 Hz was followed by iontophoretic stimulation after a refractory period of five seconds. **(B)** Representative image illustrating the incision (dashed line) and stimulation electrode with an overlay of the Alexa Fluor 594-filled CA1 pyramidal cell (scale bar: 100 µm). **(C)** Enlargement of the whole-cell patched CA1 pyramidal cell (scale bar: 40 µm) and stimulated dendrite with microiontophoresis pipette (scale bar: 5 µm).

(Figure legend continued on next page)

(D) Representative example of the relationship between iontophoretic stimulation intensity and somatic EPSP amplitude for a nonlinear integrating dendrite before (black), after 10 Hz (turquoise) and 40 Hz alveus stimulation (blue). The first dendritic spike is marked by a color-coded dashed line with the corresponding somatic traces (scale bar: 2 mV, 20 ms) and first derivatives (scale bar: 1 mV/ms, 10 ms) on the right panel. **(E)** The threshold stimulus was significantly increased after 10 Hz (0.33 ± 0.03 µA vs. 0.26 ± 0.03 µA, n = 8, p = 0.00007, post-hoc Fisher's LSD,) and 20 Hz stimulation (0.44 IQR 0.33-0.44 µA vs. 0.34 IQR 0.27-0.42 µA, n = 9, p = 0.034, post-hoc Wilcoxon signed-rank test). 4 and 40 Hz had no effect (4 Hz: 0.55 ± 0.03 µA vs. 0.55 ± 0.04 µA, n = 5, p = 1, paired t-test; 40 Hz: 0.33 ± 0.03 µA vs. 0.32 ± 0.04 µA, n = 8, p = 0.31, post-hoc Fisher's LSD). The observed change during 10 Hz was significantly bigger than observed with 4, 20 and 40 Hz stimulation (one-way ANOVA with post-hoc Fisher's LSD). **(F)** The amplitude of subthreshold EPSPs were significantly increased after 10 Hz (6.18 ± 1.77 mV vs. 7.66 ± 1.79 mV, n = 8, p = 0.0006, post-hoc Fisher's LSD) and 20 Hz stimulation (3.00 IQR 2.59-6.66 mV vs. 4.77 IQR 3.02-7.94 mV, n = 9, p = 0.008, post-hoc Wilcoxon signed-rank test) but not 4 and 40 Hz (4 Hz: 8.71 ± 1.11 mV vs. 8.57 ± 1.39 mV, n = 5, p = 0.72, paired t-test; 40 Hz: 6.18 ± 1.77 mV vs. 5.93 ± 1.61 mV, n = 8, p = 0.48, post-hoc Fisher's LSD). Comparing between the different stimulation frequencies showed a significantly bigger change in subthreshold amplitude for 10 and 20 Hz compared to 4 and 40 Hz (one-way ANOVA with post-hoc Fisher's LSD). **(G)** The NMDA receptor component of dendritic spikes was significantly increased only after 10 Hz (13.70 ± 2.47 mV vs. 15.75 ± 2.29 mV, n = 8, p < 0.0001, post-hoc Fisher's LSD) and 20 Hz stimulation (9.75 ± 1.37 mV vs. 11.08 ± 1.81 mV, n = 9, p = 0.022, post-hoc Fisher's LSD) but not 4 and 40 Hz (4 Hz: 17.97 ± 2.98 mV vs. 18.61 ± 2.94 mV, n = 5, p = 0.23, paired t-test; 40 Hz: 13.70 ± 2.47 mV vs. 14.00 ± 2.39 mV, n = 8, p = 0.41, post-hoc Fisher's LSD). Comparing between the different stimulation frequencies showed a significantly bigger change in the NMDA receptor component of dendritic spikes evoked after 10 Hz alveus stimulation (Kruskal-Wallis ANOVA with post-hoc Mann-Whitney test). **(H)** The maximum slope of the dendritic spike was only increased by retrograde activation of CA1 pyramidal cells at 10 Hz (1.72 ± 0.13 mV/ms vs. 2.02 ± 0.18 mV/ms, n = 8, p = 0.0004, post-hoc Fisher's LSD) and 20 Hz (1.59 IQR 1.10-1.95 mV/ms vs. 1.90 IQR 1.47-2.38 mV/ms, n = 9, p = 0.004, post-hoc Wilcoxon signed-rank test) and not with activation at 4 or 40 Hz (4 Hz: 2.14 IQR 1.68-11.14 mV/ms vs. 2.13 IQR 1.68-11.16 mV/ms, n = 5, p = 1, Wilcoxon signed-rank test; 40 Hz: 1.72 ± 0.13 mV/ms vs. 1.72 ± 0.13 mV/ms, n = 8, p = 0.99, post-hoc Fisher's LSD). The change between baseline and the different alveus stimulation frequencies showed a significant effect of 10 and 20 Hz over 4 and 40 Hz (one-way ANOVA with post-hoc Fisher's LSD). *Note: Data for 10 Hz and 40 Hz stimulation were collected from one cell. The three conditions (baseline, 10 Hz, 40 Hz) were recorded in alternating order. Data for 20 Hz stimulation were collected with a third measurement after a refractory period of five minutes (see Table 2). In all cases, post-hoc testing was only performed if the appropriate ANOVA reported significant overall differences. # p < 0.10, * p < 0.05, ** p < 0.01, *** p < 0.001*

The results shown indicate an interesting, previously unknown feedback loop that connects pyramidal cell firing with astrocyte calcium transients and supralinear dendritic integration. AP firing of CA1 pyramidal cells results in the mobilization of endocannabinoids. These endocannabinoids activate astrocytic CB1 receptors and thereby increase the intracellular calcium. This increase in calcium recruits the release of the NMDA receptor co-agonist D-serine. Locally at the dendrite the released D-serine maximized the recruitment of NMDA receptors during supralinear dendritic integration. Among others, this resulted in a decrease of the threshold stimulus and an increase of the slow, NMDA receptor component of dendritic spikes. Notably, the depolarization of a single neuron was not sufficient to activate this positive feedback loop but rather the recruitment of an ensemble of CA1 PCs was required. Unexpectedly, I observed a tuning of the positive modulation of dendritic integration to AP firing in the theta frequency range. This immediately raises the question, why higher frequencies do not recruit the described feedback loop.

Table 2. Pyramidal cell activity transiently promotes supralinear dendritic integration via CB1 receptor and the NMDA receptor co-agonist D-serine.

parameter	baseline mean ± SEM ∨ median IQR	treatment mean ± SEM ∨ median IQR	n	p	test
A: baseline vs. five minutes after 20 Hz alveus stimulation					
threshold stim. (µA)	0.44 IQR 0.33-0.44	0.39 IQR 0.34-0.48	9	0.21	post-hoc Wilcoxon S-R test
iEPSP (mV)	0.83 IQR 0.42-1.17	0.36 IQR 0.21-0.65	9	0.13	post-hoc Wilcoxon S-R test
subthreshold EPSP (mV)	3.00 IQR 2.59-6.66	2.82 IQR 2.46-6.53	9	0.50	post-hoc Wilcoxon S-R test
NMDAR component (mV)	9.75 ± 1.37	9.41 ± 1.56	9	0.52	post-hoc Fisher's LSD
max. slope (mV/ms)	1.59 IQR 1.10-1.95	1.71 IQR 1.19-2.10	9	0.09	post-hoc Wilcoxon S-R test
B: baseline vs. 20 Hz alveus stimulation in AM-251					
threshold stim. (µA)	0.36 ± 0.06	0.35 ± 0.05	7	0.54	paired t-test
iEPSP (mV)	0.58 ± 0.12	0.60 ± 0.10	7	0.62	paired t-test
subthreshold EPSP (mV)	6.75 ± 1.06	6.56 ± 1.03	7	0.33	paired t-test
NMDAR component (mV)	14.53 ± 2.21	14.61 ± 2.27	7	0.85	paired t-test
max. slope (mV/ms)	3.45 ± 0.72	3.29 ± 0.70	7	0.12	paired t-test
C: baseline vs. 20 Hz alveus stimulation in D-serine					
threshold stim. (µA)	0.44 ± 0.05	0.45 ± 0.05	6	0.36	paired t-test
iEPSP (mV)	1.27 ± 0.28	1.66 ± 0.26	6	0.09	paired t-test
subthreshold EPSP (mV)	11.93 ± 2.73	12.38 ± 2.73	6	0.11	paired t-test
NMDAR component (mV)	20.34 ± 2.54	20.05 ± 2.46	6	0.61	paired t-test
max. slope (mV/ms)	2.14 IQR 1.76-3.13	2.29 IQR 1.52-3.14	6	0.63	Wilcoxon S-R test
D: baseline vs. 10 Hz alveus stimulation in DAAO					
threshold stim. (µA)	0.36 ± 0.06	0.37 ± 0.07	8	0.73	paired t-test
iEPSP (mV)	1.24 ± 0.15	1.27 ± 0.18	8	0.66	paired t-test
subthreshold EPSP (mV)	7.29 ± 1.07	7.30 ± 0.98	8	0.99	paired t-test
NMDAR component (mV)	19.58 ± 3.21	18.60 ± 2.46	8	0.27	paired t-test
max. slope (mV/ms)	1.98 IQR 1.60-2.14	1.84 IQR 1.83-2.37	8	0.84	Wilcoxon S-R test

Note: Data in A were collected as part of the experiment in which the effect of 20 Hz alveus stimulation was investigated (see Figure 3.15). Post-hoc testing was only performed if the one-way repeated measurement ANOVA or Friedman ANOVA reported significant overall differences. IQR, interquartile range; NMDAR, NMDA receptor; stim, stimulation; Wilcoxon S-R test, Wilcoxon signed-rank test

3.7 Origin of Frequency Dependent Modulation of Integration

Endocannabinoid-dependent depolarization-induced suppression of inhibition (DSI) is more prominent and long-lasting with an increasing number of APs and higher AP frequency (Dubruc et al., 2013; Fortin et al., 2004). Especially, frequencies of more than 20 Hz and more than ten APs have been shown to maximize DSI. In contrast, my results showed that a stimulation frequency of 40 Hz for one second (40 APs) does not influence supralinear dendritic integration via the endocannabinoid-depending signaling cascade. The cause of these circumstances remains to be investigated. DSI is mediated by signaling from the postsynaptic to the presynaptic neuron while the described feedback loop requires activation of astrocytic calcium signaling. It is important to note that endocannabinoids are lipophilic compounds (Di Marzo et al., 1998; Piomelli et al., 2000) with a rather limited action range of approximate 10 µm (Chevaleyre and Castillo, 2003). Thus, it could be possible that distinct frequencies result in the mobilization of endocannabinoids at distinct locations. This would mean that astrocytes are not activated by alveus stimulation at a frequency of 40 Hz.

To test this hypothesis, it was investigated whether the calcium response in astrocytes differs between 10 and 40 Hz stimulation of the alveus. Astrocytic calcium imaging was performed in mice expressing the calcium-sensitive indicator GCaMP5g and the calcium-insensitive indicator tdTomato selectively in astrocytes (Figure 3.19 A; GLAST-cre ERT2 x PC-G5-tdT mice, tamoxifen injected). Viability of astrocytes was ensured through a low baseline fluorescence of GCaMP5g, which corresponds to a low intracellular calcium concentration, and the presence of spontaneous transients. After a baseline recording of three minute, CA1 axons were stimulated repetitively with either 10 Hz or 40 Hz for one second with an inter-stimulus interval of ten seconds. The frequency of astrocytic calcium transients was analyzed as an indicator for astrocytic recruitment. The baseline calcium transient frequency did not differ between the two treatment groups (Figure 3.19 B). Interestingly, 10 Hz stimulation resulted on average in a significant increase in the calcium transient frequency, while no change was observed during 40 Hz stimulation (Figure 3.19 C). Additionally, the proportion of astrocytes showing an increase in calcium transients during 10 Hz stimulation was significantly higher compared to 40 Hz stimulation. Thus, it was twice as likely that an astrocyte responded with an increase in its calcium transient frequency during 10 Hz stimulation compared to 40 Hz. But, expectedly, the calcium transient frequency showed a large variation between cells. Since my results (Figure 3.2) showed that the relative change in the integral might be used as an alternative indicator of changes in astrocyte calcium frequency, it was used as an additional parameter in these experiments. Since shifts in the recording plane could influence the integral of the fluorescence ratio (GCaMP5g/tdTomato, background corrected), it was determined during a subset of frames (> 250 frames and 1.3 minutes). Comparing the integral between baseline and stimulation revealed a significant increase during 10 Hz stimulation of the alveus. This effect was not observed during 40 Hz stimulation. The relative change in the integral was significantly larger increased during 10 Hz stimulation of the alveus compared to 40 Hz. Astrocytes that showed an increase of more than 5 % in their integral were classified as responders, similar as in the experiments performed by Eva M. Schönhense (Figure 3.17). Again, the number of astrocytes responding was significantly lager with 10 Hz than with 40 Hz stimulation (Figure 3.19 D). Notably, it was ten times more likely that an astrocyte responded with an increase in the integral after 10 Hz stimulation than after a 40 Hz.

These results support the hypothesis that astrocytes are not activated by alveus stimulation at a frequency of 40 Hz. In contrasts, DIS does take place at this frequency. However, it is mainly observed in the perisomatic region (Lee et al., 2010). Endocannabinoids are lipophilic and cannot diffuse over long distances (Di Marzo et al., 1998). This implies that for DSI the depolarization and/or calcium influx evoked would only be required to mobilize endocannabinoids close to the soma. Astrocytic calcium transients, though, require depolarization and/or calcium influx locally in the dendrites. Hence, the depolarization induced by retrograde activation of CA1 PCs needs to backpropagate into the dendritic tree to be able to mobilize endocannabinoids locally. It is known, that dendrites are more likely to respond to inputs at distinct frequencies. In CA1 pyramidal cells this resonance frequency lies within the theta frequency range (Hu et al., 2009). Hyperpolarization-activated cyclic nucleotide-gated (HCN) channels are crucial in determining the resonance frequency (Buzsáki and Draguhn, 2004; Hutcheon et al., 1996).

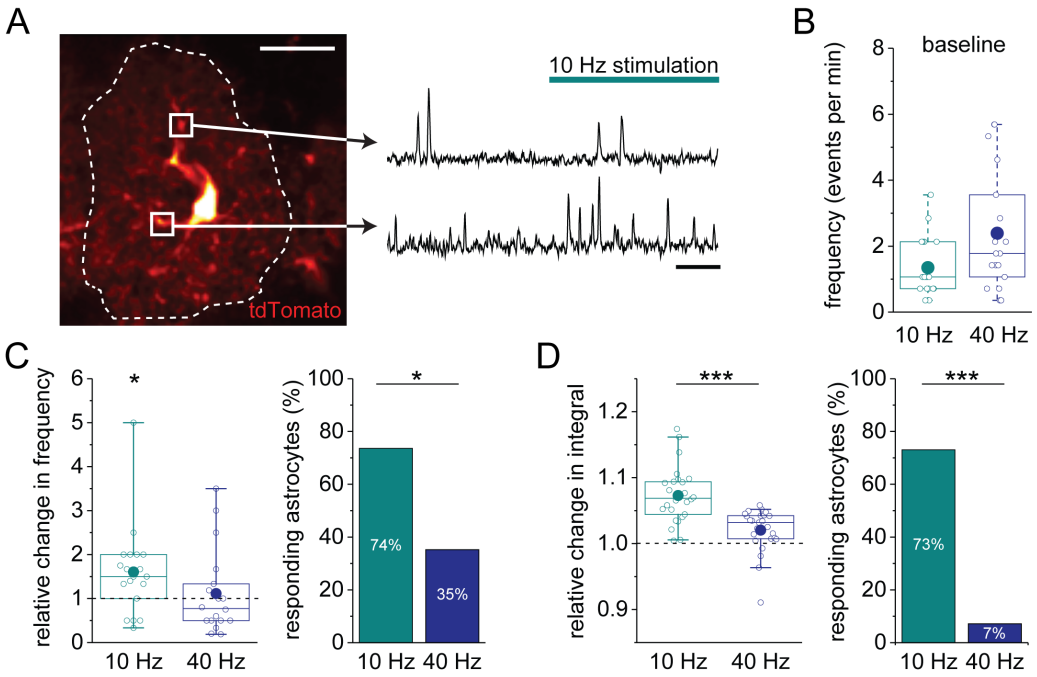

Figure 3.19. Astrocytic Ca^{2+} transients are evoked by pyramidal cell activity at 10 Hz but not 40 Hz. (A) Representative astrocyte of PC-G5-tdT x GLAST-cre ERT2 mouse showing the tdTomato expression (scale bar: 20 µm). For the analysis of the Ca^{2+}-transient frequency regions of interest were defined around visually identified Ca^{2+} transients. Sample traces show the ratio of GCaMP5g and tdTomato (background-subtracted) over time (scale bar: 50 s). For the analysis of the integral of the fluorescence ratio a region of interest around the astrocyte was drawn. The soma was excluded. **(B)** At baseline, no significant difference between the calcium event frequency during 10 Hz and 40 Hz alveus stimulation could be detected (1.07 IQR 0.71-2.13 vs. 1.78 IQR 0.89- 4.09, n = 19/17, p = 0.102, Mann-Whitney U-test). **(C)** The change in calcium frequency showed a significant increase during 10 Hz stimulation (1.5 IQR 1-2, n = 19, p = 0.011, one-population Wilcoxon signed-rank test) but not 40 Hz stimulation of the alveus (0.78 IQR 0.5-1.42, n = 18, p = 0.72, one-population Wilcoxon signed-rank test). The change was larger during 10 Hz stimulation compared to 40 Hz (p = 0.055, Mann-Whitney test). The percentage of astrocytes showing an increase in frequency was significantly higher with 10 Hz stimulation than with 40 Hz (Fisher's exact test, p = 0.042). **(D)** The integral of the fluorescence ratio showed a significantly larger change when the alveus was stimulated with 10 Hz compared to 40 Hz (1.07 IQR 1.04-1.09 vs. 1.03 IQR 1.01-1.04, n = 26/25, p < 0.0001, Mann-Whitney test). The percentage of astrocytes showing an increase of more than 5 % was significantly larger with 10 Hz stimulation than with 40 Hz (Fisher's exact test, p < 0.0001).

Owing to the relevance of HCN channels in establishing the resonance frequency, I wondered whether blockade of these channels by the antagonist ZD7288 would affect the modulation of supralinear dendritic integration during 10 Hz stimulation of the alveus (Figure 3.20 A). After establishing the whole-cell configuration and placing the microiontophoresis pipette, ZD7288 was bath applied while monitoring the resting membrane potential of the patched cell. Since HCN channels are typically open at potentials below -50 mV, they are important in setting the resting membrane potential (Pape, 1996). Hence, their block resulted in a decrease of the resting membrane potential by 4.99 ± 1.06 mV (n = 18). To ensure normal activation of voltage-dependent channels during the integration and initiation of dendritic spikes, a constant positive current was applied to set the resting membrane potential to -70 mV. Next, the dendritic integration was investigated at baseline and during 10 Hz alveus stimulation. Strikingly, no difference was detected for any parameter investigated (Figure 3.20 B-E). To ensure that the absence of an effect was not caused by a compensatory or a ceiling effect caused by the blockade of HCN channels themselves, a positive control was performed. Therefore, the release of endocannabinoids was circumvented by bath application of the agonist WIN55-212-2 in the presence of the HCN channel blocker ZD7288. This recovered the effects observed previously by 10 Hz alveus stimulation under control condition for all four parameters (Figure 3.20 B-E). This means that the dendritic integration and dendritic spike initiation is not yet maximized while HCN channels blockade and, thus, a positive modulation by endocannabinoid-dependent release of D-serine from astrocytes should be possible. However, 10 Hz stimulation could not evoke a similar effect on the integration during the blockade of HCN channels. This suggests that HCN channels impact the spread of the depolarization and/or calcium during the backpropagation of APs in the theta frequency band into the dendrites and hence, controls the local mobilization of endocannabinoids.

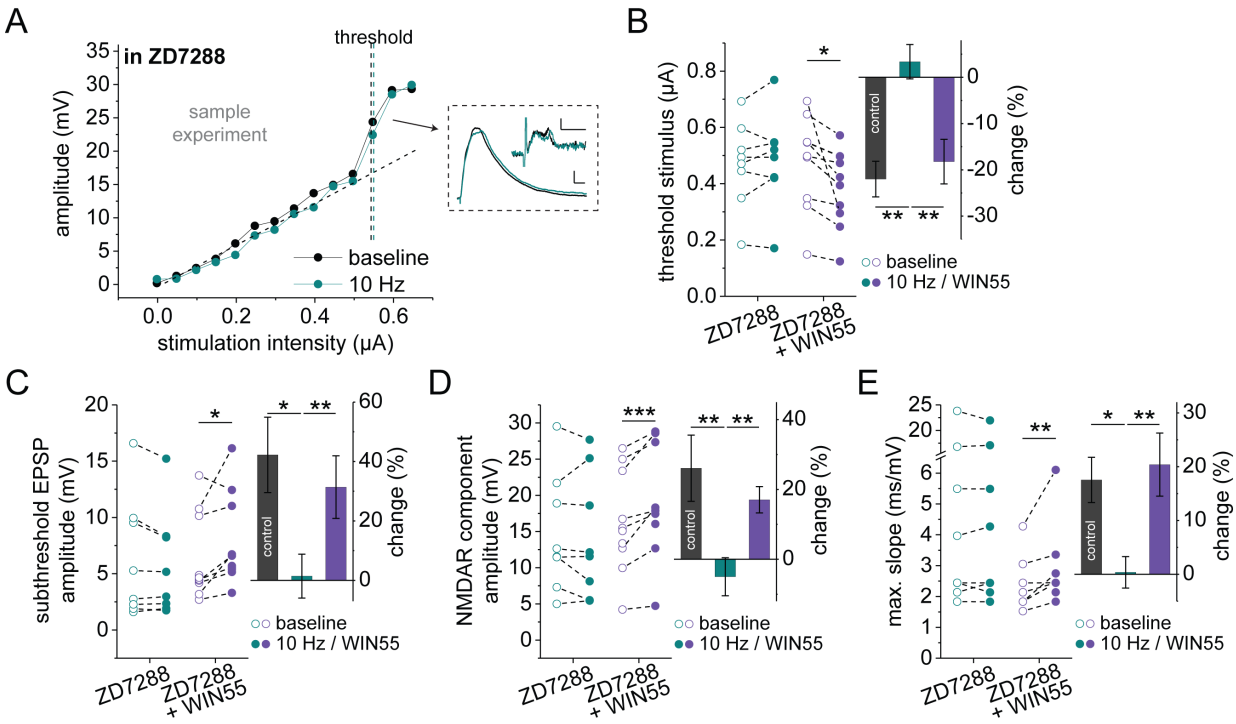

Figure 3.20. HCN channels are a key mediator in the frequency-dependent modulation of nonlinear dendritic integration. **(A)** Representative example of the relationship between iontophoretic stimulation intensity and somatic EPSP amplitude for a nonlinear integrating dendrite in the HCN channel blocker ZD7288 (10 µM) during baseline (black) and after 10 Hz alveus stimulation (turquoise). The first dendritic spike is marked by a color-coded dashed line with the corresponding somatic traces (scale bar: 2 mV, 20 ms) and first derivatives (scale bar: 1 mV/ms, 10 ms) on the right panel. **(B)** The threshold stimulus intensity for the first dendritic spike was not different with 10 Hz stimulation of the alveus in ZD7288 (0.47 ± 0.05 µA vs. 0.49 ± 0.06 µA, n = 8, p = 0.33, paired t-test), but application of the CB1 receptor agonist WIN55-212,2 (1 µM) in the presence of ZD7288 resulted in a significant decrease (0.48 ± 0.05 µA vs. 0.38 ± 0.04 µA, n = 10, p = 0.025, paired t-test). Comparing the relative changes of the stimulation intensity to the change observed under control conditions with 10 Hz stimulation (see Figure 3.18), revealed a significant difference between control and ZD7288 treated slices and compared to WIN55-212,2 application (Kruskal-Wallis ANOVA with post-hoc Mann-Whitney test). **(C)** The subthreshold EPSP amplitude was unchanged after alveus stimulation in ZD7288 (6.23 ± 1.89 mV vs. 5.74 ± 1.65 mV, n = 8, p = 0.12, paired t-test). Bath-application of WIN55-212,2 significantly enhanced the subthreshold EPSP amplitude in ZD7288 (4.57 IQR 3.94-10.30 mV vs. 6.14 IQR 5.33-11.38 mV, n = 10, p = 0.037, Wilcoxon signed-rank test). Comparing the relative changes of these experiments to the control recordings of 10 Hz stimulation revealed a significant larger increase of 10 Hz stimulation under control conditions and WIN55-212,2 application compared to 10 Hz stimulation in ZD7288 (Kruskal-Wallis ANOVA with post-hoc Mann-Whitney test). **(D)** The NMDA receptor component of dendritic spikes in presence of the HCN channel blocker remained comparable after stimulation of the alveus (14.75 ± 2.87 mV vs. 14.27 ± 3.05 mV, n = 8, p = 0.52, paired t-test) but was significantly increased by WIN55-212,2 (16.24 ± 2.21 mV vs. 18.79 ± 2.41 mV, n = 10, p = 0.001, paired t-test). The relative change of the NMDA receptor component was significantly lager with 10 Hz stimulation under control conditions and with WIN55-212,2 treatment than with 10 Hz stimulation in ZD7288 (Kruskal-Wallis ANOVA with post-hoc Mann-Whitney test). **(E)** The maximum slope of the first dendritic spike showed no significant difference after 10 Hz alveus stimulation in ZD7288 (3.20 IQR 2.21-13.96 mV/ms vs. 3.35 IQR 2.21-14.18 mV/ms, n = 8, p = 0.74, Wilcoxon signed-rank test), but significantly increased after application of the CB1 receptor agonist (2.14 IQR 1.83-2.59 mV/ms vs. 2.44 IQR 2.14-2.90 mV/ms, n = 10, p = 0.002, Wilcoxon signed-rank test). Also, the relative change was significantly larger after 10 Hz stimulation in control slices as well as slices treated with the CB1 receptor agonist in ZD7288 compared to 10 Hz stimulation and HCN channel blockade (one-way ANOVA with post-hoc Fisher's LSD). *Note: Values for the control conditions are from the experiments shown in Figure 3.18. Post-hoc testing was only performed if the appropriate ANOVA reported significant overall differences. * p < 0.05, ** p < 0.01*

3.8 Astrocytic CB1 Receptors are Essential in Regulating Dendritic Integration

The results so far show that CA1 PC AP firing selectively at a frequency of 10 Hz recruits the mobilization of endocannabinoids and results in an increase in astrocytic calcium. This in turn evoked the release of D-serine, which increases the recruitment of NMDA receptors locally at the dendrite during supralinear dendritic integration. Consequently, dendritic spikes are promoted. Endocannabinoid signaling is one of the key steps in the described frequency loop. However, CB1 receptors are not only expressed by astrocytes, but to an even greater extent by neurons (Marsicano and Lutz, 1999; Navarrete and Araque, 2008). To study specifically the involvement of astrocytic CB1 receptors in this pathway, a transgenic mouse line was used ($CB1^{f/f}$ x Ai14 x GLAST-creERT2). In these mice, tamoxifen treatment results in translocation of the cre recombinase to the nucleus selectively in cells that express the glutamate aspartate transport (GLAST). In the nucleus the cre recombinase binds and cleaves the DNA flanked by two lox-P sequences present in the coding region for the CB1 receptor and around a stop codon in front of the sequence for tdTomato. Accordingly, CB1 receptors are knocked out and the expression of tdTomato activated in GLAST-positive cells. The efficacy and specificity to astrocytes of the knock-out was determined by perfusion fixation and staining for the astrocyte marker GFAP, the neuronal marker NeuN and the nuclei marker Hoechst (Figure 3.21). tdTomato expression was used as a proxy for CB1 receptor removal. The majority of the tdTomato-expressing cells were GFAP-positive astrocytes (89.70 ± 1.42 %, n = 3) and hence, should have a knock-out for the CB1 receptor. Interestingly, a subset (7.45 ± 1.22 %, n = 3) of the tdTomato expressing cells were negative for NeuN and GFAP staining. This might suggest that some of these cells are not astrocytes. It is important to note that GFAP staining does not label all astrocytes in the hippocampus (Walz and Lang, 1998). Importantly, nearly all (98.71 ± 0.82 %, n = 3) of the GFAP-positive astrocytes also expressed tdTomato, while only a very small number (2.04 ± 1.80 %, n = 3) of the NeuN-positive neurons did. These results suggest that the CB1 receptor is deleted in the majority of astrocytes.

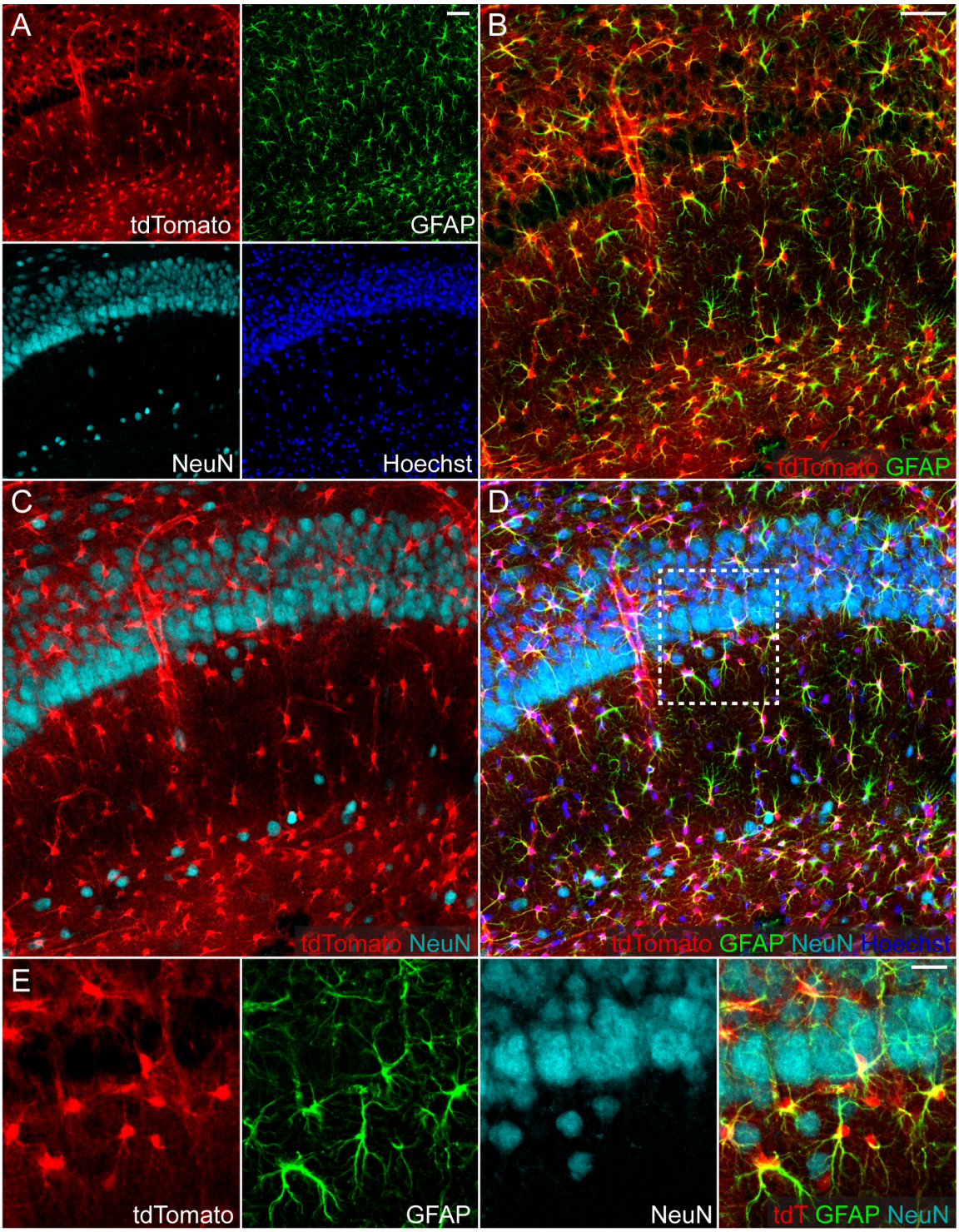

Figure 3.21. Knock-out of CB1 receptors selectively in astrocytes. Representative average projection of a confocal z-stack of 20 µm of a ventral hippocampus slice of a GLAST-CreERT2 x CB1f/f x Ai14 mouse after cre induction by tamoxifen shows the endogenous tdTomato expression and antibody staining for astrocytes (GFAP), neurons (NeuN) and nuclei (Hoechst). **(A-D)** Overview of the CA1 region in single color and multi-color overlays (scale bars: 50 µm). **(E)** Enlargement of the marked area in (D) for tdTomato, GFAP and NeuN (scale bar: 20 µm).

Using these animals, as well as sham-injected (sunflower oil with 10 % ethanol) and wild type mice as controls, the role of astrocytic CB1 receptors in alveus stimulation-mediated enhancement of dendritic integration was assessed (Figure 3.22 A&B). It is important to note that sham as well as astrocyte-specific CB1 receptor knock-out (aCB1KO) mice have a heterozygous knock-out of GLAST. Although the majority of glutamate clearance from the synapse at the age used is performed by GLT1 (Rose et al., 2018), an effect on neuronal excitability cannot be excluded. Therefore, the basic cellular properties of the whole-cell patched CA1 PCs from wild type mice were compared to the ones from sham and aCB1KO mice. The membrane resistance (R_m) and the resting membrane potential (V_m) did not differ (Table 3). However, the AP threshold showed significant differences between the three mouse lines. Both sham and aCB1KO mice showed a significant decrease compared to control (Table 3, control vs. sham: $p = 0.010$, control vs. aCB1KO $p = 0.027$, post-hoc Fisher's LSD). The shape of the APs remained comparable. Additionally, the population spike amplitude was significantly different. These population spikes were evoked by alveus stimulation with a stimulation intensity that resulted in 80% of the maximal amplitude. Post-hoc analysis revealed that the amplitude was selectively increased in sham mice (Table 3, wild type vs. sham: $p = 0.049$, sham vs. KO $p = 0.002$, post-hoc Fisher's LSD).

Table 3. Properties of CA1 pyramidal cells in wild type, sham-injected and aCB1KO mice

parameter	wild type (mean ± SEM)	sham (mean ± SEM)	aCB1KO (mean ± SEM)	n	p	test
Rm (MΩ)	136.8 ± 14.1	119.3 ± 9.7	132.8 ± 10.5	7/8/9	0.54	one-way ANOVA
Vm (mV)	-63.4 ± 2.96	-66.9 ± 1.95	-67.7 ± 1.18	7/8/9	0.21	one-way ANOVA
AP threshold (mV)	-43.1 ± 2.11	-50.0 ± 1.88	-48.9 ± 1.09	9/10/10	0.02	one-way ANOVA
AP height (mV)	93.1 ± 1.7	93.7 ± 4.0	94.1 ± 1.4	8/10/10	0.97	one-way ANOVA
AP upstroke (mV/ms)	409.3 ± 16.8	407.2 ± 9.2	400.1 ± 14.7	9/9/10	0.87	one-way ANOVA
popspike (mV)	-1.82 ± 0.25	-2.55 ± 0.31	-1.43 ± 0.13	7/8/9	0.008	one-way ANOVA

AP, action potential, aCB1KO, astrocyte-specific knock-out of CB1 receptor. popspike, population spike amplitude.

These results show that the heterozygous knock-out of GLAST possibly increased the excitability of CA1 pyramidal cells through lowering the AP threshold. However, sham-injected control mice, with the same genetic background as the aCB1KO mice, were used as controls in all further experiments. Accordingly, any effect discovered between these two groups of mice cannot be the result of an increased excitability. Furthermore, an unspecific difference in the amplitude of the population spikes was discovered. My results showed that the number of recruited CA1 PCs varies substantially between different slices (ranging from 20-80 %, Figure 3.16). Therefore, this is likely the result of the slicing procedure causing a differential connectivity and, hence, recruitment of CA1 pyramidal cells during retrograde stimulation.

Next, the effect of 10 Hz alveus stimulation on the local dendritic integration was investigated in wild type, sham-injected and aCB1KO mice. Therefore, the same experimental approach as before was used (Figure 3.22 A&B). The threshold of the dendritic spike was under control conditions (wild type and sham mice) significantly decreased during 10 Hz stimulation (Figure 3.22 C, left panel). No difference was found in the aCB1KO animals. Accordingly, the subthreshold EPSP amplitude (Figure 3.22 D, left panel), NMDA receptor component amplitude (Figure 3.22 E, left panel) and the maximum slope of dendritic spikes (Figure 3.22 F, left panel) showed an increase

during alveus stimulation in both control groups, but not in aCB1KO mice. Comparing the relative change of each parameter between the different treatments showed significant differences between both control groups and aCB1KO mice (Figure 3.22 C-F, right panel).

Selective removal of astrocytic CB1 receptors impaired the effect of 10 Hz alveus stimulation that is observed under control condition and, importantly, in sham-injected control mice. Furthermore, no differences between these two control groups was found. Therefore, the differences in excitability between wild type and transgenic mice and the unspecific increase in the population spike amplitude are not influencing these results. In accordance with these results astrocytic CB1 receptors play a key role in the modulation of supralinear dendritic integration during PC firing.

In summary, my data show that theta frequency range of CA1 PCs probably causes the mobilization of endocannabinoids likely in the stratum radiatum. Here endocannabinoids activate astrocytic CB1 receptors and subsequently an increase in the astrocytic calcium occurs. The calcium increase stimulates the release of D-serine locally at the dendrites. Under these circumstances, clustered synapses activated are now more likely to cause the initiation of dendritic spikes and possibly changes in the AP output of the CA1 PC. An interesting question, which remains, addresses the behavior that requires this positive feedback exerted by astrocytes through the activation of their CB1 receptors.

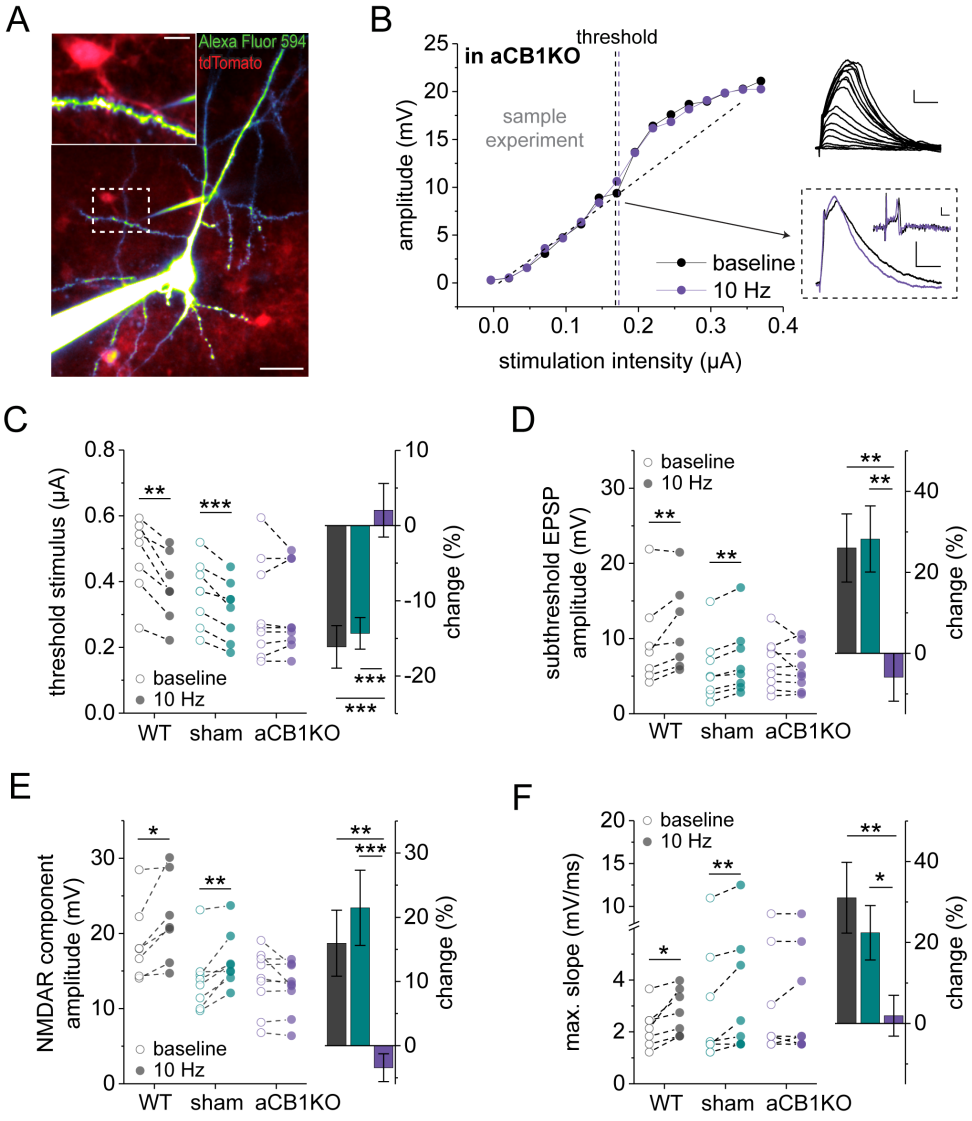

Figure 3.22. Astrocytic CB1 receptors are essential for facilitation of supralinearity. (A) Example of a CA1 pyramidal cell filled with Alexa Fluor 594 (40 µM) via a whole-cell patch clamp pipette in an aCB1RKO (GLAST-CreERT2 x CB1f/f x Ai14 mouse, tamoxifen injected) mouse (scale bar: 20 µm) and enlargement of the stimulated dendrite within the territory of a tdTomato expressing astrocyte (scale bar: 5 µm). **(B)** Representative example of the relationship between iontophoretic stimulation intensity and somatic EPSP amplitude for a nonlinear integrating dendrite in an aCB1KO mouse during baseline (black) and after 10 Hz alveus stimulation (purple). The first dendritic spike is marked by a color-coded dashed line with the corresponding somatic traces (scale bar: 3 mV, 20 ms) and first derivatives (scale bar: 2 mV/ms, 2 ms) in the right panel. **(C)** Wild type and sham injected mice showed a decrease in the threshold stimulus after 10 Hz stimulation (WT: 0.47 ± 0.04 µA vs. 0.38 ± 0.04 µA, n = 7, p = 0.002, paired t-test; sham: 0.36 ± 0.03 µA vs. 0.31 ± 0.03 µA, n = 8, p = 0.0007, paired t-test). No change was observed in aCB1RKO mice (0.26 IQR 0.19-0.45 µA vs. 0.26 IQR 0.22-0.47 µA, n = 9, p = 1, Wilcoxon signed-rank test). **(D)** The amplitude of subthreshold EPSP was significantly increased with 10 Hz stimulation of the alveus in WT and sham-injected mice (WT: 9.60 ± 2.32 mV vs. 11.44 ± 2.18 mV, n = 7, p = 0.041, paired t-test; sham: 5.92 ± 1.51 mV vs. 7.09 ± 1.62 mV, n = 8, p = 0.0002, paired t-test) but unchanged in aCB1KO mice (6.63 ± 1.09 mV vs. 6.07 ± 0.96 mV, n = 9, p = 0.32, paired t-test). **(E)** Also, the amplitude of the NMDA receptor component of the dendritic spike was significantly increased with 10 Hz stimulation in WT and sham-injected mice (WT: 18.81 ± 1.91 mV vs. 21.93 ± 2.20 mV, n = 7, p = 0.021, paired t-test; 13.83 ± 1.50 mV vs. 16.41 ± 1.29 mV, n = 8, p = 0.006, paired t-test) but not in aCB1KO mice (13.73 ± 1.36 mV vs. 12.83 ± 1.14 mV, n = 9, p = 0.14, paired t-test). **(F)** The maximum slope was increased by 10 Hz alveus stimulation in both control animals (WT: 2.18 ± 0.30 mV/ms vs. 2.79 ± 0.34 mV/ms, n = 7, p = 0.013, paired t-test; sham: 1.58 IQR 1.30-4.50 mV/ms vs. 2.13 IQR 1.53-5.03 mV/ms, n = 8, p = 0.008, Wilcoxon signed-rank test), but not in the aCB1KO ones (1.83 IQR 1.53-4.27 mV/ms vs. 1.83 IQR 1.53-4.73 mV/ms, n = 9, p = 0.91, Wilcoxon signed-rank test). **(C-F)** For all parameters a significant change of WT and sham compared to aCB1KO was present (one-way ANOVA with post-hoc Fisher's LSD). WT, wild type; aCB1RKO, astrocyte specific CB1 receptor knock-out. Note: *Post-hoc testing was only performed if the one-way ANOVA reported significant overall differences. * p < 0.05, ** p < 0.01*, *** p < 0.001.

3.9 Astrocytic CB1 Receptors Regulate Spatial Learning and Memory

To address the behavioral output this novel frequency-dependent feedback loop mediates, it is important to take several things into account. The specific tuning to activity in the theta frequency band suggests that especially behavior that induces this activity could recruit astrocytic CB1 receptors. In the hippocampus the frequency of theta oscillations correlate with the animal's speed during exploration (Kramis et al., 1975; Vanderwolf, 1969). Furthermore, it is thought that theta oscillations put the hippocampus in an active state necessary for the encoding of memory (Buzsáki, 2002; Tanaka et al., 2018). Memory processed and encoded by the CA1 microcircuit usually contains spatial aspects. For example, changes in the environment result in rearrangement of CA1 place cells and fields (Lenck-Santini et al., 2005; Lever et al., 2010). This rearrangement is accompanied by a shift in the phase precession of the place cells to the local theta rhythm. Dendritic spikes have been shown to correlate with the spatial precision, generation, persistence and disappearance of place fields in CA1 PCs (Sheffield and Dombeck, 2015; Sheffield et al., 2017). Accordingly, behavioral tests, which require spatial learning through dynamic changes in the place cell firing, are suitable to study the role of astrocytic CB1 receptors.

To investigate if astrocytic CB1 receptors modulate learning and memory formation aCB1KO mice ($CB1^{f/f}$ x Ai14 x GLAST-creERT2, tamoxifen injected) and sham-injected littermates as control mice were subjected to several tasks. The design of these experiments was developed by me with the expertise of Thoralf Opitz (senior postdoctoral fellow, laboratory of Heinz Beck). The required animals for the experiments were bred, tamoxifen injected and verified by me. I monitored the experiments and analyzed the obtained data. The performance of the behavioral experiments and the corresponding handling of these animals was the responsibility of Rebekka Zölzer (technical assistance, laboratory of Heinz Beck).

3.9.1 Astrocytic CB1 Receptors do not Influence General Exploratory Behavior

The open field test is widely used to gain insight into a mouse's locomotor ability and anxiety-like behavior (Seibenhener and Wooten, 2015). Before behavioral testing is performed, it is important to test, whether locomotion and exploration is comparable between the mice. Differences detected with the open field test may affect any result obtained using other tests. Naïve mice were placed into an open field arena (40 x 60 cm) and were allowed to explore it freely for ten minutes (Figure 3.23 A&D). The total distance travelled and the mean velocity of the mice did not differ between the groups (Figure 3.23 B&C). Thus, the locomotion between the two groups of mice is comparable. Importantly, fecal boli deposits and the relative cumulative time the animals spend in the inner or outer zone of the open field did not show differences either (Figure 3.23 A&E). Increased anxiety or stress is known to increase fecal boli deposits and will decrease the time spend in the inner zone (Seibenhener and Wooten, 2015). However, no differences were detected between the two groups of mice. Therefore, mice with an astrocytic CB1 receptors knock-out showed no impairment in locomotion or anxiety-like behavior that could confound further behavioral examination.

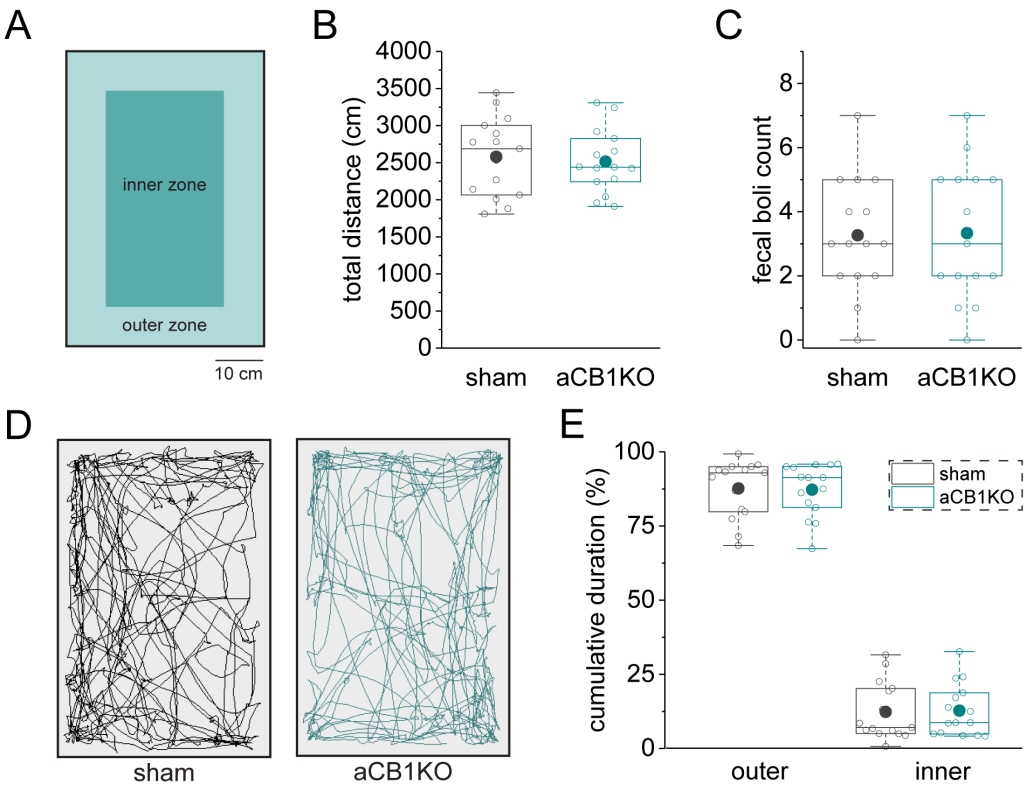

Figure 3.23. Astrocytic CB1 receptors do not influence exploratory behavior in the open field. (A) Schematic representation of the open field arena (40 x 60 cm). **(B)** Total distance the mice travelled within ten minutes of free exploration of the arena showed no difference between the two groups (2580 ± 136 cm vs. 2514 ± 109 cm, n = 15, p = 0.71, Student's t-test). **(C)** Fecal boli deposit count was comparable between the two groups (3.27 ± 0.46 vs. 3.33 ± 0.54, n = 15, p = 0.93, Student's t-test). **(D)** A representative track of a sham and aCB1KO mouse throughout the area. **(E)** Cumulative duration mice of both groups spend in the outer and inner zone, respectively, did not show differences between the two groups or an interaction effect (outer: 87.67 ± 2.50 % vs. 87.22 ± 2.27 %; inner: 12.33 ± 2.5 % vs. 12.77 ± 2.27 %, n = 15, group: p = 0.33, interaction: p = 0.90, two-way repeated measurement ANOVA).

3.9.2 Spatial Working Memory Does not Require Astrocytic CB1 Receptors

The hippocampus plays an important role in encoding spatial working memory (Spellman et al., 2015). It is thought that constant updating of spatial information takes place through direct connections with the prefrontal cortex. However, activity in several other brain regions is required as well (Lalonde, 2002). Accordingly, spatial working memory tasks are often used to investigate general cognitive deficits in rodents. Alterations in spatial working memory can influence the behavior of mice in other tasks, as it is required for exploration of unfamiliar environments and continuous adaptation of once behavior in response to rewards or threats (Baddeley, 1992). One task that investigates spatial working memory is the Y-maze (Figure 3.24 A; Lalonde, 2002). Resulting from the inherent preference to novelty, mice tend to visit the arms in alternating order. This order of arm entries is recorded to calculate the alternation index (AI). If a mouse visited all three arms after one another, the triplet is counted as an alternation. The AI measures the number of performed alternations relative to the number of possible alternations (max. number of alternations). aCB1KO mice did not show any difference in the AI (Figure 3.24 B) nor in the total number of alternations (Figure 3.24 C) compared to sham-injected control mice. In summary, aCB1KO mice did not show any deficits in spatial working memory.

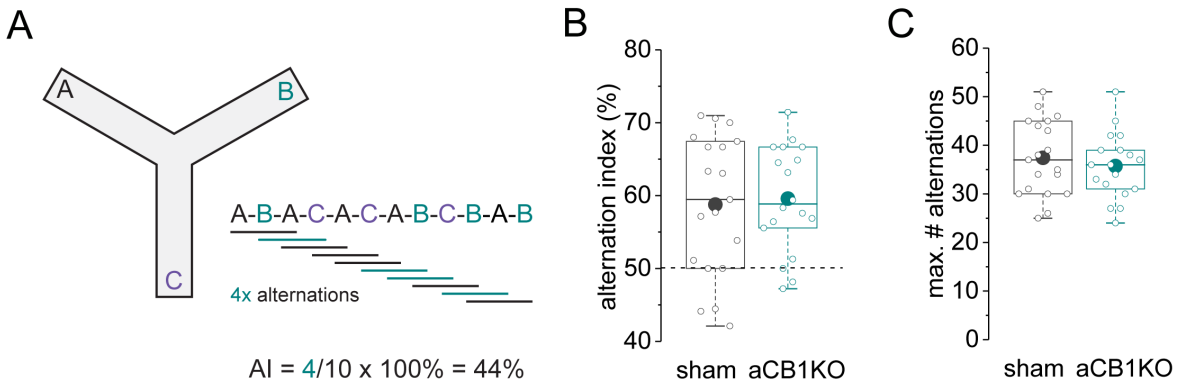

Figure 3.24. Astrocytic CB1 receptors do not influence spatial working memory. (A) Schematic representation of the arena. The sequence of arm entries was recorded and analyzed for triplets containing all three arms. This number is divided by the total number of possible triplets and multiplied by 100 to calculate the alteration index (AI). **(B)** The AI was not different between sham-injected and aCB1KO mice (58.77 ± 2.21 % vs. 59.58 ± 1.72 %, n = 19/18, p = 0.78, Student's t-test). **(C)** The maximum number of possible alterations did not differ (37.42 ± 1.78 vs. 35.72 ± 1.61, n = 19/18, p = 0.48, Student's t-test).

3.9.3 Astrocytic CB1 Receptors are Required for Long-Term Spatial Memory

The CA1 microcircuit has a central role in spatial novelty detection (Brun et al., 2002; Larkin et al., 2014; Lee et al., 2004). This requires retrieval of already encoded memory. The Schaffer collateral fibers transmit this information from the CA3 to the CA1. Accordingly, the modulation of dendritic spikes in the stratum radiatum of CA1 by astrocytic CB1 receptors could alter memory retrieval and, hence, impair novelty detection. Object recognition tasks, like the novel object recognition task (NORT) and object location task (OLT), require memory retrieval for accurate novelty detection (Ennaceur, 2018). During both tasks, the mice were freely exploring two identical objects for ten minutes. After a 24-hour delay either one object or the location of one object was changed. Since mice show an inherent preference for novelty, they are expected to show more interest in the novel object or location compared to the familiar one. Therefore, the time the animals explored each object was measured. Exploration was defined as the nose-point being within 2 cm of the object, with the body pointing towards the object. The discrimination index (DI; see section 2.6.2) was used as a parameter for analysis.

The NORT requires apart from several cortical areas also the hippocampus (Antunes and Biala, 2012) and is frequently used to study alterations in long-term memory. During acquisition of the object's identity, sham and aCB1KO mice examined both objects in a similar ratio and for a similar duration (Figure 3.25 A). After a 24 h delay, one of the objects was exchanged with a novel one that was different in shape, texture and color (Figure 3.25 B). After the delay, mice from both groups were able to distinguish the novel from the familiar object (Figure 3.25 B2, DI > 0, $p < 0.001$, one-population Student's t-test). Nevertheless, the DI was significantly lower in aCB1KO mice. The total object exploration time showed a trend to be lower in the aCB1KO mice. Examining the relationship between exploration time and DI revealed a significant correlation ($R = 0.43$, $p = 0.043$, Spearman's rank correlation). Therefore, an interpretation of the result is difficult, since the difference in discrimination could be cause by a decreased interest in the objects.

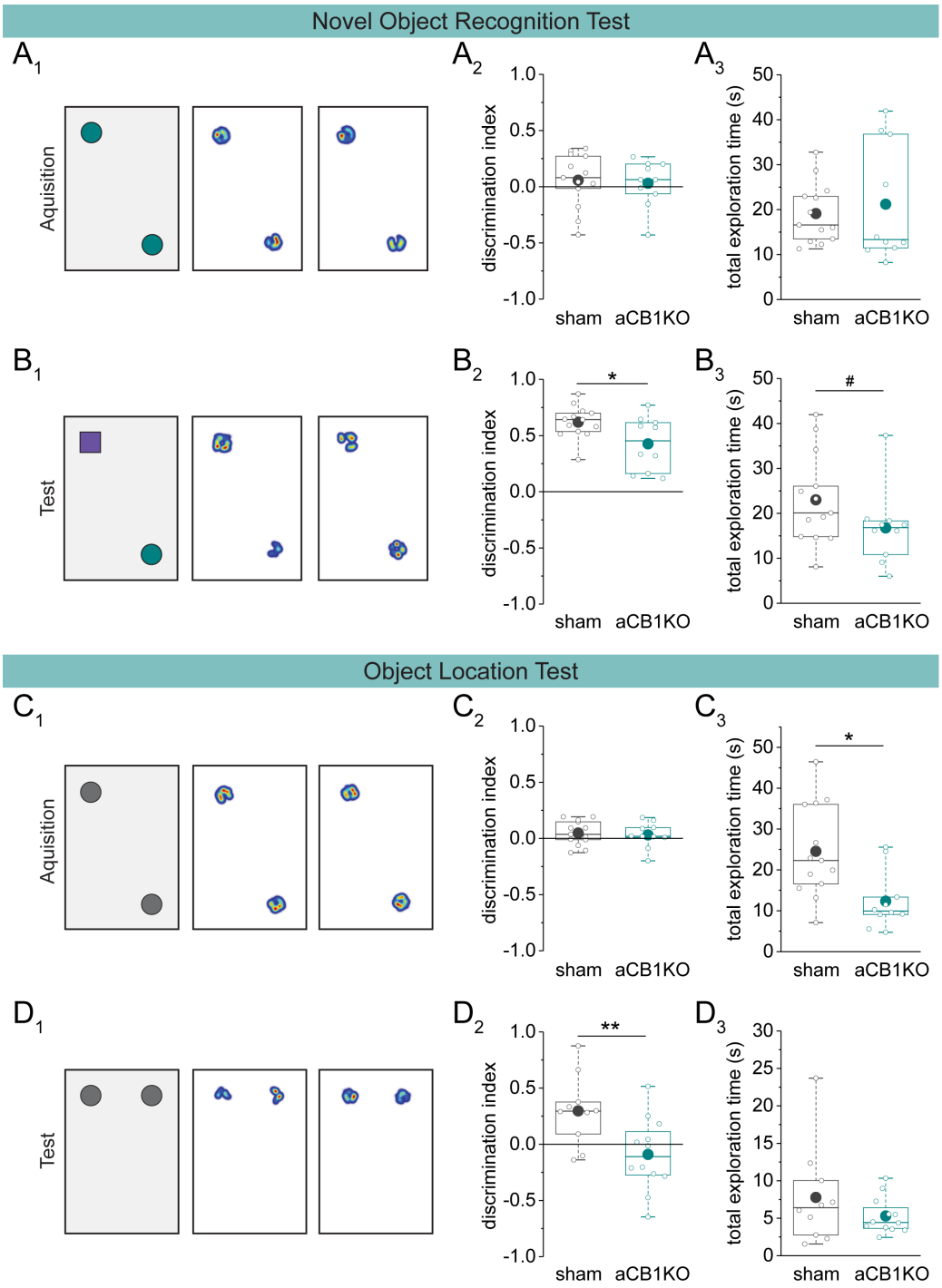

Figure 3.25. Astrocytic CB1 receptors mediate object recognition and location memory. (A1-D1) Schematic representation of the arena and representative heat maps for one mouse of each group illustrating the relative exploration time of each objects. **(A)** Acquisition of novel object recognition test. **(A2,3)** Sham-injected and aCB1KO mice show no difference in the discrimination index between objects (0.06 ± 0.07 vs. 0.03 ± 0.07, n = 13/10, p = 0.78, Student's t-test) and total exploration time (16.56 IQR 13.18-23.56 s vs. 13.34 IQR 11.36-36.99 s, n = 13/10, p = 0.74, Mann-Whitney test). **(B)** Memory test of novel object recognition test. **(B2)** aCB1KO mice had a significantly reduced discrimination index compared to sham-injected control mice (0.62 ± 0.04 vs. 0.43 ± 0.08, n = 13/10, p = 0.025, Student's t-test). **(B3)** The total exploration time of the objects was slightly reduced in aCB1KO mice (20.09 IQR 14.74-30.11 s vs. 16.83 IQR 10.40-18.42 s, n = 13/10, p = 0.10, Mann-Whitney test). **(C)** Acquisition of the object location test. **(C2)** Mice from both groups did not discriminate between the two object locations during learning (0.08 ± 0.03 vs. -0.002 ± 0.07, n = 10/12, p = 0.34, Student's t-test). **(C3)** aCB1KO mice explored the objects significantly less compared to sham-injected mice during acquisition (22.58 IQR 18.09-36.57 s vs. 10.67 IQR 9.11-24.52 s, n = 10/12, p = 0.021, Mann-Whitney test). **(D)** Memory test of object location test. **(D2)** While sham-injected mice explore the object in the novel location significantly more, aCB1KO mice did not discriminate between the objects (0.30 ± 0.010 vs. -0.09 ± 0.09, n = 10/12, p = 0.0098, Student's t-test). **(D3)** The total time the mice explored the objects was not different (6.40 IQR 2.65-10.61 s vs. 4.43 IQR 3.59-6.83 s, n = 10/12, p = 0.54, Mann-Whitney test).

In contrast to the NORT, the OLT is particularly sensitive to alterations in the hippocampal CA1 region (Assini et al., 2009). While both groups examined the two objects on the first day to a similar extent (Figure 3.25 C1&2), the total exploration time was significantly shorter in the aCB1KO mice (Figure 3.25 C3). After the 24 h delay, aCB1KO mice showed an inability to distinguish the object in the novel location from the one in the familiar location (Figure 3.25 D1&2, 0.09 ± 0.35, n = 12, p = 0.35, one-population Student's t-test). Furthermore, the DI was significantly lower compared to the sham controls (Figure 3.25 D2) without any difference in the total exploration time (Figure 3.25 D3). To determine whether the shortened exploration times during memory acquisition in aCB1KO mice might influence the DI on the second day, the relationship between the two was examined. However, no significant correlation was found (R = 0.21, p = 0.36, Spearman's rank correlation). It can be concluded that the selective knock-out of CB1 receptors from astrocytes results in impaired spatial long-term memory.

3.9.4 Astrocytic CB1 Receptors are Recruited During Spatial Reversal Learning of an Aversive Stimulus

Emotions can improve episodic memory formation (Hamann et al., 1999) and in line with this activity in the amygdala has been shown to be responsible for memory enhancement through aversive stimuli. The amygdala is strongly connected to the ventral hippocampus (Kishi et al., 2006), where the slice experiments characterizing the frequency-dependent feedback loop were performed. To examine fear-related spatial memory, the mice were subjected to a passive place avoidance task. During this task, an aversive stimulus in form of an air puff is introduced in specific locations of an O-shaped maze (Figure 3.26 A). This behavior test can be used to examine several components of aversive memory formation in relation to a spatial paradigm: the encoding (learning), the memory retention (stability) and reversal memory (flexibility); and hence activity in several neocortical areas, the amygdala and the hippocampus (Cimadevilla et al., 2000; D'Hooge and De Deyn, 2001; Lénárd and Kertes, 2002; Vafaei and Rashidy-Pour, 2004).

During the first day, the mice were habituated to the O-shaped maze. Both groups explored the maze at similar velocity (9.72 ± 0.64 cm/s vs. 9.37 ± 0.48 cm/s) and distance travelled (Figure 3.26 B). On the second day, an air puff was introduced at position A. This resulted in an overall reduction of locomotion. Mice from both groups learned the position of the air puff quickly (Figure 3.26 C). During the second half of the exploration period, mice of both groups activated the air puff less than once. Comparing these to the first half, significant learning, measured through the number of air puff activation, was observed in both groups. Notably, no significant difference between sham-injected and aCB1KO mice was detected. On the third day, long-term aversive place memory was tested, with the air puff still being present at position A. The number of air puff activations and the latency to the first activation did not differ between the two groups of mice (Figure 3.26 D). On the fourth day, on which the air puff was no longer present, no difference in retention memory was detected (Figure 3.26 E). On day five, the air puff was moved to position B on the opposite side of the maze to examine the flexibility of the aversive memory. The aCB1KO mice showed a significantly higher number of air puff activations compared to sham-injected mice, while crossings at the previous location (position A) were comparable (Figure 3.26 F, left panel). Moreover, the duration from first to last air puff activation was significantly increased in knock-out mice (Figure 3.26 F, middle left panel).

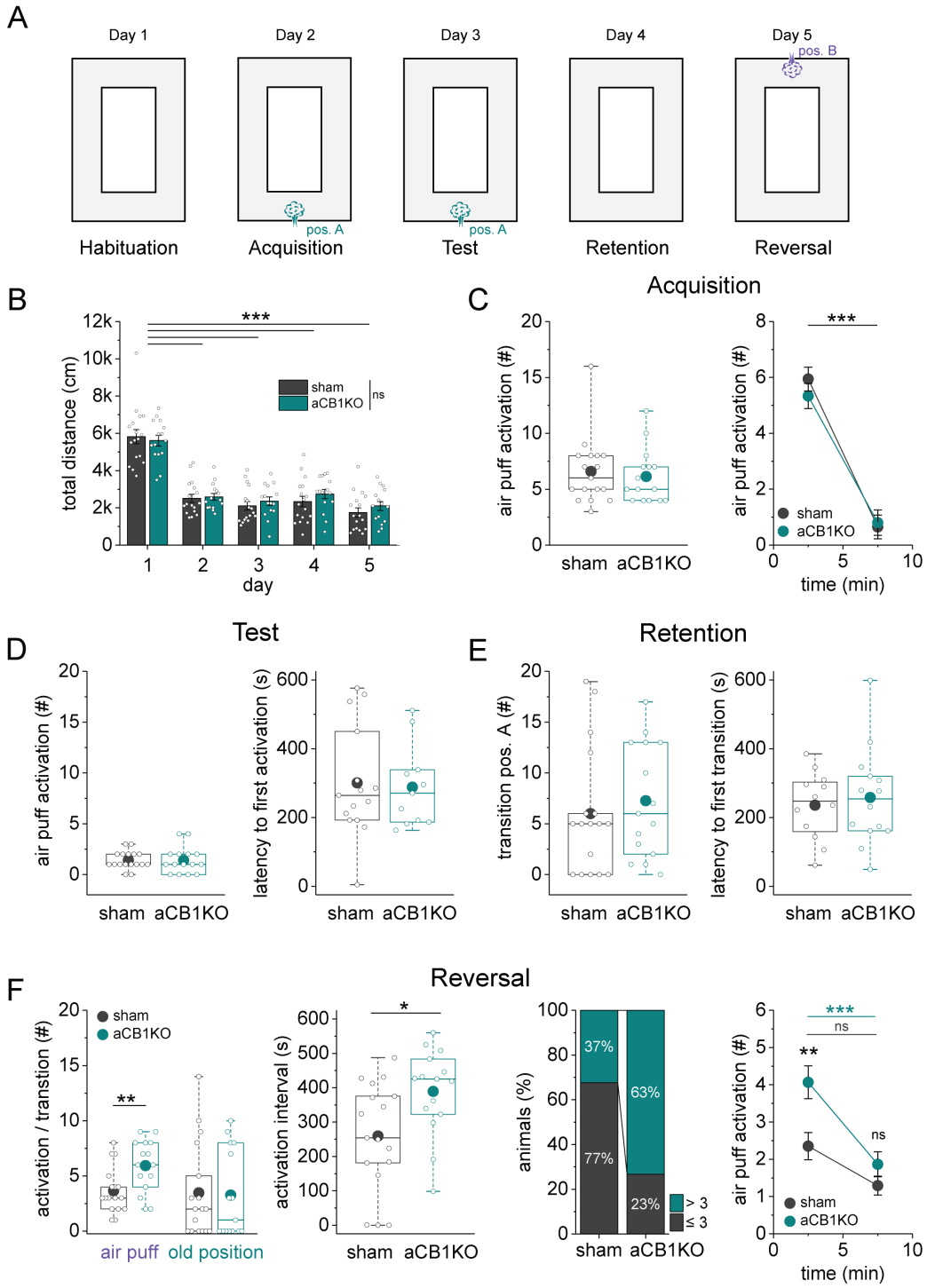

Figure 3.26. Astrocytic CB1 receptors selectively influence reversal memory in a passive place avoidance task. (A) Schematic representation of the arena with location of the air puff for each day of the task. **(B)** The total distance the mice travelled in the arena per day showed no difference between the two groups of mice (n = 17/15, p = 0.58, two-way repeated measurement ANOVA). After the introduction of the air puff, the total distance travelled significantly decreased for all mice comparing each day to day 1 (n = 17/15, p < 0001, two-way repeated measurement ANOVA with Greenhouse-Geisser correction; p < 0.001, post-hoc Tukey test). **(C)** Day 2: Acquisition. Sham-injected and aCB1KO mice activated the air puff in comparable amounts (6 IQR 4.5-8 vs. 5 IQR 4-7, n = 17/15, p = 0.62, Mann-Whitney test). Comparing the air puff activation binned by five minutes intervals revealed a significant decrease over time (n = 17/15, p < 0.001, two-way repeated measurement ANOVA). No difference between the groups of mice was detected (n = 17/15, p = 0.64, two-way repeated measurement ANOVA). **(D)** Day 3: Test. Sham-injected and aCB1KO mice activated the air puff equally often (1 IQR 1-2 vs. 1 IQR 0-2, n = 17/15, p = 0.73, Mann-Whitney test). The latency to the first air puff activation did not show a difference (300.75 ± 41.7 s vs. 288.30 ± 35.82 s, n = 15/11, p = 0.83, Student's t-test).

(Figure legend continued on next page)

(E) Day 4: Retention. At this day, the air puff was removed. The transitions at the former air puff location did not show a significant difference between both groups of mice (5 IQR 0-9 vs. 6 IQR 2-13, n = 17/15, p = 0.45, Mann-Whitney test), neither did the latency to the first transition (235.73 ± 28.42 s vs. 258.23 ± 37.43 s, n = 12/14, p = 0.65, Student's t-test). **(F)** Day 5: Reversal. At this day, the air puff was moved to the opposite arm. aCB1KO mice activated the air puff significantly more often than sham-injected control mice (3.65 ± 0.50 vs. 5.93 ± 0.61, n = 17/15, p = 0.0066, Student's t-test). The transitions at the former air puff location did not show a difference between the two groups of mice (2 IQR 0-6.5 vs. 1 IQR 0-8, n = 17/15, p = 0.77, Mann-Whitney test). The time interval between first and last activation of the air puff was significantly longer in aCB1KO mice than in sham-injected ones (259.57 ± 38.23 s vs. 389.19 ± 32.26 s, n = 17/15, p = 0.016, Student's t-test). The number of animals activating the air puff ≤ 3 or > 3 times was significantly different between the two groups of mice (p = 0.036, Fisher's exact test). Comparing the number of air puff activations binned in five minutes intervals revealed a significant influence of the time bin and the group of the mice (n = 17/15, time: p = 0.000009, group: p = 0.0066, time x group: p = 0.072, two-way repeated measure ANOVA). aCB1KO mice activated the air puff significantly more often during the first five minutes compared to sham-inject mice (2.35 ± 0.33 vs. 4.07 ± 0.35, p = 0.0007, post-hoc Tukey test), but not during the last five minutes (1.29 ± 0.33 vs. 1.87 ± 0.35, p = 0.64, post-hoc Tukey test). Additionally, sham-injected mice did not show a difference over time (2.35 ± 0.33 vs. 1.29 ± 0.33, p = 0.13, post-hoc Tukey test), while aCB1KO mice did (4.07 ± 0.35 vs. 1.87 ± 0.35, p = 0.0006, post-hoc Tukey test).

To investigate the difference on the fifth day in more detail, mice were categorized as quick-learners (≤ 3 activations) and slow-learners (> 3 activations; Figure 3.26 F, middle right panel). A significant higher proportion of aCB1KO mice were slow-learners, with a relative risk of 2.74. Nevertheless, over time a significant reduction in air puff activations was observed in the aCB1KO mice as well (Figure 3.26 F, right panel). In line with this, a significant difference in air puff activation was only observed during the first five minutes bin, with comparable activation numbers during the last bin, comparing sham and aCB1KO mice. Interestingly, significant differences in the number of air puff activations between the initial learning (day one) and reversal learning (day five) were observed (Figure 3.26 C and F, left panel: day: p = 0.013, group: p = 0.17, day x group: p = 0.028, n = 32, two-way repeated measures ANOVA). Sham-injected control mice required a significant lower number of activations on day five than on day one (6.59 ± 0.73 vs. 3.65 ± 0.50, n = 17, p= 0.0068, post-hoc Tuckey test). This difference was not detected in the aCB1KO mice (6.13 ± 0.62 vs. 5.93 ± 0.61, n= 15, p = 1.00, post-hoc Tuckey test). On the fourth day, the aversive place memory is overridden and therefore transitions at this position occurred in increasing number independent of the CB1 receptor knock-out (first time-bin: 2.2 ± 0.47 vs. second time-bin: 4.41 ± 0.68, n = 32, time: p = 0.0003, time x group: p = 0.52, group: p = 0.55, two-way repeated measures ANOVA, data not shown). However, the total number of activations varied considerably between animals, with a coefficient of variation of 1.05. As memory extinction and reversal learning are both important for cognitive flexibility (Chaby et al., 2019), the deficit in acquiring the novel spatial information of the air puff location might correlate with the inability to eliminate the previously learning position. This hypothesis was tested by investigating the relationship between the number of transitions on day four (measure of memory extinction) and the number of air puff activations on day five (measure of reversal learning). Surprisingly, the opposite was found. Mice that showed a higher number of transitions on day four (no air puff), also showed higher transition rate on day five for both locations (A: R = 0.44, n = 32, p = 0.01; B: R = 0.53, n = 32, p = 0.002, Spearman's rank correlation, data not shown). This means, that exactly those mice that display successful memory extinction, show an impairment during the reversal learning. Thus, rather unspecific general mouse-to-mouse differences in locomotion might underlie this correlation. It is important to note that a small number of mice did not cross position A on day four. These mice never discover the absence of the air puff. As no extinction of the previous memory was induced, it was investigated whether this has an impact on the result obtained. However, excluding these mice from analysis still resulted in a significant difference in total air puff activation on day five (3.75 ± 0.57 vs. 6.14 ± 0.62, n = 12/14, p = 0.0096, Student's t-test, data not shown).

In summary, the results show that aCB1KO display normal exploratory and anxiety-related behavior as well as spatial working memory. However, aCB1KO mice are unable to distinguish between an object in a familiar and novel location after a 24 h delay. Likewise, the recognition of the novel object as opposed to a familiar one was impaired. This suggests a deficit in spatial novelty detection during long-term spatial learning. Using a spatial place avoidance task, it was shown that aCB1KO mice were able to acquire, remember and extinct an aversive place memory. While these results might seem to contradict the results from the object recognition memory task, it is important to take into consideration that emotional learning enhances our learning abilities (Hamann et al., 1999). The presence of an aversive stimulus will recruit other brain regions, like the amygdala, that by connections to the hippocampus can alter memory encoding and reconsolidation (McGaugh, 2004). Therefore, more subtitle deficits in spatial learning might not be detected in the passive place avoidance task. Interestingly, aCB1KO mice showed a significant reduction in learning a second, new position of an aversive stimulus. Thus, aCB1KO mice might have a reduced memory flexibility. Taken together, these results show that astrocytic CB1 receptors play an important role in spatial long-term memory and control the adaptation of a formed aversive memory.

4 DISCUSSION

My thesis investigated how astrocytes shape dendritic integration and how this affects behavior. The integration of synaptic inputs is a fundamental feature of neurons. A hippocampal CA1 pyramidal cell (PC) receives thousands of inputs. The resulting changes in potential are summed up not only at the soma but also locally in the dendrites. Here, asynchronous or distributed inputs are integrated linearly (Gasparini et al., 2004; Losonczy and Magee, 2006). Synchronous, spatially clustered inputs, however, can evoke dendritic spikes under specific circumstances. This will result in a supralinear summation of the synaptic input. Moreover, CA1 PC dendrites can generate large local plateaus potentials in response to simultaneous activation of both input pathways, i.e., the Schaffer collateral and perforant path fibers (Takahashi and Magee, 2009). Dendritic spikes and plateau potentials modulate distinct output computations and have been implicated in place cell arrangement in vivo: changes in action potential (AP) number and timing or changes in firing mode (Bittner et al., 2017; Grienberger et al., 2014). The presented results showed that astrocytes can modulate dendritic integration. On the one hand, glutamate uptake by astrocytes is less efficient at large spines compared to small ones. The former also favors the induction of dendritic spikes and supralinear integration over linear dendritic integration without dendritic spikes. On the other hand, astrocytes can dynamic modulation of supralinear dendritic integration through the supply of the NMDA receptor co-agonist D-serine. My experiments revealed a previously unknown positive feedback loop linking activity in the theta frequency band, endocannabinoids, astrocytic CB1 receptors and calcium elevations to the release of D-serine and a subsequent increase in supralinear dendritic integration. Disrupting this signaling cascade led to specific alterations in spatial learning and memory. Furthermore, a central role of the astrocytic resting calcium concentration in mediating the shape of calcium transients was discovered. This section discusses the results and their implications.

4.1 ASTROCYTE CALCIUM TRANSIENT SHAPE AND FUNCTION

Calcium transients in astrocytes have a crucial role in regulating synaptic transmission through, for example, the release of gliotransmitters (Guerra-Gomes et al., 2018). One of the aims of my thesis was to gain a better understanding of the factors determining the shape of astrocytic calcium transients. To this extent, the relevance of the resting calcium concentration in astrocytes for peak and amplitude of calcium transients was studied. Using fluorescence lifetime imaging (FLIM) recordings of the calcium-sensitive indicator Oregon Green BAPTA-1 (OGB-1) in whole-cell patch clamped astrocytes, Claire M. King, a former Ph.D. student in our laboratory, demonstrated not only strong variations in the resting calcium concentration within individual astrocytes but also found a positive correlation between the resting and peak calcium concentration of spontaneous and evoked calcium transients (King*, Bohmbach* et al., 2020). Furthermore, she discovered a negative correlation between the resting calcium concentration and the amplitude. In further experiments, she was able to cause predictable changes in the calcium concentration of the transient's peak and amplitude by increasing or decreasing the resting calcium concentration through deactivation or release of calcium chelators by photolysis, respectively.

The experiments presented in this thesis investigated the relationship between the resting calcium concentration and the peak or amplitude of the transient in unperturbed astrocytes. Therefore, genetically modified mice, expressing the calcium sensitive indicator GCaMP5g and the calcium insensitive indicator tdTomato were used. In line with the previous findings, the data showed that the local resting calcium concentration shapes the peak and amplitude of calcium transients in astrocytes differentially (Figure 3.2). While the peak increased with increasing resting calcium, the amplitude decreased. Since this dependency was observed throughout different preparations (in vitro and in vivo) and experimental approaches (spontaneous and locomotion-induced transients), it is likely to be a universal principle.

To understand the underlying molecular mechanism, calcium influx from different sources was reduced by performing experiments in nominally 0 mM calcium or in presence of the store-depending calcium release blockers 2-APB and ryanodine. Interestingly, the positive correlation between baseline and peak was selectively reduced in nominally 0 mM calcium. On the other hand, selective impairment of the inverse relationship between baseline and amplitude was found when store-dependent calcium release was blocked. In line with these findings, Claire M. King and Daniel Minge found a negative correlation between the baseline and amplitude of astrocytic calcium transients when store-dependent calcium release was triggered through ATP, glutamate or norepinephrine (King*, Bohmbach* et al., 2020). Store-dependent calcium release is mainly regulated by IP3 receptors, albeit varying results concerning the magnitude of their contribution have been found (Agarwal et al., 2017; Kanemaru et al., 2014; Petravicz et al., 2008; Sherwood et al., 2017; Srinivasan et al., 2015). This controversy has been addressed recently by Okubo et al. (2019). Using a fluorescent calcium indicator, the authors have suggested a role for IP3 receptor 2-independent calcium release from the endoplasmic reticulum through, for instance, mitochondria. However, 2-APB does not directly block IP3 receptors but inhibits calcium refilling of the endoplasmic reticulum by store-operated calcium entry (SOCE; Okubo et al., 2020). The concentration of calcium within the endoplasmic reticulum declines rapidly after application of 2-APB and a subsequent increase in IP3 will not be able to cause an increase in the intracellular calcium. Accordingly, reductions in the amplitude of spontaneous and evoked astrocytic calcium transients have been found using this drug (Jennings et al., 2017; Vaarmann et al., 2010).

But how can the resting calcium concentration within the astrocyte modulate the efflux of calcium from the endoplasmic reticulum? Several models state that an increase in the intracellular calcium concentration does increase the open probability of IP3 receptors (Foskett et al., 2007; Hituri and Linne, 2013). Based on a resting calcium concentration of 70-90 nM in astrocytes (Zheng et al., 2015), an increase in the intracellular calcium concentration would indeed increase the opening probability of IP3 receptors (Foskett et al., 2007; Hituri and Linne, 2013). However, the negative correlation suggests the opposite. A possible explanation could be a full equilibration of the calcium concentration between the cytosol and the endoplasmic reticulum during a cytosolic transient and hence, a reduced driving force of calcium efflux from the endoplasmic reticulum in higher resting calcium concentration. Modeling by Christian Henneberger suggests that indeed this would explain the negative correlation found experimentally (King*, Bohmbach* et al., 2020).

Overall, the described relationships may have intriguing implications since they suggest that changes in the resting concentration of calcium can directly influence the magnitude of the peak. Differences in astrocytic resting calcium have been described during development (Zheng et al., 2015) as well as under physiological and pathophysiological conditions (Agarwal et al., 2017; Jennings et al., 2017; Kuchibhotla et al., 2009; Shigetomi et al., 2012; Srinivasan et al., 2015). These changes will directly influence the peak and amplitude and thus, calcium-dependent mechanisms in astrocytes (for review of mechanisms see Bazargani and Attwell, 2016). The resting calcium concentrations can therefore be seen as an integrator. It changes in response to neuronal activity, toxic deposits and pathophysiological changes in ion homeostasis and translates these in a differential output. For instance, neuronal activity can be altered through calcium-dependent uptake of extracellular potassium (Wang et al., 2012a) and in other cell types changes in free cytosolic calcium can even alter gene expression (Li et al., 1998). But changes in the intracellular calcium can, of course, also modulate the release of gliotransmitters.

In astrocytes, it has been described that changes in the resting calcium concentration modulate the extracellular D-serine concentration (Shigetomi et al., 2013b). The release of D-serine from astrocytes has been shown to (partially) depend on vesicular release mediated by SNARE proteins and intracellular calcium (Henneberger et al., 2010; Martineau et al., 2013; Papouin et al., 2017; Sultan et al., 2015). Consequently, it should follow a power law dependency, as described for neuronal release. Schneggenburger and Neher (2000) investigated the sensitivity of synaptic transmission to local calcium at the calyx of Held. They have found that the peak calcium concentration increased the release rates with an exponent of four. In astrocytes, increases in calcium as small as 50 nM have been shown to cause the release of glutamate (Parpura and Haydon, 2000). Hill coefficients, a measure of the (positive) cooperative binding of calcium ions, in astrocytes have been estimated to be between three and five (Kreft et al., 2004; Parpura and Haydon, 2000). This indicates that already changes in the local resting calcium in the nanomolar range are sufficient to cause significant increases in the peak concentration and can pose an even greater influence on the release probability.

Spontaneous calcium events in astrocytes are quite infrequent in slice preparations and can vary substantially within and between cells (1-2 per minute, our data and Gee et al., 2014; Shigetomi et al., 2013). They occur mainly in microdomains (Kanemaru et al., 2014) and display a large variability even to the same stimulus (Taheri et al., 2017). Furthermore, calcium indicators likely buffer the peak amplitude and frequency of calcium transients (Denizot et al., 2019). Thus, detection, owing to noise during the acquisition, and accurately estimating the frequency is difficult. I investigated whether a rather crude measure, the integral of the fluorescence ratio throughout the astrocytic territory, could serve as an alternative parameter to detect general changes in astrocytic calcium. The integral should be influenced by the frequency of astrocytic calcium transients but also by changes in the resting and peak calcium concentration. It is known that changes in the extracellular calcium concentration result in changes in the spontaneous frequency of calcium events (Di Castro et al., 2011; Kuchibhotla et al., 2009; Shigetomi et al., 2012; Wu et al., 2019). My recordings in nominally 0 mM calcium reproduced this effect (Figure 3.2). The integral showed a significant decrease as well. Importantly, a significant correlation between the changes in the integral and the changes in the frequency was observed. Besides decreases in calcium transients, also increases are mirrored by the integral. 10 Hz stimulation of the alveus resulted a significant increase in both, calcium transient frequency and in the integral. These results propose that the integral could indeed serve as crude, but quantitative parameter to

examine general changes in astrocytic calcium. Notably, changes in the integral were rather small in magnitude. Likely, local effects are diluted by averaging over the whole territory of the astrocyte. In agreement with this is the observation that throughout the whole territory a 5-10 % change in the integral was detected (Figure 3.19), while examination of smaller regions of interest yielded in a change of 25 % during alveus stimulation (Figure 3.17). Therefore, rather small overall changes likely represent larger local adaptations of the calcium transient dynamics. Overall, determining the integral can be used as a quantitative measure for changes in astrocytic calcium.

4.2 Astrocytes Control the Dwell Time of Glutamate at the Synapse Through Spine Size-Dependent Uptake

One aim of my thesis was to determine whether astrocyte glutamate uptake is differentially regulated at spines of different sizes. Astrocyte coverage of spines varies within the hippocampus (Ventura and Harris, 1999). Only half of the synapses have an astrocytic process in their vicinity. It is known that these fine astrocytic processes are particularly enriched in glutamate transporters (Sakers et al., 2017) and that a retraction of these processes modulates the spatial spread glutamate (Oliet et al., 2001; Sweeney et al., 2017). In the dentate gyrus, astrocytes processes can be found preferably at thin spines. Whether astrocytes target spines of different size differentially in the stratum radiatum is unknown. Unpublished data from our laboratory by Michel K. Herde have suggested that small spines have lower concentrations of perisynaptic glutamate (Herde et al., unpublished). Furthermore, he showed that the density of GLT-1 is increased at small spines. But does this difference in glutamate also cause functional implications for the synaptic transmission? To answer this question, I examined the effect of glutamate uptake inhibition on single spine NMDA receptor-mediated calcium responses to microiontophoretic glutamate application. The decay of these responses showed a significant increase selectively for small spines after glutamate transporter inhibition (Figure 3.8). Bigger spines were largely unaffected by this treatment. The decay of NMDA receptor responses has been shown to be a valuable measure for glutamate clearance rates (Armbruster et al., 2016; Pinky et al., 2018). This suggests a lower glutamate clearance rate at larger spines.

Rapid changes in spine size occur during the induction of long-term potentiation (LTP; Matsuzaki et al., 2004; Nägerl et al., 2004). In parallel changes in the astrocyte morphology are observed (Bernardinelli et al., 2014; Lushnikova et al., 2009). Whether these rapid changes in the neuron-astrocyte proximity also rapidly modify glutamate uptake needs to be determined. Monitoring of the perisynaptic glutamate levels using the optical sensor iGluSnFr before and after induction of plasticity at a single spine could provide evidence for this hypothesis.

What would be the functional implication of differential glutamate uptake? A longer glutamate dwell time at larger spines would likely cause increased recruitment of pre-, peri- and extrasynaptic receptors. Oliet et al. (2001) have observed that retraction of astrocytic processes results in reduced glutamate uptake in the hypothalamic supraoptic nucleus. This has caused an increased recruitment of presynaptic mGluRs and subsequently a decreased release of neurotransmitters. Thus, the longer glutamate dwell time selectively at larger spines could cause increased recruitment of presynaptic mGluRs at the Schaffer collaterals synapses. This could in turn influence the release probability of glutamate in a spine size dependent manner. Another interesting functional consequence is the increased recruitment of peri- and extrasynaptic NMDA receptors. Some studies have suggested an important role of extrasynaptic, GluN2B-containing

NMDA receptors in the induction of long-term depression (LTD; Liu et al., 2004; Massey et al., 2004; Papouin et al., 2012). This suggests that large spines are biased to LTD induction while small spines are more likely to exhibit LTP. However, the relevance of distinct NMDA receptors at different subcellular locations and containing different subunits in regulating plasticity is still under debate. Recruitment of extrasynaptic NMDA receptors is also required for the induction of dendritic NMDA spikes in the cortex (Chalifoux and Carter, 2011). Thus, also dendritic spikes and supralinear dendritic integration in the hippocampus could depend on the recruitment of extrasynaptic NMDA receptors.

4.3 Spine Size Regulates Mode of Integration in Dendrites

If extrasynaptic NMDA receptor recruitment is essential for the induction of dendritic spikes, then the differential regulation of astrocytic glutamate uptake at small and big spines could influence the propensity of dendritic spikes in the apical dendrites of CA1 pyramidal cells. Indeed, the presented data showed that the occurrence of a dendritic spike is more likely when big spines are stimulated with glutamate from the microiontophoresis pipette (Figure 3.7).

Is the differential glutamate uptake the cause of this effect? It is known that spatially distributed and subthreshold inputs are summed linearly, while synchronous spatially clustered inputs are more likely to evoke dendritic spikes in apical oblique or basal dendrites of CA1 PCs (Gasparini et al., 2004; Losonczy and Magee, 2006). Notably, spatially clustered inputs do not always evoke a dendritic spike. It has been shown that asynchronous activation of spatially clustered synapses with an interstimulus interval of 1-2 ms results in linear summation (Gasparini et al., 2004; Losonczy and Magee, 2006). Another important determining factor is the location along the dendritic tree. Proximally located synapses are less likely to evoke dendritic spikes, compared to distal ones (Branco and Häusser, 2011; Losonczy et al., 2008). However, these findings do not explain the increased likelihood of dendritic spikes during the activation of big spines. An important difference between small and big spines is the receptor composition. Small filopodia spines contain a smaller number of AMPA receptors than bigger mushroom spines (Matsuzaki et al., 2001). The depolarization achieved by the same amount of presynaptically released glutamate would be expected to be smaller. However, their small size increases the impedance and thus, increases the local depolarization evoked by the same ion influx. It is important to note that the large impedance will cause a greater difference to the dendritic impedance and will increase the attenuation of EPSPs when propagating to the dendrite. Next to differences in the spine head size, differences in the neck length are observes. Smaller spines tend to have a longer, narrow neck leading to compartmentalization of the spine from the dendrites (Tønnesen et al., 2014). Simulations by the authors predict that a decrease in the spine neck will only slightly increase dendritic EPSPs while it substantially decreases the EPSP in the spine. They have suggested that the recruitment of voltage-gated channels and NMDA receptors will likely be decreased in large spines compared to small ones. Induction of dendritic spikes would therefore be less likely. However, the opposite was observed in my experiments.

This leaves the differential clearance of glutamate by astrocytes as a possible cause. My results showed, that at big spines the dwell time of glutamate is less tightly regulated by astrocytes (Figure 3.8) and suggests that the recruitment of peri- and extrasynaptic NMDA receptors could be selectively increased. Notably, only the size of the initially activated spine was investigated, while the spatial extent of the ejected glutamate is several micrometers and therefore a cluster of spines will be stimulated. Several studies have shown that LTP occurs in small dendritic clusters

(Fu et al., 2012; Makino and Malinow, 2011; Roth et al., 2020; Takahashi et al., 2012) and induces bigger, mushroom-like spines (Matsuzaki et al., 2004; Nägerl et al., 2004). Thus, it can be assumed that the cluster of microiontophoretically stimulated spines are similar in size. If small spines are more tightly enwrapped by astrocytes, this might detain the ejected glutamate, thereby reducing the number of activated synapses and the recruitment of extrasynaptic receptors required for spike initiation. It is important to note that glutamate is ejected from a point source with microiontophoretic stimulation. Glutamate uptake by astrocytes and diffusion will reduce the amount of glutamate that reaches other spines. Therefore, the effect astrocytic glutamate clearance has on dendritic integration might be overestimated in these experiments. To gain additional evidence two-photon uncaging of glutamate would be a good technical approach. This technique releases glutamate from a chemical cage upon laser excitation and permits a more spatially precise stimulation of single spines. By two-photon uncaging of glutamate selectively on small or big spines the likelihood of dendritic spike initiation by activation of either subtype could be determined more directly. If indeed spine size determines the likelihood of spike initiation it suggests an interesting possibility of how the proximity of astrocytic processes and glutamate uptake can influence dendritic computations and neuronal AP output. This hypothesis could be tested by studying the dendritic spike propensity before and after a partial block of EAATs. Furthermore, it could be tested whether a partial block of EAATs can turn a linear integrating dendrite into a supralinear one with dendritic spikes. To unravel whether indeed the recruitment of extrasynaptic NMDA receptors is the cause, it could be tested whether selectively blocking the recruitment of these receptors decreases the probability of inducing dendritic spikes. Such a block could be, for example, achieved by application of the used-dependent NMDA receptor blocker MK-801. By slightly elevating the extracellular glutamate concentrations, selectively extrasynaptic receptors should be recruited and thus, become blocked by MK-801. Then the dendritic integration of the same dendrite can be studied again to detect changes caused by the selective block of extrasynaptic receptors.

4.4 Dynamic Modulation of NMDA Receptor Recruitment

Besides through glutamate uptake, astrocytes can also modulate the recruitment of NMDA receptors by, for instance, the supply of the NMDA receptor co-agonists D-serine (Henneberger et al., 2010). NMDA receptor activation requires the presence of glutamate and a co-agonist, e.g., D-serine or glycine (Ascher and Nowak, 1988; Johnson and Ascher, 1987). In combination with depolarization-induced removal of the magnesium ion from the channel pore, ion in- und efflux through the receptor can take place (Nowak et al., 1984). Experimental evidence suggests that the co-agonist binding site is usually not saturated (Henneberger et al., 2010; Papouin et al., 2017; Rasooli-Nejad et al., 2014; Shigetomi et al., 2013b). Accordingly, application of saturating concentrations of a NMDA receptors co-agonist can be used to maximize NMDA receptor recruitment. This approach can determine if dynamic modulation by astrocytic D-serine release is possible. For my thesis, I investigated the relevance of NMDA receptor recruitment for different modes of dendritic integration by application of an antagonist and the possibility of maximizing its recruitment by application of saturating concentrations of D-serine.

4.4.1 Linear Integration

The importance of NMDA receptor recruitment for linear dendritic integration by prohibiting sublinearity is known (Cash and Yuste, 1999; Losonczy and Magee, 2006) and preserved using microiontophoretic stimulation (Figure 3.9). Therefore, the potential modulation of linear integrating EPSPs by the co-agonist D-serine was explored by recording dendritic integration

before and after applying a saturating concentration of the co-agonist D-serine. Interestingly, no significant difference was found between the baseline and D-serine application (Figure 3.9). This result was particularly surprising since modulation by D-serine at nonlinear integrating dendrites took place at the subthreshold EPSP before dendritic spikes were evoked (Figure 3.12 C). It can only be speculated about possible reasons: for one, the contribution of NMDA receptors could be too small to detect a possible modulation by D-serine. However, the average change in amplitude after NMDA receptor blockade comparing the recordings from linear and supralinear integrating dendrites suggests otherwise. Another possibility is that the co-agonist binding site of the recruited NMDA receptors is already saturated under the recording conditions. Either different receptor pools are recruited during linear and supralinear integration or the extracellular D-serine concentration differs between them. To investigate this hypothesis a tool with sufficient spatial resolution would be required to detect local differences in the D-serine concentration. One approach could be an optical sensor that reports the binding of D-serine in a concentration-dependent change of its fluorescence intensity or life time. Using this sensor differences in the concentration could be correlated with distinct modes of integration. However, to date, no specific optical sensor for D-serine exists.

4.4.2 Supralinear Integration

Supralinear integration has been mainly investigated with two-photon uncaging of glutamate at and electrical stimulation of dendritic spines (Gasparini et al., 2004; Harnett et al., 2012; Losonczy and Magee, 2006). These experiments have established that NMDA receptors contribute significantly to the nonlinearity and the input-output relationship of dendrites. However, the influence of NMDA receptors has not been studied using acute application of an antagonist. Using microiontophoretic stimulation, the relevance of NMDA receptors in the nonlinear integration of a single dendrite was investigated in a paired experimental paradigm. Thereby the sensitivity to and the power of finding possible effects was increased. My results showed that both subthreshold EPSP and the NMDA receptor component of the dendritic spike were significantly decreased after acute application of the antagonist APV (Figure 3.10). Moreover, also the maximum slope of the sodium spikelet was decreased significantly. This is in contrast to earlier, unpaired observations. Losonczy and Magee (2006) have described only a minor effect of the NMDA receptor blockade on the number of spines required to evoke a dendritic spike and no difference in the maximum slope of the sodium component. To exclude that the difference in NMDA receptor recruitment caused by the different techniques that were used, our collaborators from the laboratory of Heinz Beck investigated the effect of APV on supralinear dendritic integration using two-photon uncaging of glutamate. Nicola Masala found that, indeed, the dendritic spike threshold increases and the slope of the fast and the amplitude of the slow component decrease after NMDA receptor blockade. Thus, the observed effects are not caused by different techniques. The increased sensitivity using paired recordings likely underlies the different results.

What would be the molecular mechanism by which NMDA receptors control the recruitment of voltage-gated sodium channels (VGSC)? Several possible scenarios might play a role: (1) AMPA receptors lose their driving force during depolarization (Cook and Johnston, 1999; Gasparini et al., 2004). Owing to the increased magnitude of the NMDA receptors inward current during depolarization, their contribution replaces the loss in AMPA conductance during synaptic activation. This relationship makes NMDA receptor recruitment essential for linear integration (Cash and Yuste, 1999) and dendritic spike initiation (Gasparini et al., 2004). Accordingly,

currents through both AMPA and NMDA receptors are recruited to evoke a sufficient depolarization to recruit VGSC. When NMDA receptors are blocked, a similar local depolarization for VGSC recruitment is required. Thus, the activation of a higher number of spines along a longer stretch of dendrite would be needed to achieve this. Experimentally, this effect is observed as an increase in the threshold stimulus. The reduction in AMPA receptor driving force during the depolarization could therefore also reduce the recruitment of VGSC, evident by the decrease in the maximum slope of the sodium spikelet. (2) Furthermore, a co-dependence of NMDA receptor and VGSC recruitment is likely. The current provided by NMDA receptors is essential for the recruitment of VGSC. In turn, the opening of VGSC will result in an increase of the intracellular sodium concentration. Yu and Salter (1998) have shown that NMDA receptor currents are positively modulated by the intracellular sodium concentration. Because of the slow glutamate unbinding and the increased sodium concentration, the recruitment of NMDA receptors will be further accelerated. Accordingly, the depolarization will increase and a larger number of VGSC can be recruited. With NMDA receptors being blocked, this synergy cannot take place and less VGSC are recruited. (3) The initiation of NMDA spikes in the cortex has been shown to be increased by the activation of extrasynaptic NMDA receptors (Chalifoux and Carter, 2011). VGSCs are located on the dendrites (Lorincz and Nusser, 2010). Thus, the co-dependence of VGSCs and NMDA receptors at extrasynaptic and dendritic sites specifically might be greater. Moreover, differences in the NMDA receptor subunit composition could be relevant for the recruitment of VGSCs. However, the role of sublocation-specific and or subunit-specific NMDA receptors recruitment in mediating supralinear dendritic integration in the hippocampus is unknown. Since dendritic spike induction is favored at big spines with a less tight regulation of glutamate clearance, an increased relevance for extrasynaptic NMDA receptors is suggested. Performing experiments with a selective block of extrasynaptic NMDA receptors, e.g., by a use-dependent blocker like MK-801, would be necessary to draw any conclusions on the differential contribution of synaptic and extrasynaptic receptors.

The contribution of subunit-dependent recruitment of NMDA receptors can be examined through pharmacology. I examined the contribution of GluN2B-containing NMDA receptors in supralinear dendritic integration. Similar to blockade with APV, an increase in the threshold stimulus and decreases in sub- and suprathreshold response amplitudes were observed after application of a specific GluN2B antagonist (Figure 3.11). Interestingly, GluN2B-containing NMDA receptor blockade did not affect the maximum slope of the fast sodium spikelet. Thus, the recruitment of GluN2B-containing NMDA receptors is likely not coupled to the recruitment of VGSCs. This result can be explained by the differences in the biophysical characteristics of NMDA receptor subtypes. EPSPs evoked by GluN2A-containing NMDA receptors have been shown to have a faster acceleration and decay than the ones evoked by GluN2B-containing receptors (Hansen et al., 2014; Rauner and Köhr, 2011). Thus, the slow activation of GluN2B-containing receptors does not contribute to the depolarization that recruits VGSCs. Notably, not only diheterometic NMDA receptors are found in the adult hippocampus but also triheteromeric NMDA receptors have been described to substantially contribute to synaptic transmission (Rauner and Köhr, 2011; Tovar et al., 2013). These receptors are blocked to a similar extent by Ro 25-6981, the antagonist used to test the contribution of GluN2B-containing NMDA receptors (Hawkins et al., 1999; Lü et al., 2017). The kinetics of GluN2A-GluN2B-GluN1 NMDA receptors are intermediate. The fact that the maximum slope of the sodium spikelet was uninfluenced by Ro 25-6981, therefore, suggests that also triheteromeric NMDA receptors are to “slow” to recruit VGSCs. To further study the relevance of different subunit compositions of NMDA receptors in dendritic integration, the

selective block of GluN2A-containing receptors would be of great interest. However, most antagonists lack sufficient subunit-selectivity. Nevertheless, the kinetics and my data strongly support a GluN2A-VGSC interaction, specifically at extrasynaptic locations, in modulating the maximum slope of dendritic spikes.

Because of the importance of NMDA receptors for supralinear dendritic integration, the possible modulation through co-agonist binding was investigated. The results showed, that the threshold for dendritic spike initiation decreased in saturating concentrations of D-serine (Figure 3.12). D-serine enhanced the maximum slope of the fast and the amplitude of the slow component of dendritic spikes. In contrast to linearly integrating dendrites, an increase in the amplitude of subthreshold EPSPs was also observed. These data showed, that the NMDA receptor co-agonist binding site was not saturated in baseline conditions, as found by others for field EPSPs in acute slices and in vivo (Henneberger et al., 2010; Papouin et al., 2012, 2017; Robin et al., 2018). Furthermore, this result suggests that supralinear dendritic integration in apical oblique dendrites can be modified by raising the extracellular NMDA receptor co-agonist concentration. Astrocytic release of D-serine could, therefore, decrease the amount of glutamate needed to evoke dendritic spikes and increase the amplitude of the slow component. Subsequently, astrocytes could, for instance, control somatic AP firing and modulate the initiation of place fields through adapting the local dendritic integration.

4.4.3 Dendritic Plateau Potentials

Besides supralinear dendritic integration in the apical oblique dendrites, nonlinear input computations have also been described in the apical tuft dendrites of PCs in the dorsal hippocampus and cortex (Magee and Carruth, 1999; Malik and Johnston, 2017; Pérez-Garci et al., 2006; Schiller et al., 1997; Takahashi and Magee, 2009; Tsay et al., 2007; Wei et al., 2001). These dendritic plateau potentials are characterized by an increase in the intracellular calcium concentration, for which the recruitment of NMDA receptors is essential. Here their presence and the underlying NMDA receptor recruitment was investigated in the ventral hippocampus. By using a stimulation protocol similar to Takahashi and Magee (2009), plateau potentials were evoked with an overall probability of 45 % and during the fifth stimulation train of 80 % (Figure 3.13). The probability of plateau initiation reported for the fifth stimulation train is close to 100 % (Takahashi and Magee, 2009). However, different recording sites (apical trunk dendrite vs. soma) and thus attenuation or regional differences herein between the ventral and dorsal hippocampus might be causative for the different plateau initiation probabilities (Malik and Johnston, 2017). Nevertheless, a similar after depolarization duration and calcium influx were observed in my recordings compared to published ones (Schiller et al., 1997; Takahashi and Magee, 2009). Likewise to dendritic spikes at the apical oblique dendrites, a requirement of NMDA receptor recruitment for plateau potential initiation in the apical tufts has been described (Schiller et al., 1997; Takahashi and Magee, 2009). The same observation was made in the ventral hippocampus in the present study. Both, the local calcium response in the tufts as well as the somatic potential were significantly decreased by NMDA receptors blockade. Furthermore, the results demonstrated that plateau potential initiation and duration can be modulated through NMDA receptor co-agonists. The overall probability of dendritic spikes as well as the amplitude, area and duration of the local calcium response and somatic potential were significantly increased after application of saturating concentrations of D-serine. This not only shows that the co-agonist binding site of the NMDA receptors was not saturated but also implies that additional release of D-serine can enhance the initiation of dendritic plateau potentials.

On important question is, whether the modulation by NMDA receptor co-agonists takes place in the stratum radiatum or in the stratum lacunosum moleculare. Increased recruitment of NMDA receptors in the former would increase the depolarization and will subsequently increase the somatic potential recorded. Since this depolarization is also required for the successful induction of dendritic plateau potentials (Larkum et al., 1999; Takahashi and Magee, 2009), an increase in the probability could likewise underlie an increased NMDA receptor recruitment in the stratum radiatum. Additionally, an increase in the local calcium response in the apical tuft dendrites was observed after application of D-serine. One possible explanation is increased recruitment of VGCC because of the increased depolarization in the stratum radiatum. Another explanation is that the observed effect was caused by the saturation of the co-agonist binding site of NMDA receptors in the stratum lacunosum moleculare. To separate the effects on NMDA receptors in the two strata, dendritic plateau potentials could be evoked by paring somatic depolarization with local stimulation of the apical tuft dendrites. Under these circumstances, only NMDA receptors in the stratum moleculare lacunosum should contribute to the effect observed.

4.5 Astrocytic CB1 Receptors Activation Modulates Dendritic Integration via the Release of NMDA Receptor Co-Agonist

While exogenous application of saturating concentrations of a co-agonist was used to study a potential modulation of dendritic integration, to draw a conclusion on the relevance of endogenous release this needs to be stimulated. It is known that astrocyte calcium signals can evoke the release of gliotransmitters (Guerra-Gomes et al., 2018). One stimulus for gliotransmitter release are endocannabinoids. Navarrete and Araque (2008) have shown, for instance, that application of exogenous and endogenous cannabinoids results in calcium responses in stratum radiatum astrocytes. This elevation has been mediated through cannabinoid 1 (CB1) receptors since it has been blocked by the inverse agonist AM251. Robin et al. (2018) have demonstrated that specifically astrocytic CB1 receptors mediate the increase in astrocyte calcium. Through the application of exogenous cannabinoids, an increase of the astrocytic calcium event probability has been observed in wild type mice but not in astrocyte-specific CB1 receptor knock-out (aCB1KO) mice. Both studies used pressure application of cannabinoids and studied the response of astrocytes through incubation with Fluo-4-AM, a membrane permeable calcium dye. Bulk-loading of astrocytes underestimates astrocytic calcium transients since it only labels approximately 10 % of the cell's territory with a sufficient dye concentration (Reeves et al., 2011; Shigetomi et al., 2013a). Combining whole-cell patch clamp recordings of astrocytes with time-lapse imaging, data from our lab showed that not only the soma and major branches but also the fine processes, which are in contact with synapses, display elevations in calcium during bath-application of WIN55,212-2, a specific CB1 receptor agonist (Figure 1.8). In the presence of the inverse agonist AM251 this effect was absent. Moreover, the number of astrocytes responding to WIN55,212-2 in presence of AM251 was significantly decreased.

It is important to note that the CB1 receptor agonist WIN55,212-2 has been shown to interact with TRPA1 channels at concentrations used to stimulate astrocytes (10 µM, Koch et al., 2011). In turn, TRPA1 channels have been shown to mediate the release of D-serine from astrocytes in a calcium-dependent manner (Shigetomi et al., 2013b). While the experiments in aCB1KO mice performed by Robin et al. (2018) argue against direct recruitment of TRPA1 channels in evoking astrocytic calcium transients, an involvement of these channels cannot be excluded completely. Experiments performed in cultured HEK cells and spinal cord neurons showed that TRPA1 channels can be activated through the Gβγ subunit of the Mas-related G protein-coupled receptor A3 and G protein-coupled bile acid receptor 1 (Lieu et al., 2014; Wilson et al., 2011). Thus, a similar mechanism could also be recruited by CB1 receptors. Experiments performed in the presence of a specific TRPA1 antagonist might aid to draw a conclusion if such a mechanism can also be recruited in astrocytes.

Nevertheless, it can be concluded that the application of a CB1 receptor agonist reliably increases calcium in astrocytes. Furthermore, experiments by Robin et al. (2018) have suggested that activation of astrocytic CB1 receptors increases the extracellular concentration of D-serine. Therefore, this signaling cascade was used to determine the effect of endogenously-released co-agonist on supralinear dendritic integration in the stratum radiatum (Figure 3.14). As in the case of direct application of D-serine, all parameters used to examine supralinear dendritic integration were enhanced significantly after application of WIN55,212-2. It is important to note that these experiments were conducted with a ten-times smaller concentration of WIN55,212-2 and activation of TRPA1 channels is therefore likely neglectable (Koch et al., 2011).

Previous studies have observed the release of glutamate, ATP and/or D-serine from astrocytes upon exposure to cannabinoids (Navarrete and Araque, 2008; Rasooli-Nejad et al., 2014; Robin et al., 2018). To exclude a contribution of glutamate and/or ATP release, the application of WIN55,212-2 was repeated in saturating concentrations of D-serine. If other gliotransmitters than D-serine would be released by the stimulation of CB1 receptors, modulation of dendritic integration would be expected under these conditions. However, occlusion of the effect was observed and demonstrated therefore the release of NMDA receptor co-agonist upon CB1 receptor activation. Since microiontophoretic stimulation was used, a co-release of ATP or glutamate, which might preferentially act on the presynaptic terminal cannot be excluded by these experiments. Owing to the presence of picrotoxin, a modulation of GABAergic transmission by postsynaptic P2X receptors can neither be ruled out. The activation of presynaptic mGluRs, NMDA receptors or adenosine receptors could decrease presynaptic glutamate release and thereby counteract the increased NMDA receptor recruitment caused by the release of its co-agonist. However, postsynaptic activation of P2X receptors and subsequent downregulation of GABA receptors, as described in the neocortex (Rasooli-Nejad et al., 2014), would decrease the attenuation dendritic spike propagation. Accordingly, supralinear dendritic integration would be strengthened. An interesting question along this line is how and why astrocytic CB1 receptors cause the release of varying gliotransmitters. One difference lies in the age of the animals used. While in the studies that demonstrate glutamate release, juvenile animals (11-18 days old) were used (Gómez-Gonzalo et al., 2015; Navarrete and Araque, 2008, 2010), Robin et al. (2018) and I describe the release of D-serine in (young) adult ones (> 21 days old). While this age difference might seem trivial, morphological maturation of astrocytes continues until the end of the third postnatal week (Bushong et al., 2004). Thus, the full complexity of the sponge-like astrocytic morphology might be required to efficiently regulate synaptic transmission by D-serine.

Furthermore, in the CA1 region an increasing relevance of D-serine in modulating NMDA receptor recruitment during development has been suggested (Le Bail et al., 2015). Hence, developmental regulation of the released gliotransmitter in response to CB1 receptor activation could be a likely explanation. Another difference is the incomparable NDMA receptor recruitment between the studies. Navarrete and Araque (2008, 2010) recorded the frequency of slow inward currents as a read-out for astrocytic glutamate release. To maximize the frequency of these currents, the NMDA receptor co-agonist binding site is often saturated and/or the magnesium concentration reduced to 0 mM (Fellin et al., 2004). Especially the former would occlude any effect of astrocytic released D-serine. Notably, some studies have examined the identity of the released gliotransmitters in response to CB1 receptor activation more directly. Through capillary electrophoresis in the extracellular solution, Robin et al. (2018) have detected an overall increase in the D-serine concentration but not in the glutamate concentration. However, a local short-lasting co-release of glutamate and D-serine cannot be excluded because of the low spatial resolution and sensitivity of the method. Rasooli-Nejad et al. (2014) have employed microelectrode sensors for ATP and D-serine and have found an increase in both gliotransmitters in response to astrocytic CB1 receptor activation. It is important to note, that these experiments have been conducted in the neocortex and not in the hippocampus. Thus, regional differences in gliotransmitter identity could be possible, too. To unravel the mystery of the gliotransmitter identity released in response to the activation of astrocytic CB1 receptors a spatially-precise, sensitive method would be needed. For instance, optical sensors would be a suitable technique to examine the locally released compounds from astrocytes. While these do exist for glutamate and ATP, an optical D-serine sensor is not yet available.

4.6 Neuronal Activity Recruits the Release of D-Serine From Astrocytes and Thereby Modulates Dendritic Integration

The next question of my thesis addressed the situations in which astrocytic CB1 receptor activation could occur in vivo. The release of endocannabinoids has been shown to depend on neuronal depolarization and an increase in neuronal calcium (Ohno-Shosaku et al., 2001). Likewise, astrocytic calcium elevations can be evoked through neuronal depolarization and endocannabinoids (Navarrete and Araque, 2008). In addition to an increase in depolarization-induced suppression of inhibition (DSI), the authors have observed an increase in astrocytic calcium transient probability with increasing duration of neuronal depolarization. Therefore, the effect of neuronal depolarization on dendritic integration was investigated (Figure 3.15). Surprisingly, instead of an increase in the amplitude of the slow component of the dendritic spike, a decrease was observed. This effect was specific for the amplitude of dendritic spikes as no change was detected for their maximum slope or the amplitude of subthreshold EPSPs. Differential recruitment of NMDA receptors, because of the prolonged somatic depolarization, is therefore a likely explanation. The injection of somatic current caused the induction of somatic APs, which backpropagate into the dendrites (Inoue et al., 2001; Spruston et al., 1995). In the dendrites, this will cause the activation of voltage-gated calcium channels (VGCC). The resulting calcium influx in turn can recruit calcium-activated potassium channels (Jones and Stuart, 2013; Marrion and Tavalin, 1998). Two subtypes of these channels are distinguished by their differential conductance: small potassium conductance channels (SK channels) and big potassium conductance channels (BK channels). BK channels mediate the fast afterhyperpolarization of APs, while the slow afterhyperpolarization evoked by AP bursts is mediated by SK channels (Marrion and Tavalin, 1998). Since the effect on the amplitude was

observed several seconds after the depolarization, a contribution of SK channels is more likely. SK channels have been shown to be functionally coupled to NMDA receptors (Ngo-Anh et al., 2005). Thus, their activation by the somatic depolarization could reduce the current evoked by NMDA-receptor activation. It is also important to note that the probability to observe astrocytic recruitment by neuronal depolarization is considerably lower than with the application of an exogenous agonist application, namely 30 % vs. 80 % (Navarrete and Araque, 2008). Accordingly, even if endocannabinoid mobilization is successfully evoked, a larger heterogeneity and/or smaller effect size can be expected with this method. Independent of the mechanism, the conclusion that the depolarization and AP firing of a single neuron is not able to modulate supralinear dendritic integration can be drawn.

To increase the recruitment of endocannabinoid production and mobilization while avoiding strong depolarization of the whole-cell patch clamped neuron, an ensemble of CA1 PCs was recruited by retrograde activation. Through precise incisions, a solely axonal response could be evoked by electrical stimulation of the alveus (Figure 3.16). This experimental setup recruited AP firing in 20-80 % of the investigated CA1 PCs. Importantly, also 70 % of the astrocytes responded with an increase in intracellular calcium (Figure 3.17). The increase in calcium was evoked through CB1 receptors since the change in the fluorescence ratio was significantly smaller in the presence of the inverse agonist AM251. Thus, the recruitment of CA1 PCs through retrograde stimulation in the alveus could potentially modulate dendritic integration through astrocytic release of D-serine. Since it has been described in the literature that DSI and hence, the production and mobilization of endocannabinoids depends on the frequency and number of APs (Fortin et al., 2004), different frequencies of neuronal firing that mimic behavior-associated rhythmic activity observed in the hippocampus (see section 1.1.3, for detailed information on the associated behaviors) were investigated for their impact on dendritic integration (Figure 3.18). Noteworthy, stimulation of the alveus evoked reliable AP recruitment in CA1 PCs across the used frequencies (Figure 3.17).

Stimulation with a low frequency (4 Hz) had no effect on supralinear dendritic integration. Likely, evoking 4 APs did not recruit sufficient endocannabinoid release, if any at all. But stimulation with a frequency of 20 Hz, which is commonly used to induce DSI, resulted in a significant enhancement of supralinear dendritic integration. In contrast to DSI, a further increase in the frequency and AP number by stimulating the alveus at 40 Hz, did not yield any effect on supralinear dendritic integration. Surprisingly, repetitive stimulation with 10 Hz for one second was not only sufficient to promote supralinear dendritic integration but also the most potent. This result was unexpected since DSI induced with APs at this frequency has been found to evoke only submaximal effects (Fortin et al., 2004). Notably, the observed effect only lasted for a short time (Table 2 A). These experiments suggest not only a differential efficiency of cell-type-dependent endocannabinoid signaling at distinct frequencies but show that supralinear dendritic integration can be regulated by a stimulation frequency that mimics theta oscillations.

Through a range of pharmacological interventions, it was determined that the modulation of the integration required CB1 receptors and the release of the NMDA receptor co-agonist. Both the inverse CB1 receptor agonist AM251 (Table 2 B) as well as saturating concentrations of the NMDA receptor co-agonist D-serine (Table 2 C) occluded the earlier observed effects on supralinear dendritic integration. Importantly, incubating the hippocampal slices in and recording the dendritic integration in the presence of the D-serine degrading enzyme D-amino acid oxidase (DAAO) prohibited the alveus stimulation-induced modulation of dendritic integration (Table 2 D). Thus, suggesting that the released co-agonist is D-serine instead of glycine.

Taken together, the collected data uncovered a frequency-dependent modulation of supralinear dendritic integration linking AP firing, CB1 receptor activation and the release of the NMDA receptor co-agonist D-serine. Recruitment of CA1 PCs with a stimulus in the theta frequency band yielded the strongest modulation of the integration, suggesting an interesting link of this signaling cascade to behavior. Not only can the resonance frequency of CA1 PCs be found in the theta frequency band, but also is an increase in theta oscillations commonly observed during exploration (Vanderwolf, 1969). Theta oscillations are thought to put the hippocamps in general into an active state that primes the network for learning and memory (Buzsáki, 2002). For instance, the encoding and remapping of spatial information depend on the AP timing relative to these oscillations (Lever et al., 2010; O'Keefe and Recce, 1993). Thus, this previously unknown feedback loop could have an important role in spatial learning and memory.

4.7 Astrocytic CB1 Receptors Are Required for the Amplification of Dendritic Integration by D-Serine

It is important to note that CB1 receptors are expressed not only by astrocytes but also, to an even bigger extent, by inhibitory and excitatory neurons (Marsicano and Lutz, 1999; Navarrete and Araque, 2008). To establish the importance of specifically astrocytic CB1 receptors in the uncovered signaling cascade, an inducible astrocyte-specific knock-out mouse line was used (Figure 3.21). The use of a GLAST-dependent cre driver line yielded a high efficacy and specificity in targeting astrocytes. But by the expression of tdTomato after tamoxifen injection, recombination was also identified in a subset of cells with unknown origin. Staining with a neuron-specific antibody against NeuN showed expression of tdTomato in a neglectable number of neurons, suggesting a glial origin of the unknown cells. It is important to note that not all astrocytes are stained with a GFAP-targeting antibody (Walz and Lang, 1998) and the possibility that these cells are also astrocytes does exist. Morphologically, most of these GFAP/NeuN-negative but tdTomato-positive cells displayed a small soma (small diameter of Hoechst staining and tdTomato expression) and very few visible processes. Because of their distinct location, a subset of these cells could be pericytes, lining small capillary vessels. In line with this, a pericyte subpopulation in the spinal cord is known to express GLAST (Göritz et al., 2011). Another possibility is that these cells are intermediate progenitor cells. The creators of the mouse line have identified GLAST-positive, GFAP-negative cells with a small soma to be CC1- and NG2- or Sox10-positive (Mori et al., 2006). Nevertheless, since the neuronal CB1 receptor expression should be uninfluenced while the expression in astrocytes should be substantially reduced, these mice are suitable to investigate the relevance of astrocytic CB1 receptors in supralinear dendritic integration. It is important to note, that astrocytes from this mouse line display a heterozygous knock-out of the GLAST that could cause altered glutamate clearance. Although glutamate clearance in adult rodents is mostly mediated by GLT1 (Rose et al., 2018), basic cell properties of

wild type, sham-injected control and aCB1KO mice were compared. This analysis revealed an increased excitability of CA1 PCs through a decrease in the AP threshold in both sham-injected and aCB1KO mice (Table 3) and affirming the importance of a sham-inject control group with the same genetic background as CB1KO mice.

Having confirmed the specificity and efficacy of aCB1KO mice, the effect of 10 Hz stimulation on supralinear dendritic integration was compared between wild type, sham-injected control and aCB1KO mice. In both control mice groups, the earlier in rats observed effect was preserved (Figure 3.22). The stimulation of the alveus resulted in a significant decrease in the threshold stimulus and an increase in the amplitude of the subthreshold EPSP and NMDA receptor component of the dendritic spike. Also, an increase in the maximum slope of the fast sodium component was observed. Importantly, no significant difference between both control groups was found for either parameter. In aCB1KO mice, however, none of these parameters was influenced by the retrograde activation of CA1 PCs. Moreover, the effect of 10 Hz alveus stimulation on these parameters was significantly smaller comparing aCB1KO to wild type and sham-inject control mice. On the one hand, these results demonstrate that the heterozygous GLAST knock-out does not affect the coupling of CA1 PC activity to the release of D-serine. On the other hand, these experiments prove that specifically astrocytic CB1 receptors are crucial for the positive modulation of supralinear dendritic integration by alveus stimulation.

4.8 Mechanism Underlying the Frequency-Dependency of The Feedback Loop

Since endocannabinoid-mediated DSI is stronger at higher frequencies (Fortin et al., 2004), the surprising result, that AP firing at a frequency of 40 Hz did not influence supralinear dendritic integration (Figure 3.18) raised the question concerning the origin of this effect. Experiments showed that astrocytes sense the difference in frequency, since both, the calcium transient frequency and the integral, were selectively increased during 10 Hz stimulation but not during 40 Hz stimulation (Figure 3.19). Thus, the different signaling of both stimulation paradigms must take place upstream of the increase in astrocytic calcium and suggests, for instance, a frequency-dependent mobilization of endocannabinoids at distinct subcellular locations. Because of their lipophilic structure, endocannabinoids are required to be produced and mobilized locally (Chevaleyre and Castillo, 2003; Di Marzo et al., 1998). Since mGluR-independent DSI has been observed mainly for (peri)somatic inputs (Lee et al., 2010; Younts et al., 2013), endocannabinoid mobilization would only be required there. However, to activate astrocytes in the stratum radiatum, also production and mobilization of endocannabinoids locally in the apical oblique dendrites is required. This means that APs need to backpropagate into the dendritic tree and there evoke a sufficient increase in the depolarization or influx of calcium to induce the production of endocannabinoids. Backpropagation of APs is regulated by many different voltage-dependent channels and receptors expressed in distinct density and subtypes with increasing distance to the soma (Hoffman et al., 1997; Lorincz and Nusser, 2010; Magee and Johnston, 1995).

An interesting candidate for modulating the frequency dependency are hyperpolarization-activated cation-nonselective (HCN) channels. HCN channels and the related current (I_h) influence many computational functions of neurons. For instance, they participate in establishing the resonance frequency of CA1 PCs (Hu et al., 2002; Hutcheon and Yarom, 2000; Nolan et al., 2004). The resonance frequency is the input frequency that yields the maximum response amplitude. In CA1 PCs it is within theta frequency range. Since 10 Hz stimulation of the alveus mimics a theta rhythm, an involvement of these channels in modulating the frequency-dependency was investigated. It is important to note that HCN channels are controlling the resting membrane potential and membrane resistance (Pape, 1996). In the presented experiments, a reduction of approximately 5 mV for the resting membrane potential with application of ZD7288, an HCN channel blocker, was observed. These findings are in line with studies using HCN knock-out mice or pharmacological blockade (Dougherty et al., 2013; Nolan et al., 2004). Interestingly, the effect of 10 Hz alveus stimulation on dendritic integration in the presence of an HCN channel blocker was occluded (Figure 3.20). The blockade of HCN channels will change the membrane resistance (Pape, 1996) and will influence the integration directly by increasing the amplitude and duration of EPSPs (Magee, 1998, 1999). When HCN channels are blocked, an enhanced recruitment of calcium influx through VGCCs during dendritic spikes in the apical tuft dendrites of CA1 PCs has been described (Tsay et al., 2007). Therefore, it needs to be excluded that the occlusion of the effect was not caused by an already maximal NMDA receptor recruitment under the experimental conditions. To exclude such a ceiling effect, the CB1 receptor agonist WIN55,212-2 was applied in the presence of ZD7288. The results showed that the effect of exogeneous cannabinoid application is preserved in these conditions. Thus, a decrease in the threshold and increase in the amplitude and maximum slope of dendritic spikes can be evoked even when HCN channels are blocked. Since 10 Hz stimulation of the alveus did not, it suggests that this channel blockade interferes with the production or mobilization of endocannabinoids or downstream effectors.

What could be the possible underlying molecular or computational mechanism regulating the occlusion effect that is induced by HCN channels blockade? HCN channels do not only modulate the resonance frequency of synaptic input, but also somatic current injections, which propagate into the apical dendrites, display resonance (Hu et al., 2009). Using a combination of somatic and dendritic patch clamp recordings, the authors have shown that at resting membrane potentials the resonance strength is larger in the dendrites than at the soma. This difference was abolished by application of ZD7288. The increase in HCN channel density with increasing distance from the soma is through to underly this phenomenon (Magee, 1998). Accordingly, the HCN channel-dependent regulation of the resonance frequency could underly the frequency-dependency of the coupling between neuronal activity and astrocytic calcium transients. Nevertheless, it would be important to computational model the backpropagation of APs evoked in different frequencies into the apical dendritic tree in dependence of I_h. Moreover, recording the local dendritic calcium responses to alveus stimulation at 10 and 40 Hz or in relation to HCN channel blockade by using two-photon excitation microscopy and a calcium sensitive dye could further advance our understanding of the underlying signaling cascade.

Another important point to consider is the extent of the dendritic depolarization and calcium influx evoked by the somatic activity. The evoked potentials in CA1 PCs display a decrease of the amplitude and an increase in latency with increasing distance from the soma (Inoue et al., 2001; Spruston et al., 1995). Nevertheless, APs reliably propagate into second-order basal and apical

oblique dendrites (Antic, 2003). A similar attenuation is observed for calcium transients. Modeling suggests that I_h modulates the attenuation of somatic potentials (Hu et al., 2009). At depolarized membrane potentials (- 60 mV) a removal of I_h resulted in an increased attenuation of somatic subthreshold inputs with a frequency of 10 Hz or more. Thus, an increased attenuation of the somatic APs propagating into the apical oblique dendrites could participate in the occlusion that was observed experimentally. Notably, a reduced attenuation has been described for brief high frequency trains of APs (Spruston et al., 1995; Williams and Stuart, 2000). Also, DSI and the mobilization of endocannabinoids can be induced by short AP bursts (Fortin et al., 2004). Thus, short bursts of APs might also recruit astrocytic calcium increases and subsequent release of D-serine. However, this hypothesis requires experimental testing.

Noteworthy, experimental confounders could play a role in the occlusion. For instance, the ZD7288-induced hyperpolarization was compensated by a constant somatic current injection. While this efficiently depolarizes the somatic membrane potential, the efficacy on the potential in the distant apical oblique dendrites is questionable. A hyperpolarized dendritic membrane potential would certainly reduce the depolarization and calcium influx evoked by the stimulation of the alveus, independent of the frequency. Hence, the production and mobilization could be reduced, which would cause an occlusion as well. Since experimentally this cannot be controlled, it emphasizes the advantage and need of using a computational model to draw a conclusion on the underlying mechanism regulating the frequency dependency of the uncovered feedback loop.

4.9 CA1 Microcircuit – The Feedback Loop as Part of a Network

The antidromic stimulation of CA1 PCs results in the production and mobilization of endocannabinoids likely in the stratum radiatum. Here, CB1 receptors are activated, which will cause an increase in astrocytic calcium and the release of D-serine. Subsequently, D-serine will maximize NMDA receptor recruitment and thus, increase the likelihood and extent of supralinear dendritic integration. However, the CA1 microcircuit also contains other neurons that were so far not considered in this feedback loop.

4.9.1 Axonal Recruitment of Other Neurons by Alveus Stimulation

Interneurons can, for instance, like CA1 PCs produce and mobilize endocannabinoids. Since some interneuron axons are located in the alveus, the used stimulation paradigm would recruit depolarization in these cells. Owing to the presence of a $GABA_A$ receptor blocker, direct electrical signaling from these interneurons could not influence the recorded dendritic integration. Nevertheless, interneurons could participate in the endocannabinoid mobilization. It is important to note that interneurons also express HCN channels (Hughes et al., 2013; Lupica et al., 2001; Maccaferri and McBain, 1996; Santoro et al., 2000; Sekulić et al., 2015). Thus, the experimental blockade of HCN channels would have likewise targeted interneurons. To exclude their participation, a cell-type specific activation would be required. For example, the expression of ChR2, a light-gated nonspecific cation channel could be induced selectively in (a subset of) CA1 PCs. Thus, recruitment of specifically these cells could be evoked by small laser pulses. If the positive modulation on the supralinear dendritic integration is preserved under these experimental conditions, a participation of interneuron through direct electrical stimulation of their axons can be excluded.

Alveus stimulation may also recruit fibers from the medial septum. Papouin et al. (2017) found a strong relationship between neuronal activity, theta oscillations and the release of D-serine, similar to the one presented. However, while they have observed a regulation by nicotinic AChRs, our data suggest a dependence on CB1 receptors. Importantly, in our experiments, an inverse CB1 receptor agonist abolished the astrocytic calcium increase and the modulation on the dendritic integration. Furthermore, in aCB1KO mice an enhancement of supralinear dendritic integration by alveus stimulation was not possible. Thus, a functional relevance of cholinergic modulation can be excluded. Nevertheless, it is an interesting question of how these two different mechanisms in the same microcircuit fit together? Papouin et al. (2017) have found a gradual increase in the overall D-serine concentration during the dark/active phase and a gradual decrease during the light/sleep phase. While the decrease has occurred within one to two hours, the observed increase has been even slower and highly dependent on the animal's locomotor activity. Contrastingly, the mechanism described here suggests a fast (within seconds), short-lasting (couple of minutes) increase in D-serine. The release of D-serine can be recruited through local activity and directly influence the local dendritic integration. This is in line, with the known lipophilic structure of endocannabinoids, not allowing long-distance diffusion. So overall, the medial septum may regulate circadian fluctuations, while the newly discovered feedback loop provides an acute short-term release of D-serine.

4.9.2 Interneuron Modulation of the Signaling Cascade

But even without direct electrical stimulation, CA1 PC AP firing will recruit certain interneurons that can change the functional output of the microcircuit (Megías et al., 2001) and thus, the impact the presented feedback loop has in vivo. It is important to note that all experiments were conducted in the presence of a $GABA_A$ receptor blocker. Therefore, it can only be speculated on the influence of interneurons.

Apical oblique dendrites in the stratum radiatum are mainly targeted by two types of GABAergic interneurons, bistratified and ivy cells (Freund and Buzsáki, 1996; Klausberger, 2009). They form synapses at the end or origin of dendrites depending on the distance to the soma (Bloss et al., 2016), thereby suppressing either spike initiation or spike propagation, respectively (Gidon and Segev, 2012). These interneurons are capable of inhibiting neuronal output evoked through dendritic spikes (Lovett-Barron et al., 2012; Müller et al., 2012). Repetitive activation of the alveus recruits both somatic and apical dendritic inhibition in a phase-dependent manner (Pouille and Scanziani, 2004). It has been shown that especially activity in the theta frequency band results in a higher probability of weak dendritic spikes to evoke somatic APs (Müller et al., 2012). Of note, strong dendritic spikes can propagate towards the soma albeit inhibition. An increase in excitation, as provided by D-serine release from astrocytes, could further aid to overcome inhibition (Vu and Krasne, 1992). Additionally, the mobilization of endocannabinoids will also decrease the impact of inhibition (Bezaire and Soltesz, 2013; Freund and Buzsáki, 1996; Marsicano and Lutz, 1999). Since endocannabinoid-dependent suppression of inhibition is mainly observed for perisomatic synapses (Lee et al., 2010), an increase of spike initiation and propagation would be expected. Thus, the AP firing evoked by dendritic spikes would be increased or a switch in firing mode would be initiated (Lovett-Barron et al., 2012) during the recruitment of the uncovered feedback loop.

In addition, AP in CA1 PCs will activate feedback inhibition and recruit oriens lacunosum-moleculare (OLM) interneurons that in turn innervate the apical tuft dendrites (Freund and Buzsáki, 1996; Klausberger, 2009). By forming synapses at the end of the dendrites (Bloss et al., 2016), they are highly effective in suppressing dendritic spike initiation (Gidon and Segev, 2012; Lovett-Barron et al., 2012). Interestingly, OLM cells fire predominantly during the trough of a theta waveform when CA1 PCs are most active as well (Klausberger et al., 2003). Consequently, dendritic plateaus potential initiation would be more likely at the peak and hence, increase the likelihood of synaptic potentiation (Hyman et al., 2003).

Next to local inhibition, also long-range inhibition from the entorhinal cortex modulates the computations of the CA1 microcircuit (Melzer et al., 2012). These fibers have been shown to suppress the activation of cholecystokinin (CCK)-positive interneurons recruited by Schaffer collateral activation, thereby reducing the inhibition of OLM cells (Basu et al., 2013, 2016). A precise pairing of inputs from the Schaffer collaterals and the perforant path allows initiation and propagation of dendritic plateau potentials in the apical tuft dendrites (Basu et al., 2016) and thereby enabling place cell formation (Bittner et al., 2015). How would these interneurons be recruited during activity in the theta frequency band that is necessary for activation of the presented feedback loop? It has been shown that CCK-positive interneurons fire at the ascending phase during theta oscillations (Klausberger et al., 2005) and hence disinhibit OLM interneuron output. This would permit dendritic plateau potential initiation in the apical tuft dendrite and will cause an increase of CA1 PC firing. Usually, burst-like firing of CA1 PCs with up to 20 Hz is observed within a place field (O'Keefe, 1976; O'Keefe and Recce, 1993). Consequently, D-serine release from astrocytes will be activated, enhancing dendritic spike initiation in the apical oblique dendrites. Possibly, this promotes the precise pairing between inputs from both pathways further enhancing plateau propagation. Notably, CCK-positive neurons express CB1 receptors (Katona et al., 1999; Marsicano and Lutz, 1999) that could suppress disinhibition during the trough of the theta cycle caused by post-synaptic OLM cell activity. Whether astrocytic D-serine release from stratum lacunosum moleculare astrocytes is recruited during repetitive activation of CA1 PCs was not determined by my experiments. However, theoretically, APs backpropagate into the tuft dendrites (Spruston et al., 1995; Williams and Stuart, 2000) and consequently a frequency-dependent release of co-agonists from astrocytes could be possible. But the depolarization is strongly attenuated during the propagation. To yield a better recruitment of endocannabinoid mobilization repetitive, short, high frequency bursts might be more potent since these are less attenuated. Thus, determining the influence of high frequency AP bursts on supralinear dendritic integration and the initiation of dendritic plateau potential could provide important evidence supporting such mechanisms.

4.10 Relevance of Dendritic Integration for Spatial Learning in the CA1 Microcircuit

Many of the studies investigating dendritic integration have been performed in slice preparation. This makes a tight control of the extracellular environment possible and intrinsic synaptic activation is absent. The different physiological environment in vivo will, however, influence the integrative properties of dendrites through fluctuations of ion, neurotransmitter and neuromodulator concentrations (Palmer et al., 2016). For instance, the constant synaptic input, which is present in vivo, has been described to influence the membrane potential (V_m), the membrane resistance (R_m) and membrane time constant (τ_m; Paré et al., 1998; Steriade et al.,

2001). Nevertheless, similar dendritic properties in vitro and vivo have been observed (Larkum and Zhu, 2002; Waters et al., 2003). Importantly, also clustered input patters and clustered functional recruitment of synapses have been described in the cortex (Dombeck et al., 2009; Fu et al., 2012; Jia et al., 2010; Kerlin et al., 2019; Roth et al., 2020; Takahashi et al., 2012; Wilson et al., 2016; Winnubst et al., 2015) and hippocampus (Bloss et al., 2018; Kleindienst et al., 2011; Takahashi et al., 2012). In line with these findings, dendrites in vivo show different forms of dendritic integration, like sublinear, linear and supralinear input summations, and dendritic spikes or plateau potentials (Cichon and Gan, 2015; Grienberger et al., 2014; Lavzin et al., 2012; Léger et al., 2005; Longordo et al., 2013; Palmer et al., 2014; Xu et al., 2012). But what is the function of supralinear dendritic integration in relation to behavior? Dendritic spikes and plateaus have been shown to increase AP output in vivo (Bittner et al., 2015; Grienberger et al., 2014; Lavzin et al., 2012; Palmer et al., 2014; Smith et al., 2013). Specifically, in CA1 PCs, dendritic integration has been shown to regulate spatial information processing. During exploration of a novel environment, place cell formation in the CA1 area of the hippocampus is taking place (O'Keefe, 1976), a process linked to dendritic spikes and plateau potentials (Bittner et al., 2015; Sheffield et al., 2017). But also existing place cells show regenerative dendritic events with a varying prevalence that allowed the experimenters to predicted changes in the place field, like their spatial precision, persistence of disappearance (Sheffield and Dombeck, 2015; Sheffield et al., 2017). Changes in the environment, e.g., displacement or introduction of objects, will result in increased exploration and reorganization of these place fields (Deshmukh and Knierim, 2013; Lenck-Santini et al., 2005; Manns and Eichenbaum, 2009; O'Keefe and Nadel, 1978). The related changes in synaptic efficacy and place cell formation required NMDA receptor function (Morris et al., 1986; Sheffield et al., 2017). Furthermore, theta oscillations are commonly observed during exploration (Vanderwolf, 1969) and depending on the theta phase the likelihood of LTP and place cell induction is changed (Bittner et al., 2015; Huerta and Lisman, 1996). Thus, the positive modulation of the supralinear dendritic integration by the astrocytic release of D-serine with its dependency on theta-like activity could strongly modulate place cell formation and refinement as well as spatial learning and memory in general.

4.10.1 Astrocytic CB1 Receptors Modulate Spatial Learning and Memory

Slice experiments showed that this signaling cascade is disrupted in aCB1KO mice, therefore, their spatial learning abilities were investigated. Of note, these mice have a heterozygous knock-out of GLAST (owing to the GLAST-creERT2 lines) that has been shown to not cause behavioral phenotypes (Karlsson et al., 2009). Likewise, comparing sham-injected control mice to aCB1KO littermates did not reveal changes in general locomotor or anxiety-related behavior phenotype (Figure 3.23).

Interestingly, an impairment of long-term object memory was observed comparing sham-inject control mice to aCB1KO ones during the object location task (OLT) and novel object recognition task (NORT; Figure 3.25). A similar result concerning novel object recognition memory was found by Robin et al. (2018) using a slightly different experimental setup and a different cre line to induce the astrocyte-specific knock-out of the CB1 receptor. However, the novel object recognition task (NORT) does not only rely on the hippocampus but also on several other (neo)cortical areas (Antunes and Biala, 2012; Barker and Warburton, 2011). But the object location task (OLT) has been shown to be specific for the CA1 region of the hippocampus (Assini et al., 2009; Barker and Warburton, 2011). Assuming a common underlying mechanism in the impairment of object memory, alterations in the CA1 microcircuit could underly the observed

impairment. Moreover, Robin et al. (2018) have investigated the particular relevance of this area by using a virus-injection-induced cell-type specific knock-out of astrocytic CB1 receptors and have found a similar effect. It is important to consider that the mice used in my thesis displayed differences in the object exploration time. While this did not reach significance during the NORT, a positive relationship between object exploration time and discrimination index (DI) was found. Thus, the result might be confounded by a decreased object interest during the recognition memory test. The ORT revealed no relationship between the exploration time during acquisition and DI after a 24-hour delay. Interestingly, Robin et al. (2018) have conducted experiments in which the memory performance of aCB1KO mice was rescued by an administration of D-serine before the acquisition of the object memory. In conclusion, these results illustrate the importance of astrocytic D-serine release in response of CB1 receptor activation in the acquisition of object-related long-term memory.

The molecular mechanism underlying object memory is still under debate. It has been described that specifically the place cells in CA1 are important to represent novelty by an increase in their firing rate (Larkin et al., 2014). NMDA receptors and the level of co-agonist appear to have a diverse, bidirectional role in this. While some studies describe a positive relationship between NMDA receptor recruitment and object location memory formation (Guercio et al., 2014; Yamada et al., 2017), others describe a negative (Howland and Cazakoff, 2010; Migues et al., 2019). Specifically, blockade of GluN2B-containing NMDA receptors has been shown to increase the duration of memory in these tasks. This suggests a tight bidirectional regulation of object memory by both, long-term potentiation (LTP) and depression (LTD). In line with this hypothesis is the postulation that encoding of space itself requires LTP, while spatial features as objects and their visual recognition are encoded by LTD (Dong et al., 2012; Goh and Manahan-Vaughan, 2013; Goh and Manahan-Vaughan, 2013, 2015; Griffiths et al., 2008; Kemp and Manahan-Vaughan, 2004). An impairment of LTP in aCB1KO mice has been shown in vivo (Robin et al., 2018); however, whether LTD is affected too remains unknown. Unraveling the role of dendritic spikes, LTP, LTD and NMDA receptor co-agonist levels during the encoding of object location and novel object recognition memory requires more investigation. Cannabinoids in general have been shown to have opposing effects in object memory depending on the timing at which they are administrated (for review see Chesworth et al., 2018). Especially, when cognitive functions are dysregulated in pathologies, various effects have been observed after CB1 receptor activation. The uncovered feedback loop that links network activity in the theta frequency band and endocannabinoids to the release of astrocytic D-serine and subsequent modulation of specifically supralinear dendritic integration and the initiation of dendritic spikes provides another essential puzzle piece to unravel the multidimensional regulations of object memory by endocannabinoids. Knowing mechanisms that cause the release of endocannabinoids under physiological activity patterns, their consequences and the impact on signal integration aids to understand the functional regulations within the microcircuit and its output.

4.10.2 Aversive Spatial Reversal Learning Requires Astrocytic CB1 Receptors

Place cells are not only important for object memory but also encode information about the location of an aversive stimulus (Okada et al., 2017). For the encoding of aversive memory, the ventral hippocampus is recruited, in which the here presented slice experiments were performed. Thus, aCB1KO and sham-injected control mice were subjected to a passive place avoidance task. This task has been shown to rely on several cortical and limbic brain areas, with different contribution to learning, retention memory and reversal learning (Cimadevilla et al., 2000;

D'Hooge and De Deyn, 2001; Lénárd and Kertes, 2002; Vafaei and Rashidy-Pour, 2004). The aversion of a stimulus will increase the emotional value of its location, and thus, the ventral hippocampus should play a central role during the task (Fanselow and Dong, 2010). To decrease animal suffering, an air puff was used as an aversive stimulus as opposed to many other studies, which have been using a food shock. It has been shown that an air puff can be used in fear-related behavior tasks without affecting aversive learning (Moriarty et al., 2012).

During the habituation to the circular arena, mice of both groups displayed similar exploratory behavior (Figure 3.26). Likewise, aCB1KO mice displayed normal passive avoidance behavior after introduction of the air puff as compared to sham-injected controls. Locomotion behavior, velocity and avoidance of the air puff location showed no differences during the first days of the task. While this might seem in contrast to the results obtained with the object tasks, it is important to note that the presence of the aversive stimulus will lead to the recruitment of other brain regions that could compensate for the earlier observed effect. In addition, no differences in retention memory after removal of the air puff was detected. Surprisingly, a specific alteration was discovered on the last day of the test, where the air puff is relocated to the opposite side of the maze. This so-called reversal learning is often linked to memory flexibility (Izquierdo et al., 2017; Klanker et al., 2013; Rubin et al., 2014). While the nature of the aversive stimulus is known, the previous memory needs to be "transferred" to a new location in space to avoid punishment. While many studies focus on monoaminergic regulation in the prefrontal and orbitofrontal cortex as well as the amygdala (for review see Izquierdo et al., 2017; Klanker et al., 2013), the hippocampus has also been implicated to contribute to specifically spatial reversal learning (Mahut, 1971). Treatments or modifications resulting in reduced spatial reversal abilities often coincidence with a decreased "extinction" of the previous location (Gajardo et al., 2018; Russig et al., 2003). However, the results revealed a selective impairment of spatial reversal acquisition without differences between transitions at the previous location. A possible explanation could lie in differential efficiency of strategies used to locate the air puff's position: egocentric and spatial learning. Interestingly, a lower number of air puff activations in the control mice than required during the initial learning was observed on the last day, suggesting indeed the use of spatial learning strategies in sham-inject control mice. However, aCB1KO mice seem to have no beneficial effect of the previous memory and thus, likely employing egocentric learning strategies. Importantly, no changes in spatial working memory were observed during the initial learning and in the Y-maze (Figure 3.24). Surprisingly, aCB1KO mice seemed to learn the new position of the aversive stimulus over time, as illustrated by the decrease in air puff activation during the time course of the exploration. The retention memory concerning the novel air puff location was not examined in these experiments but could provide interesting information.

The suggested different learning strategies have a distinct efficiency during spatial reversal learning. O'Keefe and Nadel (1978) postulated that hippocampal place cells are important for spatial but not egocentric learning strategies. Many studies since have reported effects of hippocampal-dependent disruption of spatial reversal learning (Balschun et al., 2010; Dong et al., 2013; Duffy et al., 2008; Oliveira et al., 1997). Using the Morris water maze (MWM) and MRI imaging of the functional connectivity, it has been shown that mice during the early acquisition days of the task rely on nonspatial strategies. However, extended training and reversal learning required spatial strategies (Shah et al., 2019). Interestingly, the dorsal hippocampus has been described to regulate stimulus-related responses, i.e., egocentric learning (Kleinknecht et al., 2012; Stevens and Cowey, 1973). In contrast, the ventral hippocampus mediates response-

related approaches and strategies. Thus, processing by the ventral hippocampus will result rather in general rules and strategies in how to respond to the air puff. In line with this hypothesis is the finding that acquisition of the platform location in a water maze was unaltered by lesions to the ventral hippocampus (Kleinknecht et al., 2012). But an impaired to solve a water-cross maze task during reversal learning, which requires the use of spatial strategies, was found. Investigating the use of different learning strategies in sham-injected control and aCB1KO mice in solving spatial tasks could shed some light on the underlying mechanism of the observed effect. Learning strategies can be, for instance, investigated with a T-maze. During training, a reward is placed in the right arm. After several trials, the mouse will learn this. However, to examine if the mouse remembers the direction or location of the reward, a probe trial is performed. Here, the maze is turned by 180°. If the mouse used a spatial strategy to learn the reward location, it will enter the left arm in anticipation of the reward. However, if the mouse used egocentric learning strategies to solve the task it will enter the right arm. Subjecting animals with a localized knock-out of CB1 receptors in astrocytes in either the dorsal or ventral hippocampus might aid to unravel the differential contribution of these subregions in spatial reversal learning and the use of different learning strategies between aCB1KO and sham-injected mice.

While the relevance of the hippocampus in spatial reversal learning is well-studied, the molecular mechanism is poorly understood. Some studies have postulated a relevance of GluN2B- and D-serine-depending LTD (Dong et al., 2013; Duffy et al., 2008), others have hypothesized a central role for LTP (Balschun et al., 2010). Inhibitory activity provides another important mechanism in gaining meaningful output of the CA1 microcircuit. Accordingly, in vivo studies have shown regulation of place cells by inhibition. Somatostatin-positive cells regulate the switch to burst firing, while parvalbumin-positive interneurons regulate phase precision (Royer et al., 2012). Additionally, place cell remapping requires disinhibition (Schoenenberger et al., 2016) and spatially uniform inhibition regulates place field precision (Grienberger et al., 2017).

How could the uncovered feedback loop influence spatial reversal learning on a molecular level? The introduction or removal of an air puff or other aversive stimulus leads to reorganization of place cells in the hippocampus (Moita et al., 2004; Okada et al., 2017). Interestingly, dendritic targeting interneurons play an essential role in this process (Lovett-Barron et al., 2014). They postulate that the aversive stimulus induced suppression of selectively perforant path inputs by OLM interneurons is required for contextual fear learning. Accordingly, a reorganization in response to spatial reversal of the air puff location would be expected under control conditions. An impairment of this reorganization in the knock-out mice would explain the decrease in aversive spatial reversal learning. Endocannabinoids have been described to be a powerful regulator of the inhibitory balance underlying place cell assembly (Dubruc et al., 2013). An interesting relevance of D-serine for reversal learning has been suggested as well (Labrie et al., 2009). Using a contextual feat memory task, the authors found that increasing the concentration of D-serine by reducing the activity of the degrading enzyme resulted in increased adaptive learning in response to changing conditions. However, to my knowledge, no study has investigated the impact of D-serine or NMDA receptor co-agonist binding site occupancy on place cell formation or reorganization. Recording place cell activity in vivo through implanted tetrodes or in vivo calcium imaging either with the application of D-serine or using sham-inject control and aCB1KO mice could yield more information on NMDA receptor co-agonist dependent place field organization and restructuring.

4.11 Universal Role of the Feedback Loop

My thesis describes a positive modulation of supralinear dendritic integration by a signaling cascade that requires neuronal activity, endocannabinoid mobilization, activation of astrocytic CB1 receptors and the release of D-serine. This feedback loop was studied and characterized in the stratum radiatum of the hippocampus. An important question to consider is, whether these findings can be transferred to other strata or brain regions. The relevance of nonlinear dendritic integration in behavioral output has been found not only in the stratum radiatum of the hippocampus but also in the stratum lacunosum moleculare and in several cortical regions (Cichon and Gan, 2015; Grienberger et al., 2014; Lavzin et al., 2012; Palmer et al., 2014; Ranganathan et al., 2018; Sivyer and Williams, 2013; Smith et al., 2013; Xu et al., 2012). Dynamic regulation of NMDA receptor co-agonists release from astrocytes would provide a powerful regulation in these behavioral paradigms. However, neuronal organization, inhibition and rhythmic activities differ within the brain. Moreover, it is established that astrocytes are a heterogenous cell population (Haim and Rowitch, 2017; Khakh and Sofroniew, 2015). Between the stratum radiatum and stratum lacunosum moleculare astrocytes show differences in density, morphology and expression patterns (Batiuk et al., 2020; Hsu et al., 2011; Jinno, 2011; Ogata and Kosaka, 2002). Between different brain regions these differences are even more pronounced (Batiuk et al., 2020; Chai et al., 2017; D'Ambrosio et al., 1998; Lanjakornsiripan et al., 2018; Miller et al., 2019; Morel et al., 2017, 2019; Takata and Hirase, 2008). Furthermore, the fraction of synapses adjacent to astrocytic processes varies between brain regions (Bernardinelli et al., 2014; Reichenbach et al., 2010; Ventura and Harris, 1999; Witcher et al., 2007). Consequently, diverse recruitment of astrocytic D-serine release in response to region-specific neuronal activity is an interesting hypothesis that needs to be explored.

Along a similar line of thought, also differences in the feedback loop along the dorso-ventral axis of the hippocampus should be considered. Evidence suggests functional and molecular differences within the hippocampus (Cembrowski et al., 2016; Dougherty et al., 2012, 2013; Kouvaros and Papatheodoropoulos, 2016; Malik and Johnston, 2017; Marcelin et al., 2012; Papatheodoropoulos and Kostopoulos, 2000). For instance, it has been shown that HCN channel expression and I_h contribution differ between the ventral and dorsal hippocampus, resulting in a depolarized membrane potential, decreased temporal summation and increased resonance in the former (Dougherty et al., 2013; Marcelin et al., 2012). Similarly, an increased expression of the A-type potassium channel Kv4.2 is observed along the dorso-ventral axis, promoting AP backpropagation differentially (Marcelin et al., 2012). These differences might permit neuronal activity in the theta frequency band to more strongly backpropagate into the dendritic arbor of ventral CA1 PCs and evoke the mobilization of endocannabinoids more potently. Interestingly, a recent study showed different integrative properties along the dorso-ventral axis (Malik and Johnston, 2017). While dendritic plateau potential initiation in the dorsal hippocampus requires precisely-timed input in both strata, they could be evoked by temporally dispersed excitatory inputs in the ventral hippocampus. This could potentially be regulated by differential inhibition and could be an important factor in the decreased spatial definition of place fields along the dorso-ventral axis (Jung et al., 1994). Since the feedback loop was uncovered in the ventral hippocampus, it cannot simply be assumed that the same mechanisms are recruited with the same efficacy in the dorsal hippocampus. To conclude whether this cascade can be recruited throughout the hippocampus, an experimental examination is required.

Another important consideration when speculating about a universal role of the discovered feedback loop is the amount of neuronal depolarization required for the production and mobilization of endocannabinoids. The present study focused on AP firing of an ensemble of neurons ranging from 20-80 %. However, other studies have shown that changes in gliotransmission can be regulated heterosynaptically (Chen et al., 2013a; Navarrete and Araque, 2010; Serrano et al., 2006; Zhang et al., 2003). This means that as little as a single neuron was able to evoke alterations in astrocytic calcium, leading to an increase in synaptic transmission in one and a decrease in another neuron. Notably, astrocytes cover nonoverlapping territories (Bushong et al., 2002; Halassa et al., 2007). This means that a single astrocyte will be in contact with several hundred dendrites located in the same area but originating from different neurons. It is estimated that a single astrocyte territory contains between 20 000 to 160 000 spines. It is an interesting question at which scale (whole territory, small microdomain, around one dendritic segment) endocannabinoid mobilization and the release of D-serine can be and are recruited. Similarly, it is important to determine whether other neurotransmitters, like dopamine, glutamate or GABA, can recruit the release of D-serine and with which potency, when this release is recruited and whether it influences the same or distinct behavior.

5 CONCLUSION

My thesis investigated the role of astrocytes in the modulation of dendritic integration and its behavioral relevance. Astrocytes can modulate NMDA receptor recruitment via the uptake of glutamate from the synaptic cleft and through the supply of the NMDA receptor co-agonist D-serine. My results revealed a negative relationship between the spine size and the efficacy of local glutamate uptake. The decreased efficacy of glutamate clearance might further underlie the increased probability of dendritic spike induction selectively at large, mushroom-like spines. Furthermore, I determined that supralinear dendritic integration with dendritic spikes in the apical oblique dendrites and dendritic plateau potentials of CA1 pyramidal cells can be modulated by the NMDA receptor co-agonist D-serine. In contrast, such modulation was not possible for linear dendritic integration without dendritic spikes. Since calcium transients underly the release of D-serine from astrocytes, the influence of the local resting calcium concentration on its shape was investigated. The presented results showed a positive relationship between the local pre-event and the peak calcium concentration. Interestingly, the pre-event concentration scaled negatively with the amplitude. Because of the power law relationship between calcium and vesicular release, this universal rule suggests that relatively small increases in the local resting calcium concentration result in larger local peak concentrations and hence, could cause even larger changes in the release of gliotransmitters. Thus, changes in the local resting calcium concentration in astrocytes, which are observed in response to neuronal activity, toxic deposits and pathophysiological changes in ion homeostasis, can affect synaptic transmission through the modulation of gliotransmitter release.

In addition, I characterized the conditions under which D-serine release from astrocytes is recruited and positively modulates supralinear dendritic integration in apical oblique dendrites. This led to the discovery of a previously unknown feedback loop linking neuronal network activity to supralinear dendritic integration in the same region (Figure 5.1). Activity of CA1 pyramidal cells in the theta frequency range can cause depolarization that backpropagates into the apical oblique dendrites. This requires the presence of hyperpolarization-activated and cyclic nucleotide-gated channels. Locally in the dendrites, the depolarization stimulates the production and mobilization of endocannabinoids. Those endocannabinoids bind to astrocytic CB1 receptors and cause an increase in the intracellular calcium concentration and transient frequency. This in turn results in an increase of the D-serine concentration within the territory of the astrocyte. Consequently, NMDA receptor recruitment will be increased promoting dendritic spike initiation during synchronous activation of spatially clustered synapses. Because of their decreased induction threshold and increased amplitude, the activation of the same number of synapses will now result in a higher chance of neuronal output in form of action potentials and/or possibly, a switch to burst firing through the increased, slow, NMDA receptor-mediated component of the dendritic spike. Proper spatial learning and memory require this signaling cascade, as disruption of it led to an impairment of object memory and aversive spatial reversal learning in mice. The latter suggests that astrocytic CB1 receptors have a central role in cognitive flexibility.

To better understand the implications of the uncovered feedback loop on spatial learning abilities of mice, exploring the place cell activity and precision in dependence of astrocytic CB1 receptors can be an important step. Furthermore, identifying other astrocytic signaling cascades resulting in an increase of intracellular calcium that can modulate dendritic integration could aid our understanding of the dendritic computations performed by pyramidal cells.

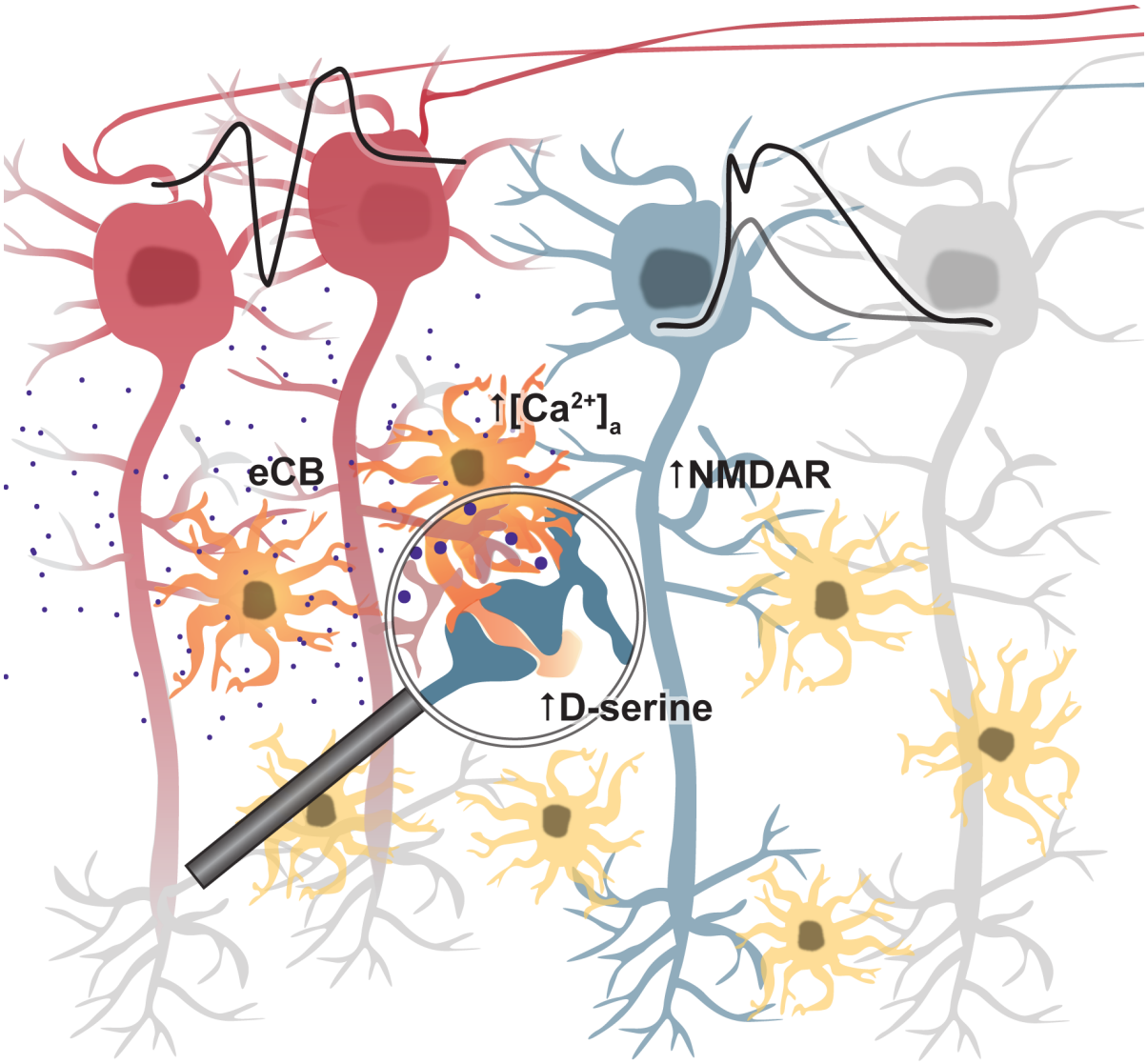

Figure 5.1. Cartoon illustrating the positive feedback loop between pyramidal cell network activity and their dendritic integration. Pyramidal cell activity in the theta frequency range (red) propagates in to the dendritic tree, causing the release of endocannabinoids (eCB, purple). These evoke an increase in the astrocytic calcium concentration through CB1 receptors (orange). Because of the elevated calcium an increased release of D-serine takes place (magnifying glass, orange at synapse). This leads to an increase recruitment of NMDA receptors and thus, promotes the supralinear dendritic integration of another pyramidal cell (blue).

6 REFERENCES

Abrahamsson, T., Cathala, L., Matsui, K., Shigemoto, R., and Digregorio, D.A. (2012). Thin dendrites of cerebellar interneurons confer sublinear synaptic integration and a gradient of short-term plasticity. Neuron *73*, 1159–1172.

Adamsky, A., Kol, A., Kreisel, T., Doron, A., Ozeri-Engelhard, N., Melcer, T., Refaeli, R., Horn, H., Regev, L., Groysman, M., et al. (2018). Astrocytic Activation Generates De Novo Neuronal Potentiation and Memory Enhancement. Cell *174*, 59-71.e14.

Agarwal, A., Wu, P.-H., Hughes, E.G., Fukaya, M., Tischfield, M.A., Langseth, A.J., Wirtz, D., and Bergles, D.E. (2017). Transient Opening of the Mitochondrial Permeability Transition Pore Induces Microdomain Calcium Transients in Astrocyte Processes. Neuron *93*, 587-605.e7.

Agulhon, C., Fiacco, T.A., and McCarthy, K.D. (2010). Hippocampal short- and long-term plasticity are not modulated by astrocyte Ca2+ signaling. Science *327*, 1250–1254.

Aika, Y., Ren, J.Q., Kosaka, K., and Kosaka, T. (1994). Quantitative analysis of GABA-like-immunoreactive and parvalbumin-containing neurons in the CA1 region of the rat hippocampus using a stereological method, the disector. Exp. Brain Res. *99*, 267–276.

Akerboom, J., Chen, T.-W., Wardill, T.J., Tian, L., Marvin, J.S., Mutlu, S., Calderón, N.C., Esposti, F., Borghuis, B.G., Sun, X.R., et al. (2012). Optimization of a GCaMP Calcium Indicator for Neural Activity Imaging. J. Neurosci. *32*, 13819–13840.

Al Awabdh, S., Gupta-Agarwal, S., Sheehan, D.F., Muir, J., Norkett, R., Twelvetrees, A.E., Griffin, L.D., and Kittler, J.T. (2016). Neuronal activity mediated regulation of glutamate transporter GLT-1 surface diffusion in rat astrocytes in dissociated and slice cultures. Glia *64*, 1252–1264.

Albrecht, J., and Zielińska, M. (2017). Mechanisms of Excessive Extracellular Glutamate Accumulation in Temporal Lobe Epilepsy. Neurochem. Res. *42*, 1724–1734.

Alger, B.E., and Kim, J. (2011). Supply and demand for endocannabinoids. Trends Neurosci. *34*, 304–315.

Alger, B.E., Pitler, T.A., Wagner, J.J., Martin, L.A., Morishita, W., Kirov, S.A., and Lenz, R.A. (1996). Retrograde signalling in depolarization-induced suppression of inhibition in rat hippocampal CA1 cells. J. Physiol. *496 (Pt 1)*, 197–209.

Ali, A.B. (2007). Presynaptic Inhibition of GABAA receptor-mediated unitary IPSPs by cannabinoid receptors at synapses between CCK-positive interneurons in rat hippocampus. J. Neurophysiol. *98*, 861–869.

Ali, A.B., and Todorova, M. (2010). Asynchronous release of GABA via tonic cannabinoid receptor activation at identified interneuron synapses in rat CA1. Eur. J. Neurosci. *31*, 1196–1207.

Allen, T.A., Salz, D.M., McKenzie, S., and Fortin, N.J. (2016). Nonspatial Sequence Coding in CA1 Neurons. J. Neurosci. *36*, 1547–1563.

Amaral, D., and Lavenex, P. (2007). Hippocampal Neuroanatomy. In The Hippocampus Book, P. Andersen, R. Morris, D. Amaral, T. Bliss, and J. O'Keefe, eds. (Oxford University Press), pp. 37–114.

Amaral, D.G., and Witter, M.P. (1989). The three-dimensional organization of the hippocampal formation: A review of anatomical data. Neuroscience *31*, 571–591.

Amemiya, S., and Redish, A.D. (2018). Hippocampal Theta-Gamma Coupling Reflects State-Dependent Information Processing in Decision Making. Cell Rep. *22*, 3328–3338.

Anders, S., Minge, D., Griemsmann, S., Herde, M.K., Steinhäuser, C., and Henneberger, C. (2014). Spatial properties of astrocyte gap junction coupling in the rat hippocampus. Philos. Trans. R. Soc. B Biol. Sci. *369*, 20130600.

Andersen, P., Bliss, T.V.P., and Skrede, K.K. (1971). Lamellar organization of hippocampal excitatory pathways. Exp. Brain Res. *13*, 222–238.

Andrade-Talavera, Y., Duque-Feria, P., Paulsen, O., and Rodríguez-Moreno, A. (2016). Presynaptic Spike Timing-Dependent Long-Term Depression in the Mouse Hippocampus. Cereb. Cortex *26*, 3637–3654.

Andriezen, W.L. (1893). The Neuroglia Elements in the Human Brain. Br. Med. J. *2*, 227–230.

Angulo, M.C., Kozlov, A.S., Charpak, S., and Audinat, E. (2004). Glutamate Released from Glial Cells Synchronizes Neuronal Activity in the Hippocampus. J. Neurosci. *24*, 6920–6927.

Antic, S.D. (2003). Action potentials in basal and oblique dendrites of rat neocortical pyramidal neurons. J. Physiol. *550*, 35–50.

Antunes, M., and Biala, G. (2012). The novel object recognition memory: neurobiology, test procedure, and its modifications. Cogn. Process. *13*, 93–110.

Araque, A., Sanzgiri, R.P., Parpura, V., and Haydon, P.G. (1998a). Calcium Elevation in Astrocytes Causes an NMDA Receptor-Dependent Increase in the Frequency of Miniature Synaptic Currents in Cultured Hippocampal Neurons. J. Neurosci. *18*, 6822–6829.

Araque, A., Parpura, V., Sanzgiri, R.P., and Haydon, P.G. (1998b). Glutamate-dependent astrocyte modulation of synaptic transmission between cultured hippocampal neurons. Eur. J. Neurosci. *10*, 2129–2142.

Araque, A., Parpura, V., Sanzgiri, R.P., and Haydon, P.G. (1999). Tripartite synapses: glia, the unacknowledged partner. Trends Neurosci. *22*, 208–215.

Arizono, M., Inavalli, V.V.G.K., Panatier, A., Pfeiffer, T., Angibaud, J., Levet, F., Veer, M.J.T.T., Stobart, J., Bellocchio, L., Mikoshiba, K., et al. (2020). Structural basis of astrocytic Ca 2+ signals at tripartite synapses. Nat. Commun. *11*, 1–15.

Armbruster, M., Hanson, E., and Dulla, C.G. (2016). Glutamate Clearance Is Locally Modulated by Presynaptic Neuronal Activity in the Cerebral Cortex. J. Neurosci. *36*, 10404–10415.

Arnth-Jensen, N., Jabaudon, D., and Scanziani, M. (2002). Cooperation between independent hippocampal synapses is controlled by glutamate uptake. Nat. Neurosci. *5*, 325–331.

Asada, A., Ujita, S., Nakayama, R., Oba, S., Ishii, S., Matsuki, N., and Ikegaya, Y. (2015). Subtle modulation of ongoing calcium dynamics in astrocytic microdomains by sensory inputs. Physiol. Rep. *3*, e12454.

Ascher, P., and Nowak, L. (1988). The role of divalent cations in the N-methyl-D-aspartate responses of mouse central neurones in culture. J. Physiol. *399*, 247–266.

Ascher, P., and Nowak, L. (2009). Early biophysics of the NMDA receptor channel. J. Physiol. *587*, 4563–4564.

Assini, F.L., Duzzioni, M., and Takahashi, R.N. (2009). Object location memory in mice: pharmacological validation and further evidence of hippocampal CA1 participation. Behav. Brain Res. *204*, 206–211.

Asztely, F., Erdemli, G., and Kullmann, D.M. (1997). Extrasynaptic glutamate spillover in the hippocampus: dependence on temperature and the role of active glutamate uptake. Neuron *18*, 281–293.

Baddeley, A. (1992). Working memory. Science *255*, 556–559.

Balschun, D., Moechars, D., Callaerts-Vegh, Z., Vermaercke, B., Van Acker, N., Andries, L., and D'Hooge, R. (2010). Vesicular Glutamate Transporter VGLUT1 Has a Role in Hippocampal Long-Term Potentiation and Spatial Reversal Learning. Cereb. Cortex *20*, 684–693.

Bannerman, D.M., Good, M.A., Butcher, S.P., Ramsay, M., and Morris, R.G. (1995). Distinct components of spatial learning revealed by prior training and NMDA receptor blockade. Nature *378*, 182–186.

Bannerman, D.M., Yee, B.K., Good, M.A., Heupel, M.J., Iversen, S.D., and Rawlins, J.N. (1999). Double dissociation of function within the hippocampus: a comparison of dorsal, ventral, and complete hippocampal cytotoxic lesions. Behav. Neurosci. *113*, 1170–1188.

Bannerman, D.M., Deacon, R.M.J., Offen, S., Friswell, J., Grubb, M., and Rawlins, J.N.P. (2002). Double dissociation of function within the hippocampus: spatial memory and hyponeophagia. Behav. Neurosci. *116*, 884–901.

Bannerman, D.M., Deacon, R.M.J., Seeburg, P.H., and Rawlins, J.N.P. (2003a). GluR-A-deficient mice display normal acquisition of a hippocampus-dependent spatial reference memory task but are impaired during spatial reversal. Behav. Neurosci. *117*, 866–870.

Bannerman, D.M., Grubb, M., Deacon, R.M.J., Yee, B.K., Feldon, J., and Rawlins, J.N.P. (2003b). Ventral hippocampal lesions affect anxiety but not spatial learning. Behav. Brain Res. *139*, 197–213.

Bannerman, D.M., Niewoehner, B., Lyon, L., Romberg, C., Schmitt, W.B., Taylor, A., Sanderson, D.J., Cottam, J., Sprengel, R., Seeburg, P.H., et al. (2008). NMDA receptor subunit NR2A is required for rapidly acquired spatial working memory but not incremental spatial reference memory. J. Neurosci. *28*, 3623–3630.

Bannerman, D.M., Bus, T., Taylor, A., Sanderson, D.J., Schwarz, I., Jensen, V., Hvalby, Ø., Rawlins, J.N.P., Seeburg, P.H., and Sprengel, R. (2012). Dissecting spatial knowledge from spatial choice by hippocampal NMDA receptor deletion. Nat. Neurosci. *15*, 1153–1159.

Barbour, B., and Häusser, M. (1997). Intersynaptic diffusion of neurotransmitter. Trends Neurosci. *20*, 377–384.

Barker, G.R.I., and Warburton, E.C. (2011). When Is the Hippocampus Involved in Recognition Memory? J. Neurosci. *31*, 10721–10731.

Barnes, J.R., Mukherjee, B., Rogers, B.C., Nafar, F., Gosse, M., and Parsons, M.P. (2020). The Relationship Between Glutamate Dynamics and Activity-Dependent Synaptic Plasticity. J. Neurosci. *40*, 2793–2807.

Barria, A., and Malinow, R. (2005). NMDA receptor subunit composition controls synaptic plasticity by regulating binding to CaMKII. Neuron *48*, 289–301.

Barria, A., Muller, D., Derkach, V., Griffith, L.C., and Soderling, T.R. (1997). Regulatory Phosphorylation of AMPA-Type Glutamate Receptors by CaM-KII During Long-Term Potentiation. Science *276*, 2042–2045.

Barrionuevo, G., Schottler, F., and Lynch, G. (1980). The effects of repetitive low frequency stimulation on control and "potentiated" synaptic responses in the hippocampus. Life Sci. *27*, 2385–2391.

Basu, J., Srinivas, K.V., Cheung, S.K., Taniguchi, H., Huang, Z.J., and Siegelbaum, S.A. (2013). A Cortico-Hippocampal Learning Rule Shapes Inhibitory Microcircuit Activity to Enhance Hippocampal Information Flow. Neuron *79*, 1208–1221.

Basu, J., Zaremba, J.D., Cheung, S.K., Hitti, F.L., Zemelman, B.V., Losonczy, A., and Siegelbaum, S.A. (2016). Gating of hippocampal activity, plasticity, and memory by entorhinal cortex long-range inhibition. Science *351*, aaa5694.

Batiuk, M.Y., Martirosyan, A., Wahis, J., Vin, F. de, Marneffe, C., Kusserow, C., Koeppen, J., Viana, J.F., Oliveira, J.F., Voet, T., et al. (2020). Identification of region-specific astrocyte subtypes at single cell resolution. Nat. Commun. *11*, 1–15.

Bayer, K.-U., De Koninck, P., Leonard, A.S., Hell, J.W., and Schulman, H. (2001). Interaction with the NMDA receptor locks CaMKII in an active conformation. Nature *411*, 801–805.

Bazargani, N., and Attwell, D. (2016). Astrocyte calcium signaling: the third wave. Nat. Neurosci. *19*, 182–189.

Beltramo, M., Stella, N., Calignano, A., Lin, S.Y., Makriyannis, A., and Piomelli, D. (1997). Functional Role of High-Affinity Anandamide Transport, as Revealed by Selective Inhibition. Science *277*, 1094–1097.

Benchenane, K., Peyrache, A., Khamassi, M., Tierney, P.L., Gioanni, Y., Battaglia, F.P., and Wiener, S.I. (2010). Coherent Theta Oscillations and Reorganization of Spike Timing in the Hippocampal-Prefrontal Network upon Learning. Neuron *66*, 921–936.

Berberich, S., Punnakkal, P., Jensen, V., Pawlak, V., Seeburg, P.H., Hvalby, Ø., and Köhr, G. (2005). Lack of NMDA receptor subtype selectivity for hippocampal long-term potentiation. J. Neurosci. Off. J. Soc. Neurosci. *25*, 6907–6910.

Bergersen, L.H., Morland, C., Ormel, L., Rinholm, J.E., Larsson, M., Wold, J.F.H., Røe, Å.T., Stranna, A., Santello, M., Bouvier, D., et al. (2012). Immunogold Detection of L-glutamate and D-serine in Small Synaptic-Like Microvesicles in Adult Hippocampal Astrocytes. Cereb. Cortex *22*, 1690–1697.

Bergles, D.E., and Jahr, C.E. (1997). Synaptic Activation of Glutamate Transporters in Hippocampal Astrocytes. Neuron *19*, 1297–1308.

Berke, J.D., Hetrick, V., Breck, J., and Greene, R.W. (2008). Transient 23–30 Hz oscillations in mouse hippocampus during exploration of novel environments. Hippocampus *18*, 519–529.

Bernardinelli, Y., Randall, J., Janett, E., Nikonenko, I., König, S., Jones, E.V., Flores, C.E., Murai, K.K., Bochet, C.G., Holtmaat, A., et al. (2014). Activity-Dependent Structural Plasticity of Perisynaptic Astrocytic Domains Promotes Excitatory Synapse Stability. Curr. Biol. *24*, 1679–1688.

Berridge, M.J., Bootman, M.D., and Roderick, H.L. (2003). Calcium signalling: dynamics, homeostasis and remodelling. Nat. Rev. Mol. Cell Biol. *4*, 517–529.

Bezaire, M.J., and Soltesz, I. (2013). Quantitative assessment of CA1 local circuits: Knowledge base for interneuron-pyramidal cell connectivity. Hippocampus *23*, 751–785.

Bezzi, P., Gundersen, V., Galbete, J.L., Seifert, G., Steinhäuser, C., Pilati, E., and Volterra, A. (2004). Astrocytes contain a vesicular compartment that is competent for regulated exocytosis of glutamate. Nat. Neurosci. *7*, 613–620.

Bibbig, A., Middleton, S., Racca, C., Gillies, M.J., Garner, H., LeBeau, F.E.N., Davies, C.H., and Whittington, M.A. (2007). Beta Rhythms (15-20 Hz) Generated by Nonreciprocal Communication in Hippocampus. J. Neurophysiol. *97*, 2812–2823.

Binder, S., Baier, P.C., Mölle, M., Inostroza, M., Born, J., and Marshall, L. (2012). Sleep enhances memory consolidation in the hippocampus-dependent object-place recognition task in rats. Neurobiol. Learn. Mem. *97*, 213–219.

Bittner, K.C., Grienberger, C., Vaidya, S.P., Milstein, A.D., Macklin, J.J., Suh, J., Tonegawa, S., and Magee, J.C. (2015). Conjunctive input processing drives feature selectivity in hippocampal CA1 neurons. Nat. Neurosci. *18*, 1133–1142.

Bittner, K.C., Milstein, A.D., Grienberger, C., Romani, S., and Magee, J.C. (2017). Behavioral time scale synaptic plasticity underlies CA1 place fields. Science *357*, 1033–1036.

Bliss, T.V., and Lomo, T. (1973). Long-lasting potentiation of synaptic transmission in the dentate area of the anaesthetized rabbit following stimulation of the perforant path. J. Physiol. *232*, 331–356.

Bloss, E.B., Cembrowski, M.S., Karsh, B., Colonell, J., Fetter, R.D., and Spruston, N. (2016). Structured Dendritic Inhibition Supports Branch-Selective Integration in CA1 Pyramidal Cells. Neuron *89*, 1016–1030.

Bloss, E.B., Cembrowski, M.S., Karsh, B., Colonell, J., Fetter, R.D., and Spruston, N. (2018). Single excitatory axons form clustered synapses onto CA1 pyramidal cell dendrites. Nat. Neurosci. *21*, 353–363.

Boehm, J., Kang, M.-G., Johnson, R.C., Esteban, J., Huganir, R.L., and Malinow, R. (2006). Synaptic Incorporation of AMPA Receptors during LTP Is Controlled by a PKC Phosphorylation Site on GluR1. Neuron *51*, 213–225.

Bohmbach, K., Schwarz, M.K., Schoch, S., and Henneberger, C. (2018). The structural and functional evidence for vesicular release from astrocytes in situ. Brain Res. Bull. *136*, 65–75.

Boisvert, M.M., Erikson, G.A., Shokhirev, M.N., and Allen, N.J. (2018). The Aging Astrocyte Transcriptome from Multiple Regions of the Mouse Brain. Cell Rep. *22*, 269–285.

Bollmann, J.H., and Engert, F. (2009). Subcellular Topography of Visually Driven Dendritic Activity in the Vertebrate Visual System. Neuron *61*, 895–905.

Bonilla-Del Río, I., Puente, N., Peñasco, S., Rico, I., Gutiérrez-Rodríguez, A., Elezgarai, I., Ramos, A., Reguero, L., Gerrikagoitia, I., Christie, B.R., et al. (2019). Adolescent ethanol intake alters cannabinoid type-1 receptor localization in astrocytes of the adult mouse hippocampus. Addict. Biol. *24*, 182–192.

Bragin, A., Jandó, G., Nádasdy, Z., Hetke, J., Wise, K., and Buzsáki, G. (1995). Gamma (40-100 Hz) oscillation in the hippocampus of the behaving rat. J. Neurosci. *15*, 47–60.

Branco, T., and Häusser, M. (2011). Synaptic Integration Gradients in Single Cortical Pyramidal Cell Dendrites. Neuron *69*, 885–892.

Brem, A.-K., Ran, K., and Pascual-Leone, A. (2013). Learning and memory. Handb. Clin. Neurol. *116*, 693–737.

Brigman, J.L., Wright, T., Talani, G., Prasad-Mulcare, S., Jinde, S., Seabold, G.K., Mathur, P., Davis, M.I., Bock, R., Gustin, R.M., et al. (2010). Loss of GluN2B-containing NMDA receptors in CA1 hippocampus and cortex impairs long-term depression, reduces dendritic spine density, and disrupts learning. J. Neurosci. Off. J. Soc. Neurosci. *30*, 4590–4600.

Brown, S.P., Brenowitz, S.D., and Regehr, W.G. (2003). Brief presynaptic bursts evoke synapse-specific retrograde inhibition mediated by endogenous cannabinoids. Nat. Neurosci. *6*, 1048–1057.

Brun, V.H., Otnass, M.K., Molden, S., Steffenach, H.-A., Witter, M.P., Moser, M.-B., and Moser, E.I. (2002). Place cells and place recognition maintained by direct entorhinal-hippocampal circuitry. Science *296*, 2243–2246.

Brun, V.H., Leutgeb, S., Wu, H.-Q., Schwarcz, R., Witter, M.P., Moser, E.I., and Moser, M.-B. (2008). Impaired spatial representation in CA1 after lesion of direct input from entorhinal cortex. Neuron *57*, 290–302.

Bushong, E.A., Martone, M.E., and Ellisman, M.H. (1999). CCDB:28, rattus norvegicus, protoplasmic astrocyte. CIL Dataset.

Bushong, E.A., Martone, M.E., Jones, Y.Z., and Ellisman, M.H. (2002). Protoplasmic Astrocytes in CA1 Stratum Radiatum Occupy Separate Anatomical Domains. J. Neurosci. *22*, 183–192.

Bushong, E.A., Martone, M.E., and Ellisman, M.H. (2004). Maturation of astrocyte morphology and the establishment of astrocyte domains during postnatal hippocampal development. Int. J. Dev. Neurosci. Off. J. Int. Soc. Dev. Neurosci. *22*, 73–86.

Buzsáki, G. (2002). Theta Oscillations in the Hippocampus. Neuron *33*, 325–340.

Buzsáki, G., and Draguhn, A. (2004). Neuronal Oscillations in Cortical Networks. Science *304*, 1926–1929.

Cain, D.P., Saucier, D., Hall, J., Hargreaves, E.L., and Boon, F. (1996). Detailed behavioral analysis of water maze acquisition under APV or CNQX: contribution of sensorimotor disturbances to drug-induced acquisition deficits. Behav. Neurosci. *110*, 86–102.

Canolty, R.T., Edwards, E., Dalal, S.S., Soltani, M., Nagarajan, S.S., Kirsch, H.E., Berger, M.S., Barbaro, N.M., and Knight, R.T. (2006). High Gamma Power Is Phase-Locked to Theta Oscillations in Human Neocortex. Science *313*, 1626–1628.

Capuani, C., Melone, M., Tottene, A., Bragina, L., Crivellaro, G., Santello, M., Casari, G., Conti, F., and Pietrobon, D. (2016). Defective glutamate and K+ clearance by cortical astrocytes in familial hemiplegic migraine type 2. EMBO Mol. Med. *8*, 967–986.

Carlisle, S.J., Marciano-Cabral, F., Staab, A., Ludwick, C., and Cabral, G.A. (2002). Differential expression of the CB2 cannabinoid receptor by rodent macrophages and macrophage-like cells in relation to cell activation. Int. Immunopharmacol. *2*, 69–82.

Cash, S., and Yuste, R. (1999). Linear summation of excitatory inputs by CA1 pyramidal neurons. Neuron *22*, 383–394.

Cavelier, P., and Attwell, D. (2005). Tonic release of glutamate by a DIDS-sensitive mechanism in rat hippocampal slices. J. Physiol. *564*, 397–410.

Cembrowski, M.S., Bachman, J.L., Wang, L., Sugino, K., Shields, B.C., and Spruston, N. (2016). Spatial Gene-Expression Gradients Underlie Prominent Heterogeneity of CA1 Pyramidal Neurons. Neuron *89*, 351–368.

Chaby, L.E., Karavidha, K., Lisieski, M.J., Perrine, S.A., and Liberzon, I. (2019). Cognitive Flexibility Training Improves Extinction Retention Memory and Enhances Cortical Dopamine With and Without Traumatic Stress Exposure. Front. Behav. Neurosci. *13*.

Chai, H., Diaz-Castro, B., Shigetomi, E., Monte, E., Octeau, J.C., Yu, X., Cohn, W., Rajendran, P.S., Vondriska, T.M., Whitelegge, J.P., et al. (2017). Neural Circuit-Specialized Astrocytes: Transcriptomic, Proteomic, Morphological, and Functional Evidence. Neuron *95*, 531-549.e9.

Chalifoux, J.R., and Carter, A.G. (2011). Glutamate Spillover Promotes the Generation of NMDA Spikes. J. Neurosci. *31*, 16435–16446.

Chamberland, S., Salesse, C., Topolnik, D., and Topolnik, L. (2010). Synapse-specific inhibitory control of hippocampal feedback inhibitory circuit. Front. Cell. Neurosci. *4*, 130.

Chen, J., Tan, Z., Zeng, L., Zhang, X., He, Y., Gao, W., Wu, X., Li, Y., Bu, B., Wang, W., et al. (2013a). Heterosynaptic long-term depression mediated by ATP released from astrocytes. Glia *61*, 178–191.

Chen, X., Rochefort, N.L., Sakmann, B., and Konnerth, A. (2013b). Reactivation of the Same Synapses during Spontaneous Up States and Sensory Stimuli. Cell Rep. *4*, 31–39.

Chesworth, R., Watt, G., and Karl, T. (2018). Cannabinoid Modulation of Object Recognition and Location Memory—A Preclinical Assessment. In Handbook of Behavioral Neuroscience, A. Ennaceur, and M.A. de Souza Silva, eds. (Elsevier), pp. 461–488.

Chevaleyre, V., and Castillo, P.E. (2003). Heterosynaptic LTD of Hippocampal GABAergic Synapses. Neuron *38*, 461–472.

Chevaleyre, V., and Castillo, P.E. (2004). Endocannabinoid-Mediated Metaplasticity in the Hippocampus. Neuron *43*, 871–881.

Cichon, J., and Gan, W.-B. (2015). Branch-specific dendritic Ca 2+ spikes cause persistent synaptic plasticity. Nature *520*, 180–185.

Cimadevilla, J.M., Fenton, A.A., and Bures, J. (2000). Functional inactivation of dorsal hippocampus impairs active place avoidance in rats. Neurosci. Lett. *285*, 53–56.

Clarke, R.J., and Johnson, J.W. (2006). NMDA receptor NR2 subunit dependence of the slow component of magnesium unblock. J. Neurosci. Off. J. Soc. Neurosci. *26*, 5825–5834.

Clayton, D.A., Mesches, M.H., Alvarez, E., Bickford, P.C., and Browning, M.D. (2002). A hippocampal NR2B deficit can mimic age-related changes in long-term potentiation and spatial learning in the Fischer 344 rat. J. Neurosci. *22*, 3628–3637.

Colbert, C.M., Magee, J.C., Hoffman, D.A., and Johnston, D. (1997). Slow Recovery from Inactivation of Na+ Channels Underlies the Activity-Dependent Attenuation of Dendritic Action Potentials in Hippocampal CA1 Pyramidal Neurons. J. Neurosci. *17*, 6512–6521.

Colgin, L.L., and Moser, E.I. (2010). Gamma Oscillations in the Hippocampus. Physiology *25*, 319–329.

Colgin, L.L., Denninger, T., Fyhn, M., Hafting, T., Bonnevie, T., Jensen, O., Moser, M.-B., and Moser, E.I. (2009). Frequency of gamma oscillations routes flow of information in the hippocampus. Nature *462*, 353–357.

Collingridge, G.L., Kehl, S.J., and McLennan, H. (1983). Excitatory amino acids in synaptic transmission in the Schaffer collateral-commissural pathway of the rat hippocampus. J. Physiol. *334*, 33–46.

Combe, C.L., Canavier, C.C., and Gasparini, S. (2018). Intrinsic Mechanisms of Frequency Selectivity in the Proximal Dendrites of CA1 Pyramidal Neurons. J. Neurosci. *38*, 8110–8127.

Cook, E.P., and Johnston, D. (1999). Voltage-Dependent Properties of Dendrites That Eliminate Location-Dependent Variability of Synaptic Input. J. Neurophysiol. *81*, 535–543.

Cornell-Bell, A.H., Finkbeiner, S.M., Cooper, M.S., and Smith, S.J. (1990). Glutamate induces calcium waves in cultured astrocytes: long-range glial signaling. Science *247*, 470–473.

Coultrap, S.J., Freund, R.K., O'Leary, H., Sanderson, J.L., Roche, K.W., Dell'Acqua, M.L., and Bayer, K.U. (2014). Autonomous CaMKII Mediates Both LTP and LTD Using a Mechanism for Differential Substrate Site Selection. Cell Rep. *6*, 431–437.

Dabaghian, Y., Brandt, V.L., and Frank, L.M. (2014). Reconceiving the hippocampal map as a topological template. ELife *3*, e03476.

D'Ambrosio, R., Wenzel, J., Schwartzkroin, P.A., McKhann, G.M., and Janigro, D. (1998). Functional Specialization and Topographic Segregation of Hippocampal Astrocytes. J. Neurosci. *18*, 4425–4438.

Danbolt, N.C. (2001). Glutamate uptake. Prog. Neurobiol. *65*, 1–105.

Danbolt, N.C., Storm-Mathisen, J., and Kanner, B.I. (1992). An [Na+ + K+]coupled L-glutamate transporter purified from rat brain is located in glial cell processes. Neuroscience *51*, 295–310.

Danbolt, N.C., Furness, D.N., and Zhou, Y. (2016). Neuronal vs glial glutamate uptake: Resolving the conundrum. Neurochem. Int. *98*, 29–45.

Dani, J.W., Chernjavsky, A., and Smith, S.J. (1992). Neuronal activity triggers calcium waves in hippocampal astrocyte networks. Neuron *8*, 429–440.

D'Ascenzo, M., Fellin, T., Terunuma, M., Revilla-Sanchez, R., Meaney, D.F., Auberson, Y.P., Moss, S.J., and Haydon, P.G. (2007). mGluR5 stimulates gliotransmission in the nucleus accumbens. Proc. Natl. Acad. Sci. *104*, 1995–2000.

Davis, S., Butcher, S.P., and Morris, R.G. (1992). The NMDA receptor antagonist D-2-amino-5-phosphonopentanoate (D-AP5) impairs spatial learning and LTP in vivo at intracerebral concentrations comparable to those that block LTP in vitro. J. Neurosci. *12*, 21–34.

Degen, J., Dublin, P., Zhang, J., Dobrowolski, R., Jokwitz, M., Karram, K., Trotter, J., Jabs, R., Willecke, K., Steinhäuser, C., et al. (2012). Dual reporter approaches for identification of Cre efficacy and astrocyte heterogeneity. FASEB J. *26*, 4576–4583.

Delekate, A., Füchtemeier, M., Schumacher, T., Ulbrich, C., Foddis, M., and Petzold, G.C. (2014). Metabotropic P2Y1 receptor signalling mediates astrocytic hyperactivity in vivo in an Alzheimer's disease mouse model. Nat. Commun. *5*, 5422.

Denizot, A., Arizono, M., Nägerl, U.V., Soula, H., and Berry, H. (2019). Simulation of calcium signaling in fine astrocytic processes: Effect of spatial properties on spontaneous activity. PLOS Comput. Biol. *15*, e1006795.

Deshmukh, S.S., and Knierim, J.J. (2013). Influence of local objects on hippocampal representations: Landmark vectors and memory. Hippocampus *23*, 253–267.

Devane, W.A., Hanus, L., Breuer, A., Pertwee, R.G., Stevenson, L.A., Griffin, G., Gibson, D., Mandelbaum, A., Etinger, A., and Mechoulam, R. (1992). Isolation and structure of a brain constituent that binds to the cannabinoid receptor. Science *258*, 1946–1949.

D'Hooge, R., and De Deyn, P.P. (2001). Applications of the Morris water maze in the study of learning and memory. Brain Res. Rev. *36*, 60–90.

Di Castro, M.A., Chuquet, J., Liaudet, N., Bhaukaurally, K., Santello, M., Bouvier, D., Tiret, P., and Volterra, A. (2011). Local Ca2+ detection and modulation of synaptic release by astrocytes. Nat. Neurosci. *14*, 1276–1284.

Di Marzo, V. (2011). Endocannabinoid signaling in the brain: biosynthetic mechanisms in the limelight. Nat. Neurosci. *14*, 9–15.

Di Marzo, V., Melck, D., Bisogno, T., and De Petrocellis, L. (1998). Endocannabinoids: endogenous cannabinoid receptor ligands with neuromodulatory action. Trends Neurosci. *21*, 521–528.

Diamantaki, M., Coletta, S., Nasr, K., Zeraati, R., Laturnus, S., Berens, P., Preston-Ferrer, P., and Burgalossi, A. (2018). Manipulating Hippocampal Place Cell Activity by Single-Cell Stimulation in Freely Moving Mice. Cell Rep. *23*, 32–38.

Diamond, J.S. (2001). Neuronal glutamate transporters limit activation of NMDA receptors by neurotransmitter spillover on CA1 pyramidal cells. J. Neurosci. *21*, 8328–8338.

Dombeck, D.A., Khabbaz, A.N., Collman, F., Adelman, T.L., and Tank, D.W. (2007). Imaging large-scale neural activity with cellular resolution in awake, mobile mice. Neuron *56*, 43–57.

Dombeck, D.A., Graziano, M.S., and Tank, D.W. (2009). Functional clustering of neurons in motor cortex determined by cellular resolution imaging in awake behaving mice. J. Neurosci. *29*, 13751–13760.

Dong, Z., Gong, B., Li, H., Bai, Y., Wu, X., Huang, Y., He, W., Li, T., and Wang, Y.T. (2012). Mechanisms of Hippocampal Long-Term Depression Are Required for Memory Enhancement by Novelty Exploration. J. Neurosci. *32*, 11980–11990.

Dong, Z., Bai, Y., Wu, X., Li, H., Gong, B., Howland, J.G., Huang, Y., He, W., Li, T., and Wang, Y.T. (2013). Hippocampal long-term depression mediates spatial reversal learning in the Morris water maze. Neuropharmacology *64*, 65–73.

Dougherty, K.A., Islam, T., and Johnston, D. (2012). Intrinsic excitability of CA1 pyramidal neurones from the rat dorsal and ventral hippocampus. J. Physiol. *590*, 5707–5722.

Dougherty, K.A., Nicholson, D.A., Diaz, L., Buss, E.W., Neuman, K.M., Chetkovich, D.M., and Johnston, D. (2013). Differential expression of HCN subunits alters voltage-dependent gating of h-channels in CA1 pyramidal neurons from dorsal and ventral hippocampus. J. Neurophysiol. *109*, 1940–1953.

Dubruc, F., Dupret, D., and Caillard, O. (2013). Self-tuning of inhibition by endocannabinoids shapes spike-time precision in CA1 pyramidal neurons. J. Neurophysiol. *110*, 1930–1944.

Dudman, J.T., Tsay, D., and Siegelbaum, S.A. (2007). A novel role for synaptic inputs at distal dendrites: instructive signals for hippocampal long-term plasticity. Neuron *56*, 866–879.

Duffy, S., Labrie, V., and Roder, J.C. (2008). D -Serine Augments NMDA-NR2B Receptor-Dependent Hippocampal Long-Term Depression and Spatial Reversal Learning. Neuropsychopharmacology *33*, 1004–1018.

Duran, R.C.-D., Wang, C.-Y., Zheng, H., Deneen, B., and Wu, J.Q. (2019). Brain Region-Specific Gene Signatures Revealed by Distinct Astrocyte Subpopulations Unveil Links to Glioma and Neurodegenerative Diseases. ENeuro *6*.

Durkee, C.A., Covelo, A., Lines, J., Kofuji, P., Aguilar, J., and Araque, A. (2019). Gi/o protein-coupled receptors inhibit neurons but activate astrocytes and stimulate gliotransmission. Glia *67*, 1076–1093.

Edwards, D.A. (2005). Multiple Mechanisms of Endocannabinoid Response Initiation in Hippocampus. J. Neurophysiol. *95*, 67–75.

Edwards, D.A., Zhang, L., and Alger, B.E. (2008). Metaplastic control of the endocannabinoid system at inhibitory synapses in hippocampus. Proc. Natl. Acad. Sci. *105*, 8142–8147.

Ellis-Davies, G.C.R. (2019). Two-Photon Uncaging of Glutamate. Front. Synaptic Neurosci. *10*.

Emsley, J.G., and Macklis, J.D. (2006). Astroglial heterogeneity closely reflects the neuronal-defined anatomy of the adult murine CNS. Neuron Glia Biol. *2*, 175–186.

Engel, A.K., Fries, P., and Singer, W. (2001). Dynamic predictions: Oscillations and synchrony in top–down processing. Nat. Rev. Neurosci. *2*, 704–716.

von Engelhardt, J., Doganci, B., Jensen, V., Hvalby, Ø., Göngrich, C., Taylor, A., Barkus, C., Sanderson, D.J., Rawlins, J.N.P., Seeburg, P.H., et al. (2008). Contribution of hippocampal and extra-hippocampal NR2B-containing NMDA receptors to performance on spatial learning tasks. Neuron *60*, 846–860.

Ennaceur, A. (2018). Chapter 1 - Object Novelty Recognition Memory. In Handbook of Behavioral Neuroscience, A. Ennaceur, and M.A. de Souza Silva, eds. (Elsevier), pp. 1–22.

Enoki, R., Hu, Y.-L., Hamilton, D., and Fine, A. (2009). Expression of long-term plasticity at individual synapses in hippocampus is graded, bidirectional, and mainly presynaptic: optical quantal analysis. Neuron *62*, 242–253.

Epsztein, J., Brecht, M., and Lee, A.K. (2011). Intracellular determinants of hippocampal CA1 place and silent cell activity in a novel environment. Neuron *70*, 109–120.

Erreger, K., Dravid, S.M., Banke, T.G., Wyllie, D.J.A., and Traynelis, S.F. (2005). Subunit-specific gating controls rat NR1/NR2A and NR1/NR2B NMDA channel kinetics and synaptic signalling profiles. J. Physiol. *563*, 345–358.

Faas, G.C., Adwanikar, H., Gereau, R.W., and Saggau, P. (2002). Modulation of presynaptic calcium transients by metabotropic glutamate receptor activation: a differential role in acute depression of synaptic transmission and long-term depression. J. Neurosci. *22*, 6885–6890.

Faas, G.C., Raghavachari, S., Lisman, J.E., and Mody, I. (2011). Calmodulin as a direct detector of Ca2+ signals. Nat. Neurosci. *14*, 301–304.

Fanselow, M.S., and Dong, H.-W. (2010). Are the Dorsal and Ventral Hippocampus Functionally Distinct Structures? Neuron *65*, 7–19.

Fellin, T., Pascual, O., Gobbo, S., Pozzan, T., Haydon, P.G., and Carmignoto, G. (2004). Neuronal Synchrony Mediated by Astrocytic Glutamate through Activation of Extrasynaptic NMDA Receptors. Neuron *43*, 729–743.

Fiacco, T.A., Agulhon, C., Taves, S.R., Petravicz, J., Casper, K.B., Dong, X., Chen, J., and McCarthy, K.D. (2007). Selective Stimulation of Astrocyte Calcium In Situ Does Not Affect Neuronal Excitatory Synaptic Activity. Neuron *54*, 611–626.

Findley, C.A., Bartke, A., Hascup, K.N., and Hascup, E.R. (2019). Amyloid Beta-Related Alterations to Glutamate Signaling Dynamics During Alzheimer's Disease Progression. ASN NEURO *11*.

Fitzjohn, S.M., Palmer, M.J., May, J.E., Neeson, A., Morris, S.A., and Collingridge, G.L. (2001). A characterisation of long-term depression induced by metabotropic glutamate receptor activation in the rat hippocampus in vitro. J. Physiol. *537*, 421–430.

Fleming, T.M., Scott, V., Naskar, K., Joe, N., Brown, C.H., and Stern, J.E. (2011). State-dependent changes in astrocyte regulation of extrasynaptic NMDA receptor signalling in neurosecretory neurons. J. Physiol. *589*, 3929–3941.

Fonseca, R., Vabulas, R.M., Hartl, F.U., Bonhoeffer, T., and Nägerl, U.V. (2006). A Balance of Protein Synthesis and Proteasome-Dependent Degradation Determines the Maintenance of LTP. Neuron *52*, 239–245.

Forsythe, I.D., and Westbrook, G.L. (1988). Slow excitatory postsynaptic currents mediated by N-methyl-D-aspartate receptors on cultured mouse central neurones. J. Physiol. *396*, 515–533.

Fortin, D.A., Trettel, J., and Levine, E.S. (2004). Brief Trains of Action Potentials Enhance Pyramidal Neuron Excitability Via Endocannabinoid-Mediated Suppression of Inhibition. J. Neurophysiol. *92*, 2105–2112.

Foskett, J.K., White, C., Cheung, K.-H., and Mak, D.-O.D. (2007). Inositol trisphosphate receptor Ca2+ release channels. Physiol. Rev. *87*, 593–658.

Foster, K.A., McLaughlin, N., Edbauer, D., Phillips, M., Bolton, A., Constantine-Paton, M., and Sheng, M. (2010). Distinct roles of NR2A and NR2B cytoplasmic tails in long-term potentiation. J. Neurosci. Off. J. Soc. Neurosci. *30*, 2676–2685.

Freund, T.F., and Buzsáki, G. (1996). Interneurons of the hippocampus. Hippocampus *6*, 347–470.

Frey, U., Huang, Y.Y., and Kandel, E.R. (1993). Effects of cAMP simulate a late stage of LTP in hippocampal CA1 neurons. Science *260*, 1661–1664.

Fu, M., Yu, X., Lu, J., and Zuo, Y. (2012). Repetitive motor learning induces coordinated formation of clustered dendritic spines in vivo. Nature *483*, 92–95.

Fyhn, M., Molden, S., Witter, M.P., Moser, E.I., and Moser, M.-B. (2004). Spatial representation in the entorhinal cortex. Science *305*, 1258–1264.

Gajardo, I., Salazar, C.S., Lopez-Espíndola, D., Estay, C., Flores-Muñoz, C., Elgueta, C., Gonzalez-Jamett, A.M., Martínez, A.D., Muñoz, P., and Ardiles, Á.O. (2018). Lack of Pannexin 1 Alters Synaptic GluN2 Subunit Composition and Spatial Reversal Learning in Mice. Front. Mol. Neurosci. *11*, 114.

Galiègue, S., Mary, S., Marchand, J., Dussossoy, D., Carrière, D., Carayon, P., Bouaboula, M., Shire, D., Le Fur, G., and Casellas, P. (1995). Expression of central and peripheral cannabinoid receptors in human immune tissues and leukocyte subpopulations. Eur. J. Biochem. *232*, 54–61.

Gao, Y., Vasilyev, D.V., Goncalves, M.B., Howell, F.V., Hobbs, C., Reisenberg, M., Shen, R., Zhang, M.-Y., Strassle, B.W., Lu, P., et al. (2010). Loss of Retrograde Endocannabinoid Signaling and Reduced Adult Neurogenesis in Diacylglycerol Lipase Knock-out Mice. J. Neurosci. *30*, 2017–2024.

Gasparini, S., Migliore, M., and Magee, J.C. (2004). On the Initiation and Propagation of Dendritic Spikes in CA1 Pyramidal Neurons. J. Neurosci. *24*, 11046–11056.

Gavrilov, N., Golyagina, I., Brazhe, A., Scimemi, A., Turlapov, V., and Semyanov, A. (2018). Astrocytic Coverage of Dendritic Spines, Dendritic Shafts, and Axonal Boutons in Hippocampal Neuropil. Front. Cell. Neurosci. *12*, 248.

Gee, J.M., Smith, N.A., Fernandez, F.R., Economo, M.N., Brunert, D., Rothermel, M., Morris, S.C., Talbot, A., Palumbos, S., Ichida, J.M., et al. (2014). Imaging Activity in Neurons and Glia with a Polr2a-Based and Cre-Dependent GCaMP5G-IRES-tdTomato Reporter Mouse. Neuron *83*, 1058–1072.

Giaume, C., Koulakoff, A., Roux, L., Holcman, D., and Rouach, N. (2010). Astroglial networks: a step further in neuroglial and gliovascular interactions. Nat. Rev. Neurosci. *11*, 87–99.

Gidon, A., and Segev, I. (2012). Principles Governing the Operation of Synaptic Inhibition in Dendrites. Neuron *75*, 330–341.

Goh, J.J., and Manahan-Vaughan, D. (2013). Endogenous hippocampal LTD that is enabled by spatial object recognition requires activation of NMDA receptors and the metabotropic glutamate receptor, mGlu5. Hippocampus *23*, 129–138.

Goh, J.J., and Manahan-Vaughan, D. (2013). Spatial Object Recognition Enables Endogenous LTD that Curtails LTP in the Mouse Hippocampus. Cereb. Cortex *23*, 1118–1125.

Goh, J.J., and Manahan-Vaughan, D. (2015). Role of inhibitory autophosphorylation of calcium/calmodulin-dependent kinase II (αCAMKII) in persistent (>24h) hippocampal LTP and in LTD facilitated by novel object-place learning and recognition in mice. Behav. Brain Res. *285*, 79–88.

Gokce, O., Stanley, G.M., Treutlein, B., Neff, N.F., Camp, J.G., Malenka, R.C., Rothwell, P.E., Fuccillo, M.V., Südhof, T.C., and Quake, S.R. (2016). Cellular Taxonomy of the Mouse Striatum as Revealed by Single-Cell RNA-Seq. Cell Rep. *16*, 1126–1137.

Gómez-Gonzalo, M., Navarrete, M., Perea, G., Covelo, A., Martín-Fernández, M., Shigemoto, R., Luján, R., and Araque, A. (2015). Endocannabinoids Induce Lateral Long-Term Potentiation of Transmitter Release by Stimulation of Gliotransmission. Cereb. Cortex *25*, 3699–3712.

Gómez-Gonzalo, M., Martin-Fernandez, M., Martínez-Murillo, R., Mederos, S., Hernández-Vivanco, A., Jamison, S., Fernandez, A.P., Serrano, J., Calero, P., Futch, H.S., et al. (2017). Neuron–astrocyte signaling is preserved in the aging brain. Glia *65*, 569–580.

Göritz, C., Dias, D.O., Tomilin, N., Barbacid, M., Shupliakov, O., and Frisén, J. (2011). A Pericyte Origin of Spinal Cord Scar Tissue. Science *333*, 238–242.

Govindarajan, A., Israely, I., Huang, S.-Y., and Tonegawa, S. (2011). The Dendritic Branch Is the Preferred Integrative Unit for Protein Synthesis-Dependent LTP. Neuron *69*, 132–146.

Grienberger, C., Chen, X., and Konnerth, A. (2014). NMDA Receptor-Dependent Multidendrite Ca2+ Spikes Required for Hippocampal Burst Firing In Vivo. Neuron *81*, 1274–1281.

Grienberger, C., Milstein, A.D., Bittner, K.C., Romani, S., and Magee, J.C. (2017). Inhibitory suppression of heterogeneously tuned excitation enhances spatial coding in CA1 place cells. Nat. Neurosci. *20*, 417–426.

Griffiths, S., Scott, H., Glover, C., Bienemann, A., Ghorbel, M.T., Uney, J., Brown, M.W., Warburton, E.C., and Bashir, Z.I. (2008). Expression of Long-Term Depression Underlies Visual Recognition Memory. Neuron *58*, 186–194.

Groen, T.V., and Wyss, J.M. (1990). Extrinsic projections from area CA1 of the rat hippocampus: Olfactory, cortical, subcortical, and bilateral hippocampal formation projections. J. Comp. Neurol. *302*, 515–528.

Gruber, M.J., Hsieh, L.-T., Staresina, B.P., Elger, C.E., Fell, J., Axmacher, N., and Ranganath, C. (2018). Theta Phase Synchronization between the Human Hippocampus and Prefrontal Cortex Increases during Encoding of Unexpected Information: A Case Study. J. Cogn. Neurosci. *30*, 1646–1656.

Gu, Z., Alexander, G., Dudek, S.M., and Yakel, J.L. (2017). Hippocampus and entorhinal cortex recruit cholinergic and NMDA receptors separately to generate hippocampal theta oscillations. Cell Rep. *21*, 3585–3595.

Guercio, G.D., Bevictori, L., Vargas-Lopes, C., Madeira, C., Oliveira, A., Carvalho, V.F., d'Avila, J.C., and Panizzutti, R. (2014). D-serine prevents cognitive deficits induced by acute stress. Neuropharmacology *86*, 1–8.

Guerra-Gomes, S., Sousa, N., Pinto, L., and Oliveira, J.F. (2018). Functional Roles of Astrocyte Calcium Elevations: From Synapses to Behavior. Front. Cell. Neurosci. *11*, 427.

Gulyas, A.I., Cravatt, B.F., Bracey, M.H., Dinh, T.P., Piomelli, D., Boscia, F., and Freund, T.F. (2004). Segregation of two endocannabinoid-hydrolyzing enzymes into pre- and postsynaptic compartments in the rat hippocampus, cerebellum and amygdala. Eur. J. Neurosci. *20*, 441–458.

Gurevicius, K., Gureviciene, I., Sivukhina, E., Irintchev, A., Schachner, M., and Tanila, H. (2007). Increased hippocampal and cortical beta oscillations in mice deficient for the HNK-1 sulfotransferase. Mol. Cell. Neurosci. *34*, 189–198.

Gustafsson, B., Wigstrom, H., Abraham, W.C., and Huang, Y.Y. (1987). Long-term potentiation in the hippocampus using depolarizing current pulses as the conditioning stimulus to single volley synaptic potentials. J. Neurosci. *7*, 774–780.

Gutiérrez-Rodríguez, A., Bonilla-Del Río, I., Puente, N., Gómez-Urquijo, S.M., Fontaine, C.J., Egaña-Huguet, J., Elezgarai, I., Ruehle, S., Lutz, B., Robin, L.M., et al. (2018). Localization of the cannabinoid type-1 receptor in subcellular astrocyte compartments of mutant mouse hippocampus. Glia *66*, 1417–1431.

Gutnick, M.J., Connors, B.W., and Ransom, B.R. (1981). Dye-coupling between glial cells in the guinea pig neocortical slice. Brain Res. *213*, 486–492.

Hafting, T., Fyhn, M., Molden, S., Moser, M.-B., and Moser, E.I. (2005). Microstructure of a spatial map in the entorhinal cortex. Nature *436*, 801–806.

Haim, L.B., and Rowitch, D.H. (2017). Functional diversity of astrocytes in neural circuit regulation. Nat. Rev. Neurosci. *18*, 31–41.

Halassa, M.M., Fellin, T., Takano, H., Dong, J.-H., and Haydon, P.G. (2007). Synaptic Islands Defined by the Territory of a Single Astrocyte. J. Neurosci. *27*, 6473–6477.

Halassa, M.M., Florian, C., Fellin, T., Munoz, J.R., Lee, S.-Y., Abel, T., Haydon, P.G., and Frank, M.G. (2009). Astrocytic Modulation of Sleep Homeostasis and Cognitive Consequences of Sleep Loss. Neuron *61*, 213–219.

Hamann, S.B., Ely, T.D., Grafton, S.T., and Kilts, C.D. (1999). Amygdala activity related to enhanced memory for pleasant and aversive stimuli. Nat. Neurosci. *2*, 289–293.

Han, J., Kesner, P., Metna-Laurent, M., Duan, T., Xu, L., Georges, F., Koehl, M., Abrous, D.N., Mendizabal-Zubiaga, J., Grandes, P., et al. (2012). Acute Cannabinoids Impair Working Memory through Astroglial CB1 Receptor Modulation of Hippocampal LTD. Cell *148*, 1039–1050.

Hansen, K.B., Ogden, K.K., Yuan, H., and Traynelis, S.F. (2014). Distinct functional and pharmacological properties of triheteromeric GluN1/GluN2A/GluN2B NMDA receptors. Neuron *81*, 1084–1096.

Hardingham, G.E., Fukunaga, Y., and Bading, H. (2002). Extrasynaptic NMDARs oppose synaptic NMDARs by triggering CREB shut-off and cell death pathways. Nat. Neurosci. *5*, 405–414.

Harnett, M.T., Makara, J.K., Spruston, N., Kath, W.L., and Magee, J.C. (2012). Synaptic amplification by dendritic spines enhances input cooperativity. Nature *491*, 599–602.

Harris, A.Z., and Pettit, D.L. (2007). Extrasynaptic and synaptic NMDA receptors form stable and uniform pools in rat hippocampal slices. J. Physiol. *584*, 509–519.

Harris, K.M., and Stevens, J.K. (1989). Dendritic spines of CA 1 pyramidal cells in the rat hippocampus: serial electron microscopy with reference to their biophysical characteristics. J. Neurosci. *9*, 2982–2997.

Harris, K.M., Jensen, F.E., and Tsao, B. (1992). Three-dimensional structure of dendritic spines and synapses in rat hippocampus (CA1) at postnatal day 15 and adult ages: implications for the maturation of synaptic physiology and long-term potentiation. J. Neurosci. *12*, 2685–2705.

Harvey, C.D., Collman, F., Dombeck, D.A., and Tank, D.W. (2009). Intracellular dynamics of hippocampal place cells during virtual navigation. Nature *461*, 941–946.

Hashimotodani, Y., Ohno-Shosaku, T., Tanimura, A., Kita, Y., Sano, Y., Shimizu, T., Di Marzo, V., and Kano, M. (2013). Acute inhibition of diacylglycerol lipase blocks endocannabinoid-mediated retrograde signalling: evidence for on-demand biosynthesis of 2-arachidonoylglycerol. J. Physiol. *591*, 4765–4776.

Hawkins, L.M., Chazot, P.L., and Stephenson, F.A. (1999). Biochemical evidence for the co-association of three N-methyl-D-aspartate (NMDA) R2 subunits in recombinant NMDA receptors. J. Biol. Chem. *274*, 27211–27218.

Hayashi, Y., Shi, S.-H., Esteban, J.A., Piccini, A., Poncer, J.-C., and Malinow, R. (2000). Driving AMPA Receptors into Synapses by LTP and CaMKII: Requirement for GluR1 and PDZ Domain Interaction. Science *287*, 2262–2267.

Hebb, D.O. (1949). The organization of behavior; a neuropsychological theory (Oxford, England: Wiley).

Heinbockel, T., Brager, D.H., Reich, C.G., Zhao, J., Muralidharan, S., Alger, B.E., and Kao, J.P.Y. (2005). Endocannabinoid Signaling Dynamics Probed with Optical Tools. J. Neurosci. *25*, 9449–9459.

Henke, P.G. (1990). Hippocampal pathway to the amygdala and stress ulcer development. Brain Res. Bull. *25*, 691–695.

Henneberger, C., Papouin, T., Oliet, S.H.R., and Rusakov, D.A. (2010). Long-term potentiation depends on release of d-serine from astrocytes. Nature *463*, 232–236.

Herkenham, M., Lynn, A.B., Little, M.D., Johnson, M.R., Melvin, L.S., de Costa, B.R., and Rice, K.C. (1990). Cannabinoid receptor localization in brain. Proc. Natl. Acad. Sci. *87*, 1932–1936.

Heynen, A.J., Abraham, W.C., and Bear, M.F. (1996). Bidirectional modification of CA1 synapses in the adult hippocampus in vivo. Nature *381*, 163–166.

Hirase, H., Qian, L., Barthó, P., and Buzsáki, G. (2004). Calcium Dynamics of Cortical Astrocytic Networks In Vivo. PLOS Biol. *2*, E96.

Hituri, K., and Linne, M.-L. (2013). Comparison of Models for IP3 Receptor Kinetics Using Stochastic Simulations. PLOS ONE *8*, e59618.

Hock, B.J., and Bunsey, M.D. (1998). Differential effects of dorsal and ventral hippocampal lesions. J. Neurosci. *18*, 7027–7032.

Hoffman, A.F., and Lupica, C.R. (2000). Mechanisms of Cannabinoid Inhibition of GABAASynaptic Transmission in the Hippocampus. J. Neurosci. *20*, 2470–2479.

Hoffman, D.A., Magee, J.C., Colbert, C.M., and Johnston, D. (1997). K + channel regulation of signal propagation in dendrites of hippocampal pyramidal neurons. Nature *387*, 869–875.

Holmseth, S., Dehnes, Y., Huang, Y.H., Follin-Arbelet, V.V., Grutle, N.J., Mylonakou, M.N., Plachez, C., Zhou, Y., Furness, D.N., Bergles, D.E., et al. (2012). The density of EAAC1 (EAAT3) glutamate transporters expressed by neurons in the mammalian CNS. J. Neurosci. *32*, 6000–6013.

Howland, J.G., and Cazakoff, B.N. (2010). Effects of acute stress and GluN2B-containing NMDA receptor antagonism on object and object–place recognition memory. Neurobiol. Learn. Mem. *93*, 261–267.

Hsu, M.S., Seldin, M., Lee, D.J., Seifert, G., Steinhäuser, C., and Binder, D.K. (2011). Laminar-specific and developmental expression of aquaporin-4 in the mouse hippocampus. Neuroscience *178*, 21–32.

Hu, H., Vervaeke, K., and Storm, J.F. (2002). Two forms of electrical resonance at theta frequencies, generated by M-current, h-current and persistent Na+ current in rat hippocampal pyramidal cells. J. Physiol. *545*, 783–805.

Hu, H., Vervaeke, K., Graham, L.J., and Storm, J.F. (2009). Complementary Theta Resonance Filtering by Two Spatially Segregated Mechanisms in CA1 Hippocampal Pyramidal Neurons. J. Neurosci. *29*, 14472–14483.

Hua, X., Malarkey, E.B., Sunjara, V., Rosenwald, S.E., Li, W.-H., and Parpura, V. (2004). C(a2+)-dependent glutamate release involves two classes of endoplasmic reticulum Ca(2+) stores in astrocytes. J. Neurosci. Res. *76*, 86–97.

Huang, A.Y.-S., Woo, J., Sardar, D., Lozzi, B., Huerta, N.A.B., Lin, C.-C.J., Felice, D., Jain, A., Paulucci-Holthauzen, A., and Deneen, B. (2020). Region-Specific Transcriptional Control of Astrocyte Function Oversees Local Circuit Activities. Neuron *in press*.

Huang, Y.H., Sinha, S.R., Tanaka, K., Rothstein, J.D., and Bergles, D.E. (2004). Astrocyte glutamate transporters regulate metabotropic glutamate receptor-mediated excitation of hippocampal interneurons. J. Neurosci. *24*, 4551–4559.

Huerta, P.T., and Lisman, J.E. (1995). Bidirectional synaptic plasticity induced by a single burst during cholinergic theta oscillation in CA1 in vitro. Neuron *15*, 1053–1063.

Huerta, P.T., and Lisman, J.E. (1996). Synaptic plasticity during the cholinergic theta-frequency oscillation in vitro. Hippocampus *6*, 58–61.

Hughes, D.I., Boyle, K.A., Kinnon, C.M., Bilsland, C., Quayle, J.A., Callister, R.J., and Graham, B.A. (2013). HCN4 subunit expression in fast-spiking interneurons of the rat spinal cord and hippocampus. Neuroscience *237*, 7–18.

Hunsaker, M.R., and Kesner, R.P. (2008). Dissociations across the dorsal–ventral axis of CA3 and CA1 for encoding and retrieval of contextual and auditory-cued fear. Neurobiol. Learn. Mem. *89*, 61–69.

Hutcheon, B., and Yarom, Y. (2000). Resonance, oscillation and the intrinsic frequency preferences of neurons. Trends Neurosci. *23*, 216–222.

Hutcheon, B., Miura, R.M., and Puil, E. (1996). Models of subthreshold membrane resonance in neocortical neurons. J. Neurophysiol. *76*, 698–714.

Hyman, J.M., Wyble, B.P., Goyal, V., Rossi, C.A., and Hasselmo, M.E. (2003). Stimulation in Hippocampal Region CA1 in Behaving Rats Yields Long-Term Potentiation when Delivered to the Peak of Theta and Long-Term Depression when Delivered to the Trough. J. Neurosci. *23*, 11725–11731.

Iacobucci, G.J., and Popescu, G.K. (2017). NMDA Receptors: Linking Physiological Output to Biophysical Operation. Nat. Rev. Neurosci. *18*, 236–249.

Igarashi, K.M., Lu, L., Colgin, L.L., Moser, M.-B., and Moser, E.I. (2014). Coordination of entorhinal–hippocampal ensemble activity during associative learning. Nature *510*, 143–147.

Innocenti, B., Parpura, V., and Haydon, P.G. (2000). Imaging Extracellular Waves of Glutamate during Calcium Signaling in Cultured Astrocytes. J. Neurosci. *20*, 1800–1808.

Inoue, M., Hashimoto, Y., Kudo, Y., and Miyakawa, H. (2001). Dendritic attenuation of synaptic potentials in the CA1 region of rat hippocampal slices detected with an optical method. Eur. J. Neurosci. *13*, 1711–1721.

Izquierdo, A., Brigman, J.L., Radke, A.K., Rudebeck, P.H., and Holmes, A. (2017). The neural basis of reversal learning: An updated perspective. Neuroscience *345*, 12–26.

Izumi, Y., and Zorumski, C.F. (2016). GABA and Endocannabinoids Mediate Depotentiation of Schaffer Collateral Synapses Induced by Stimulation of Temperoammonic Inputs. PLOS ONE *11*, e0149034.

Izumi, Y., and Zorumski, C.F. (2019). Temperoammonic Stimulation Depotentiates Schaffer Collateral LTP via p38 MAPK Downstream of Adenosine A1 Receptors. J. Neurosci. *39*, 1783–1792.

Jaffe, D.B., and Carnevale, N.T. (1999). Passive normalization of synaptic integration influenced by dendritic architecture. J. Neurophysiol. *82*, 3268–3285.

Jeffery, K.J., and Morris, R.G.M. (1993). Cumulative long-term potentiation in the rat dentate gyrus correlates with, but does not modify, performance in the water maze. Hippocampus *3*, 133–140.

Jennings, A., Tyurikova, O., Bard, L., Zheng, K., Semyanov, A., Henneberger, C., and Rusakov, D.A. (2017). Dopamine elevates and lowers astroglial Ca2+ through distinct pathways depending on local synaptic circuitry. Glia *65*, 447–459.

Jensen, O., and Colgin, L.L. (2007). Cross-frequency coupling between neuronal oscillations. Trends Cogn. Sci. *11*, 267–269.

Jeremic, A., Jeftinija, K., Stevanovic, J., Glavaski, A., and Jeftinija, S. (2001). ATP stimulates calcium-dependent glutamate release from cultured astrocytes. J. Neurochem. *77*, 664–675.

Ji, D., and Wilson, M.A. (2007). Coordinated memory replay in the visual cortex and hippocampus during sleep. Nat. Neurosci. *10*, 100–107.

Jia, H., Rochefort, N.L., Chen, X., and Konnerth, A. (2010). Dendritic organization of sensory input to cortical neurons in vivo. Nature *464*, 1307–1312.

Jinno, S. (2011). Regional and laminar differences in antigen profiles and spatial distributions of astrocytes in the mouse hippocampus, with reference to aging. Neuroscience *180*, 41–52.

Johnson, A., and Redish, A.D. (2007). Neural ensembles in CA3 transiently encode paths forward of the animal at a decision point. J. Neurosci. *27*, 12176–12189.

Johnson, J.W., and Ascher, P. (1987). Glycine potentiates the NMDA response in cultured mouse brain neurons. Nature *325*, 529–531.

Jones, S.L., and Stuart, G.J. (2013). Different Calcium Sources Control Somatic versus Dendritic SK Channel Activation during Action Potentials. J. Neurosci. *33*, 19396–19405.

Jourdain, P., Bergersen, L.H., Bhaukaurally, K., Bezzi, P., Santello, M., Domercq, M., Matute, C., Tonello, F., Gundersen, V., and Volterra, A. (2007). Glutamate exocytosis from astrocytes controls synaptic strength. Nat. Neurosci. *10*, 331–339.

Jung, H.Y., Mickus, T., and Spruston, N. (1997). Prolonged sodium channel inactivation contributes to dendritic action potential attenuation in hippocampal pyramidal neurons. J. Neurosci. *17*, 6639–6646.

Jung, M.W., Wiener, S.I., and McNaughton, B.L. (1994). Comparison of spatial firing characteristics of units in dorsal and ventral hippocampus of the rat. J. Neurosci. *14*, 7347–7356.

Kanemaru, K., Sekiya, H., Xu, M., Satoh, K., Kitajima, N., Yoshida, K., Okubo, Y., Sasaki, T., Moritoh, S., Hasuwa, H., et al. (2014). In Vivo Visualization of Subtle, Transient, and Local Activity of Astrocytes Using an Ultrasensitive Ca2+ Indicator. Cell Rep. *8*, 311–318.

Kang, J., Jiang, L., Goldman, S.A., and Nedergaard, M. (1998). Astrocyte-mediated potentiation of inhibitory synaptic transmission. Nat. Neurosci. *1*, 683–692.

Kang, N., Xu, J., Xu, Q., Nedergaard, M., and Kang, J. (2005). Astrocytic Glutamate Release-Induced Transient Depolarization and Epileptiform Discharges in Hippocampal CA1 Pyramidal Neurons. J. Neurophysiol. *94*, 4121–4130.

Kang-Park, M.-H., Wilson, W.A., Kuhn, C.M., Moore, S.D., and Swartzwelder, H.S. (2007). Differential Sensitivity of GABAA Receptor-Mediated IPSCs to Cannabinoids in Hippocampal Slices From Adolescent and Adult Rats. J. Neurophysiol. *98*, 1223–1230.

Karlsson, R.-M., Tanaka, K., Saksida, L.M., Bussey, T.J., Heilig, M., and Holmes, A. (2009). Assessment of glutamate transporter GLAST (EAAT1)-deficient mice for phenotypes relevant to the negative and executive/cognitive symptoms of schizophrenia. Neuropsychopharmacology *34*, 1578–1589.

Kartvelishvily, E., Shleper, M., Balan, L., Dumin, E., and Wolosker, H. (2006). Neuron-derived D-Serine Release Provides a Novel Means to Activate N-Methyl-D-aspartate Receptors. J. Biol. Chem. *281*, 14151–14162.

Katagiri, H., Tanaka, K., and Manabe, T. (2001). Requirement of appropriate glutamate concentrations in the synaptic cleft for hippocampal LTP induction. Eur. J. Neurosci. *14*, 547–553.

Katona, I., Sperlágh, B., Sík, A., Käfalvi, A., Vizi, E.S., Mackie, K., and Freund, T.F. (1999). Presynaptically Located CB1 Cannabinoid Receptors Regulate GABA Release from Axon Terminals of Specific Hippocampal Interneurons. J. Neurosci. *19*, 4544–4558.

Kawamura, Y., Fukaya, M., Maejima, T., Yoshida, T., Miura, E., Watanabe, M., Ohno-Shosaku, T., and Kano, M. (2006). The CB1 Cannabinoid Receptor Is the Major Cannabinoid Receptor at Excitatory Presynaptic Sites in the Hippocampus and Cerebellum. J. Neurosci. *26*, 2991–3001.

Kelso, S.R., Ganong, A.H., and Brown, T.H. (1986). Hebbian synapses in hippocampus. Proc. Natl. Acad. Sci. *83*, 5326–5330.

Kemp, A., and Manahan-Vaughan, D. (2004). Hippocampal long-term depression and long-term potentiation encode different aspects of novelty acquisition. Proc. Natl. Acad. Sci. *101*, 8192–8197.

Kerlin, A., Boaz, M., Flickinger, D., MacLennan, B.J., Dean, M.B., Davis, C., Spruston, N., and Svoboda, K. (2019). Functional clustering of dendritic activity during decision-making. ELife *8*, e46966.

Kettenmann, H., and Ransom, B.R. (2013). Neuroglia (New York: Oxford University Press).

Kettenmann, H., and Verkhratsky, A. (2008). Neuroglia: the 150 years after. Trends Neurosci. *31*, 653–659.

Khakh, B.S., and Deneen, B. (2019). The Emerging Nature of Astrocyte Diversity. Annu. Rev. Neurosci. *42*, 187–207.

Khakh, B.S., and Sofroniew, M.V. (2015). Diversity of astrocyte functions and phenotypes in neural circuits. Nat. Neurosci. *18*, 942–952.

Kim, J., Isokawa, M., Ledent, C., and Alger, B.E. (2002). Activation of Muscarinic Acetylcholine Receptors Enhances the Release of Endogenous Cannabinoids in the Hippocampus. J. Neurosci. *22*, 10182–10191.

Kim, J.-I., Lee, H.-R., Sim, S., Baek, J., Yu, N.-K., Choi, J.-H., Ko, H.-G., Lee, Y.-S., Park, S.-W., Kwak, C., et al. (2011). PI3Kγ is required for NMDA receptor–dependent long-term depression and behavioral flexibility. Nat. Neurosci. *14*, 1447–1454.

King, C.M., Bohmbach, K., Minge, D., Delekate, A., Zheng, K., Reynolds, J., Rakers, C., Zeug, A., Petzold, G.C., Rusakov, D.A., et al. (2020). Local Resting Ca2+ Controls the Scale of Astroglial Ca2+ Signals. Cell Rep. *30*, 3466-3477.e4.

Kiryk, A., Aida, T., Tanaka, K., Banerjee, P., Wilczynski, G.M., Meyza, K., Knapska, E., Filipkowski, R.K., Kaczmarek, L., and Danysz, W. (2008). Behavioral characterization of GLT1 (+/-) mice as a model of mild glutamatergic hyperfunction. Neurotox. Res. *13*, 19–30.

Kishi, T., Tsumori, T., Yokota, S., and Yasui, Y. (2006). Topographical projection from the hippocampal formation to the amygdala: a combined anterograde and retrograde tracing study in the rat. J. Comp. Neurol. *496*, 349–368.

Kjelstrup, K.B., Solstad, T., Brun, V.H., Hafting, T., Leutgeb, S., Witter, M.P., Moser, E.I., and Moser, M.-B. (2008). Finite scale of spatial representation in the hippocampus. Science *321*, 140–143.

Kjelstrup, K.G., Tuvnes, F.A., Steffenach, H.-A., Murison, R., Moser, E.I., and Moser, M.-B. (2002). Reduced fear expression after lesions of the ventral hippocampus. Proc. Natl. Acad. Sci. *99*, 10825–10830.

Klanker, M., Feenstra, M., and Denys, D. (2013). Dopaminergic control of cognitive flexibility in humans and animals. Front. Neurosci. *7*.

Klausberger, T. (2009). GABAergic interneurons targeting dendrites of pyramidal cells in the CA1 area of the hippocampus. Eur. J. Neurosci. *30*, 947–957.

Klausberger, T., and Somogyi, P. (2008). Neuronal Diversity and Temporal Dynamics: The Unity of Hippocampal Circuit Operations. Science *321*, 53–57.

Klausberger, T., Magill, P.J., Márton, L.F., Roberts, J.D.B., Cobden, P.M., Buzsáki, G., and Somogyi, P. (2003). Brain-state- and cell-type-specific firing of hippocampal interneurons in vivo. Nature *421*, 844–848.

Klausberger, T., Marton, L.F., O'Neill, J., Huck, J.H.J., Dalezios, Y., Fuentealba, P., Suen, W.Y., Papp, E., Kaneko, T., Watanabe, M., et al. (2005). Complementary roles of cholecystokinin- and parvalbumin-expressing GABAergic neurons in hippocampal network oscillations. J. Neurosci. *25*, 9782–9793.

Kleckner, N.W., and Dingledine, R. (1988). Requirement for glycine in activation of NMDA-receptors expressed in Xenopus oocytes. Science *241*, 835–837.

Klegeris, A., Bissonnette, C.J., and McGeer, P.L. (2003). Reduction of human monocytic cell neurotoxicity and cytokine secretion by ligands of the cannabinoid-type CB2 receptor. Br. J. Pharmacol. *139*, 775–786.

Kleindienst, T., Winnubst, J., Roth-Alpermann, C., Bonhoeffer, T., and Lohmann, C. (2011). Activity-Dependent Clustering of Functional Synaptic Inputs on Developing Hippocampal Dendrites. Neuron *72*, 1012–1024.

Kleinknecht, K.R., Bedenk, B.T., Kaltwasser, S.F., Gruenecker, B., Yen, Y.-C., Czisch, M., and Wotjak, C.T. (2012). Hippocampus-dependent place learning enables spatial flexibility in C57BL6/N mice. Front. Behav. Neurosci. *6*, 87.

Klimesch, W. (1999). EEG alpha and theta oscillations reflect cognitive and memory performance: a review and analysis. Brain Res. Rev. *29*, 169–195.

Klingauf, J., and Neher, E. (1997). Modeling Buffered Ca2+ Diffusion Near the Membrane: Implications for Secretion in Neuroendocrine Cells. Biophys. J. *72*, 674–690.

Koch, M., Kreutz, S., Böttger, C., Grabiec, U., Ghadban, C., Korf, H.-W., and Dehghani, F. (2011). The cannabinoid WIN 55,212-2-mediated protection of dentate gyrus granule cells is driven by CB1 receptors and modulated by TRPA1 and Cav2.2 channels. Hippocampus *21*, 554–564.

Kolhekar, R., Meller, S.T., and Gebhart, G.F. (1994). N-methyl-d-aspartate receptor-mediated changes in thermal nociception: Allosteric modulation at glycine and polyamine recognition sites. Neuroscience *63*, 925–936.

Komorowski, R.W., Garcia, C.G., Wilson, A., Hattori, S., Howard, M.W., and Eichenbaum, H. (2013). Ventral Hippocampal Neurons Are Shaped by Experience to Represent Behaviorally Relevant Contexts. J. Neurosci. *33*, 8079–8087.

Kopec, C.D., Li, B., Wei, W., Boehm, J., and Malinow, R. (2006). Glutamate Receptor Exocytosis and Spine Enlargement during Chemically Induced Long-Term Potentiation. J. Neurosci. *26*, 2000–2009.

Korol, D.L., Abel, T.W., Church, L.T., Barnes, C.A., and McNaughton, B.L. (1993). Hippocampal synaptic enhancement and spatial learning in the morris swim task. Hippocampus *3*, 127–132.

Kouvaros, S., and Papatheodoropoulos, C. (2016). Major dorsoventral differences in the modulation of the local CA1 hippocampal network by NMDA, mGlu5, adenosine A2A and cannabinoid CB1 receptors. Neuroscience *317*, 47–64.

Kramis, R., Vanderwolf, C.H., and Bland, B.H. (1975). Two types of hippocampal rhythmical slow activity in both the rabbit and the rat: Relations to behavior and effects of atropine, diethyl ether, urethane, and pentobarbital. Exp. Neurol. *49*, 58–85.

Kreft, M., Stenovec, M., Rupnik, M., Grilc, S., Kržan, M., Potokar, M., Pangršič, T., Haydon, P.G., and Zorec, R. (2004). Properties of Ca2+-dependent exocytosis in cultured astrocytes. Glia *46*, 437–445.

Kristensen, A.S., Jenkins, M.A., Banke, T.G., Schousboe, A., Makino, Y., Johnson, R.C., Huganir, R., and Traynelis, S.F. (2011). Mechanism of Ca 2+ /calmodulin-dependent kinase II regulation of AMPA receptor gating. Nat. Neurosci. *14*, 727–735.

Kuchibhotla, K.V., Lattarulo, C.R., Hyman, B.T., and Bacskai, B.J. (2009). Synchronous hyperactivity and intercellular calcium waves in astrocytes in Alzheimer mice. Science *323*, 1211–1215.

Kuffler, S.W. (1967). The Ferrier Lecture - Neuroglial cells: physiological properties and a potassium mediated effect of neuronal activity on the glial membrane potential. Proc. R. Soc. Lond. B Biol. Sci. *168*, 1–21.

Kullmann, D.M., Min, M.Y., Asztely, F., and Rusakov, D.A. (1999). Extracellular glutamate diffusion determines the occupancy of glutamate receptors at CA1 synapses in the hippocampus. Philos. Trans. R. Soc. Lond. B. Biol. Sci. *354*, 395–402.

Labrie, V., Duffy, S., Wang, W., Barger, S.W., Baker, G.B., and Roder, J.C. (2009). Genetic inactivation of D-amino acid oxidase enhances extinction and reversal learning in mice. Learn. Mem. *16*, 28–37.

Lafourcade, C.A., and Alger, B.E. (2008). Distinctions among GABAA and GABAB responses revealed by calcium channel antagonists, cannabinoids, opioids, and synaptic plasticity in rat hippocampus. Psychopharmacology (Berl.) *198*, 539–549.

Lalonde, R. (2002). The neurobiological basis of spontaneous alternation. Neurosci. Biobehav. Rev. *26*, 91–104.

Lanjakornsiripan, D., Pior, B.-J., Kawaguchi, D., Furutachi, S., Tahara, T., Katsuyama, Y., Suzuki, Y., Fukazawa, Y., and Gotoh, Y. (2018). Layer-specific morphological and molecular differences in neocortical astrocytes and their dependence on neuronal layers. Nat. Commun. *9*, 1–15.

Lansink, C.S., Meijer, G.T., Lankelma, J.V., Vinck, M.A., Jackson, J.C., and Pennartz, C.M.A. (2016). Reward Expectancy Strengthens CA1 Theta and Beta Band Synchronization and Hippocampal-Ventral Striatal Coupling. J. Neurosci. *36*, 10598–10610.

Larkin, M.C., Lykken, C., Tye, L.D., Wickelgren, J.G., and Frank, L.M. (2014). Hippocampal output area CA1 broadcasts a generalized novelty signal during an object-place recognition task. Hippocampus *24*, 773–783.

Larkum, M.E., and Zhu, J.J. (2002). Signaling of layer 1 and whisker-evoked Ca2+ and Na+ action potentials in distal and terminal dendrites of rat neocortical pyramidal neurons in vitro and in vivo. J. Neurosci. *22*, 6991–7005.

Larkum, M.E., Zhu, J.J., and Sakmann, B. (1999). A new cellular mechanism for coupling inputs arriving at different cortical layers. Nature *398*, 338–341.

Larkum, M.E., Zhu, J.J., and Sakmann, B. (2001). Dendritic mechanisms underlying the coupling of the dendritic with the axonal action potential initiation zone of adult rat layer 5 pyramidal neurons. J. Physiol. *533*, 447–466.

Lauckner, J.E., Hille, B., and Mackie, K. (2005). The cannabinoid agonist WIN55,212-2 increases intracellular calcium via CB1 receptor coupling to Gq/11 G proteins. Proc. Natl. Acad. Sci. *102*, 19144–19149.

Lavrentovich, M., and Hemkin, S. (2008). A mathematical model of spontaneous calcium(II) oscillations in astrocytes. J. Theor. Biol. *251*, 553–560.

Lavzin, M., Rapoport, S., Polsky, A., Garion, L., and Schiller, J. (2012). Nonlinear dendritic processing determines angular tuning of barrel cortex neurons in vivo. Nature *490*, 397–401.

Le Bail, M., Martineau, M., Sacchi, S., Yatsenko, N., Radzishevsky, I., Conrod, S., Ait Ouares, K., Wolosker, H., Pollegioni, L., Billard, J.-M., et al. (2015). Identity of the NMDA receptor coagonist is synapse specific and developmentally regulated in the hippocampus. Proc. Natl. Acad. Sci. *112*, E204–E213.

Lee, H.-K., Kameyama, K., Huganir, R.L., and Bear, M.F. (1998). NMDA Induces Long-Term Synaptic Depression and Dephosphorylation of the GluR1 Subunit of AMPA Receptors in Hippocampus. Neuron *21*, 1151–1162.

Lee, H.-K., Barbarosie, M., Kameyama, K., Bear, M.F., and Huganir, R.L. (2000). Regulation of distinct AMPA receptor phosphorylation sites during bidirectional synaptic plasticity. Nature *405*, 955–959.

Lee, H.-K., Takamiya, K., Han, J.-S., Man, H., Kim, C.-H., Rumbaugh, G., Yu, S., Ding, L., He, C., Petralia, R.S., et al. (2003). Phosphorylation of the AMPA Receptor GluR1 Subunit Is Required for Synaptic Plasticity and Retention of Spatial Memory. Cell *112*, 631–643.

Lee, H.S., Ghetti, A., Pinto-Duarte, A., Wang, X., Dziewczapolski, G., Galimi, F., Huitron-Resendiz, S., Piña-Crespo, J.C., Roberts, A.J., Verma, I.M., et al. (2014). Astrocytes contribute to gamma oscillations and recognition memory. Proc. Natl. Acad. Sci. *111*, E3343–E3352.

Lee, I., Rao, G., and Knierim, J.J. (2004). A Double Dissociation between Hippocampal Subfields: Differential Time Course of CA3 and CA1 Place Cells for Processing Changed Environments. Neuron *42*, 803–815.

Lee, S.-H., Földy, C., and Soltesz, I. (2010). Distinct Endocannabinoid Control of GABA Release at Perisomatic and Dendritic Synapses in the Hippocampus. J. Neurosci. *30*, 7993–8000.

Lee, S.-J.R., Escobedo-Lozoya, Y., Szatmari, E.M., and Yasuda, R. (2009). Activation of CaMKII in single dendritic spines during long-term potentiation. Nature *458*, 299–304.

Léger, J.-F., Stern, E.A., Aertsen, A., and Heck, D. (2005). Synaptic Integration in Rat Frontal Cortex Shaped by Network Activity. J. Neurophysiol. *93*, 281–293.

Lehre, K.P., Levy, L.M., Ottersen, O.P., Storm-Mathisen, J., and Danbolt, N.C. (1995). Differential expression of two glial glutamate transporters in the rat brain: quantitative and immunocytochemical observations. J. Neurosci. *15*, 1835–1853.

Lénárd, L., and Kertes, E. (2002). Influence of Passive Avoidance Learning by Substance P in the Basolateral Amygdala. Acta Biol. Hung. *53*, 95–104.

Lenck-Santini, P.-P., Rivard, B., Muller, R.U., and Poucet, B. (2005). Study of CA1 place cell activity and exploratory behavior following spatial and nonspatial changes in the environment. Hippocampus *15*, 356–369.

Lenhossék, M. (1895). Der feinere Bau des Nervensystems im Lichte neuester Forschungen: eine allgemeine Betrachtung der Strukturprinzipien des Nervensystems, nebst einer Darstellung des feineren Baues des Rückenmarkes (Berlin: H. Kornfeld).

Lenz, R.A., and Alger, B.E. (1999). Calcium dependence of depolarization-induced suppression of inhibition in rat hippocampal CA1 pyramidal neurons. J. Physiol. *521 Pt 1*, 147–157.

Lenz, R.A., Wagner, J.J., and Alger, B.E. (1998). N- and L-type calcium channel involvement in depolarization-induced suppression of inhibition in rat hippocampal CA1 cells. J. Physiol. *512 (Pt 1)*, 61–73.

Leung, L.-W.S., and Borst, J.G.G. (1987). Electrical activity of the cingulate cortex. I. Generating mechanisms and relations to behavior. Brain Res. *407*, 68–80.

Lever, C., Burton, S., Jeewajee, A., Wills, T.J., Cacucci, F., Burgess, N., and O'Keefe, J. (2010). Environmental novelty elicits a later theta phase of firing in CA1 but not subiculum. Hippocampus *20*, 229–234.

Levy, W.B., and Steward, O. (1979). Synapses as associative memory elements in the hippocampal formation. Brain Res. *175*, 233–245.

Li, X. (2005). Endothelin-1-Induced Arrhythmogenic Ca2+ Signaling Is Abolished in Atrial Myocytes of Inositol-1,4,5-Trisphosphate(IP3)-Receptor Type 2-Deficient Mice. Circ. Res. *96*, 1274–1281.

Li, S., Cullen, W.K., Anwyl, R., and Rowan, M.J. (2003). Dopamine-dependent facilitation of LTP induction in hippocampal CA1 by exposure to spatial novelty. Nat. Neurosci. *6*, 526–531.

Li, W., Llopis, J., Whitney, M., Zlokarnik, G., and Tsien, R.Y. (1998). Cell-permeant caged InsP 3 ester shows that Ca 2+ spike frequency can optimize gene expression. Nature *392*, 936–941.

Lieu, T., Jayaweera, G., Zhao, P., Poole, D.P., Jensen, D., Grace, M., McIntyre, P., Bron, R., Wilson, Y.M., Krappitz, M., et al. (2014). The bile acid receptor TGR5 activates the TRPA1 channel to induce itch in mice. Gastroenterology *147*, 1417–1428.

Lin, C.-C.J., Yu, K., Hatcher, A., Huang, T.-W., Lee, H.K., Carlson, J., Weston, M.C., Chen, F., Zhang, Y., Zhu, W., et al. (2017). Identification of diverse astrocyte populations and their malignant analogs. Nat. Neurosci. *20*, 396–405.

Lisman, J.E., and Idiart, M.A. (1995). Storage of 7 +/- 2 short-term memories in oscillatory subcycles. Science *267*, 1512–1515.

Liu, L., Wong, T.P., Pozza, M.F., Lingenhoehl, K., Wang, Y., Sheng, M., Auberson, Y.P., and Wang, Y.T. (2004). Role of NMDA receptor subtypes in governing the direction of hippocampal synaptic plasticity. Science *304*, 1021–1024.

Liu, P., Bilkey, D.K., Darlington, C.L., and Smith, P.F. (2003). Cannabinoid CB1 receptor protein expression in the rat hippocampus and entorhinal, perirhinal, postrhinal and temporal cortices: regional variations and age-related changes. Brain Res. *979*, 235–239.

Livet, J., Weissman, T.A., Kang, H., Draft, R.W., Lu, J., Bennis, R.A., Sanes, J.R., and Lichtman, J.W. (2007). Transgenic strategies for combinatorial expression of fluorescent proteins in the nervous system. Nature *450*, 56–62.

Lockmann, A.L.V., Laplagne, D.A., and Tort, A.B.L. (2018). Olfactory bulb drives respiration-coupled beta oscillations in the rat hippocampus. Eur. J. Neurosci. *48*, 2663–2673.

Longordo, F., To, M.-S., Ikeda, K., and Stuart, G.J. (2013). Sublinear integration underlies binocular processing in primary visual cortex. Nat. Neurosci. *16*, 714–723.

Lopes-Dos-Santos, V., van de Ven, G.M., Morley, A., Trouche, S., Campo-Urriza, N., and Dupret, D. (2018). Parsing Hippocampal Theta Oscillations by Nested Spectral Components during Spatial Exploration and Memory-Guided Behavior. Neuron *100*, 940-952.e7.

Lorente De Nó, R. (1934). Studies on the structure of the cerebral cortex. II. Continuation of the study of the ammonic system. J. Für Psychol. Neurol. *46*, 113–177.

Lorincz, A., and Nusser, Z. (2010). Molecular Identity of Dendritic Voltage-Gated Sodium Channels. Science *328*, 906–909.

Losonczy, A., and Magee, J.C. (2006). Integrative properties of radial oblique dendrites in hippocampal CA1 pyramidal neurons. Neuron *50*, 291–307.

Losonczy, A., Makara, J.K., and Magee, J.C. (2008). Compartmentalized dendritic plasticity and input feature storage in neurons. Nature *452*, 436–441.

Lovett-Barron, M., Turi, G.F., Kaifosh, P., Lee, P.H., Bolze, F., Sun, X.-H., Nicoud, J.-F., Zemelman, B.V., Sternson, S.M., and Losonczy, A. (2012). Regulation of neuronal input transformations by tunable dendritic inhibition. Nat. Neurosci. *15*, 423–430.

Lovett-Barron, M., Kaifosh, P., Kheirbek, M.A., Danielson, N., Zaremba, J.D., Reardon, T.R., Turi, G.F., Hen, R., Zemelman, B.V., and Losonczy, A. (2014). Dendritic Inhibition in the Hippocampus Supports Fear Learning. Science *343*, 857–863.

Lu, W., Isozaki, K., Roche, K.W., and Nicoll, R.A. (2010). Synaptic targeting of AMPA receptors is regulated by a CaMKII site in the first intracellular loop of GluA1. Proc. Natl. Acad. Sci. *107*, 22266–22271.

Lü, W., Du, J., Goehring, A., and Gouaux, E. (2017). Cryo-EM structures of the triheteromeric NMDA receptor and its allosteric modulation. Science *355*.

Lundqvist, M., Rose, J., Herman, P., Brincat, S.L., Buschman, T.J., and Miller, E.K. (2016). Gamma and Beta Bursts Underlie Working Memory. Neuron *90*, 152–164.

Lupica, C.R., Bell, J.A., Hoffman, A.F., and Watson, P.L. (2001). Contribution of the hyperpolarization-activated current (I(h)) to membrane potential and GABA release in hippocampal interneurons. J. Neurophysiol. *86*, 261–268.

Lushnikova, I., Skibo, G., Muller, D., and Nikonenko, I. (2009). Synaptic potentiation induces increased glial coverage of excitatory synapses in CA1 hippocampus. Hippocampus *19*, 753–762.

Lutz, B., and Marsicano, G. (2009). Endocannabinoid Role in Synaptic Plasticity and Learning. In Encyclopedia of Neuroscience, L.R. Squire, ed. (Oxford: Academic Press), pp. 963–975.

Lynch, G., Larson, J., Kelso, S., Barrionuevo, G., and Schottler, F. (1983). Intracellular injections of EGTA block induction of hippocampal long-term potentiation. Nature *305*, 719–721.

Maccaferri, G., and McBain, C.J. (1996). The hyperpolarization-activated current (Ih) and its contribution to pacemaker activity in rat CA1 hippocampal stratum oriens-alveus interneurones. J. Physiol. *497 (Pt 1)*, 119–130.

MacDermott, A.B., Mayer, M.L., Westbrook, G.L., Smith, S.J., and Barker, J.L. (1986). NMDA-receptor activation increases cytoplasmic calcium concentration in cultured spinal cord neurones. Nature *321*, 519–522.

Madisen, L., Zwingman, T.A., Sunkin, S.M., Oh, S.W., Zariwala, H.A., Gu, H., Ng, L.L., Palmiter, R.D., Hawrylycz, M.J., Jones, A.R., et al. (2010). A robust and high-throughput Cre reporting and characterization system for the whole mouse brain. Nat. Neurosci. *13*, 133–140.

Magee, J.C. (1998). Dendritic Hyperpolarization-Activated Currents Modify the Integrative Properties of Hippocampal CA1 Pyramidal Neurons. J. Neurosci. *18*, 7613–7624.

Magee, J.C. (1999). Dendritic Ih normalizes temporal summation in hippocampal CA1 neurons. Nat. Neurosci. *2*, 508–514.

Magee, J.C. (2016). Dendritic voltage-gated ion channels. In Dendrites, G. Stuart, N. Spruston, and M. Häusser, eds. (Oxford University Press), pp. 259–284.

Magee, J.C., and Carruth, M. (1999). Dendritic Voltage-Gated Ion Channels Regulate the Action Potential Firing Mode of Hippocampal CA1 Pyramidal Neurons. J. Neurophysiol. *82*, 1895–1901.

Magee, J.C., and Cook, E.P. (2000). Somatic EPSP amplitude is independent of synapse location in hippocampal pyramidal neurons. Nat. Neurosci. *3*, 895–903.

Magee, J.C., and Johnston, D. (1995). Characterization of single voltage-gated Na+ and Ca2+ channels in apical dendrites of rat CA1 pyramidal neurons. J. Physiol. *487*, 67–90.

Mahut, H. (1971). Spatial and object reversal learning in monkeys with partial temporal lobe ablations. Neuropsychologia *9*, 409–424.

Makara, J.K., Mor, M., Fegley, D., Szabó, S.I., Kathuria, S., Astarita, G., Duranti, A., Tontini, A., Tarzia, G., Rivara, S., et al. (2005). Selective inhibition of 2-AG hydrolysis enhances endocannabinoid signaling in hippocampus. Nat. Neurosci. *8*, 1139–1141.

Makara, J.K., Losonczy, A., Wen, Q., and Magee, J.C. (2009). Experience-dependent compartmentalized dendritic plasticity in rat hippocampal CA1 pyramidal neurons. Nat. Neurosci. *12*, 1485–1487.

Makino, H., and Malinow, R. (2011). Compartmentalized versus Global Synaptic Plasticity on Dendrites Controlled by Experience. Neuron *72*, 1001–1011.

Malenka, R.C., and Bear, M.F. (2004). LTP and LTD: An Embarrassment of Riches. Neuron *44*, 5–21.

Malik, R., and Johnston, D. (2017). Dendritic GIRK Channels Gate the Integration Window, Plateau Potentials, and Induction of Synaptic Plasticity in Dorsal But Not Ventral CA1 Neurons. J. Neurosci. *37*, 3940–3955.

Malinow, R., and Miller, J.P. (1986). Postsynaptic hyperpolarization during conditioning reversibly blocks induction of long-term potentiation. Nature *320*, 529.

Manns, J.R., and Eichenbaum, H. (2009). A cognitive map for object memory in the hippocampus. Learn. Mem. *16*, 616–624.

Marcelin, B., Lugo, J.N., Brewster, A.L., Liu, Z., Lewis, A.S., McClelland, S., Chetkovich, D.M., Baram, T.Z., Anderson, A.E., Becker, A., et al. (2012). Differential Dorso-ventral Distributions of Kv4.2 and HCN Proteins Confer Distinct Integrative Properties to Hippocampal CA1 Pyramidal Cell Distal Dendrites. J. Biol. Chem. *287*, 17656–17661.

Maren, S. (2005). Synaptic Mechanisms of Associative Memory in the Amygdala. Neuron *47*, 783–786.

Mariotti, L., Losi, G., Sessolo, M., Marcon, I., and Carmignoto, G. (2016). The inhibitory neurotransmitter GABA evokes long-lasting Ca2+ oscillations in cortical astrocytes. Glia *64*, 363–373.

Marrion, N.V., and Tavalin, S.J. (1998). Selective activation of Ca2+-activated K+ channels by co-localized Ca2+ channels in hippocampal neurons. Nature *395*, 900–905.

Marshall, L., and Born, J. (2007). The contribution of sleep to hippocampus-dependent memory consolidation. Trends Cogn. Sci. *11*, 442–450.

Marshall, L., Helgadóttir, H., Mölle, M., and Born, J. (2006). Boosting slow oscillations during sleep potentiates memory. Nature *444*, 610–613.

Marsicano, G., and Lafenêtre, P. (2009). Roles of the Endocannabinoid System in Learning and Memory. In Behavioral Neurobiology of the Endocannabinoid System, D. Kendall, and S. Alexander, eds. (Berlin, Heidelberg: Springer), pp. 201–230.

Marsicano, G., and Lutz, B. (1999). Expression of the cannabinoid receptor CB1 in distinct neuronal subpopulations in the adult mouse forebrain. Eur. J. Neurosci. *11*, 4213–4225.

Marsicano, G., Goodenough, S., Monory, K., Hermann, H., Eder, M., Cannich, A., Azad, S.C., Cascio, M.G., Gutiérrez, S.O., Stelt, M. van der, et al. (2003). CB1 Cannabinoid Receptors and On-Demand Defense Against Excitotoxicity. Science *302*, 84–88.

Martin, L.A., and Alger, B.E. (1999). Muscarinic facilitation of the occurrence of depolarization-induced suppression of inhibition in rat hippocampus. Neuroscience *92*, 61–71.

Martin, C., Beshel, J., and Kay, L.M. (2007). An Olfacto-Hippocampal Network Is Dynamically Involved in Odor-Discrimination Learning. J. Neurophysiol. *98*, 2196–2205.

Martineau, M., Shi, T., Puyal, J., Knolhoff, A.M., Dulong, J., Gasnier, B., Klingauf, J., Sweedler, J.V., Jahn, R., and Mothet, J.-P. (2013). Storage and Uptake of d-Serine into Astrocytic Synaptic-Like Vesicles Specify Gliotransmission. J. Neurosci. *33*, 3413–3423.

Mas-Herrero, E., Ripollés, P., HajiHosseini, A., Rodríguez-Fornells, A., and Marco-Pallarés, J. (2015). Beta oscillations and reward processing: Coupling oscillatory activity and hemodynamic responses. NeuroImage *119*, 13–19.

Massey, P.V., Johnson, B.E., Moult, P.R., Auberson, Y.P., Brown, M.W., Molnar, E., Collingridge, G.L., and Bashir, Z.I. (2004). Differential Roles of NR2A and NR2B-Containing NMDA Receptors in Cortical Long-Term Potentiation and Long-Term Depression. J. Neurosci. *24*, 7821–7828.

Matsugami, T.R., Tanemura, K., Mieda, M., Nakatomi, R., Yamada, K., Kondo, T., Ogawa, M., Obata, K., Watanabe, M., Hashikawa, T., et al. (2006). From the Cover: Indispensability of the glutamate transporters GLAST and GLT1 to brain development. Proc. Natl. Acad. Sci. *103*, 12161–12166.

Matsui, T., Sekiguchi, M., Hashimoto, A., Tomita, U., Nishikawa, T., and Wada, K. (1995). Functional comparison of D-serine and glycine in rodents: The effect on cloned NMDA receptors and the extracellular concentration. J. Neurochem. *65*, 454–458.

Matsuzaki, M., Ellis-Davies, G.C., Nemoto, T., Miyashita, Y., Iino, M., and Kasai, H. (2001). Dendritic spine geometry is critical for AMPA receptor expression in hippocampal CA1 pyramidal neurons. Nat. Neurosci. *4*, 1086–1092.

Matsuzaki, M., Honkura, N., Ellis-Davies, G.C.R., and Kasai, H. (2004). Structural basis of long-term potentiation in single dendritic spines. Nature *429*, 761–766.

Maurer, A.P., VanRhoads, S.R., Sutherland, G.R., Lipa, P., and McNaughton, B.L. (2005). Self-motion and the origin of differential spatial scaling along the septo-temporal axis of the hippocampus. Hippocampus *15*, 841–852.

Mayer, M.L., Westbrook, G.L., and Guthrie, P.B. (1984). Voltage-dependent block by Mg 2+ of NMDA responses in spinal cord neurones. Nature *309*, 261–263.

McCormick, D.A., and Bal, T. (1997). SLEEP AND AROUSAL: Thalamocortical Mechanisms. Annu. Rev. Neurosci. *20*, 185–215.

McGaugh, J.L. (2004). The amygdala modulates the consolidation of memories of emotionally arousing experiences. Annu. Rev. Neurosci. *27*, 1–28.

McHugh, S.B., Deacon, R.M.J., Rawlins, J.N.P., and Bannerman, D.M. (2004). Amygdala and ventral hippocampus contribute differentially to mechanisms of fear and anxiety. Behav. Neurosci. *118*, 63–78.

McHugh, T.J., Blum, K.I., Tsien, J.Z., Tonegawa, S., and Wilson, M.A. (1996). Impaired Hippocampal Representation of Space in CA1-Specific NMDAR1 Knockout Mice. Cell *87*, 1339–1349.

McKernan, M.G., and Shinnick-Gallagher, P. (1997). Fear conditioning induces a lasting potentiation of synaptic currents in vitro. Nature *390*, 607–611.

Medvedev, N., Popov, V., Henneberger, C., Kraev, I., Rusakov, D.A., and Stewart, M.G. (2014). Glia selectively approach synapses on thin dendritic spines. Philos. Trans. R. Soc. B Biol. Sci. *369*, 20140047.

Megías, M., Emri, Z., Freund, T.F., and Gulyás, A.I. (2001). Total number and distribution of inhibitory and excitatory synapses on hippocampal CA1 pyramidal cells. Neuroscience *102*, 527–540.

Melzer, S., Michael, M., Caputi, A., Eliava, M., Fuchs, E.C., Whittington, M.A., and Monyer, H. (2012). Long-Range–Projecting GABAergic Neurons Modulate Inhibition in Hippocampus and Entorhinal Cortex. Science *335*, 1506–1510.

Meur, K.L., Galante, M., Angulo, M.C., and Audinat, E. (2007). Tonic activation of NMDA receptors by ambient glutamate of non-synaptic origin in the rat hippocampus. J. Physiol. *580*, 373–383.

Mickus, T., Jung, H.-Y., and Spruston, N. (1999). Slow Sodium Channel Inactivation in CA1 Pyramidal Cells. Ann. N. Y. Acad. Sci. *868*, 97–101.

Migliore, M., and Shepherd, G.M. (2002). Emerging rules for the distributions of active dendritic conductances. Nat. Rev. Neurosci. *3*, 362–370.

Migues, P.V., Wong, J., Lyu, J., and Hardt, O. (2019). NMDA receptor activity bidirectionally controls active decay of long-term spatial memory in the dorsal hippocampus. Hippocampus *29*, 883–888.

Mikulovic, S., Restrepo, C.E., Siwani, S., Bauer, P., Pupe, S., Tort, A.B.L., Kullander, K., and Leão, R.N. (2018). Ventral hippocampal OLM cells control type 2 theta oscillations and response to predator odor. Nat. Commun. *9*, 3638.

Miller, S.J., Philips, T., Kim, N., Dastgheyb, R., Chen, Z., Hsieh, Y.-C., Daigle, J.G., Datta, M., Chew, J., Vidensky, S., et al. (2019). Molecularly defined cortical astroglia subpopulation modulates neurons via secretion of Norrin. Nat. Neurosci. *22*, 741–752.

Min, R., and Nevian, T. (2012). Astrocyte signaling controls spike timing-dependent depression at neocortical synapses. Nat. Neurosci. *15*, 746–753.

Min, R., Testa-Silva, G., Heistek, T.S., Canto, C.B., Lodder, J.C., Bisogno, T., Di Marzo, V., Brussaard, A.B., Burnashev, N., and Mansvelder, H.D. (2010). Diacylglycerol lipase is not involved in depolarization-induced suppression of inhibition at unitary inhibitory connections in mouse hippocampus. J. Neurosci. *30*, 2710–2715.

Mitchell, S.J., and Ranck, J.B. (1980). Generation of theta rhythm in medial entorhinal cortex of freely moving rats. Brain Res. *189*, 49–66.

Miwa, H., Fukaya, M., Watabe, A.M., Watanabe, M., and Manabe, T. (2008). Functional contributions of synaptically localized NR2B subunits of the NMDA receptor to synaptic transmission and long-term potentiation in the adult mouse CNS. J. Physiol. *586*, 2539–2550.

Moita, M.A.P., Rosis, S., Zhou, Y., LeDoux, J.E., and Blair, H.T. (2004). Putting Fear in Its Place: Remapping of Hippocampal Place Cells during Fear Conditioning. J. Neurosci. *24*, 7015–7023.

Moldavski, A., Behr, J., Bading, H., and Bengtson, C.P. (2020). A novel method using ambient glutamate for the electrophysiological quantification of extrasynaptic NMDA receptor function in acute brain slices. J. Physiol. *598*, 633–650.

Montana, V., Ni, Y., Sunjara, V., Hua, X., and Parpura, V. (2004). Vesicular Glutamate Transporter-Dependent Glutamate Release from Astrocytes. J. Neurosci. *24*, 2633–2642.

Morel, L., Chiang, M.S.R., Higashimori, H., Shoneye, T., Iyer, L.K., Yelick, J., Tai, A., and Yang, Y. (2017). Molecular and Functional Properties of Regional Astrocytes in the Adult Brain. J. Neurosci. *37*, 8706–8717.

Morel, L., Men, Y., Chiang, M.S.R., Tian, Y., Jin, S., Yelick, J., Higashimori, H., and Yang, Y. (2019). Intracortical astrocyte subpopulations defined by astrocyte reporter Mice in the adult brain. Glia *67*, 171–181.

Mori, T., Tanaka, K., Buffo, A., Wurst, W., Kühn, R., and Götz, M. (2006). Inducible gene deletion in astroglia and radial glia—A valuable tool for functional and lineage analysis. Glia *54*, 21–34.

Moriarty, O., Roche, M., McGuire, B.E., and Finn, D.P. (2012). Validation of an air-puff passive-avoidance paradigm for assessment of aversive learning and memory in rat models of chronic pain. J. Neurosci. Methods *204*, 1–8.

Morice, E., Billard, J.-M., Denis, C., Mathieu, F., Betancur, C., Epelbaum, J., Giros, B., and Nosten-Bertrand, M. (2007). Parallel Loss of Hippocampal LTD and Cognitive Flexibility in a Genetic Model of Hyperdopaminergia. Neuropsychopharmacology *32*, 2108–2116.

Morishita, W., Lu, W., Smith, G.B., Nicoll, R.A., Bear, M.F., and Malenka, R.C. (2007). Activation of NR2B-containing NMDA receptors is not required for NMDA receptor-dependent long-term depression. Neuropharmacology *52*, 71–76.

Morris, R.G. (1989). Synaptic plasticity and learning: selective impairment of learning rats and blockade of long-term potentiation in vivo by the N-methyl-D- aspartate receptor antagonist AP5. J. Neurosci. *9*, 3040–3057.

Morris, R.G.M. (1981). Spatial localization does not require the presence of local cues. Learn. Motiv. *12*, 239–260.

Morris, R.G., Garrud, P., Rawlins, J.N., and O'Keefe, J. (1982). Place navigation impaired in rats with hippocampal lesions. Nature *297*, 681–683.

Morris, R.G.M., Anderson, E., Lynch, G.S., and Baudry, M. (1986). Selective impairment of learning and blockade of long-term potentiation by an N -methyl-D-aspartate receptor antagonist, AP5. Nature *319*, 774–776.

Moser, M.-B., and Moser, E.I. (1998). Functional differentiation in the hippocampus. Hippocampus *8*, 608–619.

Moser, E., Moser, M.B., and Andersen, P. (1993). Spatial learning impairment parallels the magnitude of dorsal hippocampal lesions, but is hardly present following ventral lesions. J. Neurosci. *13*, 3916–3925.

Moser, M.B., Moser, E.I., Forrest, E., Andersen, P., and Morris, R.G. (1995). Spatial learning with a minislab in the dorsal hippocampus. Proc. Natl. Acad. Sci. *92*, 9697–9701.

Mothet, J.-P., Parent, A.T., Wolosker, H., Brady, R.O., Linden, D.J., Ferris, C.D., Rogawski, M.A., and Snyder, S.H. (2000). D-serine is an endogenous ligand for the glycine site of the N-methyl-D-aspartate receptor. Proc. Natl. Acad. Sci. *97*, 4926–4931.

Mothet, J.-P., Pollegioni, L., Ouanounou, G., Martineau, M., Fossier, P., and Baux, G. (2005). Glutamate receptor activation triggers a calcium-dependent and SNARE protein-dependent release of the gliotransmitter D-serine. Proc. Natl. Acad. Sci. *102*, 5606–5611.

Mulholland, P.J., Carpenter-Hyland, E.P., Hearing, M.C., Becker, H.C., Woodward, J.J., and Chandler, L.J. (2008). Glutamate Transporters Regulate Extrasynaptic NMDA Receptor Modulation of Kv2.1 Potassium Channels. J. Neurosci. *28*, 8801–8809.

Müller, C., Beck, H., Coulter, D., and Remy, S. (2012). Inhibitory Control of Linear and Supralinear Dendritic Excitation in CA1 Pyramidal Neurons. Neuron *75*, 851–864.

Murphy-Royal, C., Dupuis, J.P., Varela, J.A., Panatier, A., Pinson, B., Baufreton, J., Groc, L., and Oliet, S.H.R. (2015). Surface diffusion of astrocytic glutamate transporters shapes synaptic transmission. Nat. Neurosci. *18*, 219–226.

Mysin, I.E., Kitchigina, V.F., and Kazanovich, Y.B. (2019). Phase relations of theta oscillations in a computer model of the hippocampal CA1 field: Key role of Schaffer collaterals. Neural Netw. Off. J. Int. Neural Netw. Soc. *116*, 119–138.

Nägerl, U.V., Eberhorn, N., Cambridge, S.B., and Bonhoeffer, T. (2004). Bidirectional activity-dependent morphological plasticity in hippocampal neurons. Neuron *44*, 759–767.

Navarrete, M., and Araque, A. (2008). Endocannabinoids Mediate Neuron-Astrocyte Communication. Neuron *57*, 883–893.

Navarrete, M., and Araque, A. (2010). Endocannabinoids potentiate synaptic transmission through stimulation of astrocytes. Neuron *68*, 113–126.

Navarrete, M., Perea, G., Sevilla, D.F. de, Gómez-Gonzalo, M., Núñez, A., Martín, E.D., and Araque, A. (2012). Astrocytes Mediate In Vivo Cholinergic-Induced Synaptic Plasticity. PLOS Biol. *10*, e1001259.

Navarrete, M., Perea, G., Maglio, L., Pastor, J., García de Sola, R., and Araque, A. (2013). Astrocyte Calcium Signal and Gliotransmission in Human Brain Tissue. Cereb. Cortex *23*, 1240–1246.

Nedergaard, M. (1994). Direct signaling from astrocytes to neurons in cultures of mammalian brain cells. Science *263*, 1768–1771.

Neske, G.T. (2016). The Slow Oscillation in Cortical and Thalamic Networks: Mechanisms and Functions. Front. Neural Circuits *9*, 88.

Nett, W.J., Oloff, S.H., and McCarthy, K.D. (2002). Hippocampal Astrocytes In Situ Exhibit Calcium Oscillations That Occur Independent of Neuronal Activity. J. Neurophysiol. *87*, 528–537.

Neu, A., Földy, C., and Soltesz, I. (2007). Postsynaptic origin of CB1-dependent tonic inhibition of GABA release at cholecystokinin-positive basket cell to pyramidal cell synapses in the CA1 region of the rat hippocampus. J. Physiol. *578*, 233–247.

Nevian, T., Larkum, M.E., Polsky, A., and Schiller, J. (2007). Properties of basal dendrites of layer 5 pyramidal neurons: a direct patch-clamp recording study. Nat. Neurosci. *10*, 206–214.

Newman, E.A., and Zahs, K.R. (1997). Calcium Waves in Retinal Glial Cells. Science *275*, 844–847.

Ngo-Anh, T.J., Bloodgood, B.L., Lin, M., Sabatini, B.L., Maylie, J., and Adelman, J.P. (2005). SK channels and NMDA receptors form a Ca 2+ -mediated feedback loop in dendritic spines. Nat. Neurosci. *8*, 642–649.

Nicholls, R.E., Alarcon, J.M., Malleret, G., Carroll, R.C., Grody, M., Vronskaya, S., and Kandel, E.R. (2008). Transgenic Mice Lacking NMDAR-Dependent LTD Exhibit Deficits in Behavioral Flexibility. Neuron *58*, 104–117.

Nimmerjahn, A., Kirchhoff, F., Kerr, J.N.D., and Helmchen, F. (2004). Sulforhodamine 101 as a specific marker of astroglia in the neocortex in vivo. Nat. Methods *1*, 31–37.

Nixdorf-Bergweiler, B.E., Albrecht, D., and Heinemann, U. (1994). Developmental changes in the number, size, and orientation of GFAP-positive cells in the CA1 region of rat hippocampus. Glia *12*, 180–195.

Nolan, M.F., Malleret, G., Dudman, J.T., Buhl, D.L., Santoro, B., Gibbs, E., Vronskaya, S., Buzsáki, G., Siegelbaum, S.A., Kandel, E.R., et al. (2004). A Behavioral Role for Dendritic Integration: HCN1 Channels Constrain Spatial Memory and Plasticity at Inputs to Distal Dendrites of CA1 Pyramidal Neurons. Cell *119*, 719–732.

Nowak, L., Bregestovski, P., Ascher, P., Herbet, A., and Prochiantz, A. (1984). Magnesium gates glutamate-activated channels in mouse central neurones. Nature *307*, 462–465.

Ogata, K., and Kosaka, T. (2002). Structural and quantitative analysis of astrocytes in the mouse hippocampus. Neuroscience *113*, 221–233.

Oh, S.-J., Han, K.-S., Park, H., Woo, D. ho, Kim, H.Y., Traynelis, S.F., and Lee, C.J. (2012). Protease activated receptor 1-induced glutamate release in cultured astrocytes is mediated by Bestrophin-1 channel but not by vesicular exocytosis. Mol. Brain *5*, 38.

Ohno-Shosaku, T., Maejima, T., and Kano, M. (2001). Endogenous Cannabinoids Mediate Retrograde Signals from Depolarized Postsynaptic Neurons to Presynaptic Terminals. Neuron *29*, 729–738.

Ohno-Shosaku, T., Tsubokawa, H., Mizushima, I., Yoneda, N., Zimmer, A., and Kano, M. (2002a). Presynaptic Cannabinoid Sensitivity Is a Major Determinant of Depolarization-Induced Retrograde Suppression at Hippocampal Synapses. J. Neurosci. *22*, 3864–3872.

Ohno-Shosaku, T., Shosaku, J., Tsubokawa, H., and Kano, M. (2002b). Cooperative endocannabinoid production by neuronal depolarization and group I metabotropic glutamate receptor activation. Eur. J. Neurosci. *15*, 953–961.

Ohno-Shosaku, T., Matsui, M., Fukudome, Y., Shosaku, J., Tsubokawa, H., Taketo, M.M., Manabe, T., and Kano, M. (2003). Postsynaptic M1 and M3 receptors are responsible for the muscarinic enhancement of retrograde endocannabinoid signalling in the hippocampus. Eur. J. Neurosci. *18*, 109–116.

Okada, S., Igata, H., Sasaki, T., and Ikegaya, Y. (2017). Spatial Representation of Hippocampal Place Cells in a T-Maze with an Aversive Stimulation. Front. Neural Circuits *11*, 101.

Okamoto, K.-I., Nagai, T., Miyawaki, A., and Hayashi, Y. (2004). Rapid and persistent modulation of actin dynamics regulates postsynaptic reorganization underlying bidirectional plasticity. Nat. Neurosci. *7*, 1104–1112.

O'Keefe, J. (1976). Place units in the hippocampus of the freely moving rat. Exp. Neurol. *51*, 78–109.

O'Keefe, J., and Dostrovsky, J. (1971). The hippocampus as a spatial map. Preliminary evidence from unit activity in the freely-moving rat. Brain Res. *34*, 171–175.

O'Keefe, J., and Nadel, L. (1978). The Hippocampus as a Cognitive Map (Oxford: Clarendon Press).

O'Keefe, J., and Recce, M.L. (1993). Phase relationship between hippocampal place units and the EEG theta rhythm. Hippocampus *3*, 317–330.

Okubo, Y., Kanemaru, K., Suzuki, J., Kobayashi, K., Hirose, K., and Iino, M. (2019). Inositol 1,4,5-trisphosphate receptor type 2-independent Ca2+ release from the endoplasmic reticulum in astrocytes. Glia *67*, 113–124.

Okubo, Y., Iino, M., and Hirose, K. (2020). Store-operated Ca2+ entry-dependent Ca2+ refilling in the endoplasmic reticulum in astrocytes. Biochem. Biophys. Res. Commun. *522*, 1003–1008.

Oliet, S.H.R., Piet, R., and Poulain, D.A. (2001). Control of Glutamate Clearance and Synaptic Efficacy by Glial Coverage of Neurons. Science *292*, 923–926.

Oliveira, J.F., Sardinha, V.M., Guerra-Gomes, S., Araque, A., and Sousa, N. (2015). Do stars govern our actions? Astrocyte involvement in rodent behavior. Trends Neurosci. *38*, 535–549.

Oliveira, M.G.M., Bueno, O.F.A., Pomarico, A.C., and Gugliano, E.B. (1997). Strategies Used by Hippocampal- and Caudate-Putamen-Lesioned Rats in a Learning Task. Neurobiol. Learn. Mem. *68*, 32–41.

Opazo, P., Labrecque, S., Tigaret, C.M., Frouin, A., Wiseman, P.W., De Koninck, P., and Choquet, D. (2010). CaMKII triggers the diffusional trapping of surface AMPARs through phosphorylation of stargazin. Neuron *67*, 239–252.

Orr, A.G., Hsiao, E.C., Wang, M.M., Ho, K., Kim, D.H., Wang, X., Guo, W., Kang, J., Yu, G.-Q., Adame, A., et al. (2015). Astrocytic adenosine receptor A 2A and G s -coupled signaling regulate memory. Nat. Neurosci. *18*, 423–434.

O'Shaughnessy, W.B. (1843). On the Preparations of the Indian Hemp, or Gunjah. Prov. Med. J. Retrosp. Med. Sci. *5*, 363–369.

Otmakhov, N., Tao-Cheng, J.-H., Carpenter, S., Asrican, B., Dosemeci, A., Reese, T.S., and Lisman, J. (2004). Persistent accumulation of calcium/calmodulin-dependent protein kinase II in dendritic spines after induction of NMDA receptor-dependent chemical long-term potentiation. J. Neurosci. *24*, 9324–9331.

Otte, D.-M., Arellano, M.L.B. de, Bilkei-Gorzo, A., Albayram, Ö., Imbeault, S., Jeung, H., Alferink, J., and Zimmer, A. (2013). Effects of Chronic D-Serine Elevation on Animal Models of Depression and Anxiety-Related Behavior. PLOS ONE *8*, e67131.

Palmer, L., Murayama, M., and Larkum, M. (2016). Dendritic Integration in vivo. In Dendrites, G. Stuart, N. Spruston, and M. Häusser, eds. (Oxford University Press), pp. 399–428.

Palmer, L.M., Shai, A.S., Reeve, J.E., Anderson, H.L., Paulsen, O., and Larkum, M.E. (2014). NMDA spikes enhance action potential generation during sensory input. Nat. Neurosci. *17*, 383–390.

Pan, B., Wang, W., Long, J.Z., Sun, D., Hillard, C.J., Cravatt, B.F., and Liu, Q. (2009). Blockade of 2-Arachidonoylglycerol Hydrolysis by Selective Monoacylglycerol Lipase Inhibitor 4-Nitrophenyl 4-(Dibenzo[d][1,3]dioxol-5-yl(hydroxy)methyl)piperidine-1-carboxylate (JZL184) Enhances Retrograde Endocannabinoid Signaling. J. Pharmacol. Exp. Ther. *331*, 591–597.

Panatier, A., Theodosis, D.T., Mothet, J.-P., Touquet, B., Pollegioni, L., Poulain, D.A., and Oliet, S.H.R. (2006). Glia-Derived d-Serine Controls NMDA Receptor Activity and Synaptic Memory. Cell *125*, 775–784.

Pannasch, U., Freche, D., Dallérac, G., Ghézali, G., Escartin, C., Ezan, P., Cohen-Salmon, M., Benchenane, K., Abudara, V., Dufour, A., et al. (2014). Connexin 30 sets synaptic strength by controlling astroglial synapse invasion. Nat. Neurosci. *17*, 549–558.

Paoletti, P. (2011). Molecular basis of NMDA receptor functional diversity. Eur. J. Neurosci. *33*, 1351–1365.

Paoletti, P., and Neyton, J. (2007). NMDA receptor subunits: function and pharmacology. Curr. Opin. Pharmacol. *7*, 39–47.

Paoletti, P., Bellone, C., and Zhou, Q. (2013). NMDA receptor subunit diversity: impact on receptor properties, synaptic plasticity and disease. Nat. Rev. Neurosci. *14*, 383–400.

Papatheodoropoulos, C., and Kostopoulos, G. (2000). Dorsal-ventral differentiation of short-term synaptic plasticity in rat CA1 hippocampal region. Neurosci. Lett. *286*, 57–60.

Pape, H.-C. (1996). Queer Current and Pacemaker: The Hyperpolarization-Activated Cation Current in Neurons. Annu. Rev. Physiol. *58*, 299–327.

Papouin, T., Ladépêche, L., Ruel, J., Sacchi, S., Labasque, M., Hanini, M., Groc, L., Pollegioni, L., Mothet, J.-P., and Oliet, S.H.R. (2012). Synaptic and Extrasynaptic NMDA Receptors Are Gated by Different Endogenous Coagonists. Cell *150*, 633–646.

Papouin, T., Dunphy, J.M., Tolman, M., Dineley, K.T., and Haydon, P.G. (2017). Septal Cholinergic Neuromodulation Tunes the Astrocyte-Dependent Gating of Hippocampal NMDA Receptors to Wakefulness. Neuron *94*, 840-854.e7.

Paré, D., and Collins, D.R. (2000). Neuronal Correlates of Fear in the Lateral Amygdala: Multiple Extracellular Recordings in Conscious Cats. J. Neurosci. *20*, 2701–2710.

Paré, D., Shink, E., Gaudreau, H., Destexhe, A., and Lang, E.J. (1998). Impact of Spontaneous Synaptic Activity on the Resting Properties of Cat Neocortical Pyramidal Neurons In Vivo. J. Neurophysiol. *79*, 1450–1460.

Park, H., Han, K.-S., Oh, S.-J., Jo, S., Woo, J., Yoon, B.-E., and Lee, C.J. (2013). High glutamate permeability and distal localization of Best1 channel in CA1 hippocampal astrocyte. Mol. Brain *6*, 54.

Parpura, V., and Haydon, P.G. (2000). Physiological astrocytic calcium levels stimulate glutamate release to modulate adjacent neurons. Proc. Natl. Acad. Sci. *97*, 8629–8634.

Parpura, V., Basarsky, T.A., Liu, F., Jeftinija, K., Jeftinija, S., and Haydon, P.G. (1994). Glutamate-mediated astrocyte–neuron signalling. Nature *369*, 744–747.

Parri, H.R., and Crunelli, V. (2003). The role of Ca2+ in the generation of spontaneous astrocytic Ca2+ oscillations. Neuroscience *120*, 979–992.

Parri, H.R., Gould, T.M., and Crunelli, V. (2001). Spontaneous astrocytic Ca2+ oscillations in situ drive NMDAR-mediated neuronal excitation. Nat. Neurosci. *4*, 803–812.

Pasti, L., Zonta, M., Pozzan, T., Vicini, S., and Carmignoto, G. (2001). Cytosolic Calcium Oscillations in Astrocytes May Regulate Exocytotic Release of Glutamate. J. Neurosci. *21*, 477–484.

Patel, J., Fujisawa, S., Berényi, A., Royer, S., and Buzsáki, G. (2012). Traveling Theta Waves along the Entire Septotemporal Axis of the Hippocampus. Neuron *75*, 410–417.

Patterson, M.A., Szatmari, E.M., and Yasuda, R. (2010). AMPA receptors are exocytosed in stimulated spines and adjacent dendrites in a Ras-ERK-dependent manner during long-term potentiation. Proc. Natl. Acad. Sci. *107*, 15951–15956.

Pawelzik, H., Hughes, D.I., and Thomson, A.M. (2002). Physiological and morphological diversity of immunocytochemically defined parvalbumin- and cholecystokinin-positive interneurones in CA1 of the adult rat hippocampus. J. Comp. Neurol. *443*, 346–367.

Pentkowski, N.S., Blanchard, D.C., Lever, C., Litvin, Y., and Blanchard, R.J. (2006). Effects of lesions to the dorsal and ventral hippocampus on defensive behaviors in rats. Eur. J. Neurosci. *23*, 2185–2196.

Perea, G., and Araque, A. (2005). Properties of Synaptically Evoked Astrocyte Calcium Signal Reveal Synaptic Information Processing by Astrocytes. J. Neurosci. *25*, 2192–2203.

Perea, G., and Araque, A. (2007). Astrocytes Potentiate Transmitter Release at Single Hippocampal Synapses. Science *317*, 1083–1086.

Perea, G., Navarrete, M., and Araque, A. (2009). Tripartite synapses: astrocytes process and control synaptic information. Trends Neurosci. *32*, 421–431.

Perez-Alvarez, A., Navarrete, M., Covelo, A., Martin, E.D., and Araque, A. (2014). Structural and Functional Plasticity of Astrocyte Processes and Dendritic Spine Interactions. J. Neurosci. *34*, 12738–12744.

Pérez-Garci, E., Gassmann, M., Bettler, B., and Larkum, M.E. (2006). The GABAB1b Isoform Mediates Long-Lasting Inhibition of Dendritic Ca2+ Spikes in Layer 5 Somatosensory Pyramidal Neurons. Neuron *50*, 603–616.

Petralia, R.S., Wang, Y.X., Hua, F., Yi, Z., Zhou, A., Ge, L., Stephenson, F.A., and Wenthold, R.J. (2010). Organization of NMDA receptors at extrasynaptic locations. Neuroscience *167*, 68–87.

Petravicz, J., Fiacco, T.A., and McCarthy, K.D. (2008). Loss of IP3 Receptor-Dependent Ca2+ Increases in Hippocampal Astrocytes Does Not Affect Baseline CA1 Pyramidal Neuron Synaptic Activity. J. Neurosci. *28*, 4967–4973.

Petravicz, J., Boyt, K.M., and McCarthy, K.D. (2014). Astrocyte IP3R2-dependent Ca2+ signaling is not a major modulator of neuronal pathways governing behavior. Front. Behav. Neurosci. *8*, 384.

Petrelli, F., and Bezzi, P. (2016). Novel insights into gliotransmitters. Curr. Opin. Pharmacol. *26*, 138–145.

Pinky, N.F., Wilkie, C.M., Barnes, J.R., and Parsons, M.P. (2018). Region- and Activity-Dependent Regulation of Extracellular Glutamate. J. Neurosci. *38*, 5351–5366.

Piomelli, D., Giuffrida, A., Calignano, A., and Rodríguez de Fonseca, F. (2000). The endocannabinoid system as a target for therapeutic drugs. Trends Pharmacol. Sci. *21*, 218–224.

Pita-Almenar, J.D., Collado, M.S., Colbert, C.M., and Eskin, A. (2006). Different mechanisms exist for the plasticity of glutamate reuptake during early long-term potentiation (LTP) and late LTP. J. Neurosci. *26*, 10461–10471.

Pita-Almenar, J.D., Zou, S., Colbert, C.M., and Eskin, A. (2012). Relationship between increase in astrocytic GLT-1 glutamate transport and late-LTP. Learn. Mem. Cold Spring Harb. N *19*, 615–626.

Pitler, T.A., and Alger, B.E. (1992). Postsynaptic spike firing reduces synaptic GABAA responses in hippocampal pyramidal cells. J. Neurosci. *12*, 4122–4132.

Pitler, T.A., and Alger, B.E. (1994). Depolarization-induced suppression of GABAergic inhibition in rat hippocampal pyramidal cells: G protein involvement in a presynaptic mechanism. Neuron *13*, 1447–1455.

Pologruto, T.A., Sabatini, B.L., and Svoboda, K. (2003). ScanImage: Flexible software for operating laser scanning microscopes. Biomed. Eng. OnLine *2*, 13.

Porter, J.T., and McCarthy, K.D. (1996). Hippocampal Astrocytes In Situ Respond to Glutamate Released from Synaptic Terminals. J. Neurosci. *16*, 5073–5081.

Poskanzer, K.E., and Yuste, R. (2016). Astrocytes regulate cortical state switching in vivo. Proc. Natl. Acad. Sci. *113*, E2675–E2684.

Pothuizen, H.H.J., Zhang, W.-N., Jongen-Rêlo, A.L., Feldon, J., and Yee, B.K. (2004). Dissociation of function between the dorsal and the ventral hippocampus in spatial learning abilities of the rat: a within-subject, within-task comparison of reference and working spatial memory. Eur. J. Neurosci. *19*, 705–712.

Pouille, F., and Scanziani, M. (2004). Routing of spike series by dynamic circuits in the hippocampus. Nature *429*, 717–723.

Pu, Y., Cornwell, B.R., Cheyne, D., and Johnson, B.W. (2018). High-gamma activity in the human hippocampus and parahippocampus during inter-trial rest periods of a virtual navigation task. NeuroImage *178*, 92–103.

Rall, W. (1962). Electrophysiology of a Dendritic Neuron Model. Biophys. J. *2*, 145–167.

Rall, W. (1964). Theoretical significance of dendritic trees for neuronal input output relations. In Neural Theory and Modeling, R. Reiss, ed. (Standford University Press), pp. 122–146.

Ranganathan, G.N., Apostolides, P.F., Harnett, M.T., Xu, N.-L., Druckmann, S., and Magee, J.C. (2018). Active dendritic integration and mixed neocortical network representations during an adaptive sensing behavior. Nat. Neurosci. *21*, 1583–1590.

Rasooli-Nejad, S., Palygin, O., Lalo, U., and Pankratov, Y. (2014). Cannabinoid receptors contribute to astroglial Ca2+-signalling and control of synaptic plasticity in the neocortex. Philos. Trans. R. Soc. B Biol. Sci. *369*, 20140077.

Rauner, C., and Köhr, G. (2011). Triheteromeric NR1/NR2A/NR2B Receptors Constitute the Major N-Methyl-d-aspartate Receptor Population in Adult Hippocampal Synapses. J. Biol. Chem. *286*, 7558–7566.

Reeves, A.M.B., Shigetomi, E., and Khakh, B.S. (2011). Bulk Loading of Calcium Indicator Dyes to Study Astrocyte Physiology: Key Limitations and Improvements Using Morphological Maps. J. Neurosci. *31*, 9353–9358.

Reichenbach, A., Derouiche, A., and Kirchhoff, F. (2010). Morphology and dynamics of perisynaptic glia. Brain Res. Rev. *63*, 11–25.

Remy, S., Csicsvari, J., and Beck, H. (2009). Activity-Dependent Control of Neuronal Output by Local and Global Dendritic Spike Attenuation. Neuron *61*, 906–916.

Rinzel, J., and Rall, W. (1974). Transient Response in a Dendritic Neuron Model for Current Injected at One Branch. Biophys. J. *14*, 759–790.

Robin, L.M., Oliveira da Cruz, J.F., Langlais, V.C., Martin-Fernandez, M., Metna-Laurent, M., Busquets-Garcia, A., Bellocchio, L., Soria-Gomez, E., Papouin, T., Varilh, M., et al. (2018). Astroglial CB1 Receptors Determine Synaptic D-Serine Availability to Enable Recognition Memory. Neuron *98*, 935-944.e5.

Rogan, M.T., Stäubli, U.V., and LeDoux, J.E. (1997). Fear conditioning induces associative long-term potentiation in the amygdala. Nature *390*, 604–607.

Romanos, J., Benke, D., Saab, A.S., Zeilhofer, H.U., and Santello, M. (2019). Differences in glutamate uptake between cortical regions impact neuronal NMDA receptor activation. Commun. Biol. *2*, 1–15.

Romanos, J., Benke, D., Pietrobon, D., Zeilhofer, H.U., and Santello, M. (2020). Astrocyte dysfunction increases cortical dendritic excitability and promotes cranial pain in familial migraine. Sci. Adv. *6*, eaaz1584.

Rose, C.R., Felix, L., Zeug, A., Dietrich, D., Reiner, A., and Henneberger, C. (2018). Astroglial Glutamate Signaling and Uptake in the Hippocampus. Front. Mol. Neurosci. *10*, 451.

Rose, E.M., Koo, J.C.P., Antflick, J.E., Ahmed, S.M., Angers, S., and Hampson, D.R. (2009). Glutamate transporter coupling to Na,K-ATPase. J. Neurosci. Off. J. Soc. Neurosci. *29*, 8143–8155.

Rosenberg, D., Kartvelishvily, E., Shleper, M., Klinker, C.M.C., Bowser, M.T., and Wolosker, H. (2010). Neuronal release of D-serine: a physiological pathway controlling extracellular D-serine concentration. FASEB J. *24*, 2951–2961.

Rosenberg, D., Artoul, S., Segal, A.C., Kolodney, G., Radzishevsky, I., Dikopoltsev, E., Foltyn, V.N., Inoue, R., Mori, H., Billard, J.-M., et al. (2013). Neuronal D-Serine and Glycine Release Via the Asc-1 Transporter Regulates NMDA Receptor-Dependent Synaptic Activity. J. Neurosci. *33*, 3533–3544.

Rosenmund, C., and Westbrook, G.L. (1993). Calcium-induced actin depolymerization reduces NMDA channel activity. Neuron *10*, 805–814.

Roth, R.H., Cudmore, R.H., Tan, H.L., Hong, I., Zhang, Y., and Huganir, R.L. (2020). Cortical Synaptic AMPA Receptor Plasticity during Motor Learning. Neuron *105*, 895-908.e5.

Rothstein, J.D., Dykes-Hoberg, M., Pardo, C.A., Bristol, L.A., Jin, L., Kuncl, R.W., Kanai, Y., Hediger, M.A., Wang, Y., Schielke, J.P., et al. (1996). Knockout of Glutamate Transporters Reveals a Major Role for Astroglial Transport in Excitotoxicity and Clearance of Glutamate. Neuron *16*, 675–686.

Royer, S., Sirota, A., Patel, J., and Buzsáki, G. (2010). Distinct Representations and Theta Dynamics in Dorsal and Ventral Hippocampus. J. Neurosci. *30*, 1777–1787.

Royer, S., Zemelman, B.V., Losonczy, A., Kim, J., Chance, F., Magee, J.C., and Buzsáki, G. (2012). Control of timing, rate and bursts of hippocampal place cells by dendritic and somatic inhibition. Nat. Neurosci. *15*, 769–775.

Rubin, R.D., Watson, P.D., Duff, M.C., and Cohen, N.J. (2014). The role of the hippocampus in flexible cognition and social behavior. Front. Hum. Neurosci. *8*, 742.

Rungta, R.L., Bernier, L.-P., Dissing-Olesen, L., Groten, C.J., LeDue, J.M., Ko, R., Drissler, S., and MacVicar, B.A. (2016). Ca2+ transients in astrocyte fine processes occur via Ca2+ influx in the adult mouse hippocampus. Glia *64*, 2093–2103.

Rusakov, D.A., and Kullmann, D.M. (1998). Extrasynaptic glutamate diffusion in the hippocampus: ultrastructural constraints, uptake, and receptor activation. J. Neurosci. Off. J. Soc. Neurosci. *18*, 3158–3170.

Rusakov, D.A., Bard, L., Stewart, M.G., and Henneberger, C. (2014). Diversity of astroglial functions alludes to subcellular specialisation. Trends Neurosci. *37*, 228–242.

Russig, H., Durrer, A., Yee, B.K., Murphy, C.A., and Feldon, J. (2003). The acquisition, retention and reversal of spatial learning in the morris water maze task following withdrawal from an escalating dosage schedule of amphetamine in wistar rats. Neuroscience *119*, 167–179.

Sah, P., Hestrin, S., and Nicoll, R.A. (1989). Tonic activation of NMDA receptors by ambient glutamate enhances excitability of neurons. Science *246*, 815–818.

Sainsbury, R.S., Heynen, A., and Montoya, C.P. (1987). Behavioral correlates of hippocampal type 2 theta in the rat. Physiol. Behav. *39*, 513–519.

Sakers, K., Lake, A.M., Khazanchi, R., Ouwenga, R., Vasek, M.J., Dani, A., and Dougherty, J.D. (2017). Astrocytes locally translate transcripts in their peripheral processes. Proc. Natl. Acad. Sci. *114*, E3830–E3838.

Sakimura, K., Kutsuwada, T., Ito, I., Manabe, T., Takayama, C., Kushiya, E., Yagi, T., Aizawa, S., Inoue, Y., and Sugiyama, H. (1995). Reduced hippocampal LTP and spatial learning in mice lacking NMDA receptor epsilon 1 subunit. Nature *373*, 151–155.

Santoro, B., Chen, S., Lüthi, A., Pavlidis, P., Shumyatsky, G.P., Tibbs, G.R., and Siegelbaum, S.A. (2000). Molecular and Functional Heterogeneity of Hyperpolarization-Activated Pacemaker Channels in the Mouse CNS. J. Neurosci. *20*, 5264–5275.

Saucier, D., and Cain, D.P. (1995). Spatial learning without NMDA receptor-dependent long-term potentiation. Nature *378*, 186–189.

Schaefer, A.T., Larkum, M.E., Sakmann, B., and Roth, A. (2003). Coincidence Detection in Pyramidal Neurons Is Tuned by Their Dendritic Branching Pattern. J. Neurophysiol. *89*, 3143–3154.

Schatz, A.R., Lee, M., Condie, R.B., Pulaski, J.T., and Kaminski, N.E. (1997). Cannabinoid Receptors CB1 and CB2: A Characterization of Expression and Adenylate Cyclase Modulation within the Immune System. Toxicol. Appl. Pharmacol. *142*, 278–287.

Schell, M.J., Molliver, M.E., and Snyder, S.H. (1995). D-serine, an endogenous synaptic modulator: localization to astrocytes and glutamate-stimulated release. Proc. Natl. Acad. Sci. *92*, 3948–3952.

Schell, M.J., Jr, R.O.B., Molliver, M.E., and Snyder, S.H. (1997). d-Serine as a Neuromodulator: Regional and Developmental Localizations in Rat Brain Glia Resemble NMDA Receptors. J. Neurosci. *17*, 1604–1615.

Schiller, J., Schiller, Y., Stuart, G., and Sakmann, B. (1997). Calcium action potentials restricted to distal apical dendrites of rat neocortical pyramidal neurons. J. Physiol. *505*, 605–616.

Schneggenburger, R., and Neher, E. (2000). Intracellular calcium dependence of transmitter release rates at a fast central synapse. Nature *406*, 889–893.

Schoenenberger, P., O'Neill, J., and Csicsvari, J. (2016). Activity-dependent plasticity of hippocampal place maps. Nat. Commun. *7*, 11824.

Schönhense, E.M. (2015). Pathways controlling astrocyte Ca2+ signaling and dendritic integration. Master Thesis. Rheinische Friedrich-Wilhelms University of Bonn.

Schwartzkroin, P.A., and Wester, K. (1975). Long-lasting facilitation of a synaptic potential following tetanization in thein vitro hippocampal slice. Brain Res. *89*, 107–119.

Scimemi, A., Fine, A., Kullmann, D.M., and Rusakov, D.A. (2004). NR2B-Containing Receptors Mediate Cross Talk among Hippocampal Synapses. J. Neurosci. *24*, 4767–4777.

Scoville, W.B., and Milner, B. (1957). Loss of Recent Memory after Bilateral Hippocampal Lesions. J. Neurol. Neurosurg. Psychiatry *20*, 11–21.

Seibenhener, M.L., and Wooten, M.C. (2015). Use of the Open Field Maze to Measure Locomotor and Anxiety-like Behavior in Mice. J. Vis. Exp. e52434.

Sekulić, V., Chen, T.-C., Lawrence, J.J., and Skinner, F.K. (2015). Dendritic distributions of Ih channels in experimentally-derived multi-compartment models of oriens-lacunosum/moleculare (O-LM) hippocampal interneurons. Front. Synaptic Neurosci. *7*, 2.

Senior, T.J., Huxter, J.R., Allen, K., O'Neill, J., and Csicsvari, J. (2008). Gamma oscillatory firing reveals distinct populations of pyramidal cells in the CA1 region of the hippocampus. J. Neurosci. *28*, 2274–2286.

Serrano, A., Haddjeri, N., Lacaille, J.-C., and Robitaille, R. (2006). GABAergic Network Activation of Glial Cells Underlies Hippocampal Heterosynaptic Depression. J. Neurosci. *26*, 5370–5382.

Shah, D., Verhoye, M., Van der Linden, A., and D'Hooge, R. (2019). Acquisition of Spatial Search Strategies and Reversal Learning in the Morris Water Maze Depend on Disparate Brain Functional Connectivity in Mice. Cereb. Cortex *29*, 4519–4529.

Sharma, S., Rakoczy, S., and Brown-Borg, H. (2010). Assessment of spatial memory in mice. Life Sci. *87*, 521–536.

Sheffield, M.E.J., and Dombeck, D.A. (2015). Calcium transient prevalence across the dendritic arbour predicts place field properties. Nature *517*, 200–204.

Sheffield, M.E.J., Adoff, M.D., and Dombeck, D.A. (2017). Increased Prevalence of Calcium Transients across the Dendritic Arbor during Place Field Formation. Neuron *96*, 490-504.e5.

Sherwood, M.W., Arizono, M., Hisatsune, C., Bannai, H., Ebisui, E., Sherwood, J.L., Panatier, A., Oliet, S.H.R., and Mikoshiba, K. (2017). Astrocytic IP3 Rs: Contribution to Ca2+ signalling and hippocampal LTP. Glia *65*, 502–513.

Shigetomi, E., Bowser, D.N., Sofroniew, M.V., and Khakh, B.S. (2008). Two Forms of Astrocyte Calcium Excitability Have Distinct Effects on NMDA Receptor-Mediated Slow Inward Currents in Pyramidal Neurons. J. Neurosci. *28*, 6659–6663.

Shigetomi, E., Kracun, S., Sofroniew, M.V., and Khakh, B.S. (2010). A genetically targeted optical sensor to monitor calcium signals in astrocyte processes. Nat. Neurosci. *13*, 759–766.

Shigetomi, E., Tong, X., Kwan, K.Y., Corey, D.P., and Khakh, B.S. (2012). TRPA1 channels regulate astrocyte resting calcium and inhibitory synapse efficacy through GAT-3. Nat. Neurosci. *15*, 70–80.

Shigetomi, E., Bushong, E.A., Haustein, M.D., Tong, X., Jackson-Weaver, O., Kracun, S., Xu, J., Sofroniew, M.V., Ellisman, M.H., and Khakh, B.S. (2013a). Imaging calcium microdomains within entire astrocyte territories and endfeet with GCaMPs expressed using adeno-associated viruses. J. Gen. Physiol. *141*, 633–647.

Shigetomi, E., Jackson-Weaver, O., Huckstepp, R.T., O'Dell, T.J., and Khakh, B.S. (2013b). TRPA1 channels are regulators of astrocyte basal calcium levels and long-term potentiation via constitutive D-serine release. J. Neurosci. *33*, 10143–10153.

Shimada, M., Akagi, N., Goto, H., Watanabe, H., Nakanishi, M., Hirose, Y., and Watanabe, M. (1992). Microvessel and astroglial cell densities in the mouse hippocampus. J. Anat. *180*, 89–95.

Short, S.M., Oikonomou, K.D., Zhou, W.-L., Acker, C.D., Popovic, M.A., Zecevic, D., and Antic, S.D. (2017). The stochastic nature of action potential backpropagation in apical tuft dendrites. J. Neurophysiol. *118*, 1394–1414.

Siegel, A., and Tassoni, J.P. (1971). Differential Efferent Projections from the Ventral and Dorsal Hippocampus of the Cat. Brain. Behav. Evol. *4*, 185–200.

Sivyer, B., and Williams, S.R. (2013). Direction selectivity is computed by active dendritic integration in retinal ganglion cells. Nat. Neurosci. *16*, 1848–1856.

Sjöström, P.J., and Häusser, M. (2006). A cooperative switch determines the sign of synaptic plasticity in distal dendrites of neocortical pyramidal neurons. Neuron *51*, 227–238.

Smith, N.A., Bekar, L.K., and Nedergaard, M. (2020). Astrocytic Endocannabinoids Mediate Hippocampal Transient Heterosynaptic Depression. Neurochem. Res. *45*, 100–108.

Smith, S.L., Smith, I.T., Branco, T., and Häusser, M. (2013). Dendritic spikes enhance stimulus selectivity in cortical neurons in vivo. Nature *503*, 115–120.

Snyder, E.M., Philpot, B.D., Huber, K.M., Dong, X., Fallon, J.R., and Bear, M.F. (2001). Internalization of ionotropic glutamate receptors in response to mGluR activation. Nat. Neurosci. *4*, 1079–1085.

Soltesz, I., and Deschênes, M. (1993). Low- and high-frequency membrane potential oscillations during theta activity in CA1 and CA3 pyramidal neurons of the rat hippocampus under ketamine-xylazine anesthesia. J. Neurophysiol. *70*, 97–116.

Somogyi, P., and Klausberger, T. (2005). Defined types of cortical interneurone structure space and spike timing in the hippocampus. J. Physiol. *562*, 9–26.

Song, S., Miller, K.D., and Abbott, L.F. (2000). Competitive Hebbian learning through spike-timing-dependent synaptic plasticity. Nat. Neurosci. *3*, 919–926.

Spellman, T., Rigotti, M., Ahmari, S.E., Fusi, S., Gogos, J.A., and Gordon, J.A. (2015). Hippocampal–prefrontal input supports spatial encoding in working memory. Nature *522*, 309–314.

Sperling, G. (1960). The information available in brief visual presentations. Psychol. Monogr. Gen. Appl. *74*, 1–29.

Spruston, N. (2008). Pyramidal neurons: dendritic structure and synaptic integration. Nat. Rev. Neurosci. *9*, 206–221.

Spruston, N., Schiller, Y., Stuart, G., and Sakmann, B. (1995). Activity-dependent action potential invasion and calcium influx into hippocampal CA1 dendrites. Science *268*, 297–300.

Srinivasan, R., Huang, B.S., Venugopal, S., Johnston, A.D., Chai, H., Zeng, H., Golshani, P., and Khakh, B.S. (2015). Ca(2+) signaling in astrocytes from Ip3r2(-/-) mice in brain slices and during startle responses in vivo. Nat. Neurosci. *18*, 708–717.

Stanton, P.K., and Sarvey, J.M. (1984). Blockade of long-term potentiation in rat hippocampal CA1 region by inhibitors of protein synthesis. J. Neurosci. *4*, 3080–3088.

Staubli, U., and Lynch, G. (1990). Stable depression of potentiated synaptic responses in the hippocampus with 1–5 Hz stimulation. Brain Res. *513*, 113–118.

Stella, N. (2010). Cannabinoid and cannabinoid-like receptors in microglia, astrocytes, and astrocytomas. Glia *58*, 1017–1030.

Steriade, M., Timofeev, I., and Grenier, F. (2001). Natural waking and sleep states: a view from inside neocortical neurons. J. Neurophysiol. *85*, 1969–1985.

Stevens, R., and Cowey, A. (1973). Effects of dorsal and ventral hippocampal lesions on spontaneous alternation, learned alternation and probability learning in rats. Brain Res. *52*, 203–224.

Stocca, G., and Vicini, S. (1998). Increased contribution of NR2A subunit to synaptic NMDA receptors in developing rat cortical neurons. J. Physiol. *507*, 13–24.

Straiker, A., Hu, S.S.-J., Long, J.Z., Arnold, A., Wager-Miller, J., Cravatt, B.F., and Mackie, K. (2009). Monoacylglycerol lipase limits the duration of endocannabinoid-mediated depolarization-induced suppression of excitation in autaptic hippocampal neurons. Mol. Pharmacol. *76*, 1220–1227.

Stuart, G.J., and Häusser, M. (2001). Dendritic coincidence detection of EPSPs and action potentials. Nat. Neurosci. *4*, 63–71.

Stuart, G., Schiller, J., and Sakmann, B. (1997). Action potential initiation and propagation in rat neocortical pyramidal neurons. J. Physiol. *505*, 617–632.

Stumpf, C. (1965). THE FAST COMPONENT IN THE ELECTRICAL ACTIVITY OF RABBIT'S HIPPOCAMPUS. Electroencephalogr. Clin. Neurophysiol. *18*, 477–486.

Sullivan, J.M. (1999). Mechanisms of cannabinoid-receptor-mediated inhibition of synaptic transmission in cultured hippocampal pyramidal neurons. J. Neurophysiol. *82*, 1286–1294.

Sultan, S., Li, L., Moss, J., Petrelli, F., Cassé, F., Gebara, E., Lopatar, J., Pfrieger, F.W., Bezzi, P., Bischofberger, J., et al. (2015). Synaptic Integration of Adult-Born Hippocampal Neurons Is Locally Controlled by Astrocytes. Neuron *88*, 957–972.

Sutherland, R.J., Dringenberg, H.C., and Hoesing, J.M. (1993). Induction of long-term potentiation at perforant path dentate synapses does not affect place learning or memory. Hippocampus *3*, 141–147.

Sweeney, A.M., Fleming, K.E., McCauley, J.P., Rodriguez, M.F., Martin, E.T., Sousa, A.A., Leapman, R.D., and Scimemi, A. (2017). PAR1 activation induces rapid changes in glutamate uptake and astrocyte morphology. Sci. Rep. *7*, 43606.

Szabo, B., Urbanski, M.J., Bisogno, T., Marzo, V.D., Mendiguren, A., Baer, W.U., and Freiman, I. (2006). Depolarization-induced retrograde synaptic inhibition in the mouse cerebellar cortex is mediated by 2-arachidonoylglycerol. J. Physiol. *577*, 263–280.

Szabó, G.G., Lenkey, N., Holderith, N., Andrási, T., Nusser, Z., and Hájos, N. (2014). Presynaptic calcium channel inhibition underlies CB_1 cannabinoid receptor-mediated suppression of GABA release. J. Neurosci. *34*, 7958–7963.

Taheri, M., Handy, G., Borisyuk, A., and White, J.A. (2017). Diversity of Evoked Astrocyte Ca2+ Dynamics Quantified through Experimental Measurements and Mathematical Modeling. Front. Syst. Neurosci. *11*.

Takahashi, H., and Magee, J.C. (2009). Pathway Interactions and Synaptic Plasticity in the Dendritic Tuft Regions of CA1 Pyramidal Neurons. Neuron *62*, 102–111.

Takahashi, N., Kitamura, K., Matsuo, N., Mayford, M., Kano, M., Matsuki, N., and Ikegaya, Y. (2012). Locally Synchronized Synaptic Inputs. Science *335*, 353–356.

Takata, N., and Hirase, H. (2008). Cortical layer 1 and layer 2/3 astrocytes exhibit distinct calcium dynamics in vivo. PLOS ONE *3*, e2525.

Tanaka, M., Shih, P.-Y., Gomi, H., Yoshida, T., Nakai, J., Ando, R., Furuichi, T., Mikoshiba, K., Semyanov, A., and Itohara, S. (2013). Astrocytic Ca2+ signals are required for the functional integrity of tripartite synapses. Mol. Brain *6*, 6.

Tanaka, N., Sano, K., Rahman, M.A., Miyata, R., Capi, G., and Kawahara, S. (2018). Change in hippocampal theta oscillation associated with multiple lever presses in a bimanual two-lever choice task for robot control in rats. PLOS ONE *13*, e0192593.

Tang, Y.P., Shimizu, E., Dube, G.R., Rampon, C., Kerchner, G.A., Zhuo, M., Liu, G., and Tsien, J.Z. (1999). Genetic enhancement of learning and memory in mice. Nature *401*, 63–69.

Tanimura, A., Yamazaki, M., Hashimotodani, Y., Uchigashima, M., Kawata, S., Abe, M., Kita, Y., Hashimoto, K., Shimizu, T., Watanabe, M., et al. (2010). The Endocannabinoid 2-Arachidonoylglycerol Produced by Diacylglycerol Lipase α Mediates Retrograde Suppression of Synaptic Transmission. Neuron *65*, 320–327.

Tavares, R.M., Mendelsohn, A., Grossman, Y., Williams, C.H., Shapiro, M., Trope, Y., and Schiller, D. (2015). A Map for Social Navigation in the Human Brain. Neuron *87*, 231–243.

Thiels, E., Barrionuevo, G., and Berger, T.W. (1994). Excitatory stimulation during postsynaptic inhibition induces long-term depression in hippocampus in vivo. J. Neurophysiol. *72*, 3009–3016.

Thiels, E., Xie, X., Yeckel, M.F., Barrionuevo, G., and Berger, T.W. (1996). NMDA Receptor-dependent LTD in different subfields of hippocampus in vivo and in vitro. Hippocampus *6*, 43–51.

Thome, C., Kelly, T., Yanez, A., Schultz, C., Engelhardt, M., Cambridge, S.B., Both, M., Draguhn, A., Beck, H., and Egorov, A.V. (2014). Axon-Carrying Dendrites Convey Privileged Synaptic Input in Hippocampal Neurons. Neuron *83*, 1418–1430.

Tolman, E.C. (1948). Cognitive maps in rats and men. Psychol. Rev. *55*, 189–208.

Tomita, S., Stein, V., Stocker, T.J., Nicoll, R.A., and Bredt, D.S. (2005). Bidirectional synaptic plasticity regulated by phosphorylation of stargazin-like TARPs. Neuron *45*, 269–277.

Tønnesen, J., Katona, G., Rózsa, B., and Nägerl, U.V. (2014). Spine neck plasticity regulates compartmentalization of synapses. Nat. Neurosci. *17*, 678–685.

Touw, M. (1981). The religious and medicinal uses of Cannabis in China, India and Tibet. J. Psychoactive Drugs *13*, 23–34.

Tovar, K.R., McGinley, M.J., and Westbrook, G.L. (2013). Triheteromeric NMDA Receptors at Hippocampal Synapses. J. Neurosci. *33*, 9150–9160.

Trimper, J.B., Galloway, C.R., Jones, A.C., Mandi, K., and Manns, J.R. (2017). Gamma Oscillations in Rat Hippocampal Subregions Dentate Gyrus, CA3, CA1, and Subiculum Underlie Associative Memory Encoding. Cell Rep. *21*, 2419–2432.

Tsay, D., Dudman, J.T., and Siegelbaum, S.A. (2007). HCN1 Channels Constrain Synaptically Evoked Ca2+ Spikes in Distal Dendrites of CA1 Pyramidal Neurons. Neuron *56*, 1076–1089.

Tsien, J.Z., Huerta, P.T., and Tonegawa, S. (1996). The essential role of hippocampal CA1 NMDA receptor-dependent synaptic plasticity in spatial memory. Cell *87*, 1327–1338.

Tsubokawa, H., and Ross, W.N. (1996). IPSPs modulate spike backpropagation and associated [Ca2+]i changes in the dendrites of hippocampal CA1 pyramidal neurons. J. Neurophysiol. *76*, 2896–2906.

Twitchell, W., Brown, S., and Mackie, K. (1997). Cannabinoids Inhibit N- and P/Q-Type Calcium Channels in Cultured Rat Hippocampal Neurons. J. Neurophysiol. *78*, 43–50.

Tyan, L., Chamberland, S., Magnin, E., Camiré, O., Francavilla, R., David, L.S., Deisseroth, K., and Topolnik, L. (2014). Dendritic Inhibition Provided by Interneuron-Specific Cells Controls the Firing Rate and Timing of the Hippocampal Feedback Inhibitory Circuitry. J. Neurosci. *34*, 4534–4547.

Vaarmann, A., Gandhi, S., and Abramov, A.Y. (2010). Dopamine Induces Ca2+ Signaling in Astrocytes through Reactive Oxygen Species Generated by Monoamine Oxidase. J. Biol. Chem. *285*, 25018–25023.

Vafaei, A.A., and Rashidy-Pour, A. (2004). Reversible lesion of the rat's orbitofrontal cortex interferes with hippocampus-dependent spatial memory. Behav. Brain Res. *149*, 61–68.

Vago, D.R., and Kesner, R.P. (2008). Disruption of the direct perforant path input to the CA1 subregion of the dorsal hippocampus interferes with spatial working memory and novelty detection. Behav. Brain Res. *189*, 273–283.

Vanderwolf, C.H. (1969). Hippocampal electrical activity and voluntary movement in the rat. Electroencephalogr. Clin. Neurophysiol. *26*, 407–418.

Varma, N., Carlson, G.C., Ledent, C., and Alger, B.E. (2001). Metabotropic Glutamate Receptors Drive the Endocannabinoid System in Hippocampus. J. Neurosci. *21*, RC188.

Ventura, R., and Harris, K.M. (1999). Three-Dimensional Relationships between Hippocampal Synapses and Astrocytes. J. Neurosci. *19*, 6897–6906.

Verkhratsky, A., Rodríguez, J.J., and Parpura, V. (2012). Calcium signalling in astroglia. Mol. Cell. Endocrinol. *353*, 45–56.

Verkhratsky, A., Matteoli, M., Parpura, V., Mothet, J.-P., and Zorec, R. (2016). Astrocytes as secretory cells of the central nervous system: idiosyncrasies of vesicular secretion. EMBO J. *35*, 239–257.

Vertes, R.P., Albo, Z., and Viana Di Prisco, G. (2001). Theta-rhythmically firing neurons in the anterior thalamus: implications for mnemonic functions of Papez's circuit. Neuroscience *104*, 619–625.

Viader, A., Blankman, J.L., Zhong, P., Liu, X., Schlosburg, J.E., Joslyn, C.M., Liu, Q.-S., Tomarchio, A.J., Lichtman, A.H., Selley, D.E., et al. (2015). Metabolic Interplay between Astrocytes and Neurons Regulates Endocannabinoid Action. Cell Rep. *12*, 798–808.

Virchow, R. (1859). Die Cellularpathologie in ihrer Begründung auf physiologische und pathologische Gewebelehre: zwanzig Vorlesungen, gehalten während der Monate Februar, März und April 1858 im pathologischen Institute zu Berlin (Berlin: A. Hirschwald).

Vu, E.T., and Krasne, F.B. (1992). Evidence for a computational distinction between proximal and distal neuronal inhibition. Science *255*, 1710–1712.

Vyklický, L., Benveniste, M., and Mayer, M.L. (1990). Modulation of N-methyl-D-aspartic acid receptor desensitization by glycine in mouse cultured hippocampal neurones. J. Physiol. *428*, 313–331.

Wallraff, A., Köhling, R., Heinemann, U., Theis, M., Willecke, K., and Steinhäuser, C. (2006). The Impact of Astrocytic Gap Junctional Coupling on Potassium Buffering in the Hippocampus. J. Neurosci. *26*, 5438–5447.

Walter, L., Franklin, A., Witting, A., Wade, C., Xie, Y., Kunos, G., Mackie, K., and Stella, N. (2003). Nonpsychotropic Cannabinoid Receptors Regulate Microglial Cell Migration. J. Neurosci. *23*, 1398–1405.

Walz, W., and Lang, M.K. (1998). Immunocytochemical evidence for a distinct GFAP-negative subpopulation of astrocytes in the adult rat hippocampus. Neurosci. Lett. *257*, 127–130.

Wang, J., and Zucker, R.S. (2001). Photolysis-induced suppression of inhibition in rat hippocampal CA1 pyramidal neurons. J. Physiol. *533*, 757–763.

Wang, D., Cui, Z., Zeng, Q., Kuang, H., Wang, L.P., Tsien, J.Z., and Cao, X. (2009). Genetic enhancement of memory and long-term potentiation but not CA1 long-term depression in NR2B transgenic rats. PloS One *4*, e7486.

Wang, F., Smith, N.A., Xu, Q., Fujita, T., Baba, A., Matsuda, T., Takano, T., Bekar, L., and Nedergaard, M. (2012a). Astrocytes Modulate Neural Network Activity by Ca2+-Dependent Uptake of Extracellular K+. Sci. Signal. *5*, ra26.

Wang, X., Lou, N., Xu, Q., Tian, G.-F., Peng, W.G., Han, X., Kang, J., Takano, T., and Nedergaard, M. (2006). Astrocytic Ca 2+ signaling evoked by sensory stimulation in vivo. Nat. Neurosci. *9*, 816–823.

Wang, Y., Rattner, A., Zhou, Y., Williams, J., Smallwood, P.M., and Nathans, J. (2012b). Norrin/Frizzled4 Signaling in Retinal Vascular Development and Blood Brain Barrier Plasticity. Cell *151*, 1332–1344.

Watabe, A.M., Carlisle, H.J., and O'Dell, T.J. (2002). Postsynaptic induction and presynaptic expression of group 1 mGluR-dependent LTD in the hippocampal CA1 region. J. Neurophysiol. *87*, 1395–1403.

Waters, J., Larkum, M., Sakmann, B., and Helmchen, F. (2003). Supralinear Ca2+ Influx into Dendritic Tufts of Layer 2/3 Neocortical Pyramidal Neurons In Vitro and In Vivo. J. Neurosci. *23*, 8558–8567.

Wei, D.-S., Mei, Y.-A., Bagal, A., Kao, J.P.Y., Thompson, S.M., and Tang, C.-M. (2001). Compartmentalized and Binary Behavior of Terminal Dendrites in Hippocampal Pyramidal Neurons. Science *293*, 2272–2275.

Weitlauf, C., Honse, Y., Auberson, Y.P., Mishina, M., Lovinger, D.M., and Winder, D.G. (2005). Activation of NR2A-containing NMDA receptors is not obligatory for NMDA receptor-dependent long-term potentiation. J. Neurosci. Off. J. Soc. Neurosci. *25*, 8386–8390.

Williams, S.R., and Stuart, G.J. (2000). Backpropagation of Physiological Spike Trains in Neocortical Pyramidal Neurons: Implications for Temporal Coding in Dendrites. J. Neurosci. *20*, 8238–8246.

Wilson, M.A., and McNaughton, B.L. (1993). Dynamics of the hippocampal ensemble code for space. Science *261*, 1055–1058.

Wilson, R.I., and Nicoll, R.A. (2001). Endogenous cannabinoids mediate retrograde signalling at hippocampal synapses. Nature *410*, 588–592.

Wilson, D.E., Whitney, D.E., Scholl, B., and Fitzpatrick, D. (2016). Orientation selectivity and the functional clustering of synaptic inputs in primary visual cortex. Nat. Neurosci. *19*, 1003–1009.

Wilson, R.I., Kunos, G., and Nicoll, R.A. (2001). Presynaptic Specificity of Endocannabinoid Signaling in the Hippocampus. Neuron *31*, 453–462.

Wilson, S.R., Gerhold, K.A., Bifolck-Fisher, A., Liu, Q., Patel, K.N., Dong, X., and Bautista, D.M. (2011). TRPA1 is required for histamine-independent, Mas-related G protein-coupled receptor-mediated itch. Nat. Neurosci. *14*, 595–602.

Winnubst, J., Cheyne, J.E., Niculescu, D., and Lohmann, C. (2015). Spontaneous Activity Drives Local Synaptic Plasticity In Vivo. Neuron *87*, 399–410.

Winson, J. (1974). Patterns of hippocampal theta rhythm in the freely moving rat. Electroencephalogr. Clin. Neurophysiol. *36*, 291–301.

Witcher, M.R., Kirov, S.A., and Harris, K.M. (2007). Plasticity of perisynaptic astroglia during synaptogenesis in the mature rat hippocampus. Glia *55*, 13–23.

Wolansky, T., Clement, E.A., Peters, S.R., Palczak, M.A., and Dickson, C.T. (2006). Hippocampal Slow Oscillation: A Novel EEG State and Its Coordination with Ongoing Neocortical Activity. J. Neurosci. *26*, 6213–6229.

Wolff, J. (1968). The role of the astroglia in the brain tissue. In Symposium on Neuroglia / Symposium Concernant La Neuroglie / Symposium Über Die Neuroglia, F. Erbslöh, A. Oksche, and F. Seitelberger, eds. (Springer Berlin Heidelberg), pp. 33–39.

Wolosker, H., Blackshaw, S., and Snyder, S.H. (1999). Serine racemase: A glial enzyme synthesizing d-serine to regulate glutamate-N-methyl-d-aspartate neurotransmission. Proc. Natl. Acad. Sci. *96*, 13409–13414.

Wolosker, H., Balu, D.T., and Coyle, J.T. (2016). The Rise and Fall of the d-Serine-Mediated Gliotransmission Hypothesis. Trends Neurosci. *39*, 712–721.

Woo, D.H., Han, K.-S., Shim, J.W., Yoon, B.-E., Kim, E., Bae, J.Y., Oh, S.-J., Hwang, E.M., Marmorstein, A.D., Bae, Y.C., et al. (2012). TREK-1 and Best1 Channels Mediate Fast and Slow Glutamate Release in Astrocytes upon GPCR Activation. Cell *151*, 25–40.

Woo, D.H., Bae, J.Y., Nam, M.-H., An, H., Ju, Y.H., Won, J., Choi, J.H., Hwang, E.M., Han, K.-S., Bae, Y.C., et al. (2018). Activation of Astrocytic μ-opioid Receptor Elicits Fast Glutamate Release Through TREK-1-Containing K2P Channel in Hippocampal Astrocytes. Front. Cell. Neurosci. *12*, 319.

Woodson, W., Nitecka, L., and Ben-Ari, Y. (1989). Organization of the GABAergic system in the rat hippocampal formation: A quantitative immunocytochemical study. J. Comp. Neurol. *280*, 254–271.

Wu, Y.-W., Gordleeva, S., Tang, X., Shih, P.-Y., Dembitskaya, Y., and Semyanov, A. (2019). Morphological profile determines the frequency of spontaneous calcium events in astrocytic processes. Glia *67*, 246–262.

Xiao, M.Y., Zhou, Q., and Nicoll, R.A. (2001). Metabotropic glutamate receptor activation causes a rapid redistribution of AMPA receptors. Neuropharmacology *41*, 664–671.

Xu, J.-Y., and Chen, C. (2015). Endocannabinoids in Synaptic Plasticity and Neuroprotection. The Neuroscientist *21*, 152–168.

Xu, J., Antion, M.D., Nomura, T., Kraniotis, S., Zhu, Y., and Contractor, A. (2014). Hippocampal metaplasticity is required for the formation of temporal associative memories. J. Neurosci. *34*, 16762–16773.

Xu, N., Harnett, M.T., Williams, S.R., Huber, D., O'Connor, D.H., Svoboda, K., and Magee, J.C. (2012). Nonlinear dendritic integration of sensory and motor input during an active sensing task. Nature *492*, 247–251.

Yamada, K., Arai, M., Suenaga, T., and Ichitani, Y. (2017). Involvement of hippocampal NMDA receptors in encoding and consolidation, but not retrieval, processes of spontaneous object location memory in rats. Behav. Brain Res. *331*, 14–19.

Yang, C.-H., Huang, C.-C., and Hsu, K.-S. (2005). Behavioral stress enhances hippocampal CA1 long-term depression through the blockade of the glutamate uptake. J. Neurosci. *25*, 4288–4293.

Yang, Q., Zhu, G., Liu, D., Ju, J.-G., Liao, Z.-H., Xiao, Y.-X., Zhang, Y., Chao, N., Wang, J., Li, W., et al. (2017). Extrasynaptic NMDA receptor dependent long-term potentiation of hippocampal CA1 pyramidal neurons. Sci. Rep. *7*, 3045.

Yang, Y., Ge, W., Chen, Y., Zhang, Z., Shen, W., Wu, C., Poo, M., and Duan, S. (2003). Contribution of astrocytes to hippocampal long-term potentiation through release of d-serine. Proc. Natl. Acad. Sci. *100*, 15194–15199.

Yasuda, H., Huang, Y., and Tsumoto, T. (2008). Regulation of excitability and plasticity by endocannabinoids and PKA in developing hippocampus. Proc. Natl. Acad. Sci. *105*, 3106–3111.

Younts, T.J., Chevaleyre, V., and Castillo, P.E. (2013). CA1 Pyramidal Cell Theta-Burst Firing Triggers Endocannabinoid-Mediated Long-Term Depression at Both Somatic and Dendritic Inhibitory Synapses. J. Neurosci. *33*, 13743–13757.

Yu, X.-M., and Salter, M.W. (1998). Gain control of NMDA-receptor currents by intracellular sodium. Nature *396*, 469–474.

Zeisel, A., Muñoz-Manchado, A.B., Codeluppi, S., Lönnerberg, P., Manno, G.L., Juréus, A., Marques, S., Munguba, H., He, L., Betsholtz, C., et al. (2015). Cell types in the mouse cortex and hippocampus revealed by single-cell RNA-seq. Science *347*, 1138–1142.

Zhang, J., Wang, H., Ye, C., Ge, W., Chen, Y., Jiang, Z., Wu, C., Poo, M., and Duan, S. (2003). ATP Released by Astrocytes Mediates Glutamatergic Activity-Dependent Heterosynaptic Suppression. Neuron *40*, 971–982.

Zhang, Y., Yoshida, T., Katz, D.B., and Lisman, J.E. (2012). NMDAR antagonist action in thalamus imposes delta oscillations on the hippocampus. J. Neurophysiol. *107*, 3181–3189.

Zheng, C., Bieri, K.W., Hwaun, E., and Colgin, L.L. (2016). Fast Gamma Rhythms in the Hippocampus Promote Encoding of Novel Object-Place Pairings. ENeuro *3*.

Zheng, K., Bard, L., Reynolds, J.P., King, C., Jensen, T.P., Gourine, A.V., and Rusakov, D.A. (2015). Time-Resolved Imaging Reveals Heterogeneous Landscapes of Nanomolar Ca2+ in Neurons and Astroglia. Neuron *88*, 277–288.

Zhu, P.J., and Lovinger, D.M. (2007). Persistent Synaptic Activity Produces Long-Lasting Enhancement of Endocannabinoid Modulation and Alters Long-Term Synaptic Plasticity. J. Neurophysiol. *97*, 4386–4389.

Zimmermann, T., Bartsch, J.C., Beer, A., Lomazzo, E., Guggenhuber, S., Lange, M.D., Bindila, L., Pape, H.-C., and Lutz, B. (2019). Impaired anandamide/palmitoylethanolamide signaling in hippocampal glutamatergic neurons alters synaptic plasticity, learning, and emotional responses. Neuropsychopharmacology *44*, 1377–1388.

7 APPENDIX

7.1 ABBREVIATIONS

AChR	acetylcholine receptor
2-AG	2-Arachidonoylglycerol
aCB1KO	astrocyte-specific cannabinoid receptor 1 knock-out
aCSF	artificial cerebrospinal fluid
AEA	anandamide
AI	alternation index
AMPA	α-amino-3-hydroxy-5-methyl-4-isoxazolepropionic acid
AP	action potential
ATP	Adenosine triphosphate
bAP	backpropagation action potential
CA	cornu ammonis
CaMKII	calcium/calmodulin-dependent protein kinase II
CB	cannabinoid
CCK	cholecystokinin
DAAO	D-amino acid oxidase
DI	discrimination index
DSE	depolarization-induced suppression of excitation
DSI	depolarization-induced suppression of inhibition
EAAT	excitatory amino acid transporters
EPSP	excitatory postsynaptic potential
fEPSP	field excitatory postsynaptic potential
FWHM	full-width at half maximal amplitude
GABA	γ-aminobutyric acid
GFAP	glial fibrillary acidic protein
GLAST	glutamate aspartate Transporter
GLT1	glutamate transporter 1
HCN	hyperpolarization-activated cyclic nucleotide-gated
HEK cells	human embryonic kidney 293 cells
i.p.	intraperitoneal
I_A	A-type K^+ current
iEPSP	iontophoretic excitatory postsynaptic potential
I_h	hyperpolarization-activated current
iLTD	heterosynaptic, presynaptic, endocannabinoid-dependent LTP of inhibitor synapses
IP3	inositol trisphosphate
IQR	interquartile range

LTD	long-term depression
LTP	long-term potentiation
mGluR	metabotropic glutamate receptors
MWM	Morris water maze
NMDA	N-Methyl-D-aspartate
NORT	novel object recognition task
OLM	oriens-lacunosum moleculare
OLT	object location task
PAPs	perisynaptic astrocytic processes
PBS	phosphate-buffered saline
PC	pyramidal cell
REM	rapid eye movement
R_m	membrane resistance
ROI	region of interest
SEM	standard error of the mean
SICs	slow depolarizing inward currents
SNARE	soluble NSF attachment protein (SNAP) receptor
SWS	slow-wave sleep
THC	tetrahydrocannabinol
TRPA1	transient receptor potential ankyrin 1
TTX	tetrodotoxin
VGCC	voltage-gated calcium channel
VGSC	voltage-gated sodium channel
V_m	resting membrane potential
τ_m	membrane time constant

7.2 LIST OF FIGURES

7.3 LIST OF TABLES

ACKNOWLEDGEMENTS

First of all, I would like to thank Professor Dr. Christian Henneberger for the opportunity to work on this exciting project in his laboratory. His guidance, his fruitful discussions and enthusiasm for the project have made my doctoral studies very enjoyable. I am fortunate to have such an understanding and supportive supervisor.

Many thanks also to Professor Dr. Michael Hofmann for being the second referee of the examination committee and for investing his time and effort in reviewing my dissertation. I would also like to thank Professor Dr. Walter Witke and Professor Dr. Ulrich Ettinger for their participation in my examination committee.

Additionally, I would also like to express my sincere thanks to my collaborators: Professor Dr. Heinz Beck was a great help throughout the entire project, both personally and professionally. The collaboration during the behavior experiments with him, Rebekka Zölzer and Thoralf Opitz were crucial for the project and very gratifying. I would also like to thank Nicola Masalla and Toni Kelly for the constructive criticism and collaboration regarding the dendritic integration project. Furthermore, I would like to thank Professor Dr. Gabor Petzold, Dr. Andrea Delekante and Dr. Cordula Rakers for their collaboration on the astrocyte resting calcium project.

Special thanks go to the members of my workgroup Alberto, Anne, Björn, Catia, Charlotte, Claire K., Claire S., Daniel, Eva, Katharina, Michel, Nariman, Petr, Stefan and Steffi. You created a unique work environment with your endless support, fruitful discussions and understanding. I enjoyed the time in and out of the lab, at conferences and retreats a lot.

Next, I would like to say thank you to Professor Dr. Steinhäuser for his support and productive discussions. Being part of the Institute of cellular Neurosciences created a great backbone for the project. I am very thankful for PD Dr. Gerald Seifert's expertise on breeding and countless genotyping of the transgenic animals as well as Tomas Erdmann for his organizational support. Of course, I also like to express my thanks to all other members of the institute: Aline, Camille, Delaware, Ines, Julia, Lukas, Magda, Peter, Ronald, Silke, Steffi G., and Tushar, for such a great atmosphere, enjoyable conversations, interesting discussions, countless sweets and fun retreats.

Words are inadequate to express the gratitude I have for my friends for joining me on this journey. You have been patient and understanding throughout the years. Thank you for keeping me sane.

Tom and Ina, you kept me going through better and worse. With good meals, better wine, great conversations and countless laughs in a very enjoyable company but also with a helping hand when needed you supported and helped me. I am thankful to have you both in my life.

Wiebke, my best, my oldest, my closest. You are my cheerleader, my teddy bear, my psychologist and that all for more than half of our life. We have been separated through borders, continents and oceans. Nevertheless, you are always there when I need you. Thank you for also sticking around for this journey. I am already looking forward to the next one!

The last paragraphs are dedicated to my family. Jan-Eric and Kamila, you have always been there when I needed you, whether it was through moral support, distraction or just lending an ear. You are the best brother and sister(-in-law) I could have wished for.

Papa, although you were neither around anymore to see me start nor finish my thesis, you paved the way for me to get here. I did it and I could have not done it without your help.

Special thanks go out to my mom. Although you do not really understand what I am doing, you never question it and always support me going my way. Especially your help during the recent months made an unexpected, otherwise impossible situation productive and enjoyable. Thank you for this.

Most importantly, I would like to thank my son Fiete. You denominated the second half of this project by enforcing a healthy work-life balance, provided useful distractions and countless reasons to laugh and enjoy. But even more importantly, you also did your part in this process, even though you might not understand it yet. By sleeping through the night, enjoying your daycare and spending time with your grandma, you gave me the time and mind I needed to complete this project. I could not have done this without you. You are my sunshine at the end of every (rainy) lab day.